

*Proceedings of the Symposium
on the Recent Contributions
to the Geological History
of the South China Sea*

*Oct. 10-13, 1990
Hangzhou*

MARINE GEOLOGY AND GEOPHYSICS OF THE SOUTH CHINA SEA

*Edited by
Jin Xianglong
H.R. Kudrass
Guy Pautot*



CHINA OCEAN PRESS

*Proceedings of the Symposium
on the Recent Contributions
to the Geological History
of the South China Sea*

MARINE GEOLOGY AND GEOPHYSICS OF THE SOUTH CHINA SEA

*Edited by
Jin Xianglong
H.R. Kudrass
Guy Pautot*

CHINA OCEAN PRESS

Edited by
Jin Xianglong
H.R.Kudrass
Guy Pautot

Proceedings of the Symposium
on the Recent Contributions
to the Geological History
of the South China Sea

THE SOUTH CHINA SEA
GEOPHYSICS OF
MARINE GEOLOGY AND

Edited by
Jin Xianglong
H. R. Kudrass
Guy Pautot

ISBN 7-5027-1915-6 / K.66

This work is subject to copyright. All rights are reserved, whether the whole or part of the material is concerned, specifically those of translation, reprinting, re-use of illustrations, broadcasting, reproduction by photocopying machine of similar means and storage in data banks.

© by China Ocean Press 1992
Printed in China

CHINA OCEAN PRESS

PREFACE

The South China Sea is situated at the junction of the Eurasian plate, the Pacific plate and the Indian plate. It is one of the marginal seas in western Pacific and adjacent to the southeast Asian continent. The South China Sea has complicated tectonic and sedimentation histories, and abundant mineral resources, especially, natural gas and oil, which are greatly attracting geoscientists. The South China Sea basin appears to have been formed as a result of the continental margin rifting and spreading, rather than by simple back-arc spreading. The continental lithosphere here has been attenuated to the extent of spreading indicated by obvious magnetic pattern with approximately east-west trend. The South China Sea basin has developed between continental fragments (terrains) which have rifted from the Asian continent, and the sedimentation has also occurred between and on the submerged continental fragments. The South China Sea has proven to be an ideal region for the study of origin and evolution of marginal sea, and furthermore provides a vivid stage of scientific research for geoscientists from various countries to display the tremendous potential of cooperative spirits.

Since 60's, State Oceanic Administration (SOA) of China, Ministry of Geology and Mineral Resources (MGMR) of China, Chinese Academy of Sciences and China National Offshore Oil Corporation (CNOOC) have carried out a lot of investigations on marine geology and geophysics in the South China Sea. For better awareness of geology and geophysics in the South China Sea several cooperative investigations were carried out jointly by France, Germany and China. In 1985, IFREMER (French Institute of Research for Exploitation of Seas) and SOA have accomplished the Nanhai cruise using R/V Jean-Charcot. From 1987 to 1990, BGR (Federal Institute for Geosciences and Natural Resources) and SIO (Second Institute of Oceanography) of SOA, University of Hamburg and SIO, and University of Kiel and SOA, have implemented several cruises supported by BMFT (Federal Ministry for Research and Technology) of Germany, SO-49, SO-50, SO-57, SO-58, SO-69, SO-72 in the South China Sea, as well as in the East China Sea and western Pacific.

For the sake of exchanging the scientific results and ideas, and promoting the further international cooperations, according to the discussion between France and China, and the agreement between SOA of China and BMFT of Germany, the Symposium on the Recent Contribution to the Geological History of the South China Sea jointly sponsored by IFREMER of France, BMFT of Germany and SOA of China was held in Hangzhou, China, October 10-13, 1990. Seventy-five scientists from Australia, China, France and Germany attended the Symposium, at which fifty papers were presented. All scientists participating in the Symposium, conducted active exchange of opinions and detailed discussions on the marine geosciences of the South China Sea (tectonics, paleoceanography, sedimentation, geochemistry and mineral resources), and showed their enthusiastic interests in new ideas and findings. This Symposium is a contribution to developing knowledge of geological history in the South China Sea, and will encourage further cooperative study.

To review the progress presented at the Symposium, the Organizing Committee of the Symposium entrusted the colleagues from the Second Institute of Oceanography (SIO) of

SOA, with technical compilation of this volume of proceedings which has been published by China Ocean Press. Included in the proceedings twenty-seven papers selected by the Organizing Committee of the Symposium are divided into three topic groups: I. Tectonics and Geophysics, II. Paleooceanography and Sedimentation and III. Geochemistry, Mineralogy and Petroleum Geology. The emphasis in this volume is placed on the new scientific achievements and the new academic trend of tectonic evolution and paleooceanography in the South China Sea. It also deals with geophysical features and deep dynamic process, geochemistry, sedimentary structures and sedimentation, sea-bottom rocks, formation and distribution of oil-gas and solid mineral resources in the South China Sea, as well as marine geology and geophysics of its adjacent areas.

We would like to express our great and sincere appreciation to IFREMER of France, BMFT of Germany, SOA of China and NSF (National Natural Science Foundation) of China for their financial support to publish this proceedings of the Symposium. It would be impossible to publish this volume of proceedings without their kind support.

Mr. Gao Jinyao, Gao Zhixiong and Mrs. Peng Hui are thanked for their efforts in collection, technical preparation and review of the manuscripts included in this proceedings for publication, and Mr. Jin Xiaobing for cover designing and Mr. Gao Jian for assistance in typing.

Jin Xianglong (X.L. Jin)
H.R. Kudrass
Guy Pautot
December 25, 1991

CONTENTS

Tectonics and Geophysics

Tectogenesis and Origin of Northern South China Sea <i>X.L. Jin (Jin Xianglong)</i>	3
Morphostructural Analysis of the Central Ridge in South China Sea <i>Guy Pautot</i>	10
Seismic Stratigraphy and Holocene Sedimentation at the Northern Margin of the South China Sea <i>Christoph Gaedicke, How Kin Wong and Yuanbo Liang</i>	21
South-East Asian Marginal Basins (South China, Sulu and Celebes Seas): New Data and Interpretations <i>Claude Rangin</i>	38
Chronological Sequence of Two Spreading Phases of the South China Sea Basin <i>Wu Jinlong, Liu Zhongchen and Han Shuqiao</i>	52
Reconstructions of the South China Sea from Structural Data and Magnetic Anomalies <i>Anne Briais and Guy Pautot</i>	60
Docking of the Philippine Mobile Belt against the Eurasian Margin: Closure of the South China Sea <i>Manuel Pubellier, Nicolas Pinet and Claude Rangin</i>	71
Spreading Ages of Subbasins in the South China Sea and Their Relationship <i>Lu Wenzheng</i>	83
Features of Seismic Stratigraphy and Development of Sedimentary Sequence in the Central Basin of the South China Sea <i>Ke Changzhi</i>	92
The Age of the South China Sea Terrains Rift-Departing from South China Continent <i>Li Quanxing and Wu Shengdi</i>	101
Tectonic Movement of Mariana Trench-Arc-Trough System <i>Lin Changsong and Wang Guanrong</i>	108
The Early Mesozoic Orogeny in the Northern Shelf of the South China Sea and Its Adjacent Lands <i>Zhou Zuyi</i>	119
Crustal Isostasy and Mantle Anomaly in the South China Sea <i>Jiang Jiazhen</i>	126

Paleoceanography and Sedimentation

Erosion and Sedimentation in the Xisha Trough at the Continental Margin of Southern China <i>H.R. Kudrass, X.L. Jin, H. Beiersdorf and P. Cepek</i>	137
--	-----

A Preliminary Study of the Origin of Taiwan Shoal <i>Cai Aizhi, Li Yuanmi, Cai Yue'e, Zhu Xiaonin and Le Yuzan</i>	148
Oxygen / Carbon Isotopes and Paleoproductivity in the South China Sea during the Past 110000 Years <i>Kyaw Winn, Lianfu Zheng, Helmut Erlenkeuser and Peter Stoffers</i>	154
Stratigraphy and Sedimentary Events in the Philippine Sea <i>Wu Shiyong</i>	167
A Study of Volcanic Glass in Northern South China Sea during the Last 100KA <i>Chen Wenbin and Zhou Fugen</i>	174
Surface Textures of Quartz Grains in Cores KL37 and KL29 from the South China Sea and Its Significance of Sedimentology <i>He Liangbiao</i>	179
Deposition Process and Character of the Deep-Water Sediment in the Northern South China Sea <i>Zhou Fugen, Yun Zhiqiang, Feng Cuiying and Guo Liquan</i>	190

Geochemistry, Mineralogy and Petroleum Geology

Hydrocarbon Gases in Surface Sediments of the South China Sea <i>Ulrich Berner and Eckhard Faber</i>	199
Generation and Migration of Hydrocarbons of Neogene in Yinggehai and Qiongdongnan Basins <i>Zhang Qiming, Zhang Quanxing, Hu Zhongliang and Wang Zhenfeng</i>	212
The Tectonic Evolution of South China Sea and Its Control of Hydrocarbons <i>Wu Jinmin</i>	218
Particle Flux in the Northern South China Sea <i>T.C. Jennerjahn, G. Liebezeit, S. Kempe, L.Q.Xu, W.B.Chen and H.K. Wong</i>	228
Geochemistry and Their Genesis of Rare Earth Elements of Ferromanganese Nodules and Crusts from the South China Sea <i>Bao Gende and Li Quanxing</i>	236
Mineralogy and Geochemistry of Hydrothermal Silicic Chimney in the Mariana Trough <i>Zhang Deyu, Chen Suitian, Taibi, N.E., Wang Guanrong and Wu Shiyong</i>	246
Chemical Characterization of Hydrocarbons in Sediments from the South China Sea <i>Tang Yunqian, Zheng Shilong, Liu Kewen, Shi Jiyang, Xu Lian, H.K. Wong and G. Liebezeit</i>	255

Manuscript received

The tectonic evolution of the South China Sea Basin and the South China Sea is discussed in the light of the available geologic and geophysical data. It is suggested that the basin is a remnant of a larger basin which was formed during the Cretaceous and Tertiary. The basin is bounded by the South China Sea Ridge to the east and the South China Sea Trench to the west. The basin is filled with sediments of Cretaceous and Tertiary age.

TECTONICS AND GEOPHYSICS

The South China Sea Basin is a tectonic basin which is bounded to the east by the South China Sea Ridge and to the west by the South China Sea Trench. The basin is filled with sediments of Cretaceous and Tertiary age. The basin is bounded by the South China Sea Ridge to the east and the South China Sea Trench to the west. The basin is filled with sediments of Cretaceous and Tertiary age. The basin is bounded by the South China Sea Ridge to the east and the South China Sea Trench to the west. The basin is filled with sediments of Cretaceous and Tertiary age.

INTRODUCTION

The South China Sea Basin is a tectonic basin which is bounded to the east by the South China Sea Ridge and to the west by the South China Sea Trench. The basin is filled with sediments of Cretaceous and Tertiary age. The basin is bounded by the South China Sea Ridge to the east and the South China Sea Trench to the west. The basin is filled with sediments of Cretaceous and Tertiary age.

TECTOGENESIS AND ORIGIN OF NORTHERN SOUTH CHINA SEA *

X.L. JIN (JIN XIANGLONG)

Second Institute of Oceanography, SOA, Hangzhou, China

ABSTRACT

The tectonic regime in the South China Sea (SCS) and the South China had been changed by the end of Mesozoic. The tectonic pattern is assembling of terranes before Cenozoic, and is separating of terranes after Cretaceous. The general tendency of tectonic evolution in South China including northern margin of SCS and Indo-China is the southward or southeastward growth of continent due to combination of terranes or marginal accretion before Cenozoic. After Cretaceous, several terranes such as the Xisha-Zhongsha Terrain, Nansha Terrain and even, probably, a part of Borneo were separated from the South China mainland, and the South China Sea Basin (SCB) created.

The linear structure had been oriented along the NE direction before Cenozoic, and along NEE to EW direction during Cenozoic; it rotated clockwise from the former (NEE) to the latter (EW) with time. Most of fractures are compressional before Cenozoic, and extensional during Cenozoic. The later one made the sedimentary basin in northern margin of SCS, rifted the plate to make the northern Xisha Trough, and finally, with sea-floor spreading created the South China Sea Basin. The South China Sea Basin, and its three subbasins in SCB—Northwestern, Eastern and Southwestern Subbasin are all of oceanic crust. The magnetic lineation near E-W in the eastern SCB indicates two spreading episodes occurred during middle Oligocene—early Miocene, the asymmetric spreading and the symmetric spreading.

INTRODUCTION

The South China Sea as a marginal sea in western Pacific is located at the junction of the Eurasian, the Pacific and the Indian plates. The South China Sea consists of a deep-sea basin (SCB) and a terrain system (Fig.1). The SCB is divided into three subbasins which are the Northwestern Subbasin, the Eastern Subbasin and the Southwestern Subbasin. The terrain system is composed of the Nansha (Reed Bank and Dangerous Ground) Terrain, the Xisha-Zhongsha (Macclesfield Bank and Paracel Is.) Terrain and others (Jin & Ke, 1990).

A significant change of tectonic regime has been marked at the end of Mesozoic in the South China Sea and the South China. The tectonic pattern before Cenozoic is the assembling of terranes (gathering or accretion), and in Cenozoic after Cretaceous is the separating of terranes (rifting and drifting). The change of tectonic regime was demonstrated not only in the tectonic pattern but also in the orientation of linear structures. It provides a guide for fur-

* Project supported by National Natural Science Foundation of China.

ther study to trace the geological evolution of South China Sea.

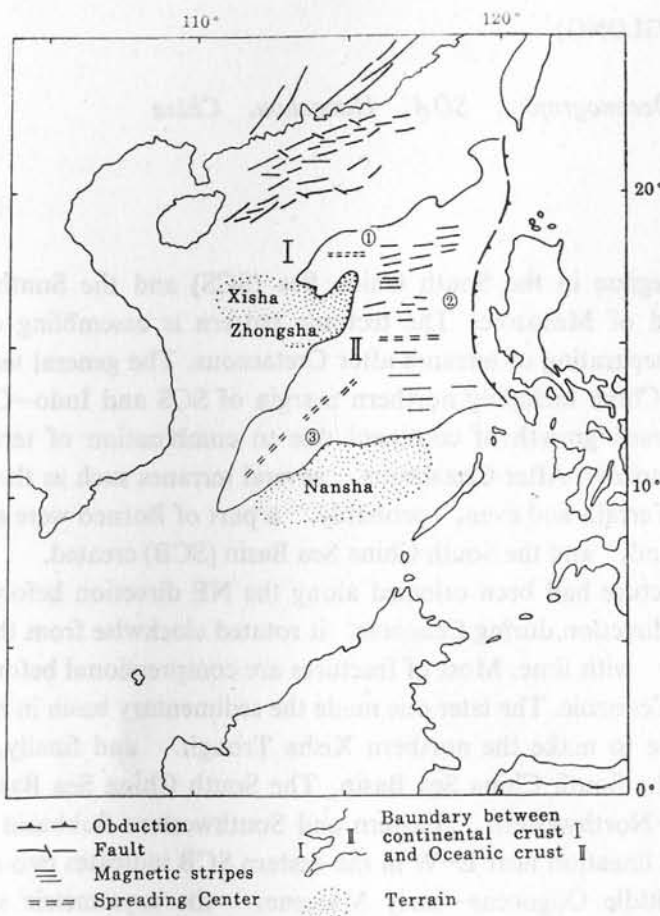


Fig.1 Tectonic setting of SCS. I. Continental crust; II. Oceanic crust: ① Northwestern Subbasin, ② Eastern Subbasin, ③ Southwestern Subbasin.

CHANGE IN TECTONIC PROCESS

Before the end of the Meozoic, the tectonic movement of lithosphere in South China Sea and Southeast China was the assembly and the accretion of plates or terrains. The small plates or terrains gradually integrated and merged into a unified plate (a part of the Eurasian Plate) (Jin & Ke, 1990). The proto-mainland in present area of the northern South China Sea and the South China mainland which had been continuously growing southward or southeastward before the Cenozoic comprised numerous collided and accreted terranes (Guo *et al.*, 1984).

The basement of the South China mainland and the northern margin of South China Sea can be divided into several tectonic provinces, such as the Caledonian province, the Hercynian province, the Yanshanian (Late Mesozoic) province and others. It displays the configuration of terrains built up in different ages and the convergence of these terrains before the Cenozoic.

The Shangda fracture zone cutting into lithosphere is an important fault system (convergence boundary) between tectonic provinces (Fig.2). The Shangda fracture zone stretching in NE-SW direction started from Shangyu of Zhejiang in north, elongated southward across Zhenhe of Fujian and Dapu of Guangdong, then branched off and extended southwestward along both the east and the west edges of Lianhuashan mountain range, through the west and the south of Hongkong, into the northern South China Sea, and reached to the east offshore of Wenchang in Hainan. The Shangda fracture zone divided the Southeast China and the northern margin of SCS into two tectonic provinces, the Caledonian province in west, the Hercynian province in east. The Caledonian province covered the most areas of Guangdong, Guangxi and Hainan Provinces, as well as the western part of northern margin in South China Sea. The Hercynian province included the southeast coastal area of Fujian, the east Guangdong province and the eastern part of northern margin in South China Sea, which consisted of Cathaysia (Huaxia old land) in basement overlaid by slightly metamorphic formation of late Paleozoic beneath late Jurassic volcanic series. The Shangda fracture zone seems to be a major suture belt in the Southeast China.



Fig.2 Shang-Da fracture zone. I. Caledonian province; II. Hercynian province.

The basic configuration in this area as the south part of the unified Eurasian plate came into being during the Indo-China movement of late Triassic by welding the Indo-China with the South China mainland along the Red River suture due to continent-continent collision.

An Andean type of continent margin presumably in the late Mesozoic has been proposed along the margin of South China and the northern margin of SCS (Taylor and Hayes, 1983; Holloway, 1982), however, the subduction zone parallel to the Andean margin is not found yet in SCS so far. Nevertheless, the tentative interpretation on existence of Andean margin is indicated by extensive distribution of the Late Mesozoic igneous rocks, the Mesozoic folding zone, and the major NE-striking compressional faults such as reverse faults and thrusts in South China and northern margin of SCS, which are thought to be made by terrain assembling or plate convergence. In fact, there is a tectonic zone of Mesozoic in the northern margin of SCS. It is a compound zone consisting of two subzones, the Yanshanian igneous zone adjacent to the coast of mainland and the Yanshanian folding zone facing the deep sea of SCS (Fig.3).

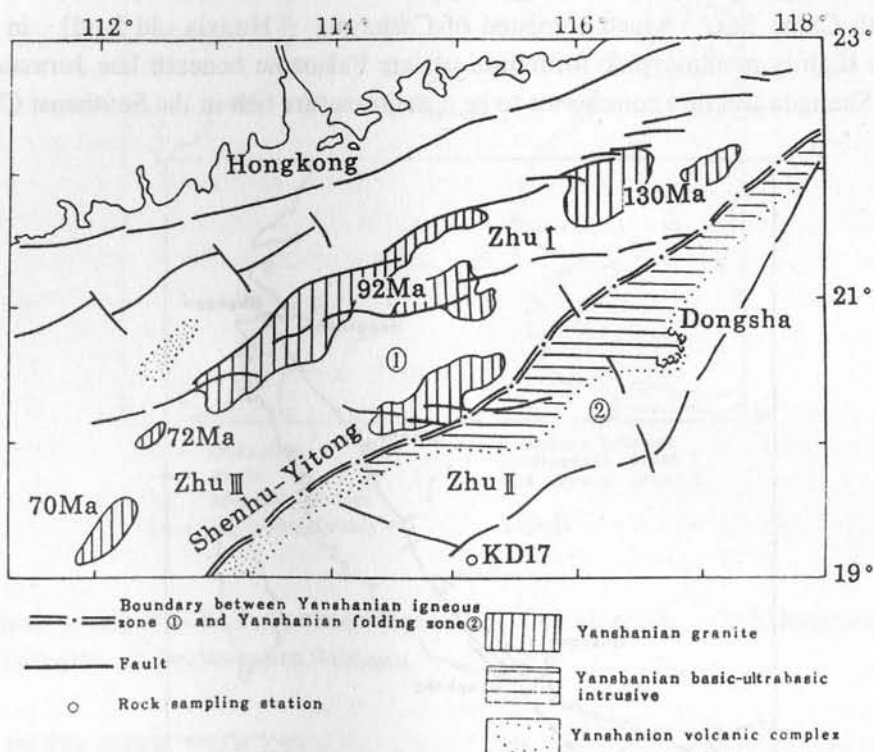


Fig.3 Mesozoic tectonic zone in northern SCS. ① Yanshanian igneous zone; ② Yanshanian folding zone. Zhu I, Zhu II and Zhu III are depressions of Zhujiang Mouth basin formed in Cenozoic. The gabbro collected from KD17 is dated of 133.95 ± 9.58 Ma (Sm/Nd).

The Yanshanian igneous zone consisted of the Late Mesozoic intermediate-acid intrusive and volcanic rocks occurred along the axes of Paleozoic structures composed of slightly metamorphic rocks. Numerous Mesozoic granites are dated in range of 70.5–130 Ma, older in east (about 92.2 Ma) and younger in west (70.5–72.9 Ma) (Yang *et al.*, 1987) (Fig.3). The Yanshanian folding zone extends along the northern margin of SCS from the Shenhu-Yitong uplift with crustal thickness of 30 km in west, across the Dongsha uplift of 29 km in crustal thickness, probably, to Beigang uplift in east near Taiwan. Dongsha-Shenhu uplift zone is composed of basic or ultrabasic rocks in its lower and

Mesozoic metamorphic rocks in its upper section with overlying sedimentary cover from Late Cretaceous to Eocene. A gabbro sample collected from station KD17 at the foot of northern continental slope of SCS during the cruise Sonne 49 was determined of 133.95 ± 9.58 Ma by Sm / Nd method (Jin *et al.*, 1989) (Fig. 3). The Mesozoic metamorphic strata of NE striking are mainly located in south of Dongsha uplift with thickness of 1.16–1.82 km, seismic velocities of 5.5–5.8 km / s, which are similar to 5.2–5.8 km / s of Mesozoic metamorphic rocks in Taiwan (Yang *et al.*, 1987). In drilling well, Tongliang No.1 of Penghu offshore of Taiwan, the Mesozoic metamorphic sandstone was found at the depth of 503.5 m; in Beigang well, there was revealed the strata containing *Ammonoidea* and *Mollusca* fauna of early Cretaceous. They are thought as a accretional margin in Yanshanian period of Late Mesozoic.

Commenced with Late Cretaceous, a drastic change in regional stress field took place in South China Sea and South China, where the regional stress changed from compressional (collision, gathering and accretion) to extensional (rifting and drifting). As mentioned above, the general tendency of pre-Cenozoic tectonic evolution in South China including northern margin of SCS and Indo-China is the southward or southeastward growth of continent due to the combination of terranes or the marginal accretion. After Cretaceous, in the south margin of South China and the northern margin of SCS has appeared the disintegration of plate due to the change of regional stress, by which the Xisha-Zhongsha Terrain and Nansha Terrain have been separated apart from the South China mainland and the South China Sea Basin has been created with time.

CHANGE IN ORIENTATION OF LINEAR STRUCTURE

The orientation of linear structures varies with time under different stress regimes. The linear structure, mainly, the fracture lineament has been oriented along the NE direction before Cenozoic, however, the dominant lineament in Cenozoic is NEE and EW direction changing from the former (NEE) to the later (EW). From view of general framework of linear structures, the arrangement (or configuration) of linear structures shows us an image of clockwise rotation in direction of structural lineament with time (Fig. 1). Most giant fracture and fold systems of pre-Cenozoic takes direction of NE in stretch of structure such as the Shangda fracture zone and others (Fig. 2). The NEE-striking faulting made the sedimentary basin in front of the Pearl River Mouth Basin—Zhujiang Mouth Basin, which has three stages of its development. The first stage is the stage of rift-valley development, the basin is controlled by NEE-striking basement faults and filled with terrigenous deposits in the rift depressions from Late Cretaceous to Late Eocene; the second stage is the stage of extensional development with the expansion of rift depressions controlled still by NEE-striking faults and led to the transition of sedimentation in basin from land facies to sea facies in Early Oligocene to Early Miocene; the third stage is the stage of subsidence, the delta and open sea appeared in the basin subsided steadily and received thick marine deposits (Su and He, 1987). It is clear that the entire process of development in Pearl River Mouth Basin is closely related to the NEE-striking fault activities.

The EW-striking faulting rifted the plate to make the northern Xisha Trough, and finally, with the sea-floor spreading created the South China Sea Basin in Oligocene to

Miocene. The magnetic lineation near E-W direction in the eastern SCB implies two episodes of the northward and southward spreading occurred during Early Oligocene—Early Miocene, the asymmetric episode of spreading indicated by NEE-striking magnetic stripes of anomaly number 11-8 (32-26 Ma, Early Oligocene - Late Oligocene) and the symmetric episode of spreading shown by EW-striking magnetic lineations of anomaly number 7-5D (26-17 Ma, Late Oligocene—end of Early Miocene). The first (asymmetric) episode only occurs in the northern part of eastern SCB, and the relict spreading axis of symmetric lineation for the second episode in eastern SCB lies along latitude 15° N. This picture of variation in orientation of magnetic stripes with time indicates the same tendency of clockwise rotation in direction of lineament (Fig.1).

As to the magnetic pattern of probable NE striking existed in the Southwestern Subbasin, it is possible to represent a NW-SE spreading and has yet to be deliberated further on account of insufficient investigation. They are three possible interpretations for its age derived from a comparison of the observed magnetic profiles with the theoretical profile from model computation and with the synthesized magnetic polarity scale: 1. Late Cretaceous - Early Tertiary (anomalies 32-27, 70-63 Ma), 2. Early Miocene (anomalies 6-5c, 20-16 Ma), and 3. Pliocene-Pleistocene (anomalies 5-1, 8 Ma-recent). It is preferred to choose the second one rather than others due to more rough relief, higher heat flow and thinner sedimentary cover on basaltic basement in SW Subbasin. In any case, it remains to be resolved the ambiguity in striking and timing of magnetic stripes in SW Subbasin.

CONCLUSION

It is shown by above-mentioned discussion that the Eurasian continent was grown and expanded southeastward before Cenozoic owing to the assembling of plates or terrains by collision, welding and accretion. However, the southeast part of the Eurasian continent—proto-mainland of South China formed before Cenozoic has been collapsed, decomposed into several terrains scattered in SCS, and the South China Sea (deep-sea) Basin has been created by rifting, drifting and spreading since Late Cretaceous due to the drastic change in regional stress field from compressional to extensional at the end of Mesozoic. The elongated orientation of major structures (convergent juncture and divergent zone) has rotated clockwise with time.

As described by McKenzie stretching model (1978), the geodynamic process of basin development in the marginal basins has been presumed to have close relation to the thermal event represented by the magmatic activities. The rifting and spreading are related to the heating of lithosphere, and the subsidence is always connected with the cooling of lithosphere heated. It is notable the oceanward migration of magmatism or heat front with time in area studied. The pattern of magmatism prior to Late Cretaceous is penetrated far into the continental interior of South China, and the igneous rocks dated of 120-190 Ma are widespread on the South China mainland. The igneous rocks of age younger than 100-130 Ma (Late Yanshanian period) are almost absent inland and merely spotted along the coastal zone of northern South China Sea. The andesite and granite dated of 98-51 Ma (Late Cretaceous to Paleocene) are found in drilling well from the Pearl River Mouth Basin on northern shelf of

SCS. The basalt samples collected from seamounts of South China Sea (deep-sea) Basin are dated in range from Middle Miocene (14.1 Ma) to Late Pliocene (3.49 Ma) (Jin *et al.*, 1989). With relation to the migration of heat front, the age of basin becomes younger and younger oceanward. The sedimentary basins on landmass of South China such as Sanshui Basin and others were formed during Late Cretaceous to Eocene; the Zhujiang Mouth (Pearl River Mouth) Basin was settled down in Late Cretaceous to Late Eocene and developed in Early Oligocene to Early Miocene; as to the SCB (deep-sea basin) with oceanic crust, it was formed in Early Oligocene to Early Miocene.

There are two kinds of crust, continental and oceanic in South China Sea. On continental margin, the Zhujiang Mouth Basin and the northern trough of Xisha were formed on the base of continental crust, and the trough could be a rifted channel, but failed in spreading, which connected with Northwestern Subbasin in east, and penetrated into continental margin in west, its crust beneath could be third one, transitional. There are several terranes and deep-sea subbasins distributed in South China Sea. The terranes with continental crust seem to be the collapsed fragments of continent in South China Sea, which are the Xisha-Zhongsha Terrain, the Nansha Terrain and others. The South China Sea Basin created by the seafloor spreading has been divided into three deep-sea subbasins—Northwestern, Eastern and Southwestern. Three subbasins in South China Sea are all oceanic in their nature of crust. The Northwestern Subbasin is older than the Eastern Subbasin, and the Southwestern Subbasin is indeterminate in age so far for now, but probably, younger.

REFERENCES

- Guo Linzhi, Shi Yangshen, Ma Ruishi, Ye Shenfu & Lu Huafu, 1984: Tectonostratigraphic terranes of Southeast China. *Jour. of Nanjing Univ, Natural Sciences (ed.)*, 20 (4), 732-739 (in Chinese).
- Holloway, N.H., 1982: North Palawan block, Philippines—Its relation to Asian mainland and role in revolution of South China Sea. *Bull. AAPG*, 66 (9), 1355-1383.
- Jin Xianglong & Ke Changzhi, 1990: Geophysical features and geological evolution of the South China Sea. *Asian Marine Geology*, 147-155, China Ocean Press, Beijing.
- Jin Xianglong *et al.*, 1989: Report on study of geosciences in South China Sea. *Donghai Marine Science*, 7 (4), 1-92 (in Chinese).
- McKenzie, D., 1978: Some remarks on the development of sedimentary basins. *Earth and Planetary Sciences Letters*, 40 (1), 25-32.
- Su Nairong and He Zhonglin, 1987: The characteristics of fault activities in the Pearl River Mouth Basin and their control of hydrocarbons. *Proceedings of Symposium on Petroleum Geology of Northern Shelf in South China Sea, Part 1*, 191-216.
- Taylor, B. and D.E. Hayes, 1983: Origin and history of the South China Sea Basin. *Tectonic and Geologic Evolution of Southeast Asian Seas and Islands, Part 2, AGU Geophysical Monograph*, 27, 23-56.
- Yang Shukan, Liu Zhaoshu, Chen Senqiang, Zhou Yan, Zhang Yixiang and Chen Hanzhong, 1987: Basement structure and evolution of Pearl River Mouth Basin. *Proceedings of Symposium on Petroleum Geology of Northern Shelf in South China Sea, Part 1*, 250-272.

MORPHOSTRUCTURAL ANALYSIS OF THE CENTRAL RIDGE IN SOUTH CHINA SEA

GUY PAUTOT

Ifremer Centre de Brest, Géosciences Marines, B.P. 70, 29263 Plouzané cédex, France

INTRODUCTION

The South China Sea (SCS) is a complex marginal oceanic basin created by rifting of the Chinese mainland during Paleogene time (Fig. 1). This basin is presently subducting eastward along the Manila Trench active until Late Tertiary time. To the north, the Chinese continental margin is a passive margin with a general NE-SW trend. The western limit of the basin is a NS straight limit along a hypothetical fault bordering to the east the Indo-China peninsula. To the south, the rifted continental block which includes North Palawan, Reed Bank and Dangerous Grounds, is the foreland of an island arc terrane (Cagayan Ridge) and Palawan Trough is generally interpreted as a relict subduction zone. Thus this rhombic shape of the basin exhibits quite different geodynamic fringes.

All the features of the SCS basin are in direct relationship with the geological behavior of the central oceanic ridge. We studied the crest and the flanks of this extinct ridge to understand the last phases of the ridge work and to obtain constraints to determine the geodynamical models of opening of this basin (Fig. 1).

DATA ACQUIRED

The Nanhai cruise was devoted to a study of the axial ridge of the South China Sea basin, between 113° E and 119° E (Fig. 1). It was the first cruise in this area to record both multibeam (Seabeam) and continuous single channel seismic data. The simultaneous deployment of these devices permits an accurate morphostructural analysis of the seafloor. To take advantage of the Seabeam's resolution, we focused the profiles on the central part of the basin, where the ridge is not buried by thick sediments (< 1000 m thick). Off ridge, the sediments are thicker (1000–2500 m), and tend to smooth the scarps, making morphologic analysis more difficult. A total of 74 profiles were obtained spaced along the 1000 km long axial ridge.

In addition to the seismic and Seabeam observations, gravity and magnetic profiles were also recorded, providing information on the age and evolution of the oceanic crust.

In complement to this cruise, Seabeam data were acquired by other French cruises on the Manila area and Indo-Chinese margin. Some additional multibeam profiles were carried out by R.V. Sonne. All these data were used to establish a more sophisticated morphological map of the central part of the SCS (Fig. 2).

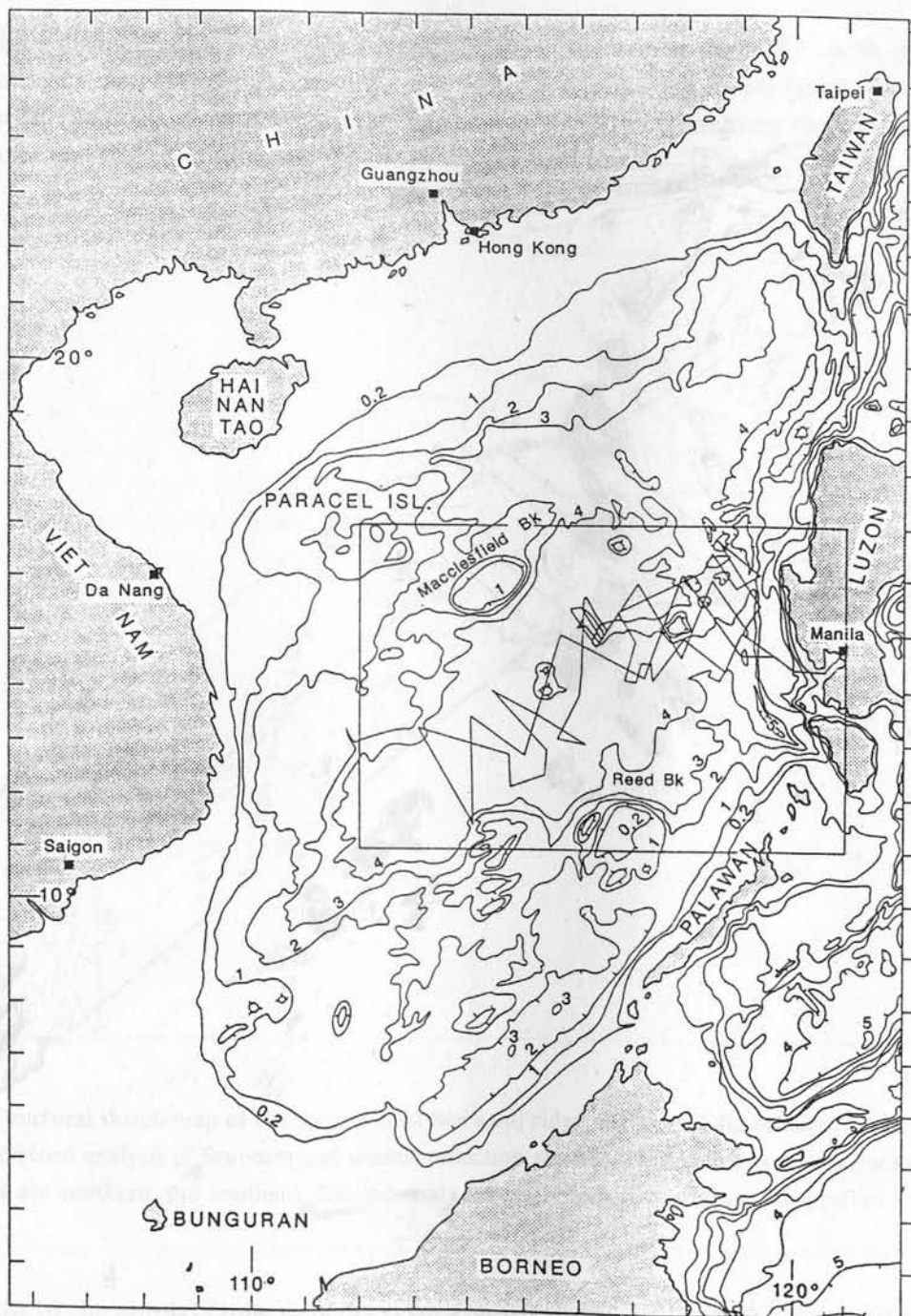


Fig.1 Schematic bathymetric map of the South China Sea showing, in the central part, the ship tracks of the R.V. Jean-Charcot during Nanhai cruise.

MORPHOSTRUCTURAL ANALYSIS OF THE CENTRAL RIDGE IN SOUTH CHINA SEA

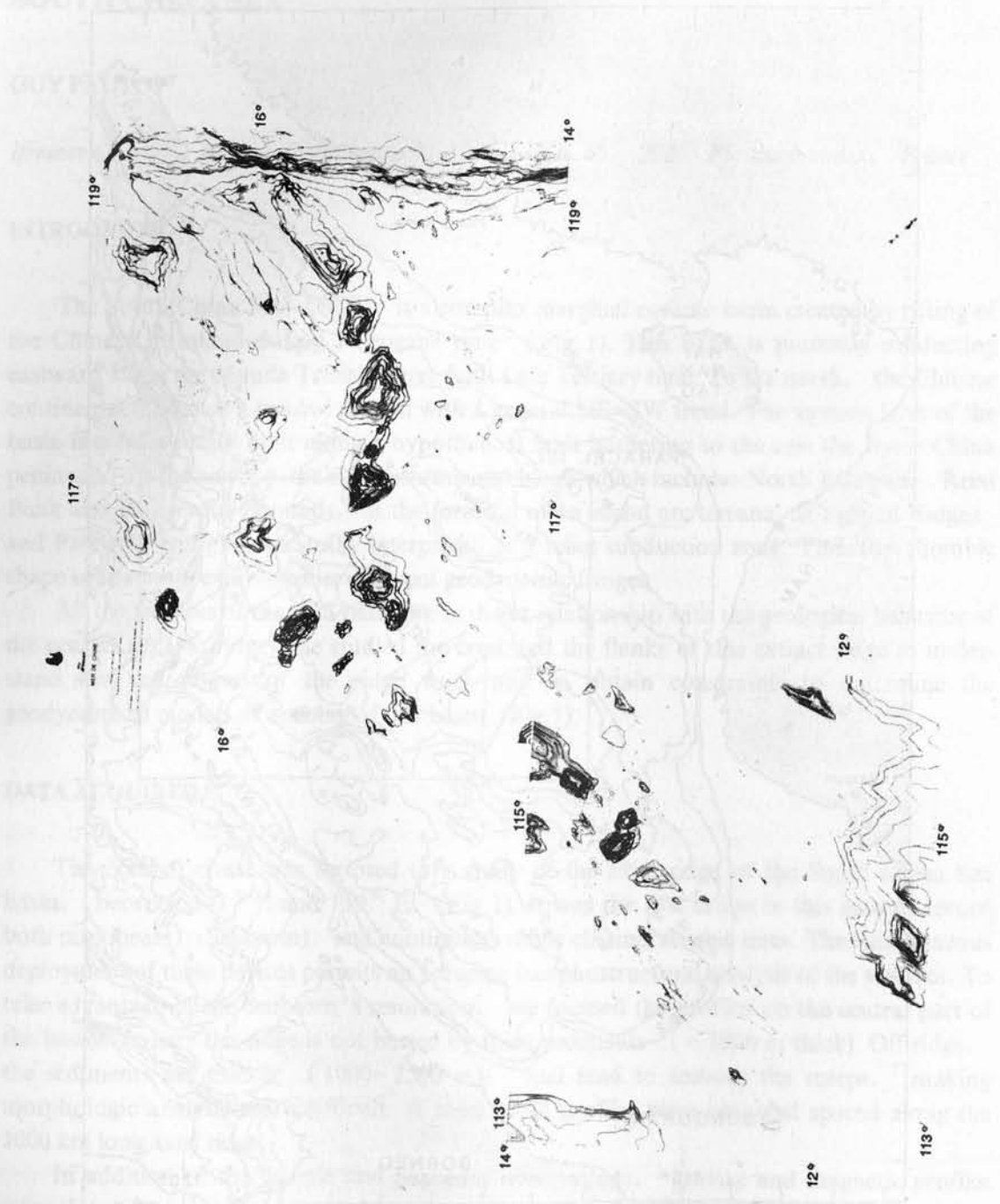


Fig. 2 New morphological map of the central South China Sea drawn from additional Seabeam data (R.V. Jean-Charcot and Sonne).

BATHYMETRY AND STRUCTURE OF THE SOUTH CHINA SEA AXIAL RIDGE

Three distinct sections have been identified along the axis of the SCS, with their own morphological and structural signature: SW and NE sections are simple linear features that bracket the complex seamount-ridden central section. After presenting the characteristics common to all three sections, we describe each one individually (Fig.3).

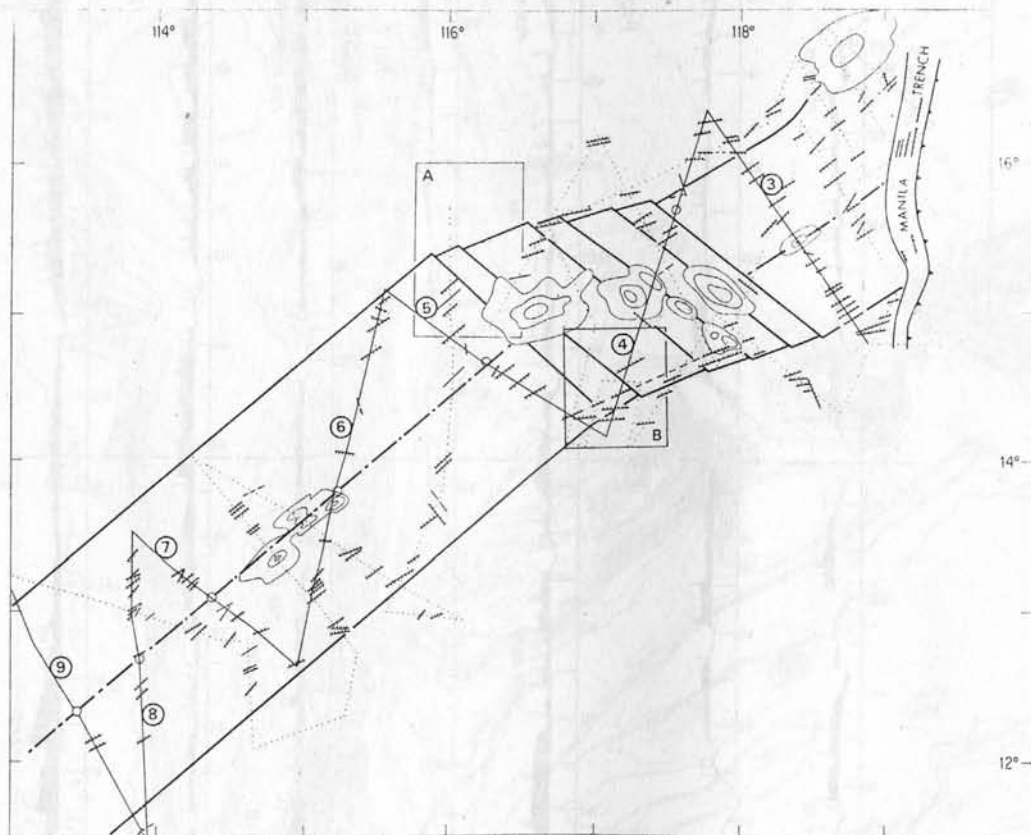


Fig.3 Structural sketch map of the South China Sea axial ridge. Strike and dip of major faults derived from combined analysis of Seabeam and seismic reflection records. Dotted lines are ship tracks. Boxes A and B are northern and southern detailed study areas. Numbers correspond to profiles shown in Fig.4.

Most of the normal faults near the ridge axis trend $N60^{\circ}E$ to $N50^{\circ}E$, while off the axis some scarps clearly trend $N80^{\circ}E$ to $N85^{\circ}E$. Most of these scarps are imaged on seismic profiles as normal faults bounding outward tilted blocks. Horst and graben structures are also observed (profiles 5 and 7 in Fig.4). The relict spreading center is generally characterized by an axial graben (profiles 5, 7 and 8 in Fig.4) locally invaded by postspreading seamounts (profile 3 in Fig.4).

Sediments are irregularly distributed along the extinct spreading center. Average sediment thickness increases from 500 m in the northeast, near the ridge, to 1000–1500 m

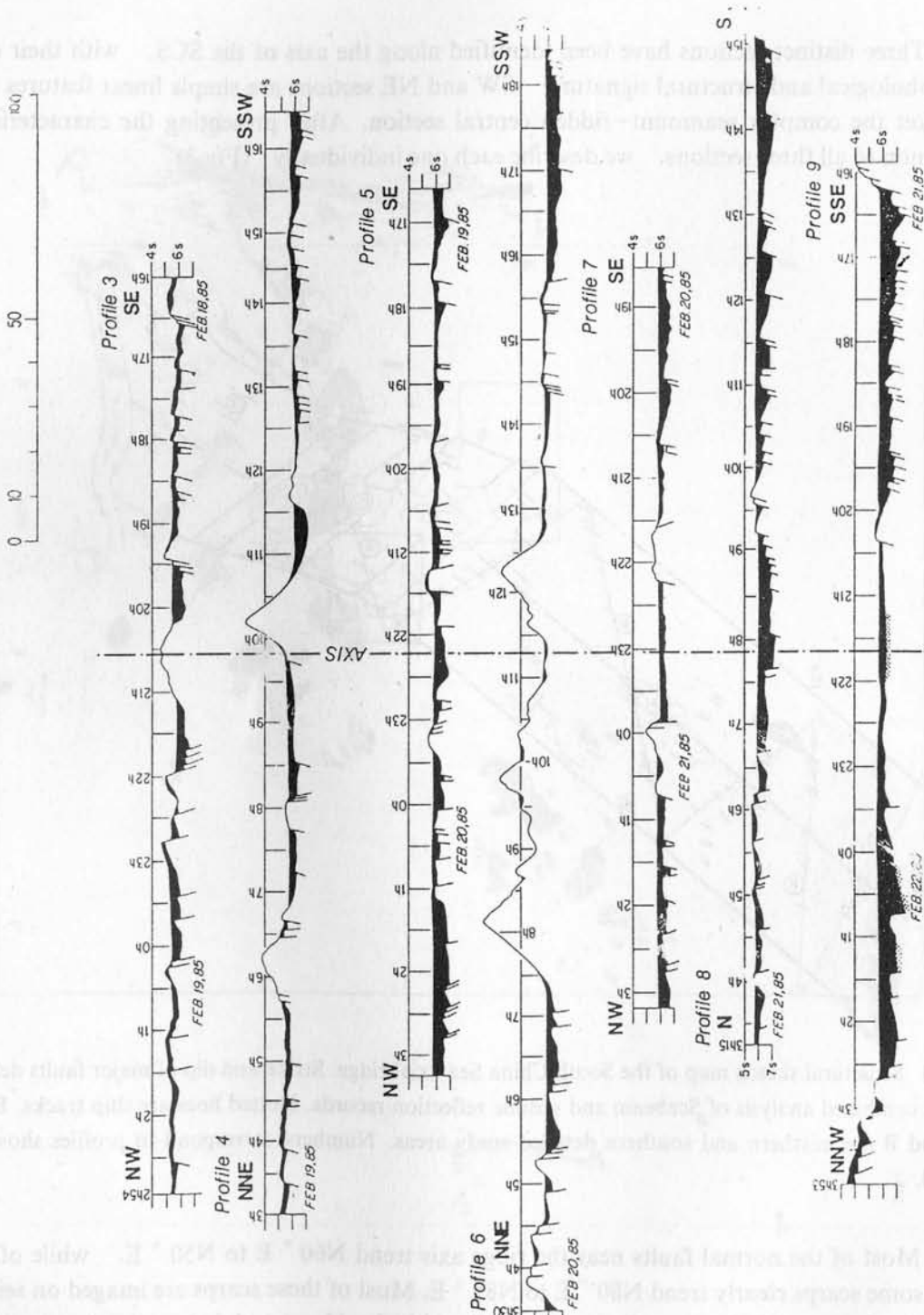


Fig.4 Interpreted single channel seismic profiles across the axial ridge. Sediments covering acoustic basement are shown in black. Vertical scales in seconds (two way travel time). Position of each profile is shown in Fig.3.

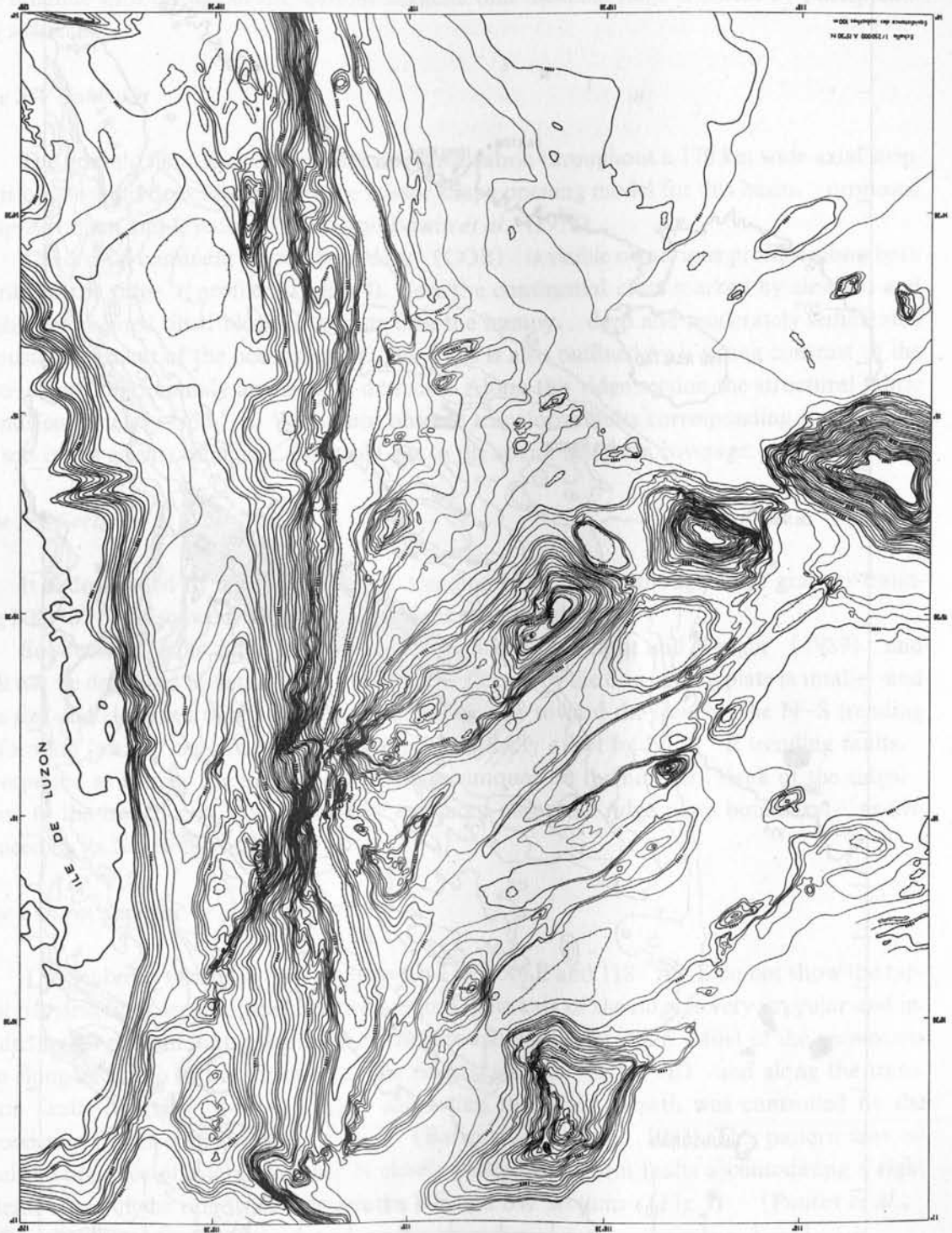


Fig. 5 Detailed bathymetric map of the eastern part of the ridge entering in subduction in Manila Trench.

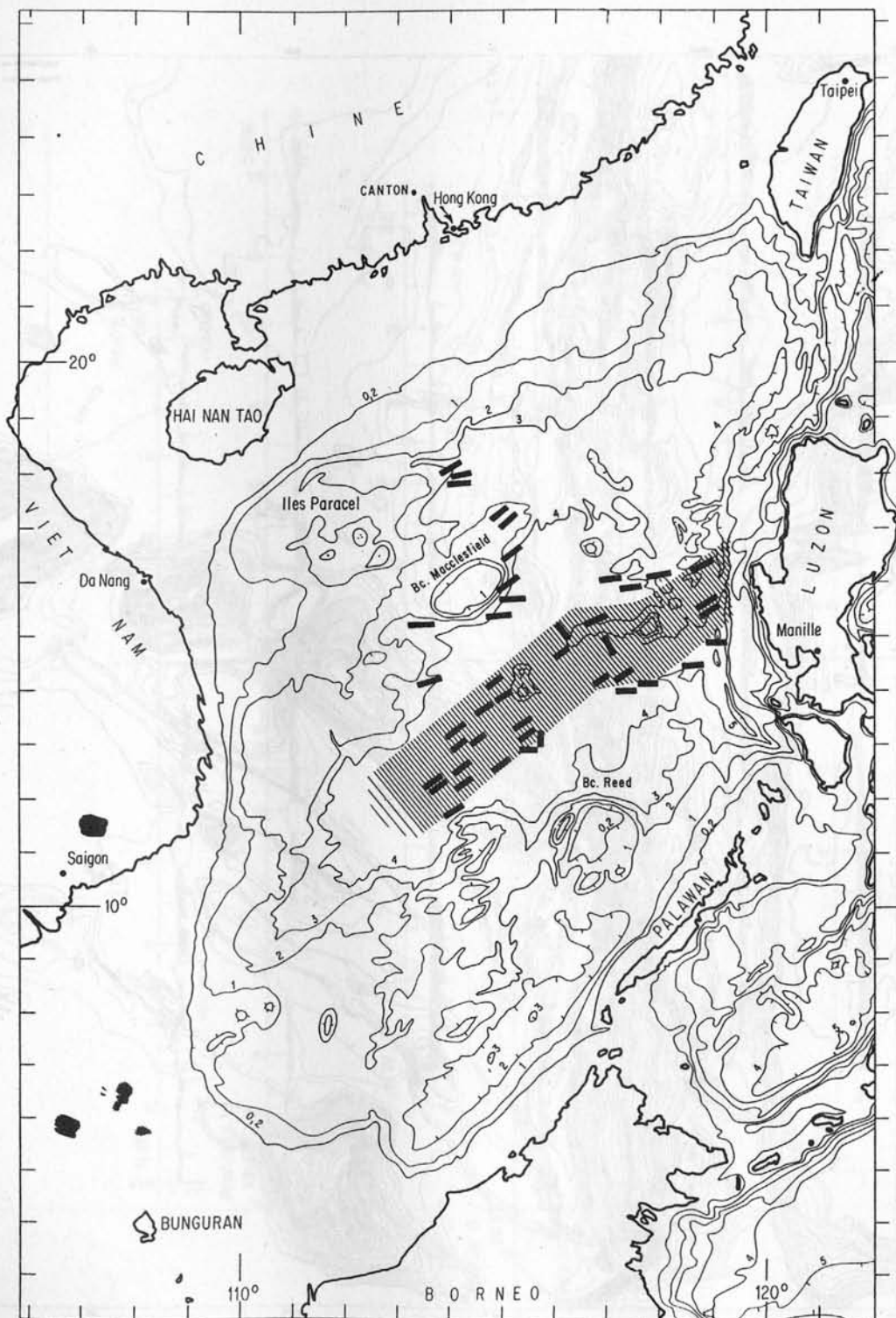


Fig.6 Heavy black lines indicate main structural directions on the extinct ridge (Nanhai cruise) and around the Macclesfield Bank (Sonne cruise).

toward the southwestern abyssal plain. The absence of a noticeable variation of the depth of the mudline with the age of the seafloor suggests that the axial ridge is buried by postspreading sediments.

The SW Subbasin

The oceanic floor shows essentially the same fabric throughout a 170 km wide axial strip. This observation does not support the scissor shape opening model for this basin, proposed Ben-Avraham and Uyeda (1973) and Bowin *et al.* (1978).

The crustal continent-ocean boundary (COB) is visible on various profiles along both flanks of the ridge (profile 9 in Fig.4). Here the continental crust marked by elevated and highly sedimented tilted blocks contrasts with the bumpy, deep and moderately sedimented acoustic basement of the oceanic crust. The COB is also outlined by a strong contrast of the free-air gravity anomaly across both domains. Along this ridge section the structural fabric trends consistently N55° E. We do not observe transform faults corresponding to the small offsets in the gravity minima, probably due to the sparse Seabeam coverage.

The NE Section

It is dominated by a structural fabric trending N50° E, although some grabens trending N80–85° E also occur along the outer flanks of the ridge.

Subduction of the ridge was previously described by Pautot and Rangin (1989) and will not be described in detail here (Fig.5). The flexure of the downgoing plate is small, and the size and elevation of the axial seamounts decrease toward the trench. The N–S trending deforming front of the accretionary prism is vertically offset by N130° E trending faults, interpreted as former fracture zones. A large seamount on the northern flank of the ridge, close to the trench axis, was probably emplaced along the ridge jump boundary, as evidenced by its NE elongation.

The Central Section

The Seabeam swaths in the area between 115° 50' E and 118° 45' E do not show the typical rift structures seen in the other two sections. The axis of the ridge is very irregular and invaded by large seamounts forming the Scarborough seamount chain. Most of the seamounts are elongated both in the direction of the ridge segments (N50° E) and along the transform faults direction (N140° E), suggesting that their growth was controlled by the preexisting fractures in the oceanic crust (Batiza and Vanko, 1983). This pattern may reveal the presence of a large number of closely spaced transform faults accommodating a right lateral offset of the ridge axis between the NE and SW sections (Fig.3) (Pautot *et al.*, 1986; Briais *et al.*, 1989).

CONCLUSIONS

The Seabeam and geophysical survey conducted at the SCS ridge axis answers several

all along the central part of the axial ridge. Additional rift structures oriented N70–N80° E were also detected along both edges of the surveyed area, suggesting a spreading reorganization (Fig.6).

Difficulties arise when we try to accommodate the N50–N60° E trend of the axial ridge structures with our observations of N80° E structures and the E–W trending magnetic anomalies (11 to 6a) of the eastern oceanic basin (Taylor and Hayes, 1980, 1983).

To reconcile the orientation of the magnetic lineations and the structural observations is to suggest that the direction of spreading rotated 20° or 30° counterclockwise about 20 Ma B. P. (Fig. 7). This is documented along the southeastern flank of the ridge where closely-spaced profiles show N80° E trending structures changing to N60° E toward the axis, and on the northern flank of the northeastern ridge section (Fig.6). The stretched continental margins of the basin are affected by both E–W and NE–SW trending normal faults. These two extensional directions are also inferred in the oceanic crust, with related transform faults.

The interpretation implies a change in the direction of spreading, which might be related to a significant kinematic reorganization around 20 Ma. According to this hypothesis, the oldest oceanic crust (32–20 Ma) is limited to the eastern part of the basin, where E–W magnetic anomalies are offset by probable N–S trending transform faults. It was created during the Oligo–Miocene spreading stage in the South China Sea, related to a general E–W spreading event, which also occurred to the north, in the Japan Sea and the Yellow Sea (Jolivet, 1986). The most recent oceanic crust trends NE–SW all across the basin, parallel to the Palawan Trench, and is dissected N140° E transform faults.

REFERENCES

- Batiza, R. and D. Vanko, 1983: Volcanic development of small oceanic central volcanoes on the flank of the East Pacific Rise inferred from narrow beam echo sounder survey. *Mar. Geol.*, 54, 53–90.
- Ben Avraham, Z. and S. Uyeda, 1973: The evolution of the China basin and the Mesozoic paleogeography of Borneo. *Earth Planet. Sci. Lett.*, 18, 365–376.
- Bowin, C., R. Lu, C. Lee and H. Schouten, 1978: Plate convergence and accretion in the Taiwan Luzon region. *Am. Ass. Petrol. Geol. Bull.*, 62, 1645–1672.
- Briaux, A., P. Tapponnier and G. Pautot, 1989: Constraints of Seabeam data on crustal fabrics and seafloor spreading in the South China Sea. *Earth Planet. Sci. Lett.*, 95, 3/4, 307–321.
- Hékinian, R. *et al.*, 1989: Volcanics from the South China Sea ridge system. *Oceanologica Acta*, 12, 2, 101–115.
- Jolivet, L., 1986: America–Eurasia plate boundary in eastern Asia and the opening of marginal basins. *Earth Planet. Sci. Lett.*, 81, 282–288.
- Pautot, G. *et al.*, 1986: Spreading direction in the central South China Sea. *Nature*, 321, 150–154.
- Pautot, G. and C. Rangin, 1989: Subduction of the South China Sea axial ridge below Luzon (Philippines): Underplating process along an oblique convergent margin. *Earth Planet. Sci. Lett.*, 92, 57–69.
- Taylor, B. and D.E. Hayes, 1980: The tectonic evolution of the South China Sea. *The Tectonic*

and Geologic Evolution of Southeast Asian Seas and Islands, D.E. Hayes (ed.), Geophys. Monogr. Am. Geophys. Un., 23, 89-104, Washington, D.C..

Taylor, B. and D.E. Hayes, 1983: Origin and history of the South China basin. The Tectonic and Geologic Evolution of Southeast Asian Seas and Islands, Part 2, D.E. Hayes (ed.), Geophys. Monogr. Am. Geophys. Un., 27, 23-56, Washington, D.C..

The interpretation implies a change in the direction of spreading, which might be related to a significant tectonic reorganization around 20 Ma. According to this hypothesis, the oldest oceanic crust (135-10 Ma) is related to the eastern part of the basin, where N-W magmatic arc-related activity probably N-S trending transform faults. It was created during the Indo-Malayan spreading stage in the South China Sea, related to a general N-W spreading event, which was coeval to the north, in the Japan Sea and the Yellow Sea (Joliver, 1988). The oldest oceanic crust from trends NE-SW all across the basin, parallel to the Palawan Trench, and is discussed (1400° E transform fault).

REFERENCES

Barber, R. and D. Yarnik, 1981: Volcanic development of small oceanic island volcanoes on the east of the East Pacific Rise inferred from magnetic anomalies. Mar. Geol., 24, 23-36.

Chen, X. and B. Uchida, 1981: The evolution of the South China basin and the Meso-Cenozoic paleogeographic reconstruction. Mar. Geol., 24, 103-117.

Chen, C. R. and C. H. Chen, 1981: Plate tectonics and evolution in the Taiwan region. Am. J. Sci., 279, 1045-1072.

Chen, A. T., T. T. Chen, and C. H. Chen, 1982: Evolution of the South China Sea and a tectonic spreading model. Earth Planet. Sci. Lett., 57, 307-321.

Chen, R. W. and J. W. Chen, 1989: Volcanic tectonic South China Sea region. Oceanologica Acta, 11, 1-10.

Joliver, L. 1988: Kinematics of the East Pacific Rise and the opening of marginal basins. Earth Planet. Sci. Lett., 88, 23-36.

Patton, C. W. 1971: Tectonic evolution in the central South China Sea. Nature, 231, 130-134.

Patton, C. W. and C. R. Scotese, 1983: Evolution of the South China Sea and the East Pacific Rise. Tectonophysics, 103, 1-10.

Patton, C. W. and C. R. Scotese, 1983: Evolution of the South China Sea and the East Pacific Rise. Tectonophysics, 103, 1-10.

Patton, C. W. and C. R. Scotese, 1983: Evolution of the South China Sea and the East Pacific Rise. Tectonophysics, 103, 1-10.

SEISMIC STRATIGRAPHY AND HOLOCENE SEDIMENTATION AT THE NORTHERN MARGIN OF THE SOUTH CHINA SEA

CHRISTOPH GAEDICKE¹⁾, HOW KIN WONG²⁾ & YUANBO LIANG³⁾

- 1) *Fachbereich Geowissenschaften, Universität Bremen, P.O. Box 33 04 40, D-2800 Bremen 33, Germany. Formerly at the Institut für Biogeochemie und Meereschemie, Universität Hamburg, Bundesstraße 55, D-2000 Hamburg 13, Germany*
- 2) *Institut für Biogeochemie und Meereschemie, Universität Hamburg, Bundesstraße 55, D-2000 Hamburg 13, Germany*
- 3) *South China Sea Institute of Oceanology, Academia Sinica, 164 West Xingang Road, Guangzhou 510301, China*

ABSTRACT

Four distinct seismic sequences each having its own seismic facies characteristics have been recognized at the northern continental margin of the South China Sea south of Hong Kong. The basement sequence undergoes an abrupt change in seismic facies at the ocean-continent boundary. The Paleocene to Lower Oligocene syn-rift sequence is separated from the Oligocene to Miocene syn-drift sequence by the regionally mappable unconformity T_6 . The latter is in turn separated from the overlying post-drift sequence by the unconformity T_2 .

Relative sea level changes have led to a multiphase progradation and erosional truncation of the shelfbreak, resulting in three distinct, seaward-tilting clinoforms.

The continental margin may be divided into three sedimentary provinces which correlate with the physiographic provinces. The continental shelf and uppermost slope is characterized by non-deposition or erosion, the slope proper by sediment mass wasting, and the deep sea by pelagic or turbiditic sedimentation.

INTRODUCTION

The South China Sea is a Cenozoic, Atlantic-type marginal sea of the western Pacific (Pautot *et al.*, 1986; Taylor & Hayes, 1980, 1983). It is bordered to the north, west and south by passive continental margins underlain by continental crust and to the east by the eastward-dipping subduction zone of the Manila Trench (Katili, 1981). The abyssal central basin is over 4000 m deep and consists of oceanic crust.

The structural evolution of the South China Sea has been the subject of many intensive studies during the past decade (Taylor & Hayes, 1980, 1983; Pautot *et al.*, 1986; Fontaine & Mainguy, 1985; Guo & Lin, 1982; Hayes, 1985; Wu, 1985a & b; Hinz & Schluter, 1985; Ru & Pigott, 1986; Scsio, 1982-1985). Although other opinions exist, it is generally accepted that in the Late Mesozoic, extensive stretching and thinning of the continental crust under China and Borneo took place as a result of sustained subduction at the western margin of the Pacific. Arkosic, terrigenous sediments were depos-

ited in the evolving continental basins. Crustal thinning culminated in a phase of seafloor spreading from the Lower Oligocene to the Lower Miocene (magnetic anomalies 11 to 5D) with the formation of the present-day South China Sea as a backarc basin (He, 1988; Jin, 1989; Li, 1988; *op. cit.*). The drift-onset event (Brice *et al.*, 1982) is marked by a regional unconformity (T_6). During the drift phase, northern Palawan and microcontinents such as Dangerous Grounds, Reed Bank and Macclesfield Bank migrated away from the Chinese mainland (Holloway, 1982; Hinz & Schluter, 1985). On the continental margin, organic-rich kaolinitic sediments became deposited as the Zhuhai Formation (Table 1), while the overlying Zhujiang Formation consists of non-marine coastal mudstones and siltstones. The dolomitic sandstone intercalations are associated with marine transgressions (Jin *et al.*, 1984, 1986). Evolution of the Zhujiang delta started in the Lower Miocene as seafloor spreading terminated (regional unconformity T_2) and the depo-environment changed from a half-enclosed sea to open marine conditions. Sustained thermal subsidence led to a rapid growth of the prograding delta and the step-like continental margin off southern China. The Hanjiang, Yuehai and Wanshan formations comprise largely of coarse clastics, while reef buildups are found on distal banks.

Table 1 The chronostratigraphy, depositional environment and major tectonic events of the Pearl River Mouth Basin. Compiled from and modified after Haq *et al.* (1987), Jin *et al.* (1984), Taylor & Hayes (1983), Holloway (1982) and Guo & Lin (1982).

Time Series	Age (ma)	Magnetic Anomaly	Zhujiang Formation	Depositional Environment	Major Tectonic Events
Quaternary			Quaternary	neritic	
	1.55				
Pliocene			Wanshan	open sea	subsidence of continental margins
	5.2				
Upper			Yuehai	littoral	
	10.2				
Mid-Miocene			Hanjiang	transitional	
	16.2				
	17				T_2
Lower		5D 5E 6A-6C 7-8	Zhujiang	half-enclosed sea	sea-floor spreading in the South China Sea
	25.2	9			
Oligocene		10 11	Zhuhai	continental river-lake	T_6
	32				
	36				
Eocene				varying	rifting
	54			greatly (mainly continental)	(stretching, faulting, subsidence)
Paleocene					
	66.5				
Cretaceous					
	131				Yenshanian Orogeny
Jurassic					
	210				

During cruise 50 of the German R/V Sonne from July to September, 1987, about 86000 km² of the shelf, slope and deep sea provinces off the mouth of the Zhujiang (Pearl River) was studied using geophysical, sedimentological, geochemical and hydrochemical means. The geophysical work consisted of 1465 km of seismic reflection profiling (Fig.1), whereby a Prakla Seismos VLF air gun with a maximum chamber volume of 2.51 and a Bolt Par 600 air gun with a volume of 0.441 were used as the sound source. The receiver was a Prakla Seismos streamer array with 8 active sections, each having 10 hydrophones connected in parallel. High resolution profiling with a hull-mounted ORE pinger transducer energized at a frequency of 3.5 kHz was conducted simultaneously to better define the structure of the topmost several tens of meters of the sedimentary column. Navigation was carried out using the ship's GPS and Magnavox satellite navigation systems.

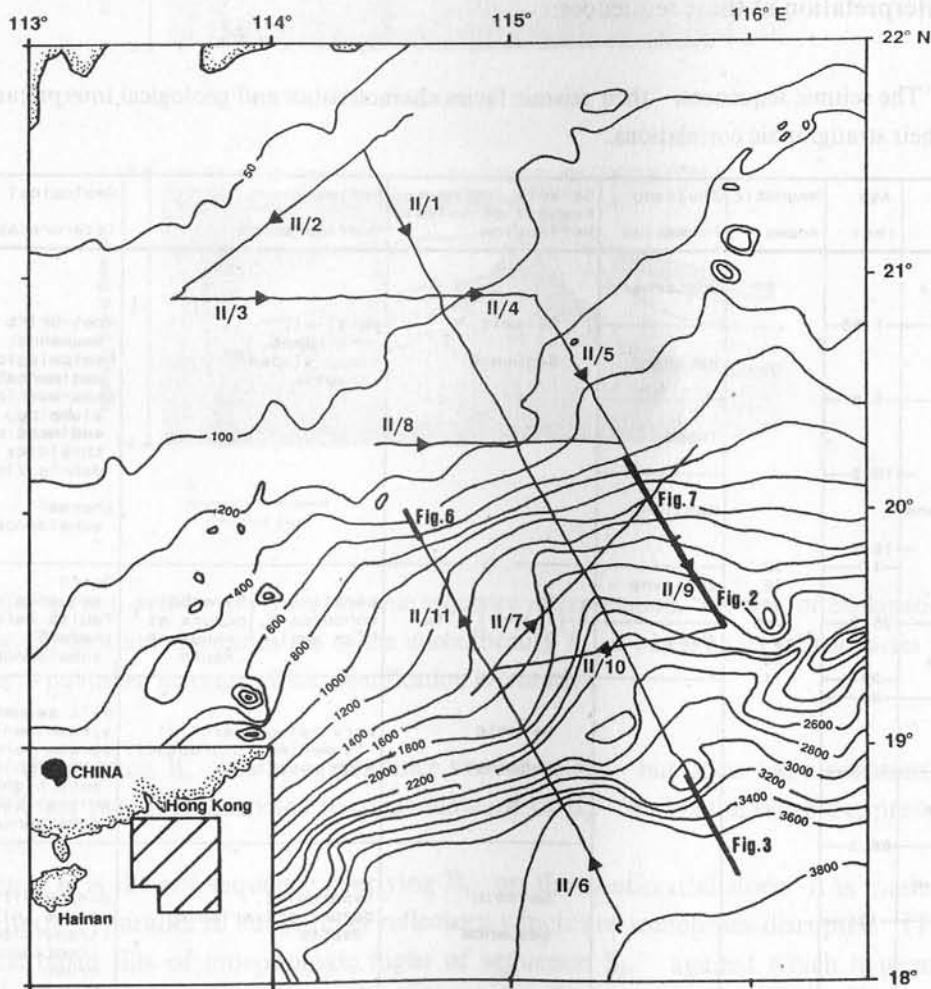


Fig.1 Chart showing the location of the reflection seismic lines. Profiles presented in this paper are marked by thick lines and by the corresponding figure numbers. The isobaths are in meters.

In this paper, we report the results of reflection seismic profiling. Three questions will be addressed. These are: 1. How did the northern continental margin of the South China Sea evolve structurally since its opening as a backarc basin? 2. How did sea level changes af-

fect the processes of sedimentation at the shelfbreak? and 3. Which recent sedimentation processes can be distinguished on the continental shelf, the continental slope and in the deep sea?

SEISMIC STRATIGRAPHY

At the deep northern continental margin of the South China Sea south of Hong Kong, four seismic sequences each having its own seismic facies characteristics have been recognized (Table 2). Correlations with other seismic data (e.g. Taylor & Hayes, 1980; 1983) and with published data on wells drilled into the Zhujiang Mouth Basin (Jin *et al.*, 1984, 1986; Liang & Liu, 1990) have made possible a stratigraphic, tectonic and sedimentary facies interpretation of these sequences:

Table 2 The seismic sequences, their seismic facies characteristics and geological interpretations, as well as their stratigraphic correlations.

Time Series	Age (ma)	Magnetic Anomaly	Zhujiang Formation	Seismic Sequence; Key Bed of Seismic Reflection	Reflection Configuration	Geological Interpretation
Quaternary			Quaternary	Seismic Sequence P	parallel, concordant, steep slopes-chaotic	Post-Drift sequence; hemipelagic sedimentation, mass-wasting: slumping, sediment creep, turbidity currents, debris flow
Pliocene	1.55		Wanshan			
Upper	5.2		Yuehai			
Mid-Miocene	10.2		Hanjiang			
Lower	16.2		Zhujiang			
Oligocene	17	5D	Zhuhai	D (T ₄) D	parallel, concordant, high ampl. hyperbolic, occurs at constant depth	Drift sequence; faults rare, thermal subsidence
	25.2	6A-6C				
	32	7-8				
	36	9				
Eocene				Seismic Sequence R	parallel-subparallel (sometimes disrupted), high amplitude	Rift sequence; synsedimentary faults strata terminate updip-onlap at basement highs, initial tectonic subsidence
Paleocene	54					
Cretaceous	66.5					
Jurassic	131			Seismic Sequence B _t	hyperbolic, occurs at variable depths	during Rift-/Drift stage thinned transitional (continental) crust
	210					

Sequence B (the acoustic basement) is strongly reflecting with a hyperbolic internal configuration. It occurs in two facies subunits:

(I) the subunit B_t which is the oldest seismic sequence mapped. It occurs at varying depths, ranging from 80 ms two-way travel time (twt) to over 1.2 s in basins of the continental slope (Fig. 2). The southernmost limit of B_t is a line oriented almost east-west at

18° 50' N. This line coincides with the seaward boundary of the continental slope and represents thinned continental crust.

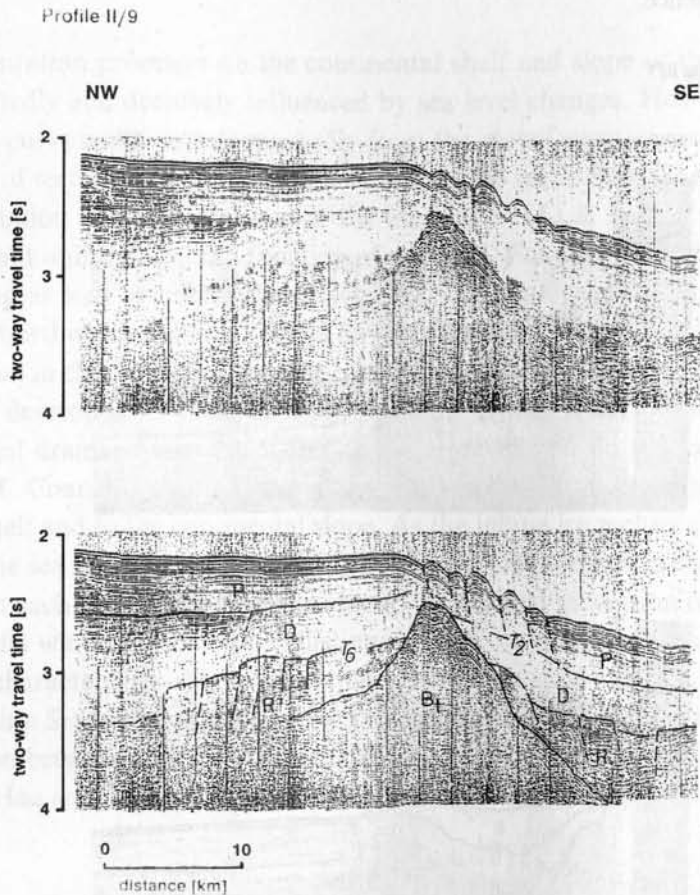


Fig.2 Part of air gun profile II / 9 and seismic sequence interpretation. See text for explanation and Fig.1 for profile location. Identification of the unconformity T_6 is based on its seismic facies and on correlations to published literature. This identification is tentative.

(II) the subunit B_0 has an appearance similar to B_1 , but occurs at a constant depth of about 700 ms twt. It is restricted to areas seaward of B_1 , and is the seismic expression of oceanic crust.

Sequence R is the rift sequence overlying B_1 on the continental slope. It is made up of high amplitude, parallel to subparallel reflectors which are sometimes disrupted (Figs.2, 3). It forms basin fills of morphologic highs of sequence B_1 , against which it terminates updip-onlap. This sequence consists of continental, fluvio-lacustrine sediments deposited during the rifting phase of the Paleocene to Lower Oligocene. It is traversed by many syn-sedimentary normal faults that characterize the fault-controlled initial subsidence of the rifting phase and is marked at its upper sequence boundary by the regional unconformity T_6 .

Sequence D is the drift sequence that succeeds R which it overlies unconformably (Figs.2, 3). It is laid down during the seafloor spreading phase from the Lower Oligocene to the Lower Miocene, and consists of a transitional, continental-marine facies with a de-

creasing continental character upsequence. It has a high amplitude, parallel, concordant internal configuration, and a sequence thickness varying from zero to over 1 s twt. Faults are rare in this sequence.

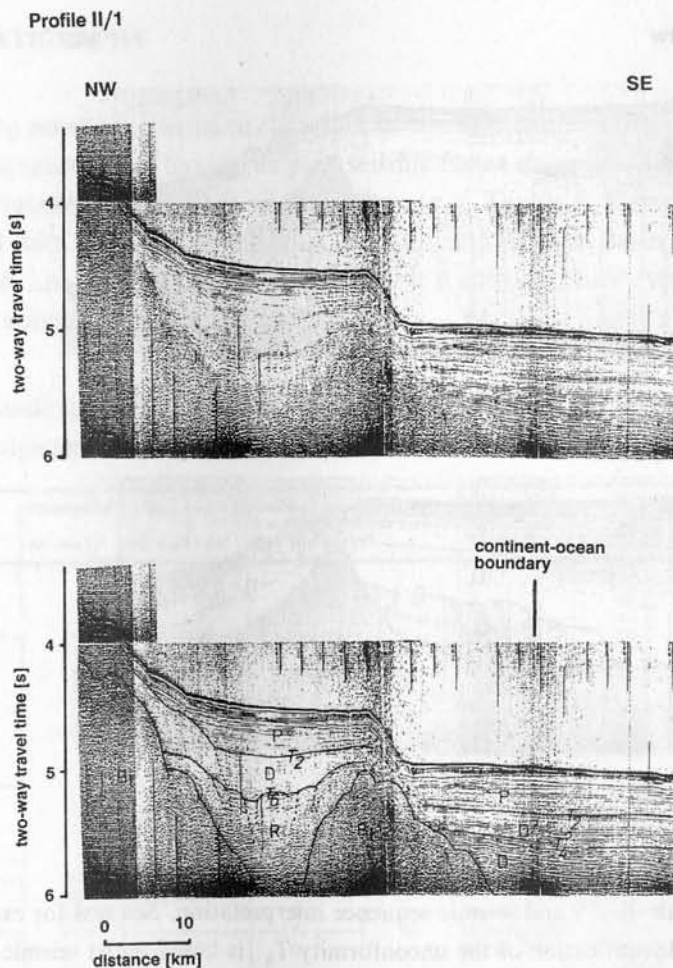


Fig.3 Part of air gun profile II / 1 and seismic sequence interpretation. See text for explanation and Fig.1 for profile location. Identification of the unconformity T_6 is based on its seismic facies and on correlations to published literature. This identification is tentative.

Sequence P is the post-drift sequence of terrigenous to fully marine sediments and is separated from the drift sequence by the regional unconformity T_2 . Its internal pattern ranges from parallel, concordant (in flat areas with pelagic sedimentation), to chaotic (on steep slopes where sediment remobilisation via mass-wasting processes such as slumping and debris flow dominates).

On the continental shelf, the internal seismic reflectors are subparallel, subhorizontal to oblique, and are typically discontinuous. Lateral continuity is intermediate and erosional channels or paleo-channels are common. The shelf slope descends in a series of steps. Reflections from the fault steps are subparallel but complicated in structure. The intervening steep slopes represent faults and exhibit hyperbolic to chaotic echoes.

HOLOCENE SEDIMENTATION AND SEDIMENT MASS TRANSPORT

The sedimentation processes on the continental shelf and slope of the South China Sea have been repeatedly and decisively influenced by sea level changes. However, the regional relative sea level curve could deviate markedly from the global eustatic sea level curve because of the influence of tectonic movements. A lowering of the sea level by as much as 130 m during the last glaciation has been reported in the literature (Li & Pang, 1990). However, this lowering is not uniform and is a function of position. For example, paleomagnetic studies, C^{14} -dating as well as micropaleontological, mineralogic and amino-acid investigations in an area northwest of Hainan Island have shown that the sea level fell about 40 m during the last glacial in this vicinity, so that over large areas of the inner shelf, a terrigenous sediment facies developed (Chen & Fan, 1988). During such phases of low sea level stand, subaerial drainage systems of the Zhujiang developed on the exposed parts of the continental shelf. Coarse, clastic material was transported from the hinterland to areas far into the outer shelf and to the continental slope. As the inland ice melted at the end of the glacial periods, the sea level rose and with it the effective depocenter was displaced towards the coast. Thus, in such a shelf-slope environment, a vertical succession of sedimentary units developed, units which can be clearly distinguished from one another using their seismo- and lithofacies characteristics. The stratigraphic development of the passive northern margin of the South China Sea is therefore a function of changes in the depo-environment as a result of the interaction between eustatic sea level change, subsidence and sediment supply (Vail *et al.*, 1984; Haq *et al.*, 1987; Galloway, 1989).

Echo Character

Damuth (1975, 1980a), Damuth & Hayes (1977) have shown that the sediment facies distribution and the sedimentation processes taking place on a continental margin may be mapped by using the echo-character observed on high frequency, high-resolution seismic profiles. For the South China Sea, they showed that by and large, these distribution patterns, regardless of whether the sediment is terrigenous, authigenic or biogenic, exhibit a zonal character (Fan *et al.*, 1987). By using the classification scheme of the echo-character of Damuth (1980b) with slight modifications, we were able to refine this pattern in our study area (Fig.4).

Table 3 shows the echo-character type distinguished, together with their interpreted sedimentary facies.

Distinct Echoes (Type I)

Type I - A1 consists of strong, sharp echoes with no subbottom reflectors. It is restricted to and dominates the continental shelf, and represents well-consolidated, relict sediments in an environment of erosion or sediment resuspension.

Type I - A2 is similar to I - A1 but has distinct, discontinuous subbottom reflectors. It is confined to filled glacial erosional channels on the continental shelf up to a maximum water depth of 60 m.

Type I - B appears as sharp, distinct echoes with multiple, parallel subbottom reflec-

tions that are fairly continuous. It is characteristic of quiet, pelagic sedimentation and is found in the deep basins as well as on flat areas of the slope and rise.

Prolonged Echoes (Type II)

Type II - A is made up of high amplitude, semi-prolonged seafloor echoes with discontinuous subbottom reflectors. It is found on steep parts of the continental slope and is typical of sediment sliding or sediment creep.

Type II - B consists of prolonged echoes without subbottom reflectors and represents debris flow or small erosional-depositional bedforms. It is confined to the boundary between the steep continental slope and the flat deep basins, where it laps out and is terminated by the echo type I - B.

Hyperbolic Echoes (Type III)

Table 3 The classification of echo-character types and their possible sedimentary facies interpretations.

Echo-Character Type	Acoustic Appearance	Possible Sedimentary Facies	Sketch of Echo-Character Type
I-A1	strong, sharp echos with no subbottom reflectors	well-consolidated, relict sediments, no recent sedimentation; erosion/resuspension	
I-A2	like I-A1 but with distinct discontinuous subbottom reflectors	filled glacial erosional channels	
I-B	distinct, sharp, with multiple continuous subbottom reflectors	quiet pelagic sedimentation in the deep sea and on flat areas of the continental slope and rise	
II-A	strong, prolonged echos; discontinuous subbottom reflectors	turbidite on the continental slope; sediment creep	
II-B	prolonged echos without subbottom reflectors	debris flow, small erosional-depositional bedforms	
III-A	large irregular hyperbolic echos with varying vertex elevations; no subbottom reflectors	slumping, basement highs on the continental slope; recent faulting	
III-B	irregular hyperbolic echos; multiple parallel subbottom reflectors	pelagic sedimentation over rugged continental slope	
III-C	sharp, regular, flat hyperbolae; dipping obliquely to the seafloor	migrating sediment waves; restricted to the shelf-break	
III-D	regular hyperbolae slightly varying vertex elevations	sediment waves induced by mass wasting processes	

Type III - A is made up of large, irregular hyperbolic echoes with varying vertex elevations and no subbottom reflections. It is found on the continental slope and is accompanied by a basement high. The environment is one of slumping and / or recent faulting.

Type III - B is characterized by irregular hyperbolae with multiple parallel subbottom reflectors. It is a result of pelagic sedimentation over rugged parts of the continental slope.

Type III-C appears as sharp, regular, flat, hyperbolic echoes dipping obliquely to the seafloor. It is typical of migrating sediment waves, but occurs only in very restricted areas near the shelfbreak (and is therefore not presented in Fig.4).

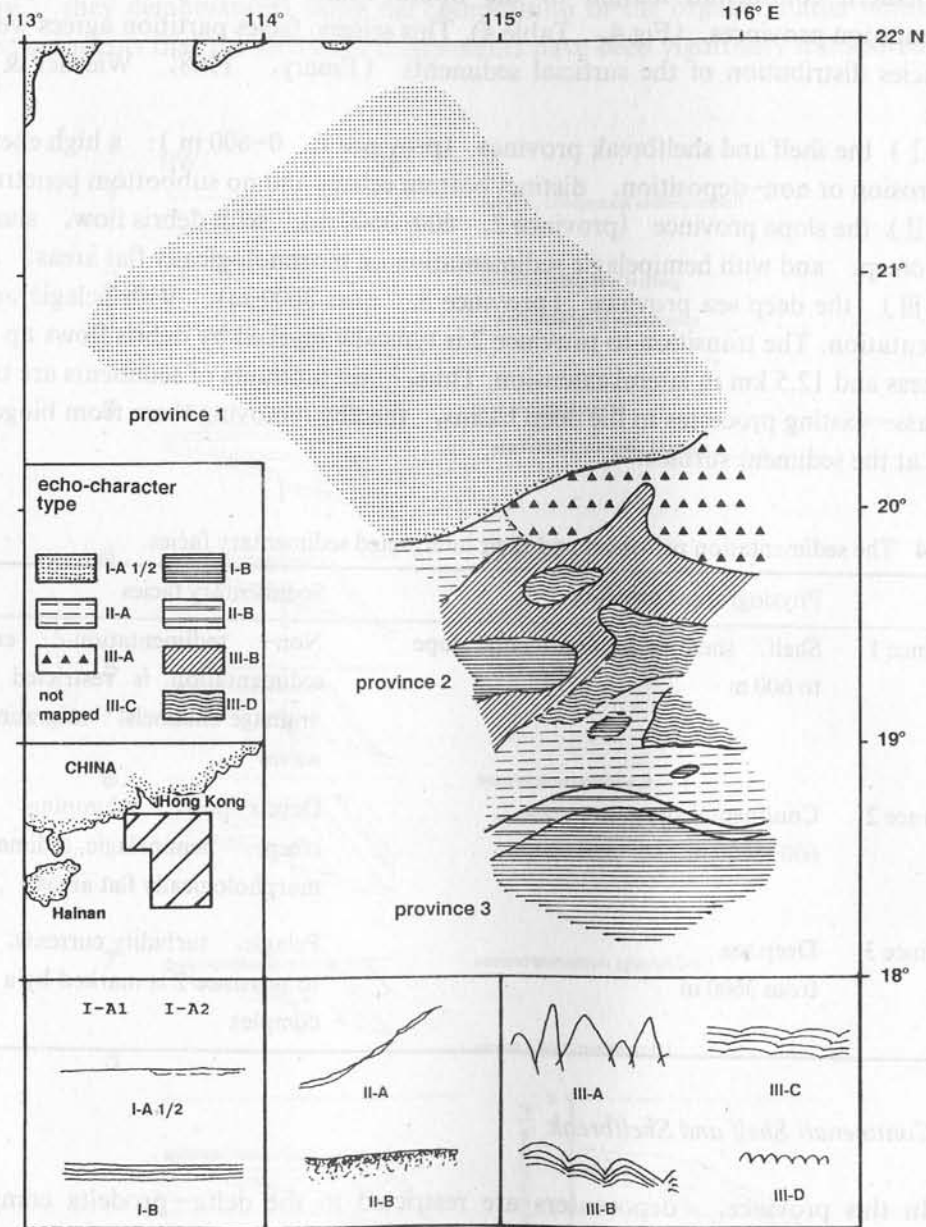


Fig.4 Seismic facies distribution (in accordance with the echo character types) and sedimentation provinces of the northern margin of the South China Sea.

Type III-D consists of regular hyperbolic echoes with a more-or-less uniform vertex elevation and no subbottom reflectors. It occurs within small basins of the continental rise and represents sediment waves induced by mass wasting processes.

Sedimentation Provinces

In accordance with the decrease in depositional energy from the shelf to the deep sea, the northern continental margin of the South China Sea may be divided into three sedimentation provinces (Fig.4, Table 4). This seismic facies partition agrees well with the lithofacies distribution of the surficial sediments (Emery, 1968; Wiesner & Anton, 1989):

(I) the shelf and shelfbreak province (province 1, 0–600 m): a high energy regime with erosion or non-deposition, distinct bottom echoes and no subbottom penetration;

(II) the slope province (province 2, 600–3600 m), with debris flow, slumping sediment creep, and with hemipelagic sedimentation on morphologically flat areas; and

(III) the deep sea province (province 3, over 3600 m), with pelagic or turbiditic sedimentation. The transition to province 2 is typically marked by debris flows up to 35 m in thickness and 12.5 km in lateral extension. Thus, vast amounts of sediments are transported via mass-wasting processes to the deep basins, thereby removing them from biogeochemical cycles at the sediment surface.

Table 4 The sedimentation provinces and their interpreted sedimentary facies.

	Physiographic province	Sedimentary facies
Province 1	Shelf, shelfbreak, continental slope to 600 m	Non-sedimentation / erosion; sedimentation is restricted to glacial drainage channels; migrating sediment waves
Province 2	Continental slope 600–3600 m	Debris flow, slumping, sediment creep, hemipelagic sedimentation on morphologically flat areas
Province 3	Deep sea from 3600 m	Pelagic, turbidity currents; boundary to province 2 is marked by a debris flow complex

The Continental Shelf and Shelfbreak

In this province, depocenters are restricted to the delta-prodelta complex of the Zhujiang formed on the inner shelf as a result of the post-glacial sea level rise and to the glacial drainage system developed on the outer shelf. They are exceptions in an environment of erosion and sediment redeposition where post-glacial currents subparallel to the coast have become established. Sandwaves with amplitudes between 2.5 to 3.5 m and wavelengths of 70–100 m at a water depth between 130 and 170 m indicate the occurrence of near-bottom currents, which from analyses of suspended matter near the bottom could achieve velocities of over 10 cm / s. The coarse clastics of the outer shelf which is texturally distinct from sediments of the inner shelf and slope are relicts of the low sea level stand during the last glacial

(Emery, 1968).

Wiesner & Anton (1989) have shown that while the fine-grained sediments of the inner shelf have a high TOC content, the high permeability of the coarser outer shelf relict deposits has led to a more efficient degradation of organic material, and hence a lower TOC. Furthermore, they demonstrated using the composition of the organic matter within the fine-grained sediments that the terrestrial components have been vigorously transported and redeposited.

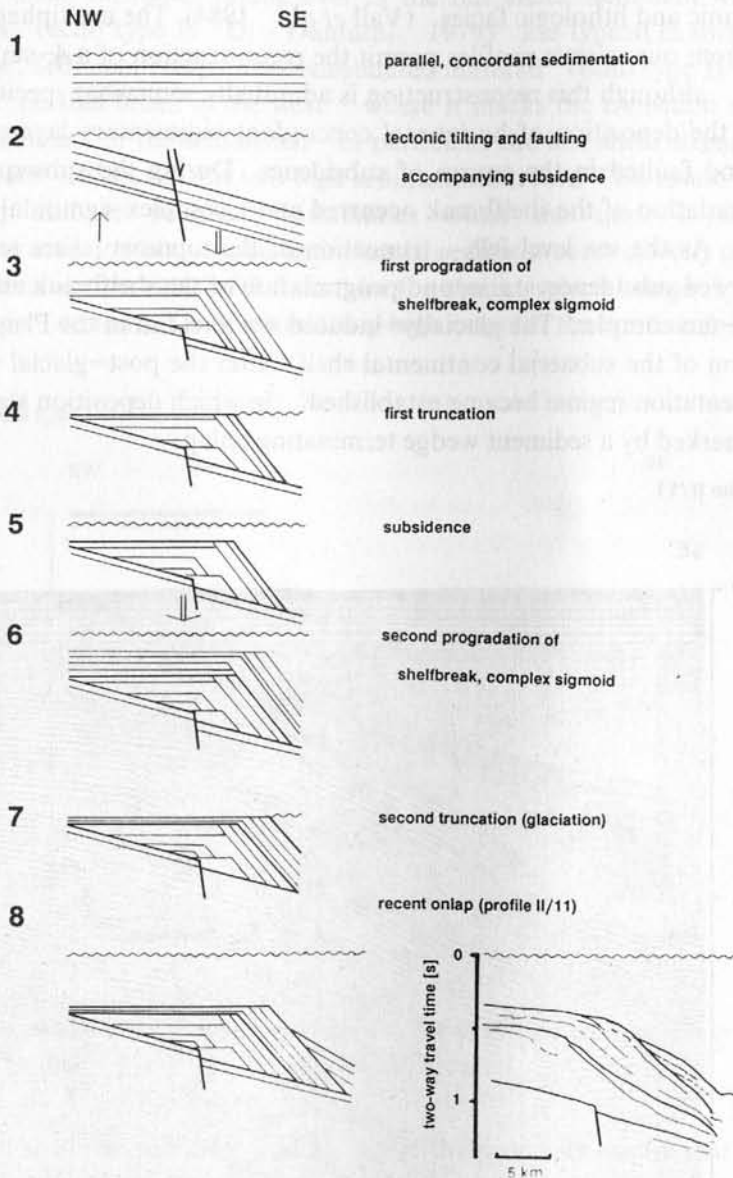


Fig. 5 A schematic, 4-stage progradation model for the evolution of the shelfbreak south of the Zhujiang estuary.

Evolution of the Shelfbreak

Because of their exposed positions and the fact that they represent the transition zone between shallow and deep waters, the shelfbreak and the adjacent upper slope are sensitive physiographic provinces that react promptly to changing physical parameters such as sea level, climate or currents (Vanney & Stanley, 1983; Vail *et al.*, 1984; Haq *et al.*, 1987; Galloway, 1989). Minor changes are sufficient to produce a new depo-environment on the shelf and hence the deposition of sediment bodies with the corresponding characteristic seismic, organic and lithologic facies (Vail *et al.*, 1984). The multiphase sea level rise and fall deduced from our seismic profiles permit the reconstruction of a 4-stage progradation of the shelfedge, although this reconstruction is admittedly somewhat speculative (Fig.5, 6). It starts with the deposition of horizontal concordant sedimentary layers, which then become tilted and faulted in the course of subsidence. During the subsequent high sea level stand, progradation of the shelfbreak occurred and a complex sigmoidal delta system came into existence. As the sea level fell, truncation of the topmost layers resulted. This is followed by renewed subsidence, a second progradation of the shelfbreak and the formation of another delta-fan complex. The glacially-induced sea level fall in the Pleistocene gave rise to another erosion of the subaerial continental shelf. After the post-glacial sea level rise, the present sedimentation regime became established, in which deposition starts at about 280 m water depth marked by a sediment wedge terminating onlap.

Profile II/11

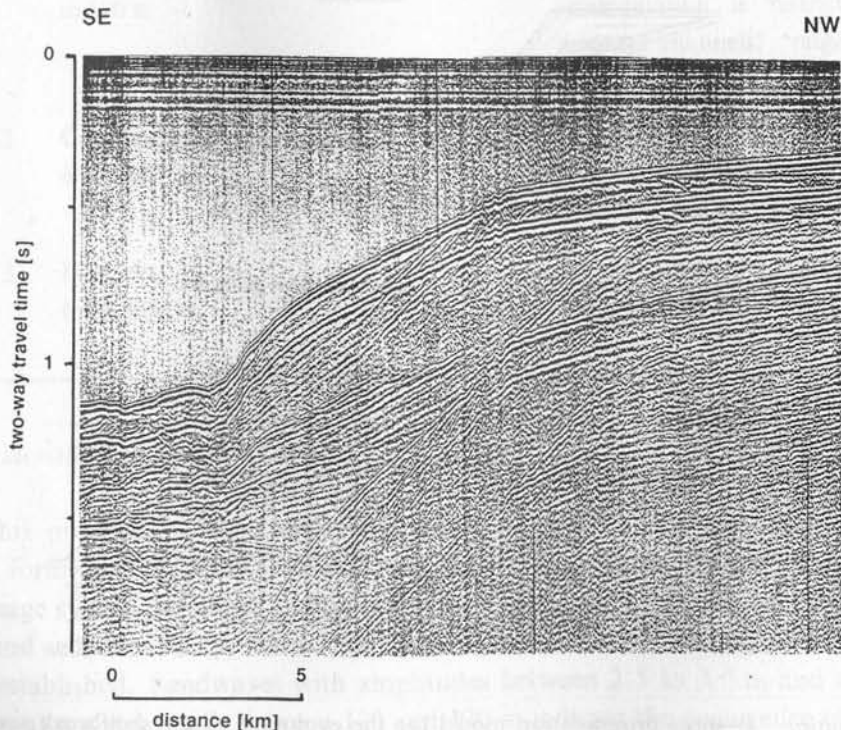


Fig.6 Part of the reflection seismic profile II / 11 showing three prograding clinoforms dipping southwards at the shelfbreak. See Fig.1 for profile location.

The Continental Slope

The northern continental slope of the South China Sea is characterized by a steplike morphology (Xie, 1981; 1983) with more-or-less flat steps (at basement highs) and seaward-dipping slopes of up to 3° gradient. Mass-wasting processes such as slump and debris flow as well as syn-sedimentary faulting dominate at the steep flanks of rotated basement blocks (He & Zhang, 1985; Liu *et al.*, 1981; Fig.7), with pelagic sedimentation and its resultant distal turbidites taking over in the flat areas. Sediment waves created by turbidity currents (echo type III-D; Damuth, 1979) are typical in small basins within the slope province. Sediment creep of unconsolidated material (echo type II-A) occurs on steep slopes near the shelfbreak in the west, where it marks the transition to the deep sea. The physical parameters of the sediments, in particular the low shear strength of the slope sediments (Holler, 1989), point to a high sedimentation rate. This results in a low degree of consolidation and to sediment instabilities when the slope is steep enough. O^{18} measurements made on planktic foraminifera in sediment cores directly off the continental shelf gave sedimentation rates of 7.5 cm/ka for the interglacial stage I (Holocene; Zheng, 1989, per. comm.). These are relatively high rates for the continental margin.

Profile II/9

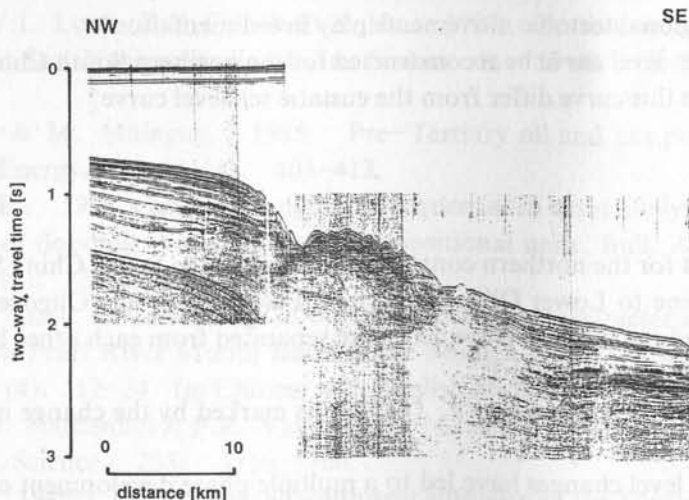


Fig.7 Sediment mass wasting at the upper continental slope of the northern margin of the South China Sea. Part of air gun profile II / 9. See Fig.1 for profile location.

The increased sedimentation rate and mass wasting processes ensure that organic matter in the sediments is rapidly buried and that the sediments are not exposed to the oxic water column for extended periods of time. Thus, high TOC contents are expected within the continental slope. Measurements show that indeed the maximum in sedimentary TOC is reached in this sedimentation province (Wiesner & Anton, 1989).

The Deep Basins

Deep basins of the northern and central South China Sea are centers of pelagic or turbiditic sedimentation. While the S2 kerogen peak in the Rock-Eval pyrograms of the organic matter from sediments of the shelf and slope is simple, that from sediments of the central and southern abyssal areas are bimodal (Wiesner & Anton, 1989). This bimodality suggests that the turbidites of the deep basins of the South China Sea have a multiple source. Thus, these turbidites originate not only from the Chinese mainland; the Mekong River with its annual suspension load of 2×10^8 t (Milliman & Meade, 1983) and the continental margin off Vietnam must also play an important role.

Open Questions

The present study has provided clues to the answer of a number of questions, such as the relationship between the distribution of seismic facies units at the seafloor and water depth or physiographic province. It has also given an insight into the sedimentation processes effective during the Quaternary which were responsible for this distribution pattern. However, a number of open questions remain. For example:

How has the facies distribution pattern changed during the Quaternary?

How and to what extent was sedimentation controlled by climatically and tectonically-induced sea level fluctuations?

What role did regional tectonic movements play in sedimentation?

Can a regional sea level curve be reconstructed for the northern South China Sea?

In what way does this curve differ from the eustatic sea level curve?

CONCLUSIONS

We conclude that for the northern continental margin of the South China Sea,

(1) the Paleocene to Lower Oligocene syn-rift sequence, the Oligocene to Miocene syn-drift sequence and the post-drift sequence are separated from each other by the regional-mappable unconformities T_6 and T_2 ;

(2) the continent-ocean boundary (COB) is marked by the change in seismic facies from B_1 to B_0 ;

(3) relative sea level changes have led to a multiple phase development of the continental margin, a record of which is most distinct at the shelfbreak; and

(4) three recent sedimentary provinces in which distinct sedimentation processes occur may be recognized. The shelf province is characterized by erosion or nondeposition, the slope province by sediment mass wasting, and the deep sea province by pelagic or turbiditic sedimentation.

REFERENCES

Brice, S. E., M. D. Cochran, G. Pardo & A. D. Edwards, 1982: Tectonics and

- sedimentation of the South Atlantic rift sequence: Cabinda, Angola. *Studies in Continental Margin Geology*, J.S. Watking & C.L. Drake (eds.), AAPG Memoir, 34, 5–20.
- Chen, X. & S. Fan, 1988: Late Quaternary deposition and environment in the sea area northwest of Hainan Island. *Tropic Oceanol.*, 8 (1), 37–45 (in Chinese).
- Damuth, J.E., 1975: Echo character of the western equatorial Atlantic floor and its relationship to dispersal and distribution of terrigenous sediments. *Marine Geology*, 18, 17–45.
- Damuth, J.E., 1979: Migrating sediment waves created by turbidity currents in the northern South China basin. *Geology*, 7, 520–523.
- Damuth, J.E., 1980a: Quaternary sedimentation processes in the South China Sea basin as revealed by echo-character mapping and piston-core studies. *The Tectonic and Geologic Evolution of South East Asian Seas and Islands*, D.E. Hayes (ed.), Amer. Geophys. Union, Geophys. Mon. Ser., 23, 105–125.
- Damuth, J.E., 1980b: Use of high-frequency (3.5–12 kHz) echograms in the study of near-bottom sedimentation processes in the deep sea: A review. *Marine Geology*, 38, 51–57.
- Damuth, J.E. & D.E. Hayes, 1977: Echo-character of the East Brazilian continental margin and its relationship to sedimentary processes. *Marine Geology*, 24, 73–95.
- Emery, K.O., 1968: Relict sediments on continental shelves of the world. *Bull. Am. Ass. Petrol. Geol.*, 52, 445–464.
- Fan, S.Q., Y.L. Luo, Z.X. Guo & D.X. Hu, 1987: Bottom sediment zonation of the South China Sea. *Nanhai Studia Marina Sinica*, 8, 55–60 (in Chinese with English abstract).
- Fontaine, H. & M. Mainguy, 1985: Pre-Tertiary oil and gas potential in the South China Sea. *Energy*, 10 (3/4), 403–412.
- Galloway, W.E., 1989: Genetic stratigraphic sequences in basin analysis I: Architecture and genesis of flooding-surface bounded depositional units. *Bull. Amer. Assoc. Petrol. Geol.*, 73 (2), 125–142.
- Guo, L. & X. Lin, 1982: Review of organic geochemical characteristics and oil origin of well No.5 in Pearl River Mouth Basin in the South China Sea. *Marine Geological Research*, 2 (4), 12–24 (in Chinese with English abstract).
- Haq, B.U., J. Hardenbol & P.R. Vail, 1987: Chronology of fluctuating sea levels since the Triassic. *Science*, 235, 1156–1166.
- Hayes, D.E., 1985: Margins of the southwest subbasin of the South China Sea—a frontier exploration target? *Energy*, 10 (3/4), 373–382.
- He, L., 1988: Formation and evolution of the South China Sea and their relation to hydrocarbon potential. *Geological Research of the South China Sea*, 1, 32–48.
- He, S. & G. Zhang, 1985: Tilted block structures in the Pearl River Mouth Basin. *Tropic Oceanology*, 4 (2), 22–29 (in Chinese).
- Hinz, K. & H.U. Schluter, 1985: Geology of the Dangerous Grounds, South China Sea, and the continental margin of the Southwest Palawan: Results of the Sonne cruises SO-23 and SO-27. *Energy*, 10 (3/4), 287–315.
- Holler, P., 1989: Sedimentphysikalische Eigenschaften von Beckensedimenten aus dem Ost- und Südchinesischen Meer. *Geochemistry and Sedimentation in the East China Sea*

- and South China Sea. Final Report to the German Ministry of Research and Technology for Projects MFG 0052, 0053, 0057.
- Holloway, N.H., 1982: North Palawan Block, Philippines—its relation to Asian mainland and role in evolution of South China Sea. *Bull. Amer. Ass. Petr. Geol.*, 66 (9), 1355–1383.
- Jin, Q.W. (ed.), 1989: *Geology and hydrocarbon potential of the South China Sea*. 417 p., Geological Press, Beijing (in Chinese).
- Jin, Q.W., Zeng, S. Zhong & Z. Wu, 1984: Analysis on petroleum geological conditions of the Pearl River Mouth Basin. *Acta Geologica Sinica*, 4, 324–336 (in Chinese with English abstract).
- Jin, Q., Z. Wu, J. Jiang & M. Lin, 1986: Preliminary study of Upper Tertiary oil source in Zhujiang River Mouth Basin. *Marine Geology & Quaternary Geology*, 6 (1), 2–16 (in Chinese with English abstract).
- Katili, J.A., 1981: *Geology of Southeast Asia with particular reference to the South China Sea*. *Energy*, 6 (11), 1077–1091.
- Li, Q. (ed.), 1988: *Geological structure and marginal extension of the South China Sea*. 398 p., Science Press, Beijing (in Chinese).
- Li.T. & G. Pang, 1990: Seismic stratigraphic study of subbottom strata in the northern South China Sea. *Abs. Proc. Symposium on the Recent Contributions to the Geological History of the South China Sea*, Oct. 10–13, 1990. 29–30.
- Liang, D. & Z.Liu, 1990: The genesis of the South China Sea and its hydrocarbon-bearing basins. *J. Petroleum Geol.*, 13 (1), 59–70.
- Liu, Y., Y. Tan & H. Liu, 1981: Fault phenomena in the northern peripheries of the South China Sea. *Nanhai Studia Narina Sinica*, 2, 13–30 (in Chinese).
- Milliman, J.D. & R.H. Meade, 1983: World-wide delivery of river sediment of the oceans. *J. Geol.*, 96, 1–21.
- Pautot, G., C. Rangin, A. Briaies, P. Tapponnier, P. Beuzert, G. Lericolais, X. Mathieu, J. Wu, S. Han, H. Li, Y. Lu & J. Zhao, 1986: Spreading direction in the central South China Sea. *Nature*, 321, 150–154.
- Ru, K. & J.D. Pigott, 1986: Episodic rifting and subsidence in the South China Sea. *Bull. Amer. Assoc. Petrol. Geol.*, 70 (9), 1136–1155.
- SCSIO (South China Sea Institute of Oceanology, Academia Sinica), 1982–1985: *Research Report on Multidisciplinary Surveys of the South China Sea*. Vol.1, 324 p., 1982; Vol.2, 436 p., 1985. Science Press, Beijing (in Chinese).
- Taylor, B. & D.E. Hayes, 1980: The tectonic evolution of the South China Sea basin. *The Tectonic and Geologic Evolution of Southeast Asian Seas and Islands*, Part 1, D.E. Hayes (ed.), *Amer. Geophys. Union Geophysical Monograph*, 23, 89–104.
- Taylor, B. & D.E. Hayes, 1983: Origin and history of the South China Sea basin. *The Tectonic and Geologic Evolution of Southeast Asian Seas and Islands*, Part 2, D.E. Hayes (ed.), *Amer. Geophys. Union Geophysical Monograph*, 27, 23–56.
- Vail, P. R., J. Hardenbol & R. G. Todd, 1984: Jurassic unconformities, chronostratigraphy and sea level change from seismic stratigraphy and biostratigraphy. *Interregional Unconformities and Hydrocarbon Exploration* J. S. Schlee (ed.), *AAPG Memoir*, 36, 129–144.
- Vanney, J.R. & D.J. Stanley, 1983: Shelfbreak physiography: An overview. *The*

- Shelfbreak: Critical Interface on Continental Margins, D.J. Stanley & G.T. Moore (ed.), SEPM Spec. Publ., 33, 1-24.
- Wiesner, M.G. & K. Anton, 1989: Organische Fazies der Oberflächensedimente des sudchinesischen Meeres. *Geochemistry and Sedimentation in the East China Sea and South China Sea*. Final Report to the Federal German Ministry of Research and Technology for Projects MFG 0052, 0053, 0057.
- Wu, J.M., 1985a: The characteristics of the geological structures of the Tertiary basins on the continental margin in the northern part of the South China Sea. *Energy*, 10 (3/4), 359-372.
- Wu, J.M., 1985b: A history of oil and gas exploration in the central and northern parts of the South China Sea. *Energy*, 10 (3/4), 413-419.
- Xie, Y., 1981: The features of submarine topography in the South China Sea. *Nanhai Studia Marina Sinica*, 2, 1-12 (in Chinese).
- Xie, X., 1983: Bottom geomorphology of the northeastern South China Sea. *Tropic Oceanology*, 2 (3), 182-190 (in Chinese).

SOUTH-EAST ASIAN MARGINAL BASINS (SOUTH CHINA, SULU AND CELEBES SEAS): NEW DATA AND INTERPRETATIONS

CLAUDE RANGIN

Departement de Geotectonique URA 1315 CNRS, Universite Pierre et Marie Curie, Paris, France

ABSTRACT

The geodynamic evolution of the South-East Asian marginal basins is discussed on the basis of recent results of scientific drilling (ODP) and geophysical cruises in these basins, as well as geologic data collected along their margins.

The Celebes and South China Seas were rifted from the Asian continental margin during the Paleogene. The present completely subducted proto-South China Sea has probably the same origin. Opening of these basins can result partly from the Indo-Asian collision and partly from slab-pull forces along the Sunda Trench.

During the Neogene, collision of the Sula Block with the southern margin of the Celebes Sea in Sulawesi, has forced progressive closure of these SE Asian basins. The proto-South China Sea was the first to subduct below the Cagayan Ridge in Early Neogene time, inducing the opening of the Sulu Sea, and spreading reorganisation in the South China Sea. Following collision of the Cagayan Ridge with the rifted margin of the South China Sea in Early Miocene time, the Sulu Sea has initiated its subduction along the Sulu Archipelago, the Celebes Sea along the North Sulawesi Trench, while intraplate shortening was registering in northern Borneo. Incipient shortening is also recorded along the axis of the South China Sea.

The Paleogene was a period of intense stretching of the Eurasian margin and opening of marginal basins, while the Neogene corresponds to the progressive subduction of these oceanic basins.

INTRODUCTION

The western Pacific region encloses a number of marginal basins displaying a variety of structural styles and settings, tectonic activity, sediment thickness and proximity to active arcs and continental margins.

The term "marginal basins" is generally restricted to those underlain by oceanic crust (Packham and Falvey, 1971; Taylor and Karner, 1983). There are several ideas on the origin of marginal basins. Among the most commonly accepted is back arc spreading (Karig, 1971), or fragmentation of the edge of a continent by extension of a global rift system. Lau and Mariana basins are examples for the first, the Tasman Sea (Weissel and Hayes, 1977) and the Coral Sea (Weissel and Watts, 1979) illustrate the second. A similar idea interprets the South China Sea as originating from the break up of the margin of Asia (Taylor and Hayes, 1980), the extrusion tectonics of the Indo-China Block providing the

model to explain the ensuing development of this basin (Tapponnier *et al.*, 1982).

Another concept is the trapping of a fragment of a once larger oceanic basin. At present the only basin that is well documented as having been a trapped fragment of a larger plate is the Bering Sea basin (Cooper *et al.*, 1976a, b). This has also been proposed for the West Philippine basin (Uyeda and Ben Abraham, 1972) and for the Banda, Sulu and Celebes Seas (Lee and McCabe, 1986) but recent kinematic reconstructions (Rangin *et al.*, 1990) and ODP drilling data do not confirm this hypothesis.

Transtensional basin formation by the movement of a major plate past a continental margin may explain the Andaman Sea, the Banda Sea or the Bismark Sea. The latter is adjacent to the colliding Ontong Java Plateau.

These different models have been applied to the SE Asian marginal basins. Forces which have induced the opening of the South China Sea are still a matter of debate, but most authors accept that this basin was rifted from mainland China (e.g. Holloway, 1982; Taylor and Hayes, 1980 and 1983). The Celebes and Sulu Seas are considerably more complex because they are surrounded by active (or recently inactive) convergent zones. Another difficulty is provided by the large amount of Neogene Island arcs developed along the margins of these basins making their earlier geological history unclear.

We have combined here recent drilling data and results of geophysical cruises from these basins with some geological data along their margins to try to unravel their origin and geological history.

AN UPDATE OF OFFSHORE DATA IN THE CELEBES AND SULU SEAS

Celebes Sea has a mean depth of over 5 km, a crustal thickness of 6–7 km, and an average heat flow of 1.6 HFU. The basin is bordered on the east by the Sangihe arc and Mindanao Island, on the south by the northern arm of Sulawesi, on the west by Borneo and on the north by the Sulu Archipelago. Subduction zones occur on the northeastern (the Cotobato Trench) and southern (North Sulawesi Trench) parts of the Celebes basin. Magnetic anomalies 18–20 have been identified in the western part of the basin (Weissiel, 1980), indicating a Middle Eocene age. Skewness analysis of the anomalies indicates no significant difference in latitude of the basin between Eocene and the present (Weissel, 1980). Sediment thickness varies from about 500 m locally in the northern part to over 3 km in the southern part. Thickness in excess of 1 km are widespread throughout the basin, filling the North Sulawesi Trench. Hemipelagics and turbidites form the remainder.

Results from ODP Drilling 124

Two sites were drilled in the Celebes Sea during leg 124 of the ODP program, and are probably the most significant data recently collected from this basin (Rangin, Silver, von Breyman *et al.*, 1990).

At site 767, a continuous section, 786 m thick, of pelagic sediments and turbidites was recovered before reaching a basaltic basement. Site 770 penetrated 420 m of pelagic sediments and recovered 110 m of basaltic basement from a fault block which is 500 m shallower than in site 767 (Fig. 1). The basalts from this basin are N-MORB in composition (Smith

and Sajona, 1991; Serri *et al.*). The distribution of major and minor elements, rare-earth elements, and Sr and Nd isotope ratios shows that the rock of the Celebes Sea are mantle derived, and they contain no subduction-related components. The isotopes are consistent with an origin in an oceanic setting, not in a back arc setting. Smith and Sajona (1991) concurred with this interpretation, on the basis of major and trace-element distributions. Although the geochemical evidence is consistent with an Indian Ocean origin, it does not rule out that the basin could have been a part of the Molucca Sea plate, or could have been derived from rifting of the edge of the China continental margin.

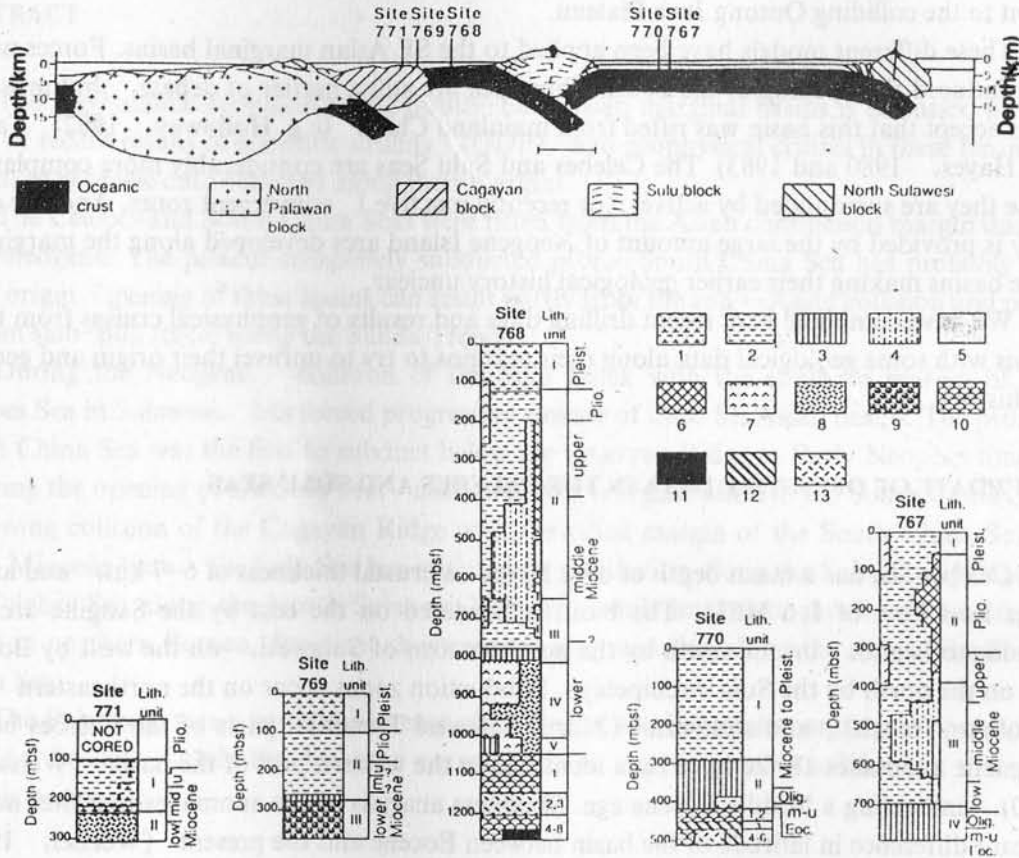


Fig.1 ODP sites in the Sulu and Celebes Seas. Symbols used are: (1) nannofossil marl or nannofossil-foraminifera marl; (2) hemipelagic sediments including clay / silt (stone); (3) pelagic brown claystone; (4) terrigenous turbidites; (5) quartz siltstone to sandstone; (6) graded carbonate turbidites; (7) fine ash / tuff; (8) pumiceous, rhyolitic to andesitic coarse tuff and lapillistone; (9) andesitic to basaltic coarse tuff and lapillistone; (10) pillow basalt; (11) basalt sheet flow; (12) brecciated massive basalt; (13) diabase sill.

Radiolarian-bearing reddish brown claystone makes up the lower parts of the section at sites 767 and 770 (Fig. 3), with a significant carbonate component at the shallower site 770. Here, a radiolarian rich layer occurs 1 cm above hyaloclastites that rest on oceanic basement (Rangin, Silver, von Breyman *et al.*, 1990). These fossils place the base of the sedimentary section in the P. chalara zone (42 Ma on the time scale of Berggren, 1985).

This supports a Middle Eocene age for the basaltic basement of the Celebes Sea. Bertrand *et al.* (1991), Nicot and Desprairies (1991) concluded that the source of a significant fraction of the brown claystone was derived from a continental source. This does not support an Indian Ocean neither a West Philippine Sea basin origin. No significant lithologic change was recorded in the basin up to 18–19 Ma. The lack of significant change in clay mineralogy means that this boundary can not be used as evidence of far-travel of the Celebes Sea.

Paleoinclinations at site 767 show a wide scatter that can be interpreted either as no significant change in latitude, or as a sudden change in latitude shortly after formation of the basement. This depends upon the interpretation of the paleomagnetic data obtained on the basement. Silver and Rangin (1991) explain the discrepancy in inclination between the basement and the overlying sediments, supporting the case of rotation of the basement block at the ridge axis. This explains the anomalously high inclinations relative to the sediments. This explanation favors for the Celebes Sea, an origin not far removed from the present latitude.

The Sulu Sea is surrounded by island arcs and continental fragments, with the Palawan and Cagayan ridges on the northwest, the Sulu Ridge on the southeast, the Philippines on the east and Borneo (Sabah) on the southwest.

The Sulu Sea has been interpreted either as the result of back arc spreading associated with the Cagayan or Sulu ridges (Holloway, 1982; Mitchell *et al.*, 1986; Rangin, 1989), or the entrapment of an old piece of oceanic crust (Lee and McCabe, 1986). To resolve this ambiguity, and trace the complex evolution of this small basin as well, various oceanographic cruises were recently conducted in the Sulu Sea. The Federal Institute for Geosciences and Natural Resources (BGR) in Germany, collected 10315 km of multichannel seismic data together with magnetic and gravimetric measurements in the Sulu Sea on six cruises from 1977 to 1987. These cruises also included heat flow measurements and dredging (Hinz and Block, 1990; Kudrass *et al.*, 1990; ODP). The French R/V J. Charcot from France made also a short survey along the Sulu and Negros trenches in 1985. All these recent data were used as a basis for drilling in the Sulu basin and the Cagayan Ridge in 1989 (Rangin, Silver, von Breyman *et al.*, 1990). Among the scientific objectives of these drillings was the determination of the age and nature of the crust of the Sulu Sea, and the record in this basin of the complex collisional history of this SE Asian area located at the junction of three major convergent lithospheric plates.

One deep site was drilled in the Sulu basin and two sites on the Cagayan Ridge (Fig.1). The tectonic objective was to determine the age for the cessation of volcanic activity along that ridge, in response to its collision with the rifted margin of China in Palawan (Reed Bank – Dangerous Grounds).

Site 768, penetrated 220 m of basaltic basement rocks, recovering pillow-basalts, massive lavas, and two diabase sills. Geochemical analyses indicate that the Sulu Sea basement is transitional between MORB and island arc tholeites, suggesting contamination of primary basaltic magmas by subduction processes (Spadea *et al.*, 1991). Just above basement, at basin site 768, lies a brown clay layer, approximately 40 m thick, dated Early Miocene (Rangin, Silver, von Breyman *et al.*, 1990).

The basement of the Cagayan Ridge was found to be a thick layer of pyroclastics blanketed by brown muds of Early Miocene age. Basaltic and andesitic clasts recovered from these pyroclastics are calcalkaline at site 769 and island arc tholeite at site 771 (Spadea *et*

al., 1991; Smith *et al.*, 1991). The chemical composition of the rocks implies continental crust contamination also indicated by the petrographic analysis (Kudrass *et al.*, 1990), and is consistent with eruption of the magmas through continental rocks. This strongly suggests that the Cagayan volcanic arc was built on a continental basement. Radiometric dates on basalts and andesites drilled on the ridge (Bellon and Rangin, 1991), show that the volcanism of this ridge ranges in age from 20–14 Ma, thus inferring two distinct magmatic events. The younger event could be coeval with that of the pyroclastics recovered at sites 769 and 771. This volcanic material is visible on seismic profiles, blanketing tilted blocks (Hinz and Block, 1990). Outpouring of these pyroclastics was interpreted by Rangin and Silver (1991) to be the last stage of magmatism during collision of the ridge with the rifted margin of China.

In the Sulu basin at site 768, a 200 m thick layer of pyroclastics rests on brown claystone deposited on the Sulu basement, but also topped by the same Early Miocene pelagic sediments (Fig.1). This indicates that the pyroclastic event of the Cagayan Ridge was short in time and probably represents the last event of magmatic activity along that ridge.

The South China Sea is one of the largest in the western Pacific region. It is bounded by the continental margins of South China, Vietnam and Borneo, and by the Manila Trench, where its crust is now being consumed by eastward-dipping subduction East of 115° E, the magnetic anomalies 11 to 5e have been identified by Taylor and Hayes (1980, 1983), and recently remodeled by Briais (1985). Recent morphological studies at the axis of the basin were conducted by R/V J. Charcot between 113° and 119° E (Pautot *et al.*, 1986). Multibeam mapping of the seafloor coupled with single channel seismic recording have documented a change from N50° E to N80° E in the strikes of normal faults 100 km away from the axis. This indicates a major counterclockwise rotation of the spreading direction 20 Ma B.P. and a major kinematic change in the spreading history of this basin at that time.

A Model for the Opening of the SE Asian Basins

These new data allow us to choose among the various interpretations proposed for the opening of these marginal basins. Concerning the Celebes Sea, a split from the west Philippine basin is unlikely because spreading rates are basically different between both basins (Silver and Rangin, 1991). Similarly an Indian Ocean origin can be disregarded because the spreading in this ocean reorganized at or just prior to anomaly 20 (Cande *et al.*, 1989) when the southeast Indian Ridge jumped to a more southern position. Earlier, the spreading system could have extended east to the possible location of the Celebes basin, but after the jump the ridge connected with spreading south of Australia, making it unlikely that the Celebes Sea was created from spreading in the Indian Ocean after anomaly 20.

Alternatively an origin by rifting from the outermost part of the East China margin is the most acceptable hypothesis as long as open circulation was maintained and continental sedimentation was restricted. However, we cannot disregard completely the hypothesis that Celebes was formerly part of a larger basin presently subducted as the Molucca Sea (Silver and Rangin, 1991). If this hypothesis for a Eurasian origin of the Celebes basin is correct, the subducted proto-South China Sea should have also opened by rifting and spreading of the China continental margin.

The Eurasian plate margin can be interpreted as subjected to extensive internal deformation in Early Paleogene, in response to the collision of India with Asia (Tapponnier *et al.*, 1982; Rangin *et al.*, 1990). Thinning of the Eurasian margin was immediately followed in Middle Eocene and Oligocene time by opening processes of oceanic floored basins (South China Sea, proto-South China Sea, and Celebes Sea), the southern boundary of the Eurasian plate being traced southward in North Sulawesi.

THE CLOSURE OF THE SE ASIA MARGINAL BASINS

The closure of these basins, which has been active since the beginning of Neogene time, can be demonstrated on the basis of volcanic arc and tectonic activity along their margins, and deposition of turbidites and ash layers into the basins.

Among the numerous data recently collected along the margin of these basins, we shall focus here on Panay Island and North Sulawesi. The reason is that significant parts of the island arcs fringing the Sulu and Celebes Seas are exposed in these key areas, providing an excellent control on the magmatic and tectonic activity along the margins of these basins.

North Sulawesi

Along the northern margin of the north arm of Sulawesi, seismic reflection lines show increasing width of the accretionary wedge toward the west (Silver *et al.*, 1983). The timing of movement along this thrust zone is not well determined, but volcanic arc activity can provide some indications. This arc volcanism is widespread along the north arm, which is truncated at its western end by the Palu Fault. Volcanic activity decreases westward and the roots of the island arc are exposed, large granodiorites were dated Early to early Middle Miocene (15 to 18.8 Ma.: Ratman *et al.*, 1976; and 22 to 18.5 Ma.: Bellon and Rangin, 1991). This old island arc is unconformably covered by a second phase of arc volcanism dated from 7 to 4 Ma. These two phases of arc magmatism can be interpreted as a shift of subduction polarity from the south to the north of the north arm of Sulawesi. Subduction of the Celebes Sea could have been initiated 8 to 7 Ma.

The Sulu and Cagayan Volcanic Arcs in Panay

Cenozoic volcanics of the Sulu and Cagayan Ridges are covered either by Plio-Pleistocene volcanism or water. However, the volcanic arc sequences are known both to the northeast and southwest of the Sulu Sea, in southern Sabah, and Panay Island. In Panay Island, in the uppermost part of the Negros Trench inner wall, the Antique Range is composed of distinct island arc terranes thrust to the northwest on the North Palawan Block (Cuyo platform). Datings of these volcanic arc sequences and timing of their accretion to the rifted margin of China were discussed by UNDP (1983) and Rangin *et al.*, (1991). We have identified three distinct island arc terranes in that range (Fig. 2).

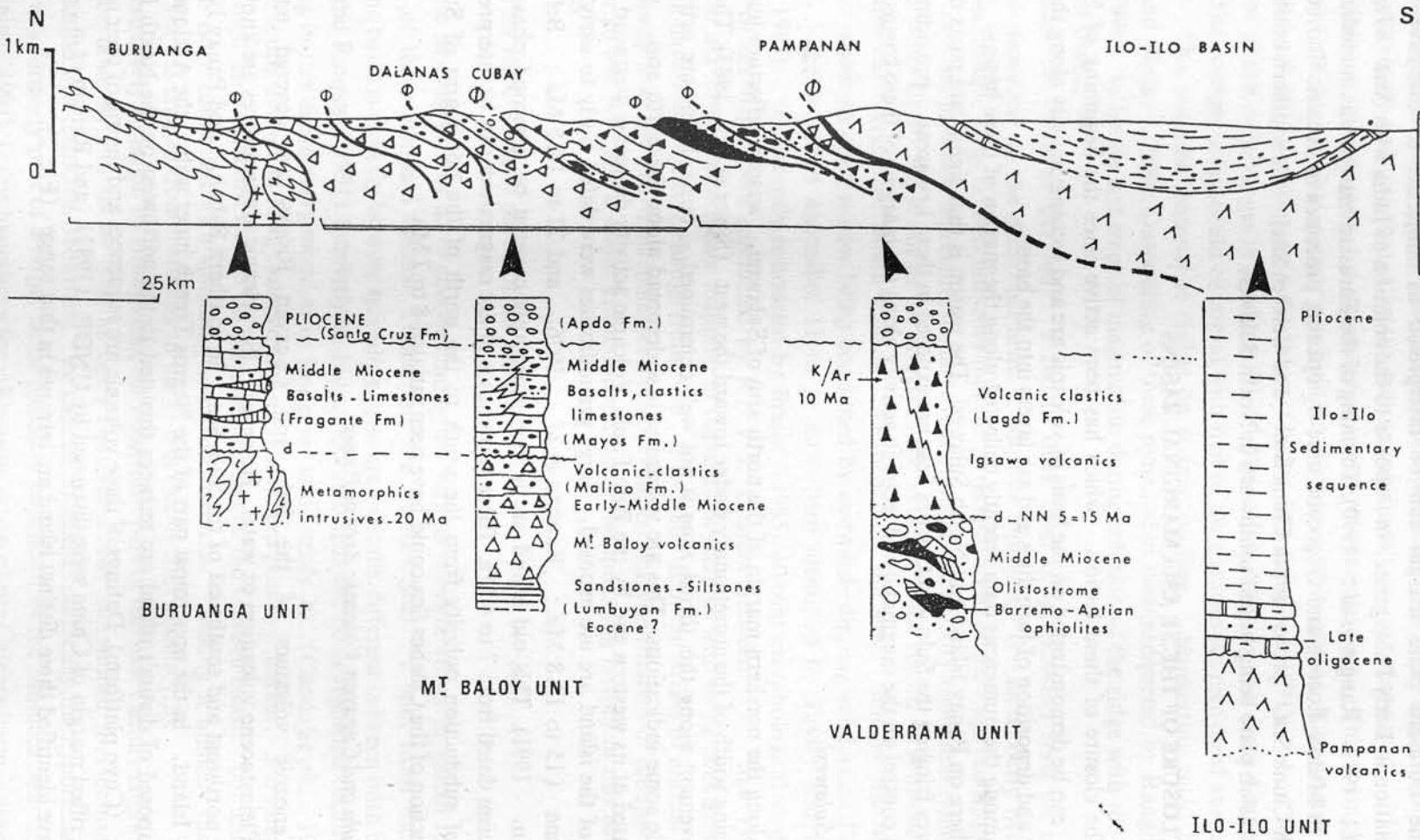


Fig. 2 Simplified cross section of the Antique Range in Panay Island and simplified logs corresponding to the various units; a = Eocene limestone; b = Radiolarian chert; c = Gabbros and ultramafics.

I) The Mt. Baloy volcanic sequence was dated 15 Ma at its top (K / Ar) and is conformably covered by Miocene carbonates and clastics (Mayos Fm). It can easily be considered as the emergence of the Cagayan Ridge. This volcanic unit is thrust over high grade metamorphics intruded by Early Miocene plutons and disconformably covered by Neogene carbonates and alkali basalts (Buruanga unit).

II) In the central part of the range, the Valderrama volcanic sequence was disconformably deposited on ophiolites and melanges. The volcanics and interlayered sediments were dated Middle Miocene (14-10 Ma). This volcanic sequence was also found in the Zamboanga Peninsula where it rests disconformably on ophiolites, testifying that the Valderrama and Zamboanga volcanics are part of the same Sulu arc.

III) In southern Panay the Valderrama volcanic arc sequence is overthrust by the Philippine arc, represented by the Iloilo volcanic sequence (26-21 Ma K / Ar) topped by the Neogene clastic sequence of the Iloilo basin.

So Panay Island is located at the tectonic contact between the welded Sulu basin volcanic margins (Cagayan Ridge / Mt. Baloy and Sulu Ridge / Valderrama) with the Philippine Sea plate.

The scenario for the evolution of the Sulu basin is summarized in the Antique Range of Panay (Fig.3):

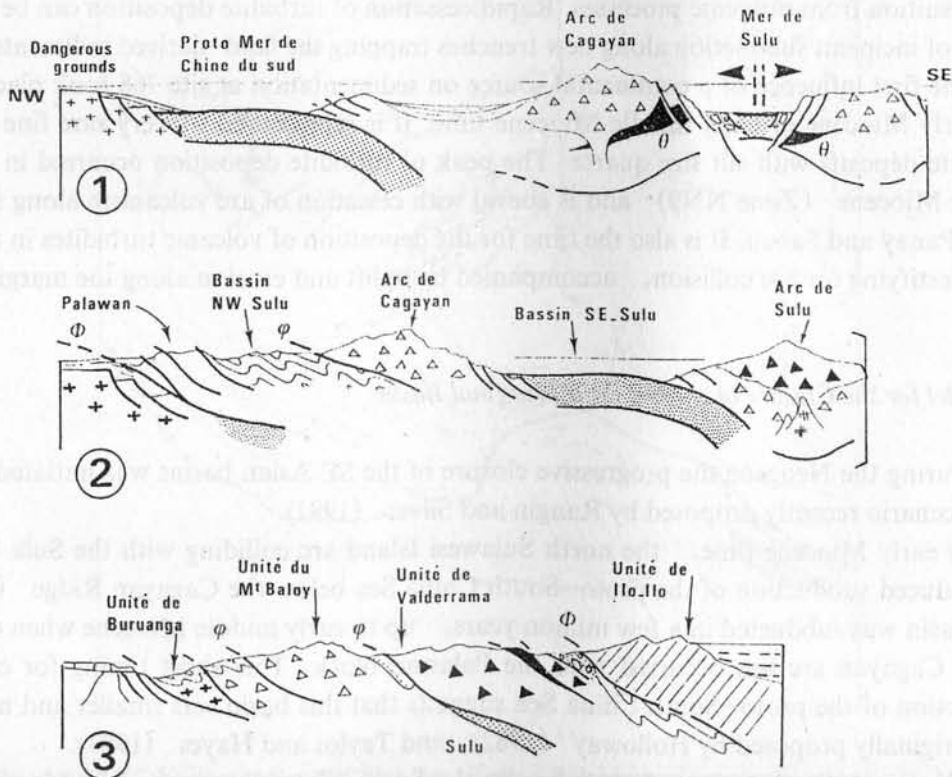


Fig.3 Interpretative sketch diagram depicting the tectonic evolution of the Antique Range during the Cenozoic.

I) the Cagayan / Mt. Baloy collided with the Palawan Block in early Middle Miocene

time, the age for the cessation of magmatic activity along this arc. Convergence was immediately accommodated along the Sulu Trench and the Sulu / Valderrama arc was rapidly developed.

II) At 10 Ma, the Sulu / Valderrama arc collided with Cagayan / Mt. Baloy, and is also accreted to the Palawan Block. This was the time for complete closure of the Sulu basin. During the same event the Iloilo volcanic unit was thrust over the Valderrama sequence along the Pampanan thrust.

In Sabah, on the other side of the Sulu basin, Late Oligocene – Early Neogene volcanic arc sequences are imbricated with melanges and Mesozoic ophiolites (Rangin *et al.*, 1990). Here, the converging Cagayan and Sulu volcanic arc sequences are difficult to differentiate in the field, and are both thrust on the Crocker sedimentary sequence, the latter being an extension in Borneo of the Palawan accretionary wedge.

Drilling Data into the Sedimentary Basins of the Sulu–Celebes Seas

A second control for the closure history of the Sulu–Celebes basins is the arrival of turbidites into the basins inducing important sedimentation changes. The source of these quartz rich turbidites can be found in the surrounding land masses affected by intensive erosion resulting from orogenic processes. Rapid cessation of turbidite deposition can be an indication of incipient subduction along new trenches trapping the land-derived sediments.

The first influence of a continental source on sedimentation at site 768 took place in the late early Miocene or early middle Miocene time. It is represented by very rare fine grained turbidite deposits with silt size quartz. The peak of turbidite deposition occurred in the late middle Miocene (Zone NN9) and is coeval with cessation of arc volcanism along the Sulu arc in Panay and Sabah. It is also the time for the deposition of volcanic turbidites in the Sulu basin testifying for arc collision, accompanied by uplift and erosion along the margin of the basin.

A Model for the Closure of the SE Asia Marginal Basins

During the Neogene the progressive closure of the SE Asian basins was initiated following a scenario recently proposed by Rangin and Silver (1991).

In early Miocene time, the north Sulawesi Island arc colliding with the Sula block, first induced subduction of the proto–South China Sea below the Cagayan Ridge (Fig. 4). This basin was subducted in a few million years, up to early middle Miocene when collision of the Cagayan arc has occurred with the Palawan block. This short timing for complete subduction of the proto–South China Sea suggests that this basin was smaller and narrower than originally proposed by Holloway (1982) and Taylor and Hayes (1983).

Change in the direction of spreading in the South China Sea around 20 Ma. is coeval with the oldest ages of volcanic activity recorded on the Cagayan ridge. This age is also in agreement with the opening of the Sulu Sea and the cessation of magmatism along the north arm of Sulawesi (Bellon and Rangin, 1991). This early Miocene event is the time for collision, in central Sulawesi, of the Australian derived Sula block with the southernmost fragment of the rifted margin of Eurasia. It is also the time for incipient collision of the

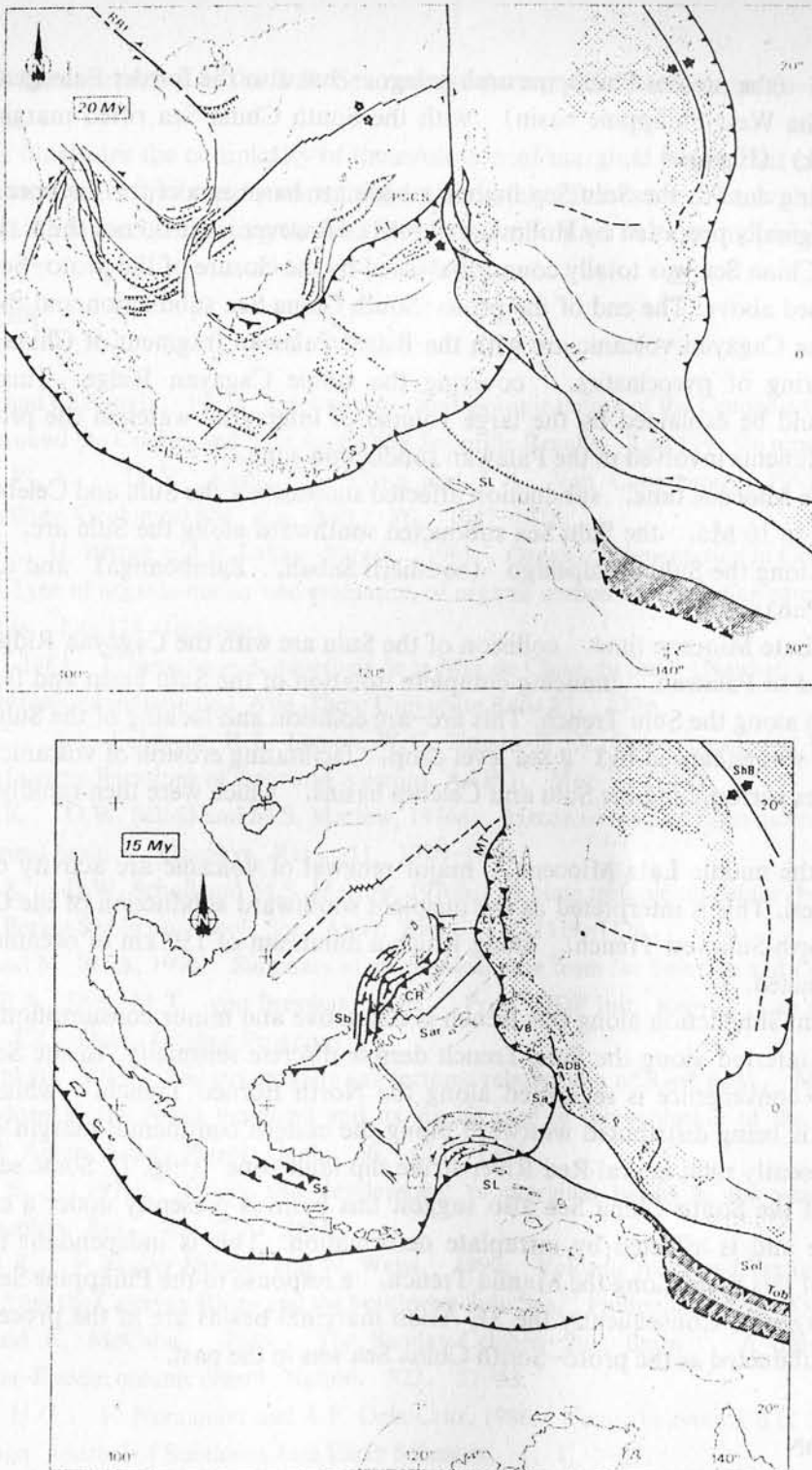


Fig. 4 The closure of the proto-South China Sea. Top: Paleotectonic reconstruction at 20 Ma. Bottom: Paleotectonic reconstruction at 15 Ma. SL= Sula Block; PT= Palawan Trough; PPF= Proto Philippine Fault; MT= Manila Trench; CR= Cagayan Ridge; Sar= Sulu Archipelago; Sb= Sabah; Tob= Tobrian Trench; Sol= Solomon Sea; ShB= Shikoku Basin; CV= Central Valley; RRF= Red River Fault; PSCS= Proto-South China Sea; S= Sumba; VB= Visayan; SS= Sunda Shelf (for more details see Rangin *et al.*, 1990).

Philippine arc (the present Philippine archipelago, but also the former Paleogene volcanic arc fringing the West Philippine basin) with the South China Sea rifted margin (north Palawan block) (Fig.4).

The drilling data in the Sulu Sea favour a back arc basin model for the opening of this basin, as originally proposed by Holloway (1982). However, we do not think the opening of the South China Sea was totally counterbalanced by the closure of the proto-South China Sea as discussed above. The end of the proto-South China Sea subduction and the incipient collision of the Cagayan volcanic arc with the Rifted Palawan fragment of China induced a large outpouring of pyroclastics, covering the whole Cagayan Ridge. This explosive volcanism could be explained by the large volume of interstitial water in the proto-South China Sea sediments involved in the Palawan subduction zone.

In Middle Miocene time, subduction affected successively the Sulu and Celebes basins.

From 15 to 10 Ma, the Sulu Sea subducted southward along the Sulu arc, volcanism being active along the Sulu archipelago (southern Sabah, Zamboanga) and its probable extension in Panay.

In early Late Miocene time, collision of the Sulu arc with the Cagayan Ridge in Panay already locked to Palawan, inducing complete isolation of the Sulu basin and fast decrease of subduction along the Sulu Trench. This arc-arc collision and locking of the Sulu basin has induced (or was enhanced by) a sea level drop, facilitating erosion of volcanic and continental terranes surrounding the Sulu and Celebes basins, which were then rapidly filled with turbidites.

During the middle Late Miocene, major renewal of volcanic arc activity occurred in North Sulawesi. This is interpreted as the incipient southward subduction of the Celebes Sea along the North Sulawesi Trench, along which a minimum of 150 km of oceanic crust was already subducted.

At present subduction along this trench is still active and minor consumption of oceanic crust can be inferred along the Sulu Trench despite discrete seismicity. In the South China Sea, active convergence is registered along the North Borneo Trench, while intraplate deformation is being distributed westward along the eastern continental margin of Vietnam up to the presently right lateral Red River strike slip fault zone (Fig. 1). Some seismic events at the axis of the South China Sea also suggest this basin is presently under a compressive stress regime and is affected by intraplate deformation. This is independent from active subduction of this basin along the Manila Trench, a response to the Philippine Sea / Eurasia plates convergence. Consequently the SE Asian marginal basins are in the process of being completely subducted as the proto-South China Sea was in the past.

CONCLUSION

Opening of the SE Asian marginal basins can be attributed to distinct processes such as fragmentation of a plate margin (Celebes and South China Seas) or back arc spreading (Sulu Sea).

The timing of spreading of these basins are also distinct. The Celebes and South China Sea basins resulted partly from intense stretching, thinning and fragmentation of the Eurasian margin in response to Indo-Asian collision and trench pull forces along the Sunda

Trench. On the other hand, the Sulu Sea opened during closure of the proto-South China Sea.

All this illustrates the complexity of the evolution of marginal basins that can be opened in a few million years and rapidly consumed immediately afterwards. The evolution of these basins is a guide for reconstructing the history ancient mountain belts with ophiolites.

REFERENCES

- Bellon, H. and C. Rangin, 1991: Geochemistry and isotopic dating of the Cenozoic volcanic arc sequences around the Celebes and Sulu Seas. ODP Scientific Results, Leg 124 (in press).
- Berggren, W. A., D. V. Kent, J. J. Flynn and J. A. Van Coovering, 1985: Cenozoic geochronology. Geological Soc. Am. Bull., 96, 1047-1418.
- Bertrand, P., U. Berner and E. Lallier-Verges, 1991: Organic sedimentation in Celebes and Sulu basins: Type of organic matter and evaluation of organic carbon accumulation rates. ODP Scientific Results, Leg 124 (in press).
- Briais, A., 1985: Cinématique d'ouverture de la Mer de Chine du Sud (Nanhai): Implications pour la Tectonique tertiaire de l'Asie. These Université Paris VI, 239p.
- Cande, S.C., J.L. Labrecque, R.L. Larson, W.C. Pitman III, X. Golovchenko and W.F. Haxby, 1989: Magnetic lineations of the world's oceans. AAPG, Map 1: 27400.
- Cooper, A.K., D.W. Scholl and M.S. Marlow, 1976a: Mesozoic magnetic lineations in the Bering Sea marginal basin. J. Geophys. Res., 11, 1916-1934.
- Cooper, A.K., D.W. Scholl and M.S. Marlow, 1976b: A plate tectonic model for the evolution of the East Bering Sea basin. Geol. Soc. Amer. Bull., 87, 1119-1126.
- Hinz, K., and M. Block, 1990: Summary of geophysical data from the Sulu Sea and Celebes Sea. C. Rangin, E.A. Siver, M.T. von Breyman *et al.*, Proc. ODP Init. Repts., Leg 124, College Station, TX (Ocean Drilling Program).
- Holloway, N.H., 1982: The stratigraphy and tectonic relationship of Reed Bank, North Palawan and Mindoro to the Asian mainland and its significance in the evolution of the South China Sea. Bull. Amer. Assoc. Petrol. Geol., 66, 1357-1383.
- Karig, D. E., 1971: Origin and development of marginal basins in the western Pacific. Jour. Geophys. Res., 76, 2542-2561.
- Kudrass, H.R., P. Muller Kresuer and W. Weiss, 1990: Volcanic rocks and Tertiary carbonates dredged from the Cagayan Ridge and the Southwest Sulu Sea, Philippines. Proc. ODP Leg 12.
- Lee, C. and R. McCabe, 1986: The Banda-Celebes-Sulu Basin: A trapped piece of Cretaceous-Eocene oceanic crust? Nature, 322, 51-53.
- Mitchell, A.H.G., F. Hernandez and A.P. Dela Cruz, 1986: Cenozoic evolution of the Philippine Archipelago. Journal of Southeast Asia Earth Sciences, 1, 1, 3-22.
- Nicot, E. and A. Desprairies, 1991: Inheritance and neof ormations in the sediments of the Celebes and Sulu basins (Leg 124). ODP Scientific Results, Leg 124 (in press).
- Packham, G.H. and D.A. Falvey, 1971: A hypothesis for the formation of marginal seas in the Western Pacific. Tectonophysics, 11, 79-109.
- Pautot, G., C. Rangin, A. Briais, P. Tapponnier, P. Beuzart, G. Lericolais, X. Mathieu, J. Wu, S. Han, H. Li, Y. Lu and Zhao, 1986: Spreading direction in the central South China Sea. Nature, 321, 6066, 150-154.

- Rangin, C., 1989: The Sulu Sea, a back-arc basin setting within a Neogene collision zone. *Tectonophysics*, 161, 119-141.
- Rangin, C., L. Jolivet and M. Pubellier, 1990: A simple model for the tectonic evolution of Southeast Asia and Indonesia region for the past 43 Ma. *Bull. Soc. Geol. Fr.*, 8, t. VI, 889-905.
- Rangin, C. and E.A. Silver, 1991: Neogene tectonic evolution of the Celebes Sulu basins: New insights from Leg 124 drilling. *ODP Scientific Results, Leg 124* (in press).
- Rangin, C., H. Bellon, F. Benard, J. Letouzey, C. Muller, S. Tahir, 1990: Neogene arc continent collision in Sabah: Northern Borneo (Malaysia). *Tectonophysics*, 183, 305-319.
- Rangin, C., E. Silver, M. von Breyman and Leg 124 Scientific Party, 1990: Volume 124 Initial Reports: Celebes and Sulu Seas. *Proc. ODP Init. Repts.*, 124, College Station TX, (Ocean Drilling Program), 916 p.
- Rangin, C., J.F. Stephan, J. Butterlin, H. Bellon, C. Muller, J. Chorowicz, D. et Baladad, 1991: Collision Neogene d'arcs volcaniques dans le centre des Philippines: Stratigraphie et structure de la chaine d'Antique (Ile de Panay). *Bull. Soc. Geol. Fr.*, 162, 465-477.
- Ratman, N., 1976: Geological map of the Tolitoli Quadrangle, North Sulawesi, 250 000e. Geological Survey of Indonesia Ministry of Mines.
- Serri, G., P. Spadea, L. Beccaluva, L. Civetta, M. Coltorti, J. Dostal, D. Sajona, C. Vaccard and O. Zeda: Petrology of igneous rocks from the Celebes Sea basement. *ODP Scientific Volume, Leg 124* (in press).
- Silver, E.A., R. McCaffrey and R.B. Smith, 1983: Collision, rotation, and the initiation of subduction in the evolution of Sulawesi, Indonesia. *Jour. Geophys. Research*, 88, 9407-9418.
- Silver, E.A. and C. Rangin, 1991: Development of the Celebes Sea basin in the context of western Pacific Marginal Basin evolution. *ODP Scientific Results* (in press).
- Smith, T.E., C.E. Huang and F.G. Sajona: Geochemistry and petrogenesis of the volcanic rocks from hole 768 and 769, Sulu Sea. *ODP Scientific Results, Leg 124* (in press).
- Smith, T.E. and F.G. Sajona, 1991: Geochemistry and petrogenesis of the volcanic rocks from holes 767C, 770B, and 770C, Celebes Sea. *ODP Scientific Results, Leg 124* (in press).
- Spadea, P., L. Beccaluva, L. Civetta, M. Coltorti, J. Dostal, D. Sajona, G. Serri, C. Vaccaro and O. Zeda, 1991: Petrology of basic igneous rocks from the floor of the Sulu Sea. *ODP Scientific Results, Leg 124* (in press).
- Tapponnier, P., G. Peltzer, A.Y. Le Dain, R. Armijo and P. Cobbold, 1982: Propagating extrusion tectonics in Asla: New insights from simple experiments with plasticine. *Geology*, 10, 611-616.
- Taylor, B. and D.E. Hayes, 1980: The tectonic evolution of the South China Basin. *The Tectonic and Geologic Evolution of Southeast Asian Seas and Islands. Geophys. Monog.*, D.E. Hayes (ed.), AGU, 27, 89-104.
- Taylor, B. and D.E. Hayes, 1983: Origin and history of the South China Sea Basin. *The Tectonic and Geologic Evolution of Southeast Asian Seas and Islands. Geophys. Monog.*, D.E. Hayes (ed.), AGU, 23-56.
- Taylor, B. and G. D. Karner, 1983: On the evolution of marginal basins. *Rev. Geophys. Space. Phys.*, 21, 1727-1741.
- The United Nations Development Program and the Philippine Bureau of Mines and Geosciences, 1983: Cenozoic geological evolution of southwestern panay and adjacent areas. *The Philippine Geologist*, Oct.-Dec., 16-36.

- Uyeda, S. and Z. Ben-Abraham, 1972: Origin and development of the Philippine Sea. *Nature Phys. Sci.*, 240, 176-178.
- Weissel, J.K., 1980: Evidence for Eocene oceanic crust in the Celebes Basin. *The Tectonic and Geologic Evolution of SE Asian Seas and Islands*. Geophys. Monogr., D.E. Hayes (ed.), 23, 37-47.
- Weissel, J.K. and A.B. Watts, 1979: Tectonic evolution of the Coral Sea basin. *Journal of Geophysical Research*, 84, B9, 4572-4582.
- Weissel, J.K. and D.E. Hayes, 1977: Evolution of the Tasman Sea reappraised. *E. P. S. L.*, 36, 77-84.

CHRONOLOGICAL SEQUENCE OF TWO SPREADING PHASES OF THE SOUTH CHINA SEA BASIN

WU JINLONG, LIU ZHONGCHEN & HAN SHUQIAO

First Institute of Oceanography, SOA, Qingdao, China

ABSTRACT

The spreading ridge is oriented along the NE direction in the east of the South China Sea between 118° E and the Manila Trench. The South China Sea has gone through two distinct phases of seafloor spreading. Seabeam maps and magnetical lineations indicate that the NE trending ridge cut off obliquely the E-W trending one. The spreading of the E-W trending ridge began earlier than that of the NE trending one. The E-W trending magnetic lineations are 11-5D. Correspondingly, the N-S seafloor spreading occurred in mid-Oligocene and terminated in Early Miocene, and age of the NE trending magnetic lineations with NW-SE seafloor spreading is about 20-16 Ma B.P. (magnetic lineation 6 to 5C).

INTRODUCTION

So far the spreading chronology of the South China Sea basin is still a problem to be debated. Taylor and Hayes (1980, 1983) dated the seafloor spreading from Mid-Oligocene to early Miocene (32-17 Ma B.P.) on the basis of magnetic lineation with the east-west direction in the mid-east of the basin. This suggestion has been supported by the data obtained afterwards and is getting more and more receivable.

During the Sino-French cooperative investigation in the South China Sea in 1985, a large number of new data were collected, including seabeam, gravity, magnetic, single channel seismic data and so on. According to those data the South China Sea has gone through two distinct phases of spreading since Mid-Oligocene. The chronological sequence of the two spreading phases is discussed below.

TOPOGRAPHIC CHARACTERISTICS OF THE CENTRAL RIDGE IN THE SOUTH CHINA SEA

Similar to an oceanic basin, the South China Sea has three large structural provinces, i.e., the central ridge, the abyssal plain and the continental margin. The seismic profile No. 9 in the southwest of the basin shows the features of three large structural provinces, but because of its later structural deposition, the central ridge has already been covered with sediments about several hundreds of meters in thickness (Fig.1), which means that the spreading activities have ceased.

By means of gravity, magnetic, seabeam and seismic reflection data, some synthetic geological and geophysical profiles of the central ridge have been plotted. These maps provide some significant evidences for researching in structural and topographic characters of the cen-

tral ridge.

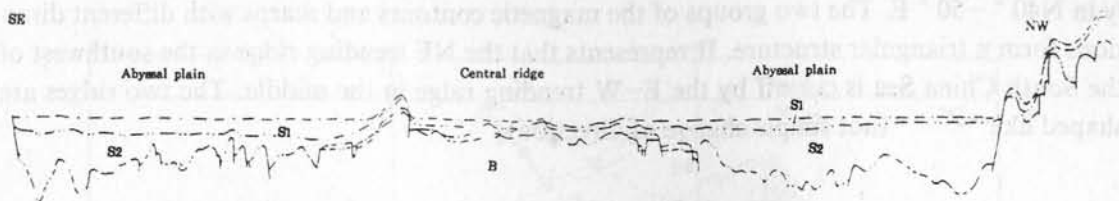


Fig.1 Seismic profile No.9 shows that the central ridge in the South China Sea has already been covered with sediments. S1—Horizontal seismic sequence, S2—Transparent sequence, B—Acoustic basement.

From Fig.2a and b, it can be seen that varieties of geologic and geophysical data are consistent with each other very well. Based on the comprehensive characteristics of geology and geophysics, the central ridges with two different directions in the axial region of the South China Sea can be distinguished. They cross each other, and form a complicated tectonic framework.

The seafloor scarps recorded by seabeam, magnetic lineations and the central rift valley observed on gravity and seismic profiles lie in NE trending in the axial region about 150 km wide between $117^{\circ} 30' E$ and Manila Trench. It indicates that the trend of northeastern section of the central ridge is in NE direction.

In the central part of the basin from $116^{\circ} E$ to $118^{\circ} E$, the structure of mid-section seems to be more complex. In this area exist some structures lying not only in E-W direction but also in NE and NW directions. However, according to the trends of seamount chain, gravity anomalies, magnetic lineations, central rift valley and seafloor scarps, its main structure still trends nearly in E-W direction. For example, the central rift valley drawn in Fig.2a by sawtooth lines with a N-S width of 90 km, the scarps and magnetic lineations located north of $15^{\circ} 40' N$ and south of $14^{\circ} 10' N$ are mainly E-W direction.

Fig.2b is a map of synthetic geological and geophysical profiles of southwest section of the ridge. Compared with the E-W trending ridge, its structural framework is more simple. All kinds of geological and geophysical features are basically in the same trend with the direction of $N40^{\circ} - 50^{\circ} E$ and are distributed symmetrically about its axis. Its central rift valley is about 30-40 km wide.

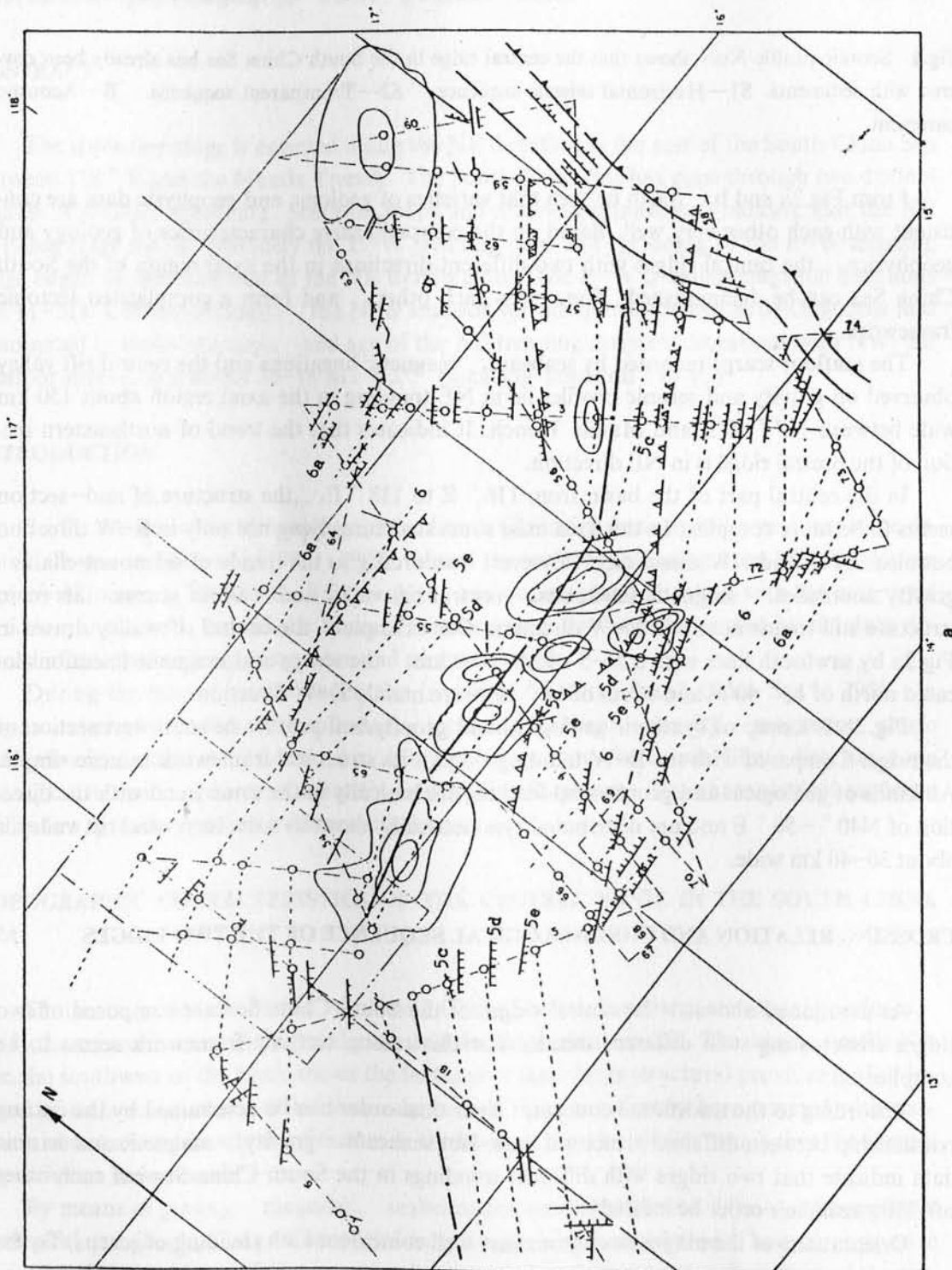
CROSSING RELATION AND CHRONOLOGICAL SEQUENCE OF THE TWO RIDGES

As mentioned above, the central ridges of the South China Sea are composed of two ridges crisscrossing with different trends. For this reason tectonic framework seems to be complicated.

According to the traditional concept, their time order can be determined by the cutting relationship between different structural lines. But seabeam, gravity, magnetic and seismic data indicate that two ridges with different trendings in the South China Sea cut each other off. How can their order be inferred?

Orientations of the magnetic contours are well coincident with trending of scarps. To the

north of $15^{\circ} 30'N$, they have a $N70^{\circ} - 80^{\circ} E$ trend and to its south, their trend are mainly in $N40^{\circ} - 50^{\circ} E$. The two groups of the magnetic contours and scarps with different directions form a triangular structure. It represents that the NE trending ridge in the southwest of the South China Sea is cut off by the E-W trending ridge in the middle. The two ridges are shaped like "7" (not simple change of direction).



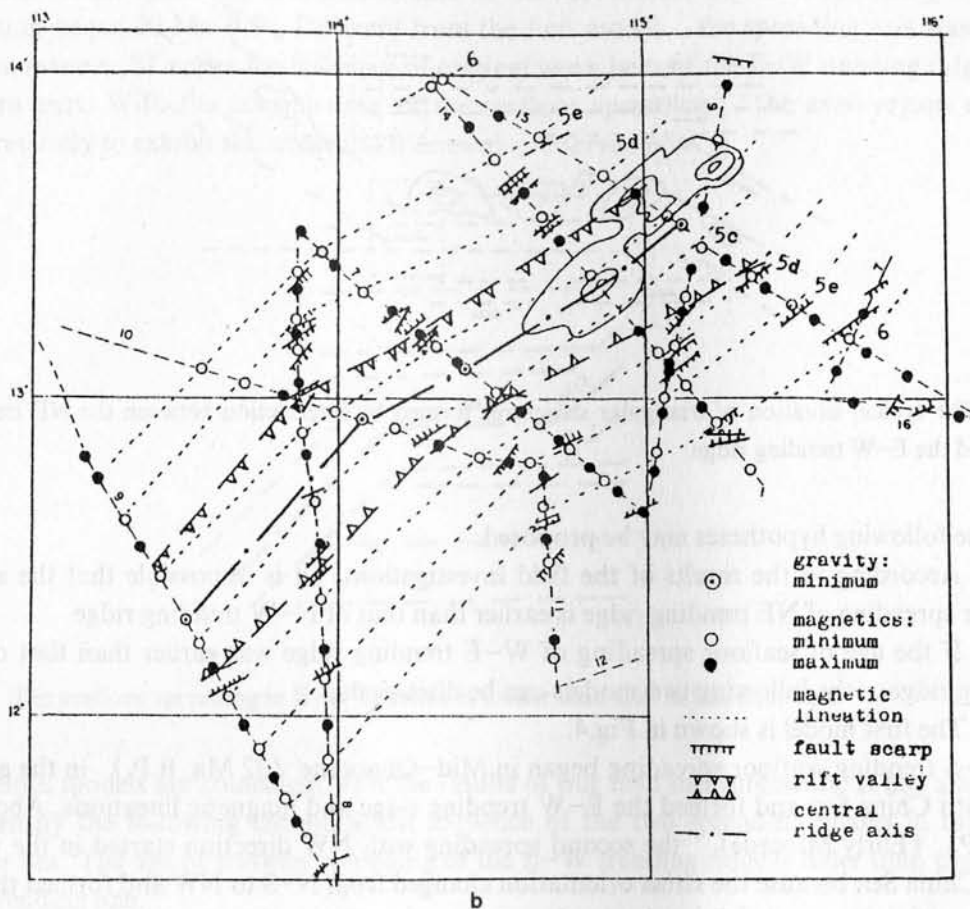


Fig.2 Structural direction of the central ridge of the South China Sea basin inferred from geology and geophysics.

The same phenomenon has been observed near $14^{\circ}30'N$, $117^{\circ}E$, where the south wing of the E-W trending ridge meets with the southeast wing of the NE trending ridge in the southwest of the South China Sea, forming the second triangular structure “ ∇ ” which implies that the NE trending ridge cuts off the E-W trending one. Similarly, there also exist two triangular structures at $16^{\circ}N$, $118^{\circ}E$ and $14^{\circ}30'N$, $118^{\circ}30'E$, where the NE trending ridge in the northeast of surveyed area is cut off by the E-W trending ridge in the middle (Fig.2a).

The typical tectonic pattern of the South China Sea discussed above is shown in Fig.3, where the E-W trending ridges cut and cross the NE trending ones and four triangular structures are formed. This geometric pattern of structure provides a valuable basis for studying the spreading chronological sequence of the South China Sea.

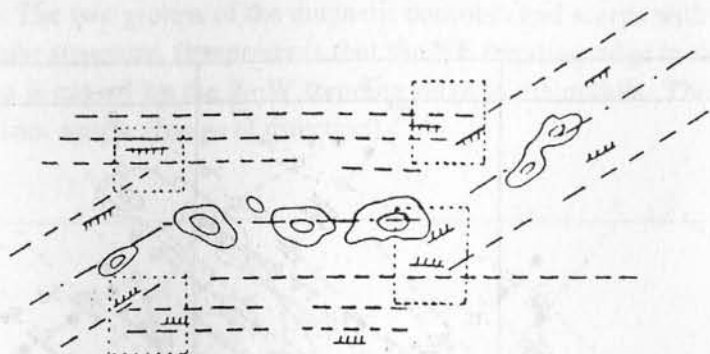


Fig.3 The typical situation of triangular structures formed by intersection between the NE trending ridge and the E-W trending ridge.

The following hypotheses may be proposed:

1. According to the results of the field investigation, it is impossible that the age of seafloor spreading of NE trending ridge is earlier than that of N-W trending ridge.

2. If the age of seafloor spreading of W-E trending ridge was earlier than that of NE trending ridge, the following two models can be discussed.

a. The first model is shown in Fig.4.

N-S trending seafloor spreading began in Mid-Oligocene (32 Ma B.P.) in the east of the South China Sea and formed the E-W trending ridge and magnetic lineations. About 20 Ma B.P. (Early Miocene), the second spreading with NW direction started in the whole South China Sea because the stress orientation changed from N-S to NW and formed the NE trending ridge. It extended from the northeastern part to the southwestern basin of the South China Sea and cut obliquely the early E-W structure line. The NW trending seafloor spreading widened the new ridge axis and pushed the EW trending fabric away from the ridge axis. Because numerous right-lateral transform faults with $N140^{\circ}E$ trend were off-set progressively eastwards, general trend of the mid-section of the central ridge turned to E-W direction.

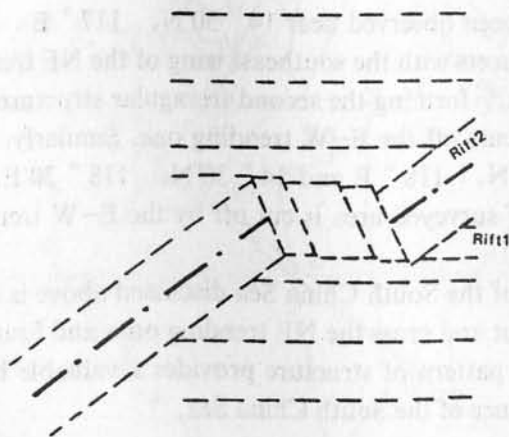


Fig.4 The seafloor spreading in E-W direction is earlier than that in NE direction.

b. The second model is shown in Fig.5.

The earlier spreading is similar to that of the first model. The later spreading with NW direction began 20 Ma B.P.. Different from the first model, the spreading axis was shaped like an inverse "S" under the influence of original weak belts of the E-W trending ridge in the eastern part. With the continuation of the seafloor spreading, the axial region widened progressively to exhibit the structural framework observed now.

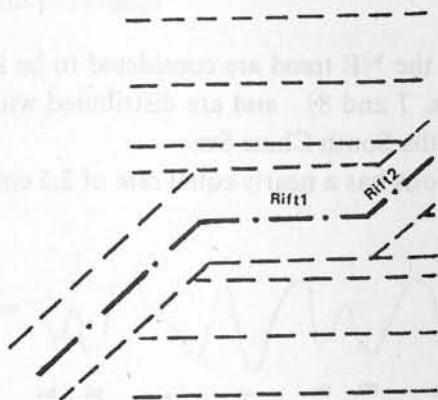


Fig.5 The seafloor spreading in E-W direction is earlier than that in NE direction.

Both models are coincident with the results of our field measurements. It has allowed us to identify the following chronological sequence of the two spreading phases in the South China Sea. The age of seafloor spreading of the E-W trending ridge is older than that of the NE trending one.

MAGNETIC LINEATIONS AND SEAFLOOR SPREADING AGE

The seafloor spreading age determined just by using magnetic lineations is often nonunique, especially in the case of a small number of magnetic anomalies. To avoid this shortage, both geological and geophysical data have been used to identify the structural geometric pattern and crisscrossing relationship of the central ridge in the South China Sea and to provide a definition of spreading age of the ridges. Then the magnetic profiles have been compared repeatedly and carefully with the theoretical models. The spreading ages of the two ridges have been dated as follows:

1. The magnetic lineations of the E-W trend in the middle part of surveyed area are identified as 5D through 6A (Fig.6) and are distributed symmetrically about the E-W trending seamount chain near 15° N. The magnetic lineations earlier than 6A, have not been compared with the theoretical profile because they are located beyond the surveyed area.

Anomaly 6A away from the ridge axis has a typical anomaly shape and keeps better symmetry about the spreading center and good continuity in the different profiles. However, it is a little difficult to identify anomalies 5D through 5E.

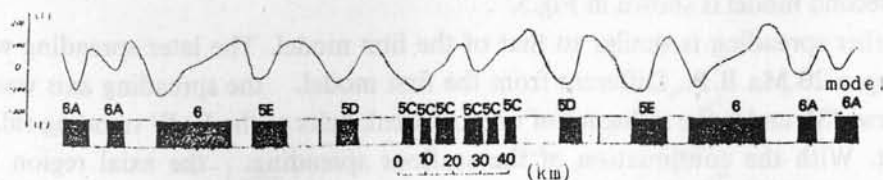


Fig.6 The theoretic model of the E-W trending magnetic lineations

2. The magnetic lineations with the NE trend are considered to be in the sequence of 5C through 6 (16–20 Ma B.P., Figs. 7 and 8) and are distributed within the southwestern part and the areas east of 118° E in the South China Sea.

3. The spreading in both directions has a nearly equal rate of 2.5 cm / a (half spreading rate).

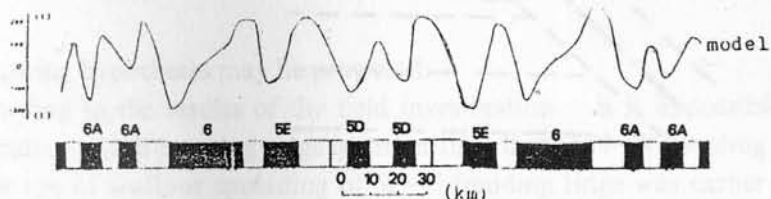


Fig.7 The theoretical model of the NE trending magnetic lineations (in the southwest of the South China Sea basin).

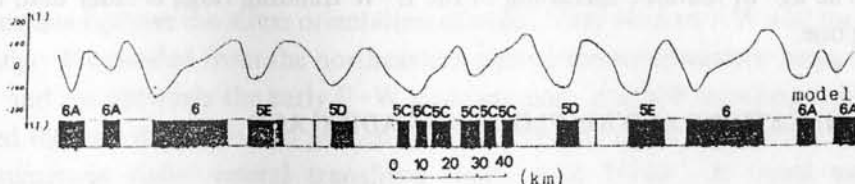


Fig.8 The theoretic model of the NE trending magnetic lineations (to the east of 118° E).

CONCLUSIONS

1. On the basis of the geological and geophysical data collected in the South China Sea, the topographic characteristics and the crisscrossing patterns of the two ridges have been studied in detail. It is possible to infer reliably the spreading chronological sequence of the two ridges and then to determine the spreading age of the NE trending ridge in the southwestern basin.

2. In order to avoid nonuniqueness of the spreading chronology, the spreading ages of the two ridges are identified not only by the magnetic lineations, but also by the spreading chronological sequence.

3. The crisscrossing relations between the different trending structures in the axial area have been explained contentedly by the current theory of seafloor spreading. It might be diffi-

cult to explain the phenomenon in the traditional concept.

ACKNOWLEDGEMENT

The Sino-French cooperative investigation is very successful in the South China Sea. It has provided us valuable information. Here we greatly appreciate our French friends, Dr. G. Pautot and his colleagues.

RECONSTRUCTIONS OF THE SOUTH CHINA SEA FROM STRUCTURAL DATA AND MAGNETIC ANOMALIES

ANNE BRIAIS¹⁾ & GUY PAUTOT²⁾

1) *Institute of Oceanographic Sciences Deacon Laboratory, Wormley, Godalming, Surrey GU8 5UB, U.K.*

2) *IFREMER, Centre de Brest, 29273 Plouzane, France*

ABSTRACT

We combine the interpretation of Sea Beam bathymetric data and seismic reflection profiles in the axial part of the South China Sea basin with an updated identification of the magnetic anomalies, to develop a model of opening of the basin. These interpretations show that oceanic spreading was very asymmetric and included at least one ridge jump. We show that anomalies in seafloor fabric, characterized by large differences in basement depth and roughness, are related to a decrease in spreading rate after the ridge jump, from about 2.5 cm / yr to 1.5 cm / yr. Spreading most probably started in the eastern part of the basin, and propagated towards the southwest in two major steps, at time of anomaly 6b-7, and at time of anomaly 6-5e. Each step is correlative of a variation of the ridge orientation, from nearly E-W to NE-SW, and of a variation in the spreading rate. The spreading stopped synchronously along the ridge, at about 15.5 Ma. From computed fits of magnetic isochrons, we calculate 10 finite poles of rotation at the times of magnetic anomalies 11 to 5c. We propose a model of opening of the basin in Oligo-Miocene time, in which oceanic spreading in South China Sea, as revealed by magnetic anomalies, and extension on its continental margins are mostly related to extrusion of the Indochina block as a consequence of the collision of India with Asia.

INTRODUCTION

In models of evolution of the basin based on structural observations on the margins and on directions of the magnetic anomalies in the eastern part of the sea, most of the oceanic crust is created with a N-S direction of spreading (Holloway, 1982; Taylor and Hayes, 1980, 1983; Ru and Pigott, 1986). A model deduced from indentation experiments on plasticine invokes the opening of the basin as a terminal pull-apart at the end of the Red River Fault, then a major left-lateral strike-slip fault allowing for the extrusion of Indochina (Tapponnier *et al.*, 1982; Peltzer and Tapponnier, 1988). To choose between these two types of model, we take yet another point of view by performing a quantitative reconstruction of the opening of the basin using the powerful constraint provided by magnetic isochrons and seafloor fabric.

We present the interpretation of the structural data, describe our preferred identification and fits of magnetic lineations, and analyze the evolution of the spreading in space and time. We investigate how extension in the basin is consistent with deformation of the adjacent

continental lithosphere. We then propose a model of opening of the basin deduced from this comparative analysis. The analyses and results presented here have been published or are in press elsewhere.

STRUCTURAL ANALYSIS

In 1985, Sea Beam bathymetric data and seismic reflection profiles were collected in the axial region of the South China Sea and on the western margin during two cruises on the R/V Jean Charcot. The fabric of the 150–200 km wide axial part of the basin is characterized by a blocky basement, with normal faults striking $N50^{\circ} E \pm 15^{\circ}$ and fracture zones striking $N140^{\circ} E \pm 15^{\circ}$, covered by sediments about 0.5 s thick (two way travel time) in the east (Fig. 1) (Taylor and Hayes, 1983; Pautot *et al.*, 1986, 1990; Briaies *et al.*, 1989). To the southwest, the fabric is homogeneous, characterized by NE striking normal fault scarps and NW striking scarps (Pautot *et al.*, 1986; Briaies *et al.*, 1989). The average sediment thickness there is higher than in the east and reaches 1–1.5 seconds (Taylor and Hayes, 1983; Pautot *et al.*, 1990). The location of the extinct spreading axis is given by a symmetry in the tilting of the blocks (Fig. 1). North and southeast of the inferred relict spreading axis, the sediment thickness increases significantly to 1.5–2 seconds and the basement becomes much smoother (Taylor and Hayes, 1983). The differences in the seafloor fabric suggest that the characteristics of the spreading varied during the opening of the basin. The axis of the ridge between $115^{\circ} 50' E$ and $118^{\circ} 45' E$ is very irregular and invaded by large seamounts forming the Scarborough seamounts chain. Most of the seamounts are elongated both in the direction of the ridge segments ($N50^{\circ} E$) and in the direction of the transform faults ($N140^{\circ} E$), suggesting that their growth was controlled by the preexisting fractures in the oceanic crust. The fabric observed in the 150–200 km wide axial part of the basin suggests that the axial area, in the east and in the southwest, was created about a spreading axis consisting of segments trending NE–SW (Pautot *et al.*, 1986), probably dissected by numerous fracture zones in order to maintain the global E–W orientation of the axis (Briaies *et al.*, 1989). Off axis some scarps trending $N70^{\circ}–80^{\circ} E$ are observed, but the structural information about the seafloor fabric is not as precise as in the axial area (Fig. 1). To the north or south, correlation of magnetic anomalies between closely-spaced profiles represents the only constraint on the evolution of the direction of extension with time.

MAGNETIC ISOCHRONS AND EVOLUTION OF THE SPREADING IN THE SOUTH CHINA SEA

This section presents the identification of the magnetic anomalies and the resulting set of magnetic lineations, and the history of the oceanic part of the basin deduced from the fit of the magnetic isochrons. The evolution of the spreading in the basin is characterized by the instability of the spreading center at the beginning of the history, and by the propagation of the oceanic spreading towards the southwest in the second half of the history.

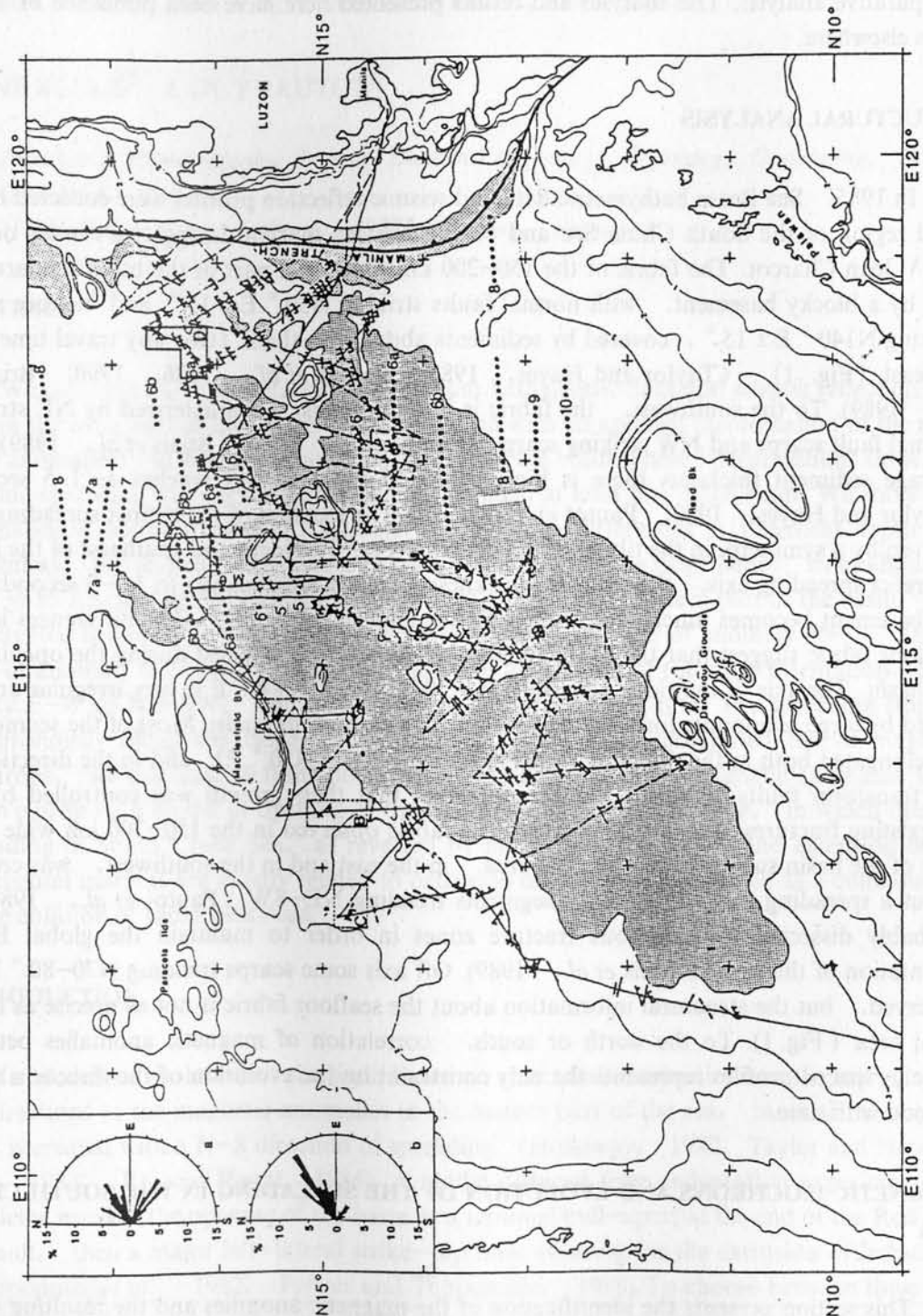


Fig.1 Structural observations in the central part of the South China Sea. Bathymetry in kilometers. Normal faults observed on Sea Beam swaths are located along tracks (barbed lines). Structural trends not interpretable as normal faults are represented by dashed segments. Dotted lines are magnetic anomaly lineations, and white lines the fracture zones interpreted by Taylor and Hayes (1983). From Briais *et al.*, 1989.

Data and methods

We compiled the magnetic data from the Charcot cruises with a map of closely-spaced magnetic profiles compiled by Chen (1987), by digitizing the magnetic anomaly profiles from the map, to get a set of data that could be easily projected and processed. In addition to these data, we have used Conrad and Vema profiles (Taylor and Hayes, 1980, 1983; Hayes *et al.*, 1987).

To identify the magnetic anomalies, we use a magnetic time scale which is a slightly modified version of that described by Patriat (1983). From the interpreted magnetic lineations, we fit the isochrons and calculate the poles and angles of rotation. A finite pole of rotation is obtained for each magnetic anomaly. For each stage between successive anomalies, we also calculated from the corresponding finite poles the rates and orientation of spreading for two points which now belong to the relict spreading axis.

The Old Crust in the Eastern and Northwestern Basins: Instability of the Spreading Center (32–25 Ma)

Our interpretation of the longest magnetic profiles from the eastern subbasin confirms the Late Oligocene–Early Miocene age (Taylor and Hayes, 1980, 1983) of the sequence of anomalies. The oldest lineations which could be identified are anomaly 11 in the north and 10 in the south (Fig.2). The beginning of the spreading in the South China Sea probably occurred about discontinuous spreading centers since anomaly 11 is not uniformly observed to the north. Just after anomaly 10 the spreading stops in the northwestern subbasin but continues in the eastern part. The isochron drawn for anomaly 10 suggests that the ridge was segmented and that the segments were globally disposed en echelon (Fig.2). Anomaly 8 appears as the most continuous isochron, and the discontinuities observed at anomalies 9 and 10 no longer exist. The direction of the spreading at this time is close to N–S.

An asymmetric distribution of the magnetic anomalies in the northern and southern off axis oceanic areas implies that the ridge jumped to the south just after anomaly 7 (Fig.2). The magnetic interpretation also suggests a variation in half spreading rate at the time of the jump, from 2.4–3.0 cm / yr before the jump, to 1.9 cm / yr for the youngest ridge, which may be correlated to a variation in the morphology of the ridge system. Spreading at intermediate rate created relatively smooth basement, and spreading at slower rate created rougher basement. Such a variation of the fabric of the oceanic crust with the spreading rate has been observed on the Mid-Indian Ridges (< 1 to 3cm / yr) (Tapscott *et al.*, 1980; Patriat, 1983).

The Axial Eastern Area and the Southwestern Basin: Propagation of the Spreading Center (25–15.5 Ma)

In the eastern area, after the ridge jump, the magnetic anomalies appear to be more and more disrupted when approaching the axis (Fig.2). For the sequence of anomalies 6b to 6 to the east, the magnetic sequences are rather symmetrical, with a half spreading rate of 1.8–2.0cm / yr. West of 117.30° E, the best fitting model involves a small ridge jump to the

south at anomalies 6a–6 time, and a half spreading rate of 1.9 cm / yr. The 6b lineation is well defined in the east, with the configuration inherited from the ridge jump. To the southwest, it only forms short segments which separates Macclesfield Bank from Reed Bank, corresponding to a first step of propagation.

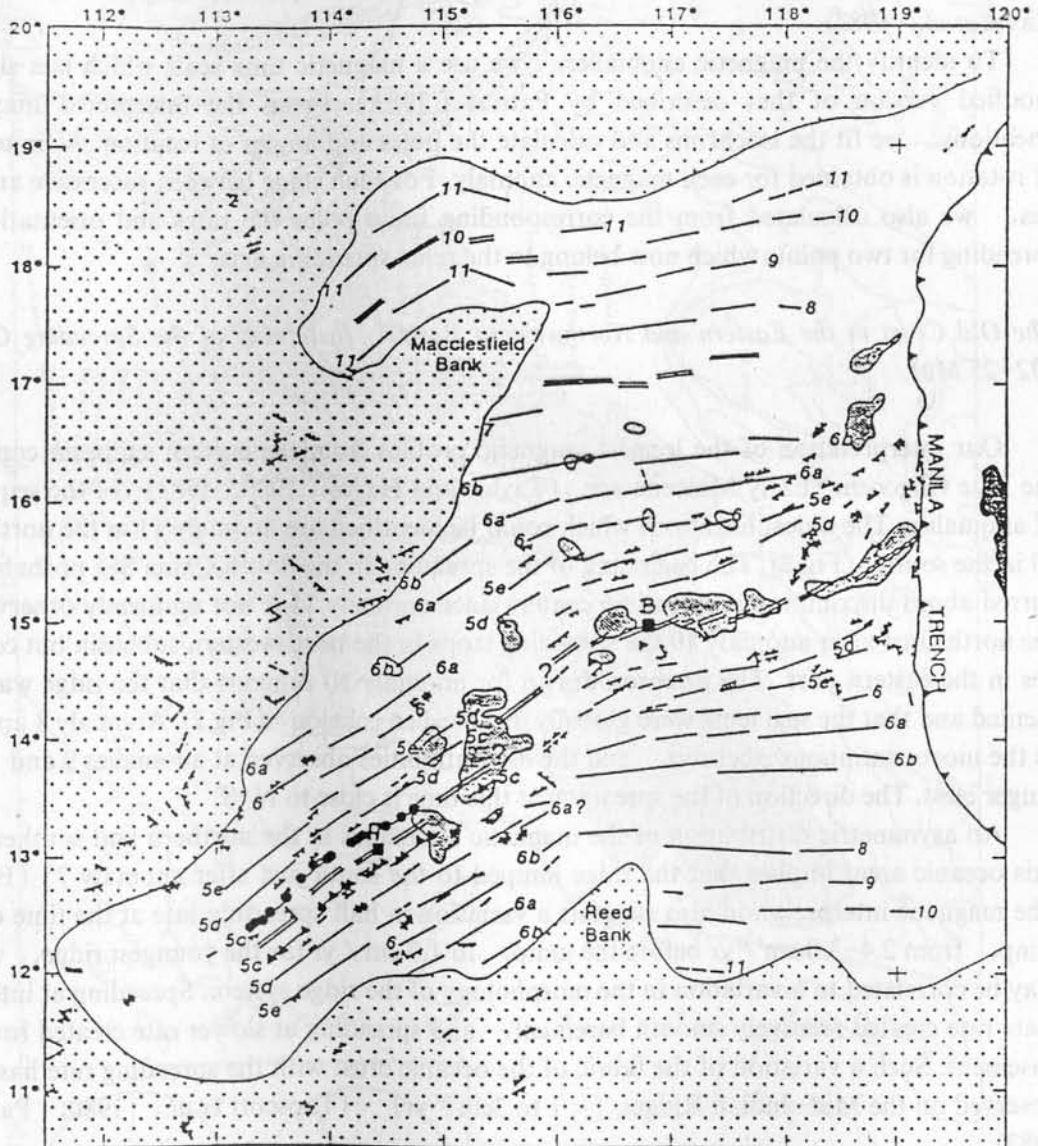


Fig.2 Magnetic lineations in the South China Sea. Also shown are tectonic features observed on Sea Beam bathymetry data, showing orientation of fault scarps in the axial area. From Biais *et al.*, 1991.

In the southwestern part of the basin the major problem is the small width of the basin (< 300 km) which implies that the match with a synthetic magnetic anomaly model is not unique. The sequences of anomalies 5c–6b, 8–13, 13–19 and 21–26 from the reversal time

scale provide synthetic profiles which resemble the observed magnetic profiles. The reconstruction corresponding to the sequence of anomalies 8 to 13 revealed a very discontinuous system of ridge segments between the east and the southwest. In our preferred model, we chose the sequence of anomalies 5c to 6b, most often with a spreading rate of 1.5 cm/yr on both sides of the axis. Several profiles, however, display a prominent asymmetry, which we model as a small ridge jump to the south at the time of anomaly 5d.

The distribution of the anomalies implies that the ridge propagated towards the southwest in two major steps, first at the time of anomalies 7–6b, then at the time of anomaly 6, when the ridge reached its longest extent (Fig. 2). The computed direction of spreading between the ridge jump and anomaly 6 is NNW–SSE, becomes closer to N–S around anomaly 6, and changes back to NW–SE after anomaly 5e. The time of anomaly 6 is also correlative of a reorientation of the spreading segments in the east, from $N80^{\circ}E$ to $N60^{\circ}E$ in average. The ridge is segmented by transform faults which appear to be more numerous to the east than to the southwest. In both areas, however, the Sea Beam bathymetry does not show as many fracture zones as suggested by the offset of the magnetic isochrons (Fig. 2). This suggests that the spreading axis may be offset along zones of rather diffuse deformation, which do not clearly appear in the Sea Beam bathymetry (Pautot *et al.*, 1990).

The last episode of spreading in the very axial eastern part of the basin may only be deduced from the model obtained for anomalies 6–5d, which suggests a cessation of spreading near anomaly 5c, assuming a constant spreading rate between anomaly 5d and the cessation of spreading. In the southwestern part, the end of the spreading is observed just after anomaly 5c. The simplest conclusion is thus that the cessation of spreading in the South China Sea was synchronous all along the ridge, just after anomaly 5c, at 15.5 Ma.

DISCUSSION: IMPLICATIONS OF THE RECONSTRUCTIONS OF THE SOUTH CHINA SEA FOR THE TERTIARY EVOLUTION OF SOUTHEAST ASIA

Because of the present-day orientation of extensional troughs north and south of the basin, and of the relict spreading axis, all models of opening of the South China basin agree on the existence of a major transcurrent system to the west of the basin. From a kinematic point of view, it is possible either to terminate the rift system against a right lateral strike-slip fault following the Vietnam margin, and to detach only small fragments of the Chinese continent along it (Holloway, 1982; Taylor and Hayes, 1983; Ru and Pigott, 1986), or to propagate left lateral strike-slip faults from the continental area into the rift system (e.g. Tapponnier *et al.*, 1986; Peltzer and Tapponnier, 1988). These two hypotheses differentiate the two types of kinematic models of evolution of the basin. They represent two mechanisms of extension in the South China Sea involving distinct driving forces: the subduction of an old oceanic crust in the North Borneo Trough in the first type of model, and the relative motion of the Indo–China Block with respect to the South China one in the second type of model. Since the existence of the North Borneo subduction zone is questionable, and the left-lateral motion along the Red River fault has been evidenced by field work, we favour the second type of model.

Compatibility of the Oceanic Spreading with a Left Lateral Motion along the Red River Fault

Models involving large horizontal displacements on strike-slip faults (e.g. Tapponnier *et al.*, 1986; Peltzer and Tapponnier, 1988) may be tested by estimating the relative motion of the blocks on either sides of the faults, the age of movement on these faults, and the compatibility of extensional deformation in the basins in which the faults end.

Field work in the region of the Ailao Shan and Dian Cang Shan along the Red River fault zone has recently evidenced that left lateral ductile shear along this zone caused the formation of a gneissic belt, characterized by vertical foliation and subhorizontal lineation. Radiometric dating of leucogranites in two locations along the belt yields an age of 23.0 ± 0.2 Ma for the ductile deformation along the shear zone (Scharer *et al.*, 1990). The kinematics and first estimates of the ages of the deformation along the Red River fault thus confirms that this fault system represents a major boundary between the China block and the Sunda block.

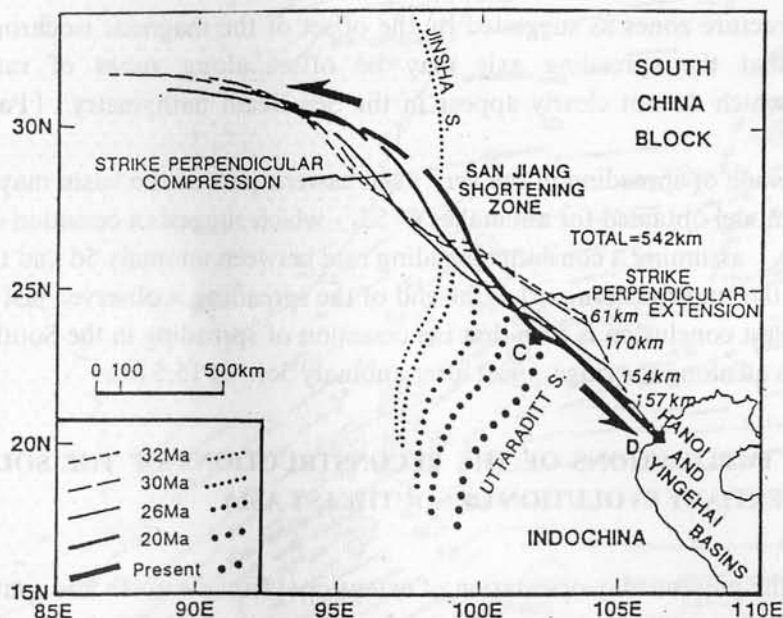


Fig.3 Successive positions, relative to South China, of the present-day Red River fault trace, assumed to be fixed to Indo-China, during seafloor spreading in the South China Sea. The positions are computed using the finite poles of rotation and the parameters of motion computed from the fit of the magnetic isochrons. Blocks south of the spreading ridge are assumed to have been part of the Sunda shelf at all time since 35 Ma. From Briais *et al.*, 1991.

We test the kinematic compatibility of the opening of the oceanic area with the movement on the Red River fault by assuming that block on the southern side of the South China Sea spreading ridge (Dangerous Grounds, Reed Bank) remained rigidly attached to Indo-China during the formation of oceanic crust in the basin. Fig. 3 represents the successive traces of the fault at the time of anomalies 11, 10, 8, 7 (ridge jump), 6 and at present, considered to represent the northeastern boundary of the Indo-China Block moving with respect to fixed South China. Overall, the positions of these successive traces sug-

gest that much of the spreading of the South China Sea may be related to transcurrent movement on this fault. The displacement resulting from the magnetic isochrons reconstruction seems fully compatible with the intense sinistral shear recently documented along the Ailao Shan and Dian Cang Shan and with the age of that shear. The total amount of left-lateral motion computed from the reconstruction (560 km) is also compatible with that estimated from the displacement of the Jinsha-Uttaraditt suture (Tapponnier *et al.*, 1986), which is seen to be completely restored on Fig. 3.

Principal Phases in the Opening of the South China Basin

Considering the compatibility of the motion along the Red River fault with the parameters of the spreading, we propose a model of opening of the basin in which the successive rotations of the Indochina block and its structural markers with respect to the China block are those computed to fit the magnetic isochrons (Fig.4).

The Beibu Gulf (Tonkin Gulf) and Yinggehai (west of Hainan Island) troughs clearly appear as pull-apart basin that opened at the southern tip of the Red River fault system (Tapponnier *et al.*, 1986). Expanding spread profiles performed on the South China margin reveal that the crust beneath the Xisha trough is anomalously thin, suggesting that this trough is also a failed rift, where no oceanic crust was created. We infer that a system of basins disposed en echelon formed at the tip of the Red River fault. In the eastern most basins only oceanic crust was generated (Fig.4a).

The instability of the oceanic spreading until anomaly 6 (20 Ma) may be interpreted as a consequence of the propagation of the Red River fault system to the south, leading to a more diffuse rifting between the termination of the strike-slip fault system and the spreading center (Fig.4). We infer that mechanical constraints, which are difficult to deduce from the present-day observed pattern of rifts and ridges, prevented the ridge to jump in a single step at the time of anomaly 10, and maintained Macclesfield Bank and Reed Bank continental blocks close together during the entire period from anomaly 10 to anomaly 7.

At anomaly 6 time an almost steady state was probably reached for the strike-slip-spreading system, implying that the propagation of the spreading system stops (Fig.4). We suggest that the cessation of spreading is related to the cessation of motion on the Red River fault, itself inferred to be due to the change in the stress field as the Indian indenter bypasses the Southeast Asian continental block (Tapponnier *et al.*, 1986; Peltzer and Tapponnier, 1988).

CONCLUSION

Clearly, the model of opening presented here and the choice of hypotheses from which it derives are not unique. Nevertheless, because the Red River-Ailaoshan fault zone is a large Oligo-Miocene discontinuity that extends into the South China Sea, with hundreds of kilometers of left-lateral displacement, the positive test of compatibility between displacement on this fault and seafloor spreading in that sea implies that it has played a leading role in the formation and evolution of the sea. Moreover, in our reconstruction, the total rotation of the Indochina block with respect to the South China Block is about 12° , which is close

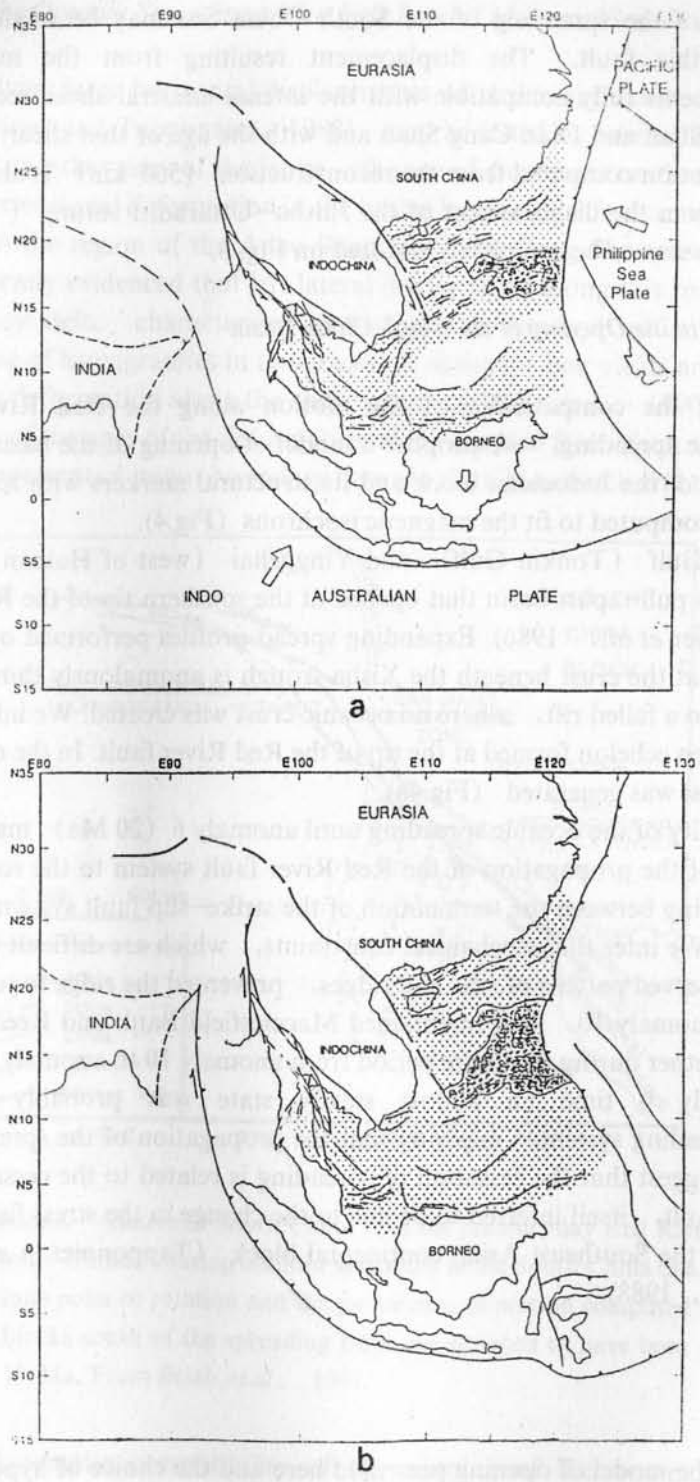


Fig.4 Reconstructions of the South China Sea. a: At the time of anomaly 7 (26 Ma), after the jump and at the beginning of the propagation of the spreading ridge. b: When spreading stopped just after anomaly 5c (15.5 Ma). From Briais *et al.*, 1991.

to the rotation measured from paleomagnetic samples ($20 \pm 10^\circ$, Achache *et al.*, 1983). The scenario presented here therefore accounts for most of the existing observations within the basin and in continental regions surrounding it to the north and west.

REFERENCES

- Achache, J., V. Courtillot and J. Besse, 1983: Paleomagnetic constraints on the Late Cretaceous and Cenozoic tectonics of southeastern Asia. *Earth Planet. Sci. Lett.*, 63, 123–136.
- Briaux, A., P. Tapponnier and G. Pautot, 1989: Constraints of Seabeam data on crustal fabrics and seafloor spreading in the South China Sea. *Earth Planet. Sci. Lett.*, 95, 307–320.
- Briaux, A., P. Patriat and P. Tapponnier, 1991: Interpretation of magnetic anomalies and reconstructions of the South China basin: Implications for the Tertiary evolution of Southeast Asia. submitted to JGR.
- Chen, S. (Compiler), 1987: Magnetic profiles. Atlas of Geology and Geophysics of the South China Sea, 1 : 2000000, Map Publishing House of Guangdong Province.
- Hayes, D.E., S. Spangler, W. Zeng, B. Yao, B. Taylor and A. Briaux, 1987: Age and evolution of the South China Sea southwest subbasin (abstract). *EOS Trans.*, AGU Annual Meeting, 68, 1496.
- Holloway, N.H., 1982: North Palawan Block, Philippines: Its relation to Asian mainland and role in evolution of the South China Sea. *Amer. Ass. Petro. Geol. Bull.*, 66, 9, 1355–1383.
- Patriat, P., 1983: L'évolution du système de dorsales de l'Océan Indien. Thèse d'Etat, Université Paris VI.
- Pautot, G., C. Rangin, A. Briaux, P. Tapponnier, P. Beuzart, G. Lericolais, X. Mathieu, J. Wu, S. Han, H. Li, Y. Lu and J. Zhao, 1986: Spreading direction in the Central South China Sea. *Nature*, 321, 150–154.
- Pautot, G., C. Rangin, A. Briaux, P. Tapponnier, J. Wu, S. Han, H. Li, Y. Lu and J. Zhao, 1990: The axial ridge of the South China Sea: A seabeam and geophysical survey. *Oceanologica Acta*, 13, 2, 129–143.
- Peltzer, G. and P. Tapponnier, 1988: Formation and evolution of strike-slip faults, rifts and basins during the India-Asia collision: An experimental approach. *J. Geophys. Res.*, 93, 15095–15117.
- Ru, K. and J.D. Pigott, 1986: Episodic rifting and subsidence in the South China Sea. *Amer. Ass. Petro. Geol. Bull.*, 70, 1136–1155.
- Scharer, U., P. Tapponnier, L. Lacassin, P.H. Leloup, D. Zhong and S. Zhi, 1990: Intraplate tectonics in Asia: A precise age for large-scale Tertiary movement along the Ailao Shan-Red River shear zone, China. *Earth Planet. Sci. Lett.*, in press.
- Tapponnier, P., R. Lacassin, P.H. Leloup, U. Scharer, D. Zhong, H. Wu, X. Liu, S. Ji, L. Zhang and J. Zhong: Tertiary left-lateral movement and metamorphism along the Ailao Shan-Red River shear zone. *Earth Planet. Sci. Lett.*, in press.
- Tapponnier, P., G. Peltzer, and R. Armijo, 1986: On the mechanics of the collision between India and Asia. *Collision tectonics*, M.P.C. a. A.C. Ries(ed.), *Geol. Soc. Spec. Publ.*, 19, 115–157.
- Tapponnier, P., G. Peltzer, A.Y. Le Dain, R. Armijo and P. Cobbold, 1982: Propagating extrusion tectonics in Asia: New insights from simple experiments with plasticine. *Geology*, 10,

611-616.

- Tapscott, C.R., P. Patriat, R.L. Fisher, J.G. Sclater, H. Hoskins and B. Parson, 1980: The Indian Ocean triple junctions. *J. Geophys. Res.*, 85, 4723-4739.
- Taylor, B. and D.E. Hayes, 1980: The tectonic evolution of the South China Basin. The tectonic and geologic evolution of southeast Asian seas and islands, D.E.Hayes(ed.), *Geophys. Monogr. Ser.*, 23, A.G.U., Washington, D.C., 89-104.
- Taylor, B. and D.E. Hayes, 1983: Origin and history of the South China Basin. The tectonic and geologic evolution of southeast Asian seas and islands, Part 2, D.E.Hayes(ed.), *Geophys. Monogr. Ser.*, 27, A.G.U., Washington, D.C., 23-56.

DOCKING OF THE PHILIPPINE MOBILE BELT AGAINST THE EURASIAN MARGIN: CLOSURE OF THE SOUTH CHINA SEA

MANUEL PUBELLIER¹⁾, NICOLAS PINET²⁾ & CLAUDE RANGIN¹⁾

- 1) *Laboratoire de Geotectonique, Université Pierre et Marie Curie., 4.pl. Jussieu, 75252 Paris Cedex 05, France*
- 2) *Institut de Géodynamique URA-CNRS 1279, Université de Nice - Sophia Antipolis, Parc Valrose, 06034 Nice, France*

ABSTRACT

The eastern border of the South China Sea is the Manila Trench which separates it from the Philippine Mobile Belt. This mobile belt includes: 1) continental fragments dragged along the Eurasian margin during the docking of the Philippine Arc, 2) large part of the Philippine arc carried by the Philippine plate, and 3) ophiolitic bodies originated in marginal basins.

Comparative study along the western edge of the Philippine plate allows to identify and date the mechanisms of its accretion along the Eurasian margin, and to propose the southward migration of the collision. Tectonic and stratigraphic evidence of tectonic activity is of the late Middle Miocene in Taiwan. Docking of the Philippine arc is of late Middle Miocene in Luzon, of Late Miocene (10 My) in the Visayas (central Philippines) and of Pliocene in Mindanao, while it is not yet completed in the Molucca Sea. The docking is rapidly followed by a renewal of subduction along the eastern edge of the South China Sea, the Sulu Sea and the Celebes Sea, showing a southward progression from 11 My, in the Manila Trench to 7 My in the Negros Trench and Late Pliocene to Pleistocene in the Celebes Sea. Subduction reversal from the western subduction front (Manila, Negros and Sulu trenches) to the Philippine Trench, is associated with the beginning of activity along the Philippine Fault S.S. and begins in late Pliocene. Decoupling between the Philippine plate and the Eurasian plate presently occurs along the Philippine Trench and the Philippine fault system.

INTRODUCTION

Most of the circum Pacific mountain belts have been formed by progressive accretion of microblocks, mainly of island arc origin against continental margins, as a result of oblique convergence (Jones, 1982; Howell *et al.*, 1985). The present-day geodynamic framework of western Pacific shows numerous examples of association of subduction zone and strike-slip fault in oblique convergence region where a mechanism of partioning is often discussed (Fitch, 1972; Woodcock, 1986; Aurelio *et al.*, 1990). The motion seems to be absorbed by two parallel decoupling zones; one of transcurrent faulting (component paralel to the trench) and one of underthrusting (component normal to the trench). The neotectonic evolution of Philippines and the eastern border of the South China Sea is closely

related to the activity of the Philippine Mobile Belt and is helpful model to understand the history of an intraoceanic volcanic belt, its migration and docking against a continental margin. Therefore, our study was extended further south all the way down to Mindanao in the southernmost Philippines (Fig.1).

GEOLOGICAL SETTING AND KINEMATICS

The oblique convergence of the Philippine plate relative to the Eurasian plate (Seno, 1977, Cardwell et al., 1983; Seno and Maruyama, 1984) has been accommodated by large strike-slip (Karig, 1983; Karig *et al.*, 1986) and collision zones (Rangin *et al.*, 1985). The orogenic belt that resulted from this tectonic framework (Fig.1) extends from Taiwan (Stephan *et al.*, 1986), Luzon where both strike-slip and shortening have occurred (Bachman *et al.* 1983), Mindoro and Panay (Irving, 1950; Rangin *et al.*, 1985, Marchadier and Rangin, 1990), to Mindanao (Hawkins *et al.*, 1985) and the Molucca Sea (Moore and Silver, 1983). Evidences of Miocene strike-slip deformation were found by microtectonic analysis of the metamorphic rocks of the Philippine arc (Geary and Kay, 1989) or of the basin edges in Luzon, Mindoro (Bachman, 1983; Maletterre *et al.*, 1988), and Mindanao (Pubellier *et al.*, 1990). Among these faults, the Philippine Fault is a neotectonic feature (Barrier *et al.*, 1990; Aurelio *et al.*, 1990), whose history is linked to the subduction along the Philippine Trench. However, some older faults crosscut the mobile belt and may be related to the collage of terranes of Philippine plate affinity to continental fragments rifted away from mainland China. They are namely from north to south: Vigan-Aggao Fault (Pinet and Stephan, 1990), the West Luzon Shear (Karig, 1983) in Luzon, the Marinduque Fault in Central Philippines and the Daguma-Cotabato fault zone in Mindanao.

Presently, the NW-SE convergence is partly absorbed by the subduction along the Manila Trench which corresponds to the eastern boundary of the South China Sea (Fig.1). Eastward subduction along the Manila Trench (Taylor and Hayes, 1980; Lewis and Hayes, 1984) is imaged by a steeply dipping Wadati-Benioff zone well defined by dense seismicity to depth of more than 200 km (Cardwell *et al.*, 1980; Hamburger *et al.*, 1983). This active margin is anchored both north in the Taiwan and south in the Mindoro collision zones (Ho, 1979; Rangin *et al.*, 1985; Marchadier and Rangin, 1990).

In this paper, we will focus on timing of arc activities and tectonic events all along the former plate boundary, using stratigraphic, radiochronologic and structural data throughout the Philippine Mobile Belt.

GEOLOGY OF THE PHILIPPINE MOBILE BELT

Two major composite terranes can be differentiated on the basis of their stratigraphic record (Fig.1). An eastern one, on the margin of the Philippine plate, is dominated by an oceanic and island arc basement on which an Eocene and Oligocene volcanic arc is developed. Neogene clastic basins controlled by N and NW faults were deposited above the arc. A

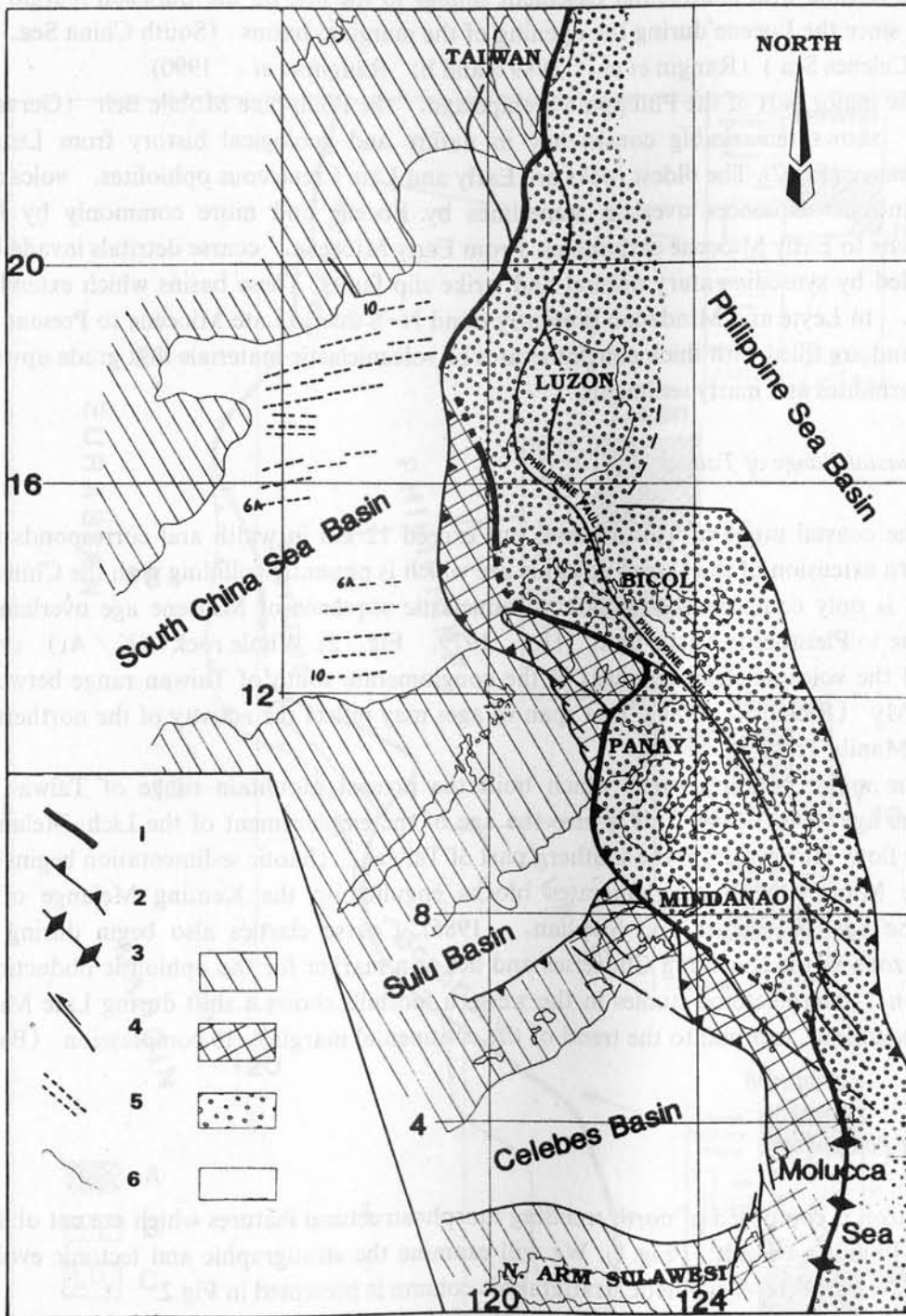


Fig.1 Overview of the plate boundary between the Philippine plate and the Eurasian plate. 1. Major tectonic contact between rocks of Eurasian and Philippine affinities (terranes boundary). 2. Subduction zones. 3. Apex of the double verging subduction of the Molucca Sea. 4. Strike-slip fault. 5. Magnetic anomalies of the South China Sea. 6. Limit of continental and oceanic crust of the marginal basins. 7. Eurasian margin fragments. 8. Continental fragments dragged along the collision zone. 9. Philippine arc (western edge of the Philippine plate). 10. Marginal or back-arc basins.

western terrane with continental basement similar to the one on the Eurasian margin is distended since the Eocene during the opening of the marginal basins (South China Sea, Sulu Sea, Celebes Sea) (Rangin *et al.*, 1989 a and b; Rangin *et al.*, 1990).

The major part of the Philippine archipelago, the Philippine Mobile Belt (Gervasio, 1966) shows remarkably consistency in nature and geological history from Luzon to Mindanao (Fig.2). The oldest rocks are Early and Late Cretaceous ophiolites, volcanic arc and plutonic sequences overlain sometimes by Eocene and more commonly by Upper Oligocene to Early Miocene carbonates. From Early Miocene, coarse detritals invade basins controlled by synsedimentary normal and strike slip faults. These basins which extend from Luzon, to Leyte and Mindanao presently trend N-S due to Late Miocene to Present shortening and are filled with thick conglomerates of volcanoclastic materials that grade upward to finer turbidites and marly sediments.

The Coastal Range of Taiwan

The coastal range of Taiwan does not exceed 12 km in width and corresponds to the northern extension of the Luzon volcanic arc which is presently colliding with the China margin. It is only composed of a thick volcanoclastic sequence of Miocene age overlain by a Pliocene to Pleistocene clastic unit (Ho, 1979, Fig. 2). Whole rock (K/Ar) isotopic ages of the volcanic clasts engulfed in the conglomerate south of Taiwan range between 16 and 4 My (Richard, 1986). This span of ages may reflect the activity of the northern part of the Manila Trench

The major collision event which built the present mountain range of Taiwan is of Pliocene age (4-3 My). This is also the age of the emplacement of the Lichi Melange by gravity flow. However, in the southern part of Taiwan, chaotic sedimentation begins in the Middle Miocene with conglomerates blocks engulfed in the Kenting Melange of Late Miocene age (Pelletier and Stephan, 1985). Coarse clastics also begin during NN6 Nannozone in the Ssujung Chi series and act as a marker for the ophiolitic obduction. In addition, microtectonic studies in the western foothills shows a shift during Late Miocene from extension (normal to the trend of the continental margin) to compression (Barrier, 1985).

Luzon (Philippines)

Luzon is composed of north trending morphostructural features which are cut obliquely by the Philippine Fault (Fig.1). We will examine the stratigraphic and tectonic evolution along two transects. A synthetic stratigraphic column is presented in Fig.2.

In the north, the core of the Luzon Central Cordillera anticlinorium exhibits magmatic rocks which belong to two distinct arcs. 1) The early arc bear ages from Lower to Upper Oligocene. Large coarse clastics of Oligocene-Miocene boundary (Klondyke Formation) come from mass wasting along the arc and are covered by late Early Miocene to early Middle Miocene platform limestones (Balce *et al.* 1981). 2) The latter, which is still active (Maletterre *et al.*, 1988), started by late Middle Miocene and its products are clearly recorded in sedimentary basins (Ilocos and Cagayan basins) on both sides of the Cordillera (Pinet and Stephan, 1990). This second arc is related to the subduction of the South

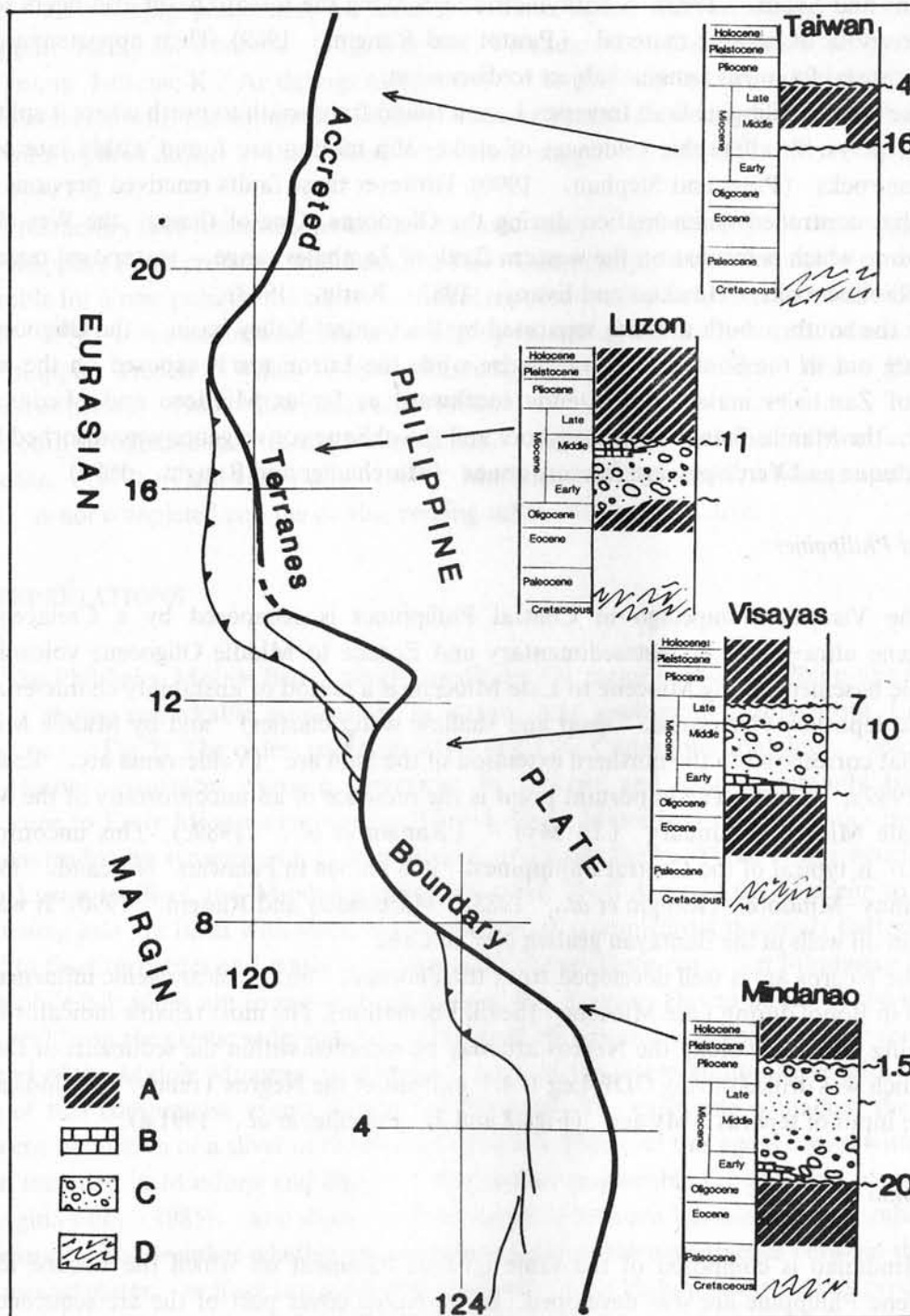


Fig.2 Schematic trace of the collision zone with synthetic stratigraphic logs in Taiwan (Coastal Range), Luzon, Visayas (Central Philippines) and Mindanao; A: Volcanic rocks; B: Limestone; C: Coarse and fine clastics; D: Ophiolitic and metavolcanic basement.

China Sea and strictly parallels the Manila Trench. Other rocks present on the western coast of Luzon includes ultra-mafic and mafic series. They range in age from Late Cretaceous in the northwest tip of the island, to Eocene in the Zambales massif (Karig, 1983; Hawkins and Evans, 1983). A bathymetric high along the forearc basin also bears seismic characteristics of oceanic material (Pautot and Rangin, 1989). Their appartenance to a unique crustal fragment remains subject to discussion.

The active Philippine fault traverses Luzon Island from south to north where it splits into several splays. Stratigraphic evidences of strike-slip motion are found within late Middle Miocene rocks (Pinet and Stephan, 1990). However these faults reactivated previous structures that controlled sedimentation during the Oligocene. One of these, the West Luzon shear zone which is located on the western flank of Zambales range, juxtaposed micashists and ophiolitic rocks (Hawkins and Evans, 1983; Karig, 1983).

In the south, both arcs are separated by the Central Valley basin, the Oligocene arc cropping out in the Southern Sierra Madre while the Luzon arc is exposed on the eastern flank of Zambales massif and extends southward as far as Mindoro and Marinduque. There, the Manila Trench passes onshore and the oblique convergence was absorbed by the Marinduque and Verde passage fracture zones (Marchadier and Rangin, 1990).

Central Philippines

The Visayan archipelago in Central Philippines is composed by a Cretaceous to Paleogene ultra-mafic, metasedimentary and Eocene to Middle Oligocene volcanic and plutonic basement. Early Miocene to Late Miocene is a period of unstability characterized by various deposits (terrestrial, deep and shallow water clastics) and by Middle Miocene tuffs that correspond to the northern extention of the Sulu arc (Valderrama arc, Rangin *et al.*, 1989 a, b & c). The important point is the presence of an unconformity at the Middle and Late Miocene boundary (10 My) (Rangin *et al.*, 1989c). This unconformity (Fig.2) is typical of the Central Philippines; it is known in Palawan (Fricaud, 1984), and Panay-Mindoro (Rangin *et al.*, 1985; Marchadier and Rangin, 1990). It was also found in oil wells in the Bantayan graben NW of Cebu.

The Negros arc is well developed from the Pliocene, but a volcanogenic influence is recorded in Bohol during Late Miocene (Sevill Formation). The most reliable indicator for the beginning of activity along the Negros arc may be recorded within the sediments of the Sulu Sea which was drilled during ODP Leg 124, in front of the Negros Trench. They indicate the sudden input of tephras 7 My ago (Figs.2 and 3, Pubellier *et al.*, 1991 a).

Mindanao

Mindanao is composed of the same igneous basement on which the Eocene to Late Oligocene Philippine arc was developed. Large basins cover part of the arc sequence. The Agusan-Davao Basin consists of an elongated structural trough, 250 km long and trending roughly north-south (Teves *et al.*, 1951; Irving, 1950; Ranneft *et al.*, 1960).

The Cotabato basin separates the East and the Central Mindanao tectonostratigraphic terranes in a presumed suture zone which is believed to be related to the docking of the eastern oceanic terrane (Philippine Mobile Belt-Halmahera arc) against the western continen-

tal terrane (Zamboanga–Daguma) in a strike–slip environment (Mitchell *et al.*, 1986; Pubellier *et al.*, 1991 b, Fig.2). The collision phase is emphasized by en echelon folds in Early Pliocene sandy marls which are sealed by horizontal Pleistocene (?) sediments. Therefore, the docking phase may be located in time earlier than in central and northern Philippine during the Pliocene (Figs.2 and 3). Volcanic series that postdate the docking are very young. Isotopic K / Ar datings range from 1.5 to 0.25 My in central Mindanao. Volcanoes associated with the subduction in the Cotabato Trench are young but undated. Correlation with tephra drilled in the Celebes Sea would suggest an age of 2.5 My (Pubellier *et al.*, 1991 b).

Preliminary field observations and neotectonic study of the drainage pattern suggest that the Philippine Fault crosscuts and folds the Plio–Quaternary carbonates and is probably responsible for a new pulse in the coarse detrital input in the Agusan–Davao basin (Pubellier *et al.*, 1990). It is a neotectonic feature probably related to the newly born subduction along the Philippine Trench (Willis, 1987; Ranneft *et al.*, 1960; Allen, 1962; Philippine Bureau of Mines, 1963; Bischke *et al.*, 1990).

South of Mindanao, in the Molucca Sea, the collision between the two facing arcs (Roeder, 1977; Cardwell *et al.*, 1980; McCaffrey *et al.*, 1980; Moore and Silver, 1983) is not completed and the double verging subduction is still active.

INTERPRETATIONS

The Philippine Mobile Belt, which constitutes the major part of the Philippine archipelago, shows remarkable consistency in nature and geological history from Luzon to Mindanao (Fig.2). The oldest rocks are Early and Late Cretaceous ophiolites, volcanic arc and plutonic sequences overlain sometimes by Eocene and more commonly by Upper Oligocene to Early Miocene carbonates. During Early Miocene, coarse clastics invade basins controlled by synsedimentary normal and strike slip faults. These basins which extend from Luzon to Bicol and Mindanao presently trend N–S due to Late Miocene to Present shortening and are filled with thick conglomerates of volcanoclastic materials that grade upward to finer turbidites and marly sediments. In the southern part, on Mindanao Island, the mobile belt series are found on both sides of the Agusan–Davao basin. In the northern part on Luzon the clastic sedimentation is replaced by volcanic and volcanoclastic series since the end of the Middle Miocene. In Taiwan, most of the interpretation agree with the existence of two compressive events during the Neogene. The early one is marked the Middle Miocene obduction of a sliver of the South China Sea. However this age is coeval with the collision recorded in Mindoro and Panay, that is also responsible for ophiolite emplacement (Rangin *et al.*, 1985), and due to the convergence between Eurasia and Australia. We, therefore cannot decipher whether this event is related to the convergence between the major continental plates, or if we can invoke the influence of the Philippine Arc in this process.

Southward migration of the collision (Fig.3) can thus be invoked. Major tectonic features in Taiwan and Luzon begin in latest Middle Miocene or Late Miocene, during Late Miocene (10 My in the Visayas (Central Philippines) and during the Pliocene in Mindanao, while it is not yet completed in the Molucca Sea. Similarly, docking is rapidly followed by a renewal of subduction along the eastern edge of the South China Sea, the Sulu

Sea and the Celebes Sea, showing a southward progression from 11 My in the Manila Trench to 7 My in the Negros Trench and Late Pliocene to Pleistocene in the Celebes Sea (Fig. 4). Subduction reversal from the western subduction zones to the Philippine Trench is contemporaneous with the beginning of activity along the Philippine Fault S.S. that initiated by Late Pliocene (Barrier *et al.*, 1990). Two major kinds of strike-slip faults are observed. Some are related to the accretion process during the docking of the Philippine plate (paleo Vigna-Aggao Fault and West Luzon Shear in Luzon, Marinduque and Sibuyan-Verde Passage fault in the northern Visayas, and Daguma-Cotabato fault in Mindanao) and others are due to the shear partitioning of the convergence vector between the Philippine and the Eurasian plates (Philippine Fault : Fitch, 1972; Barrier *et al.*, 1990). This transcurrent fault becomes a thrust fault with a minor strike-slip component in Taiwan (Longitudinal Valley Fault: Barrier, 1985).

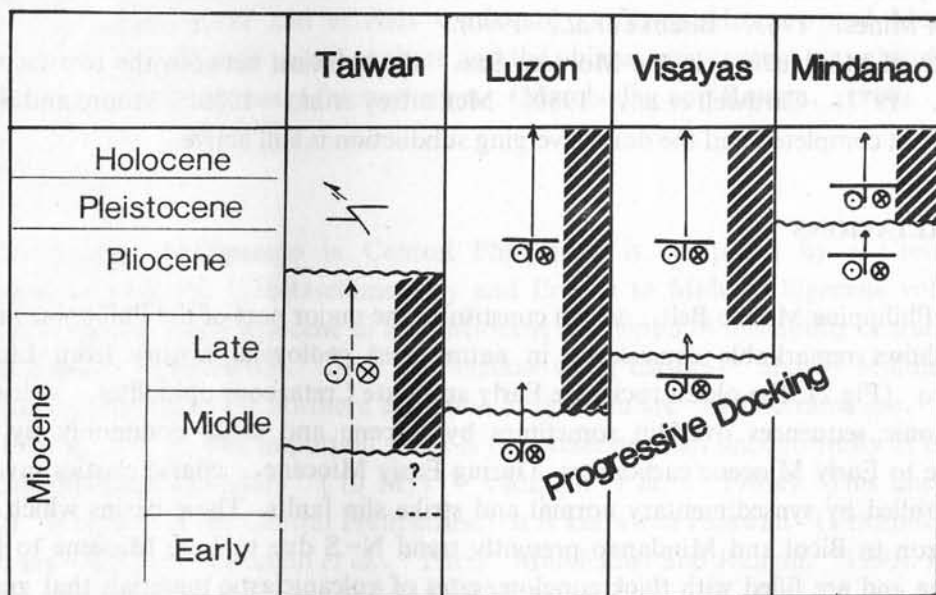


Fig.3 Time diagram of the major events of the Philippine Mobile Belt during Neogene. Solid lines pattern represents volcanic activity, and double circles occurrence of wrench faulting. Wavy lines indicates major unconformity.

Several types of fragments, therefore, compose the large belt that fringes the eastern boundary of the South China Sea. They include continental fragments dragged along the Eurasian margin during the docking of the Philippine Arc (Zambales Micaschists, eastern Mindoro and southwestern Mindanao), large part of the Philippine arc carried by the Philippine plate (Central Cordillera and southern Sierra Madre of Luzon), and ophiolitic bodies probably originated in southern marginal basins like the Celebes Sea (Zambales Ophiolites), or possibly from seamounts of the South China Sea itself accreted to the hanging wall of the Manila Trench (Pautot and Rangin, 1989).

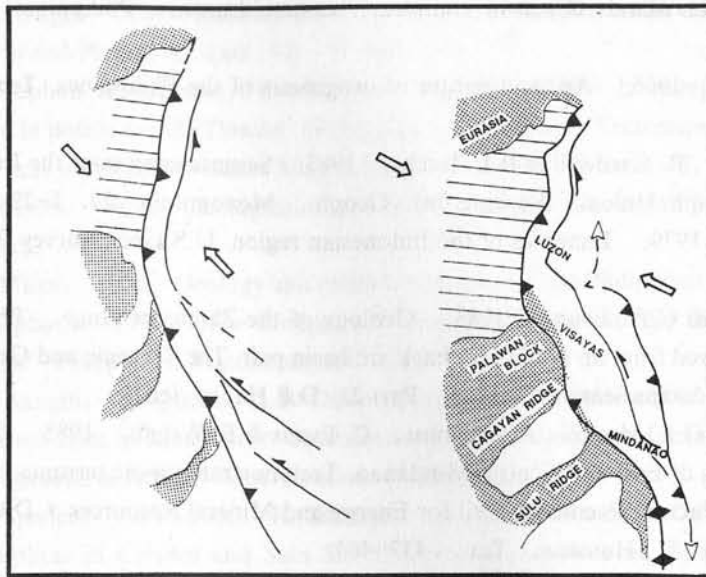


Fig.4 Evolution of the eastern Eurasian margin during the Miocene (A) and Plio-Pleistocene (B).

REFERENCES

- Allen, C.R., 1962: Circum-Pacific faulting in the Philippine-Taiwan region. *J. Geophys. Res.*, Washington, D. C., 67, 12, 4795-4812.
- Aurelio, M.A., C. Rangin, E. Barrier & C. Muller, 1990: Tectonique du segment central de la faille Philippine. *C.R. Acad. Sci. Paris*, t 310, Serie II, 403-410.
- Bachman, S.B., S. D. Lewis & W. J. Schweller, 1983: Evolution of a forearc basin. Luzon Central Valley, Philippines. *Am. Ass. of Petrol. Geol.*, 67, 7, 1143-1162.
- Balce, G.R., R.Y. Encina, A. Momongan & E. Lara, 1981: Geology of the Baguio district and its implication on the tectonic development of the Luzon Central Cordillera. *Geol. and Paleon. of Southeast Asia*, 21, Univ. Tokyo Press.
- Barrier, E., 1985: Tectonique d'une chaîne de collision active : Taiwan. *These de Doctorat d'Etat*, No. 85-29, Paris, France.
- Barrier, E., P. Huchon, M. Aurelio, 1990: The Philippine fault : A key for Philippines kinematics. *Geology*, in press.
- Bischke, R.E., J. Suppe & R. Del Pilar, 1990: A new branch of the Philippine fault system from aeromagnetic and seismic data. *Tectonophysics*, 183, 243-265.
- Cardwell, R.K., B.L. Isacks & D.E. Karig, 1980: The spacial distribution of earthquakes, focal mechanism solutions and subducted lithospheres in the Philippine and northern Indonesian region. *The Tectonic and Geologic Evolution of Southeast Asian Seas and Islands*, D.E. Hayes (ed.), Geophysical Monograph, 23, Washington, D. C., 1-35.
- Fitch, T.J., 1972: Plate convergence, transcurrent faulting and internal deformation adjacent to Southeast Asia and western Pacific. *Jour. Geophys. Res.*, 78, 188-200.
- Fricaud, L., 1984: Etude géologique et structurale de la marge Ouest Palawan (Mer de Chine meridionale). Unpublished Thesis, Univ. Paris.
- Geary, E.E. & R. W. Kay, 1989: Identification of an Early Cretaceous ophiolite in the Camarines

- Norte-Calaguas islands basement complex, eastern Luzon, Philippines. *Tectonophysics*, 168, 109-126.
- Gervasio, F.C., 1966: Age and nature of orogenesis of the Philippines. *Tectonophysics*, 4, 379-402.
- Hamburger, M., R. Cardwell & B.L. Isacks, 1983: Seismotectonics of the Luzon Philippines region. *Am. Geoph. Union, Washington, Geoph., Monograph*, 27, 1-22.
- Hamilton, W., 1979: Tectonics of the Indonesian region. *U.S. Geol. Survey Prof. Paper*, 1078, 345p.
- Hawkins, J.W. & C.A. Evans, 1983: Geology of the Zambales range, Philippines Island : Ophiolite derived from an island arc-back arc basin pair. *The Tectonic and Geologic Evolution of the Southeast Asian Seas and Islands, Part 2*, D.E. Hayes (ed) .
- Hawkins, J.W., G.F. Moore, R. Villamor, C. Evans & E. Wright, 1985: Geology of the composite terranes of East and Central Mindanao. *Tectonostratigraphic terranes of the Circum-Pacific region; Circum-Pacific Council for Energy and Mineral Resources (D.G. Howell)*, *Earth Science Series*, 1, Houston, Tex., 437-463.
- Ho, C.S., 1979: Geologic and tectonic framework of Taiwan. *Memoir of the Geological Society of China*, 3, 57-72.
- Howell, D.G., D.L. Jones & E.R. Schermer, 1985: Tectonostratigraphic terranes of the Circum Pacific region. *Circum Pacific Council for Energy and Mineral Resources, Earth Sciences Series*, 1, 3-30.
- Irving, E. M., 1950: Review of Philippine basement geology and its problem. *Phil. Jour. of Science*, 79, 267-307.
- Jones, D.L., 1982: The growth of western North America. *Scientific Amer.* 247, 70-84.
- Karig, D. E., 1983: Accreted terranes in the northern part of the Philippine Archipelago, *Tectonics*, 2, 2, 211-232, Washington, D.C..
- Karig, D.E., D.R. Sarewitz, G.D. Haeck, 1986: Role of strike-slip faulting in the evolution of allochthonous terranes in the Philippines. *Geology, Boulder Co.*, 14, 852-855.
- Lewis, S.D. & D.E. Hayes, 1984: A geophysical study of the Manila Trench, Luzon, Philippines: Forearc basin structural and stratigraphic evolution. *J. Geophys. Res.*, 89, 9196-9214.
- Maletterre, P., J.F. Stephan, P. Andreieff, H. Bellon, J. Chorowicz, J.M. Boirat & G.R. Balce, 1988: The Southern Central Cordillera of Luzon: A multistage Upper Eocene to Pleistocene arc deformed on the northern end of the Philippine strike-slip fault. *International Symposium on the Geodynamic Evolution of Eastern Eurasian Margin, Abstracts, Paris, 13-20 September, 1988.*
- Marchadier, Y. & C. Rangin, 1990: Polyphase tectonics at the southern tip of the Manila Trench: Mindoro-Tablas Islands, Philippines. *Tectonophysics*, 183, 1-4, 273-288.
- McCaffrey, R., E.A. Silver & R.W. Raitt, 1980: Crustal structure of the Molucca Sea collision zone, Indonesia. *The Tectonic and Geologic Evolution of Southeast Asian Seas and Islands. Geophysical Monograph*, 23, Washington, D. C., 161-177.
- Mitchell, A.H.G., F. Hernandez & A.P. de la Cruz, 1986: Cenozoic evolution of the Philippine archipelag. *J. of SE. Asian Earth Sci., Great Britain*, 1, 1, 3-22.
- Moore, G.F. & E.A. Silver, 1983 : Collision processes in the northern Molucca Sea. D.E. Hayes (ed.), *The Tectonic and Geologic Evolution of Southeast Asian Seas and Islands, Geophysical Monograph*, 27, Washington, D. C., 360-372.

- Pautot, G. & C. Rangin, 1989: Subduction of the South China Sea axial ridge below Luzon (Philippines). *Earth and Planet. Sci. Lett.*, 92, 57–69.
- Pelletier, B., J.F. Stephan, R. Blanchet, C. Muller & H.N. Hu, 1985: L'émergence d'une zone de collision active à la pointe sud de Taiwan (Péninsule d'Engshun): Tectoniques superposées et mise en évidence d'une obduction Miocene Moyen. *Bull. Soc. Geol., France*, 8, 2, 161–171.
- Philippine Bureau of Mines, 1963: Geological map of the Philippines. Geological Survey Division, Manila, Philippines.
- Philippine Bureau of Mines, 1982: Geology and mineral resources of the Philippines. 406 p.
- Pinet N. & J.F. Stephan, 1990: The Philippine trench fault system in the Ilocos Foothills, northwestern Luzon, Philippines. *Tectonophysics*, 183, 207–224.
- Pubellier, M., C. Rangin, R. Quebral & B. Deffontaines, 1990: Where is the extension of the Molucca Sea collision zone in Mindanao? International Interdisciplinary Meeting at the Geological Society, "Orogenesis in Action" Abst. London. 18–20 April, 1990.
- Pubellier, M., P. Spadea, A. Pouclet, R. Solidum, A. Desprairies & H. Cambray, 1991 a: Correlations of tephra in Celebes and Sulu Sea Basins: Constraints on Geodynamics. *Proc. ODP, Sci. Results*, 124, College Station, TX (Ocean Drilling Program) in press
- Pubellier, M., R. Quebral, C. Rangin, B. Deffontaines, C. Muller, J. Butterlin & J. Manzano, 1991 b: The Mindanao collision zone, a soft collision event within a continuous neogene strike-slip setting. *Journal of SE Asian Earth Sciences Sp. Iss.*, in press.
- Rangin, C., J.F. Stephan & C. Muller, 1985: Middle Oligocene oceanic crust of the South China Sea jammed into Mindoro collision zone (Philippines). *Geology*, 13, 423–425.
- Rangin, C., E.A. Silver, et l'équipe du leg 124, 1989 a: Forages dans les bassins marginaux du S.E. Asiatique: résultats préliminaires du Leg 124 (O.D.P.).
- Rangin, C., M. Pubellier, L. Jolivet, 1989 b: Collision entre les marges de l'Eurasie et de l'Australie: un processus de fermeture des bassins marginaux du Sud-Est asiatique. *C.R. Acad. Sci. Paris*, t. 309, Serie II, 1223–1229.
- Rangin, C., C. Muller & H. Porth, 1989 c: Neogene geodynamic evolution of the Visayan region. On the Geology and Hydrocarbon Prospects of the Visayan Basin, Philippines, *Geol. Jahrbuch*, B, 70. H. Porth and C. H. Von Daniels (eds.).
- Rangin, C., L. Jolivet & M. Pubellier, 1990: A simple model for the tectonic evolution of Southeast Asia and Indonesian region for the past 43 My. *Bull. Geol. Soc. France*.
- Ranneft, T.S.M., R.M.J. Hopkins, A.J. Froelich & J.W. Gwinn, 1960: Reconnaissance geology and oil possibilities of Mindanao. *Amer. Asso. of Petr. Geol. Bull.*, 4, 529–568, Tulsa, Okla.
- Richard, M., 1986: Géologie et pétrologie d'un jalon de l'arc Taiwan-Luzon: L'île de Batan, Philippines. *These Université de Brest*, 339 p.
- Roeder, D., 1977: Philippine arc system—collision or flipped subduction zone? *Geology*, 5, 203–206.
- Seno, T. & S. Maruyama, 1984: Paleogeographic reconstructions of the Philippine Sea. *Tectonophysics*, Amsterdam, 102, 53–84.
- Seno, T., 1977: The instantaneous rotation vector of the Philippine Sea plate relative to the Eurasian plate. *Tectonophysics*, 42, 209–225.
- Silver, E.A. & I.C. Moore, 1978: The Molucca Sea collision zone, Indonesia. *J. Geophys. Res.*, Washington, D.C., 83, B4, 1681–1691.
- Stephan, J.F., R. Blanchet, C. Rangin, B. Pelletier, J. Letouzey & C. Muller, 1986: Geodynamic evolution of the Taiwan-Luzon-Mindoro belt since the Late Eocene.

Tectonophysics, 125, 245-268.

Taylor, B. & D.E. Hayes, 1980: The tectonic evolution of the South China Sea basin. Geoph. Monograph. Serie, Washington, D.C., 23, 89-104.

Teves, J.S., A.A. Vergara & N. Badillo, 1951: Report on the geologic reconnaissance of Agusan. Philippine Geologist, 5, 24-50.

Willis, B., 1937: Geologic observations in the Philippines Islands. Nat. Res. Council of the Philippines Bull, 13, 127p.

Wolfe, J.A., 1981: Philippine geochronology. J. Geol. Soc. of the Philippines, Manila, 35, 1-35.

Woodcock, N.H., 1986: The role of strike-slip fault systems at plate boundaries. Phil. Trans. R. Soc. London, 317, 13-29.

SPREADING AGES OF SUBBASINS IN THE SOUTH CHINA SEA AND THEIR RELATIONSHIP*

LU WENZHENG

Second Institute of Oceanography, SOA, Hangzhou, China

ABSTRACT

Based on reidentification of the magnetic data with other information, it is suggested that the history and mechanism of the formation of the central basin in the South China Sea are complicated and characterized by multiphase spreading. The northwestern subbasin is the oldest one in the South China Sea, and the southwestern subbasin the youngest while the spreading period of the eastern subbasin is the longest among all three subbasins.

INTRODUCTION

The fact that there are magnetic anomalies in the South China Sea has been generally accepted, but the formative time of these magnetic anomalies and the relationship among its three subbasins during their evolution were still the questions under debate.

On the basis of magnetic data of approximately 60000 km in the middle of the South China Sea, the author (1987) identified these magnetic lineations in the eastern and southwestern subbasins, and put forward a model of "three phases in two periods". In 1987 and 1988, the Second Institute of Oceanography, SOA of China and BGR of Germany jointly carried out some synthetic investigations of geology and geophysics with vessel "Sonne" to obtain a lot of new data. On the basis of reidentification of magnetic lineations, along with seismic, seabeam and rock information, this paper tries to modify the spreading model of the South China Basin.

CHARACTERISTICS OF MAGNETIC LINEATIONS OF SUBBASINS IN THE SOUTH CHINA SEA

The central basin of the South China Sea is shaped like a rhombus with water depth more than 3500 m and covers about 350000 km². By the boundary of 116° E, it can be divided into three subbasins, the eastern, northwestern and southwestern subbasin (Fig.1).

The Eastern Subbasin

Magnetic lineations are best developed in this area and mainly located between 12° 30' N and 18° 30' N, 116° E and 118° E. A group of magnetic anomalies with three peaks lies

* Project supported by National Natural Science Foundation of China.

symmetrically on two flanks of the seamount chain near 15° N. From no evident correlation between the magnetic anomaly and the seafloor topography, the magnetic anomaly resulted from the seafloor spreading.

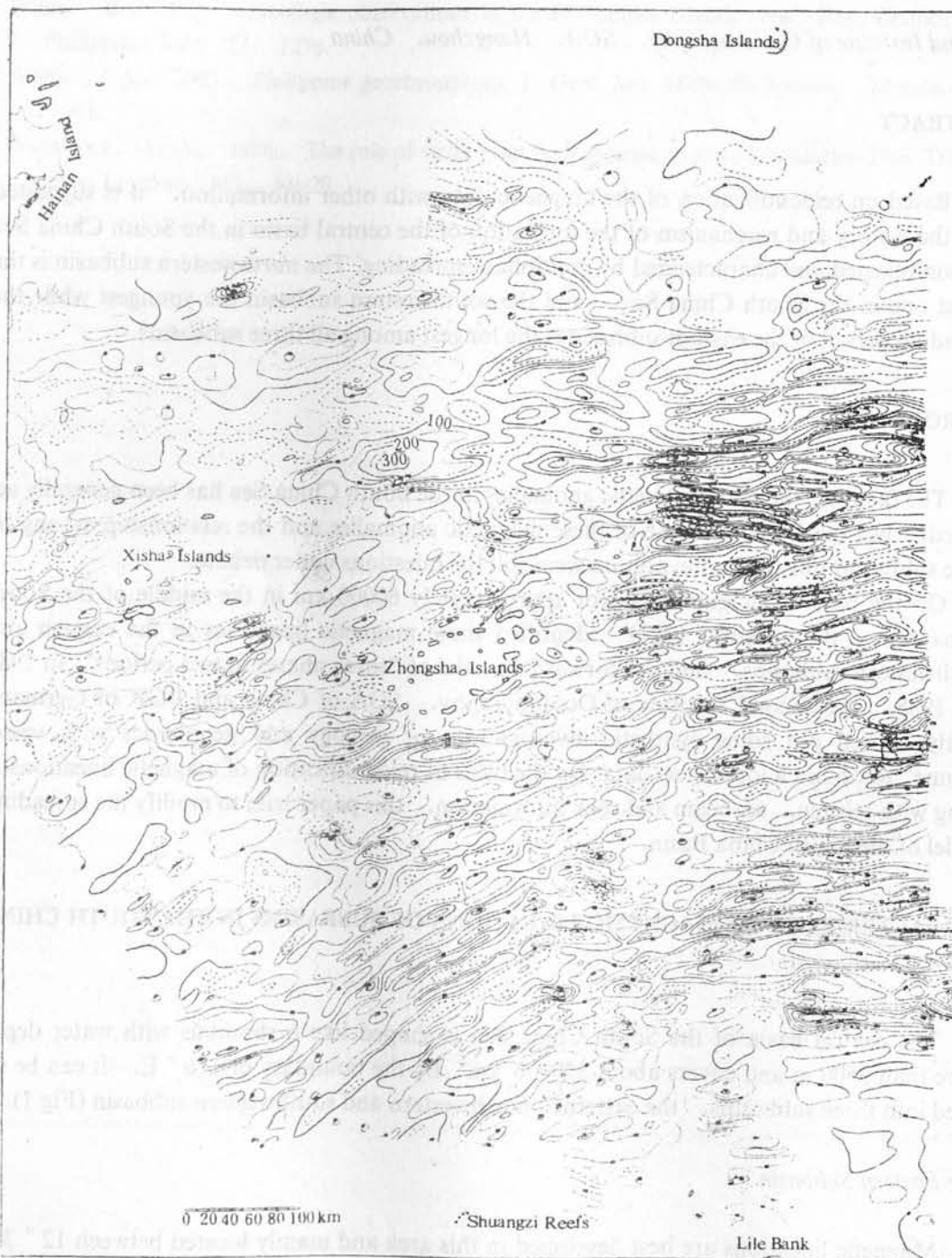


Fig.1 Contour map of magnetic anomalies (△T) in the central part of the South China Sea.

The magnetic lineations lying to the north of the spreading centre are about 400 km wide, while to the south of the spreading centre, their width is less than 300 km. This asymmetry shows that there is difference of the evolution history of two flanks.

The Northwestern Subbasin

Magnetic lineations in the subbasin are distributed only between $114^{\circ} 30' E$ and $115^{\circ} 30' E$, sitting symmetrically on both sides of the zone of negative anomalies. As shown on the seismic profile of So49-18, the zone of negative anomalies corresponds to seamount formed by the seafloor eruption and extends westwards to connect with the Xisha Trough. Though no rock of the seamounts was obtained during cruise So49 and So58, the magnetic parameters of rocks obtained from the seamounts in the eastern subbasin by the Lamont vessel "Vema" are forwarded to fit in with the magnetic anomalies satisfactorily. Therefore, we can suppose that the seamount should result from magmatism at relic spreading centre.

The Southwestern Subbasin

Magnetic lineations in this area strike in the NE direction and their amplitudes are generally about 200 nT and evidently less than those in the eastern subbasin. The subbasin can be divided into the eastern and western provinces, which is demarcated by $113^{\circ} 30' E$. The eastern province is more than 200 km wide, while the western province, gradually to be narrow eastwards, is less than 150 km wide. Seabeam and multichannel seismic demonstrate that a group of normal fault trending NE were developed in the area, and obviously the spreading centre has been offset sinistrally.

REIDENTIFICATION OF MAGNETIC ANOMALIES

Though there are many explanations about spreading of the eastern subbasin, Taylor and Hayes (1980) conclusion of 5d through 11 magnetic lineations in the eastern subbasin is generally accepted. Recognition of magnetic lineations in the southwestern subbasin is completely different from each other. The magnetic lineations in the southwestern subbasin are regarded as sequence M (He *et al.*), or 27-32 (Lu *et al.*, 1987). Some people proposed that the southwestern subbasin formed at the same stage as the eastern subbasin did or even later (Pautot *et al.*, 1986). The evolution history of the northwestern subbasin hasn't specially been discussed. By synthetically analysing new information, some recognitions about magnetic lineations of the three subbasins are given as follows.

The Eastern Subbasin

Taylor and Hayes (1980, 1983) thought that magnetic anomalies were developed symmetrically in both the south and north of the subbasin. Having analysed a series of profiles, we don't find 9 through 11 magnetic anomalies on the north flank of the Reed Bank. The anomaly No. 8 is a negative one with its amplitude of the anomaly No.9 being lower (Fig.2).

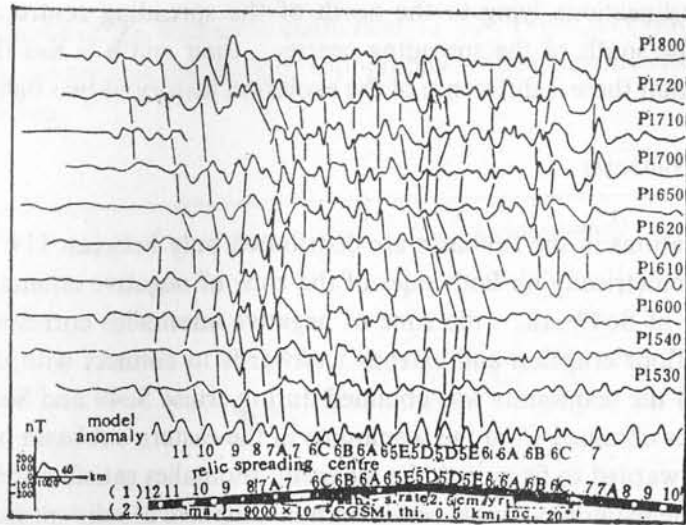


Fig.2 Correlation of the magnetic lineations in the South China Sea basin. (1) Anomaly No.; (2) Spreading model.

There is a normal fault at shot No. 10000 on the profile of So49-17, and the vertical displacement of basement is 600 m. On the south flank of the fault the surface of basement looks rough, while on the north flank it looks smooth. Features of seismic reflection are also different from each other. The fault is located right at the north boundary of the anomaly No.8, and there is no evident deformation and slip of sediment cover. All above indicate that the fault was formed at early stage, probably being a structural boundary.

Theoretical calculation shows that it is difficult for the displacement of 600 m to generate such a big magnetic anomaly. Difference between basement magnetism of both sides of the fault may be a much more important cause. Magnetization reaches 2 A/m on the north flank and 8 A/m on the south flank (Fig.3). They, as we think, were formed at different stages.

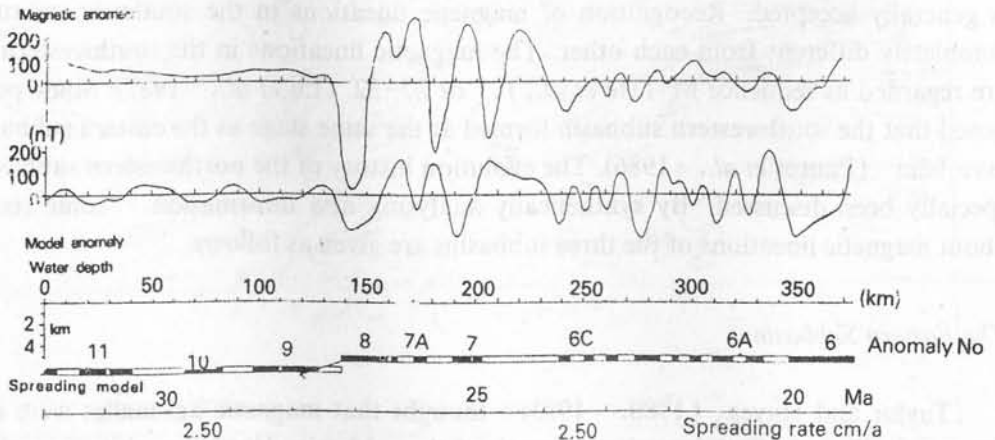


Fig.3 Correlation of magnetic lineations of SO49-17 profile

The Northwestern Subbasin

It is such a subbasin with thick sediment and thinned crust. The sedimental thickness generally is more than 2 km and its maximum is 3.5 km. Inverse computation of gravity shows that the crust thickness ranges from 7 to 8 km and the crust obviously is oceanic. According to the relationship between age and depth of basement, the northwestern subbasin is the oldest of the central basin in the South China Sea. Compared with a theoretical model, the anomaly No.9 though 11 (27–32 Ma B.P.) can be identified (Fig.4). Restricted by the Zhongsha and Xisha massif, it spread at a low rate (1.5 cm/a), and later stopped spreading and began subsiding, received thick sediment due to spreading of the southwestern subbasin.

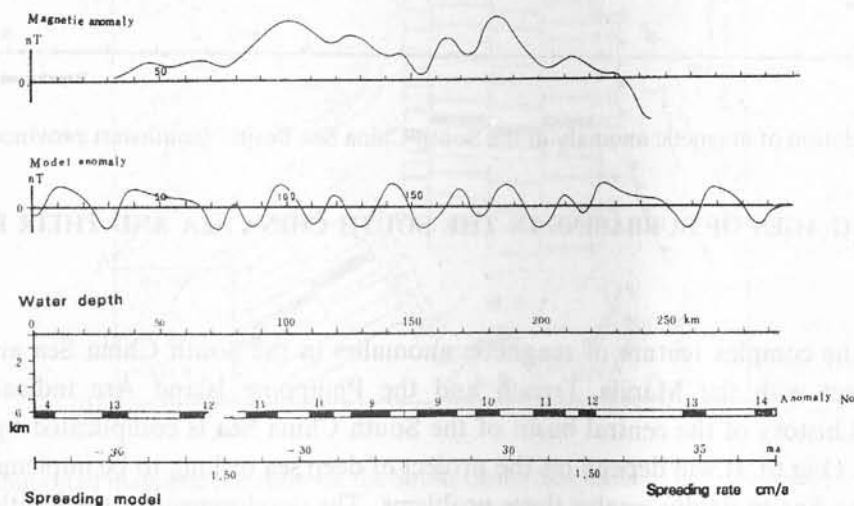


Fig.4 Correlation of magnetic anomaly in the South China Sea Basin (northwest province)

The Southwestern Subbasin

According to the distribution of magnetic anomalies in the subbasin, we think that the tectonic development of the east part is different from that of the west. In the east, the magnetic anomalies can be identified as No. 5c through 6c (16–23 Ma B.P.) In the west only exists the anomaly No. 5c to 6 (16–20 Ma B.P.) (Fig.5). The southwestern subbasin was formed over such several stages that its spreading centre gradually migrated from east to west.

Seismic profiles of So49 show that the spreading centre is covered with very thin sediment, and the sedimental thickness is about 1 km on its two sides near the margin of continental slope. There are three groups of seismic reflection which can be traced to the eastern subbasin. This also demonstrates that the spreading of the southwestern subbasin began at about the same stage as the middle of the eastern subbasin did.

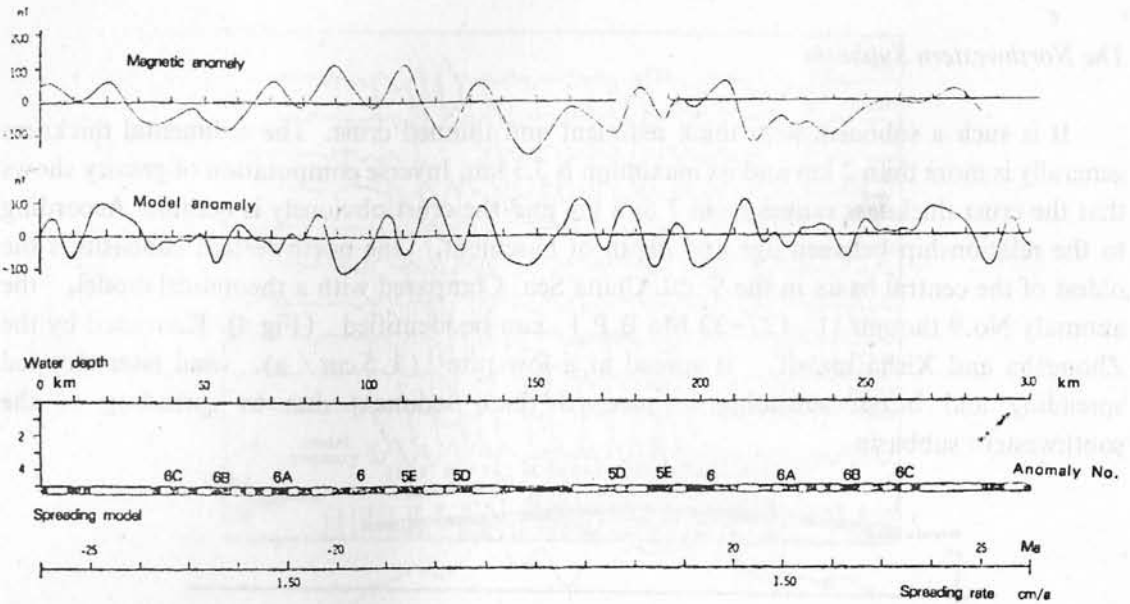


Fig.5 Correlation of magnetic anomaly in the South China Sea Basin (southwest province)

SPREADING AGES OF SUBBASINS IN THE SOUTH CHINA SEA AND THEIR RELATIONSHIPS

Both the complex feature of magnetic anomalies in the South China Sea and their oblique contact with the Manila Trench and the Philippine Island Arc indicate that the evolutionary history of the central basin of the South China Sea is complicated by polyphase spreading (Fig.6). It will depend on the project of deep sea drilling to be implemented in the South China Sea to finally resolve these problems. The development of the South China Sea can be divided into five stages as follows.

Paleogene

Basement rocks drilled from Yongxing well No.1 and Xicheng well No.2 in Xisha are Precambrian gneiss. The similar rock, micaceous has also been sampled during cruise So49 to the north of Zhongsha. In tens of drilling wells reached into the basement in the Zhujiang River Mouth Basin, there are varieties of regional metamorphic rock, migmatite and Cretaceous igneous rock unconformable under Tertiary of which the K-Ar age is 70-130 Ma B.P.. The isotopic age of gabbro, diorite and granodiorite ranges from 70 to 133 Ma B.P., dragged from the north continental slope and Zhongsha during cruise So49. All above indicate that the South China continent and Zhongsha, Xisha and Nansha had been a unity before Paleogene, and their basemental core is Precambrian metamorphic crystallization basement. From late Jurassic to Cretaceous, intensive orogenic movement (Yanshanian) took place with intermediate basic and intermediate acid magma intruding and erupting on a large scale in the region where the crust kept on uplifting in a long period. However, its south part had become an intraland shallow sea.

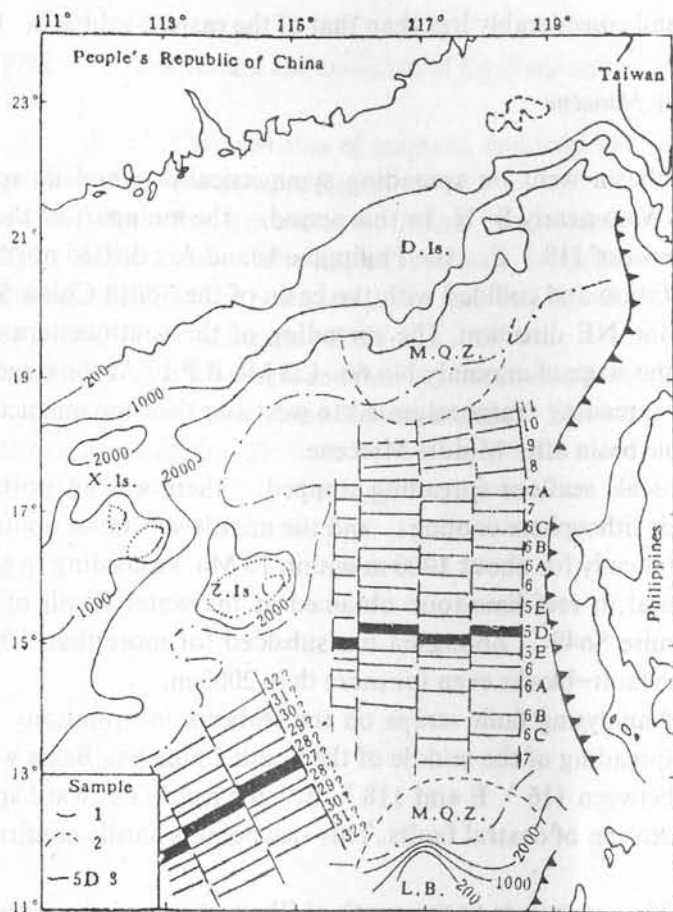


Fig.6 Distribution of magnetic lineations in the South China Sea Basin

Paleocene–Early Oligocene

In this period, the regional stress field changed from compression to relaxation. Under the influence of tension, mantle uplifted and crust thinned, so that a system of valley occurred in the north continental shelf and the middle of the South China Sea. The continental margin disintegrated by faults advanced toward the sea, and continental–crusted graben in the middle and the south of the South China Sea gradually changed into the tensional transitional–crusted one.

The isotopic age of Cenozoic volcanic rock and tuff widespread in the Zhujiang River Mouth Basin is 17.1 through 57.1 Ma B.P.. It also demonstrates that this stage was the main period of extension (Li *et al.*, 1989).

Middle Oligocene–Late Oligocene

The embryonic basin resulting from the valley spreading rapidly in the NNW–SSN direction, and was split into the northwestern and the eastern subbasin. Restricted by the Zhongsha and Xisha massif, the northwestern subbasin spread slowly, and its spreading

rate was 1.5 cm / a and considerably less than that of the eastern subbasin (2.5–3.0 cm / a).

Late Oligocene–Early Miocene

The eastern subbasin went on spreading symmetrically, and its spreading direction orientated from NNW to nearly S–N. In this period, the mainpart of the eastern subbasin was formed. To the east of 118° E, the Philippine Island Arc drifted northwestwards with a counterclockwise rotation and collided with the basin of the South China Sea to orientate regional structure to the NE direction. The spreading of the southwestern subbasin first appeared in its east at the stage of anomaly No.6c (23 Ma B.P.) At the stage of anomaly No.6 (20 Ma B.P.), the spreading centre migrated to west and then the magnetic anomaly No.5c–6 come in the whole basin after Middle Miocene.

After the large scale seafloor spreading stopped, there was an isostatic subsidence of crust with the oceanic lithosphere cooling, and the mantle substance uplifting. As a result, Xisha subsided isostatically for about 1000 m within 15 Ma. According to an identification of foraminifera and coral in reef limestone obtained at the water depth of 2800 m south of Zhongsha during cruise So49, Zhongsha has subsided for more than 1000 m since middle Miocene, and some fault-blocks even for more than 2000 m.

On the basis of analysing fault scraps on the seabeam information, Pautot (1986) concluded that the spreading of the middle of the South China Sea Basin was in the direction of NW–SE, and between 116° E and 118° E, the nearly eastward spreading centre resulted from the dislocation of dextral faults. This viewpoint is hardly confirmed by the map of magnetic anomaly.

The trough striking eastwards to the south of Zhongsha reaches a water depth of 3800 m and just corresponds to the west end of the relict spreading centre. This also demonstrates that the spreading of nearly N–S direction did exist.

The relict spreading centre of the southwestern subbasin is offset by a group of NW–trending faults with evidently sinistral slip. It is untenable in geodynamics that these faults should be formed at the same stage as those of the east did.

In short, the northwestern subbasin is the oldest one in the South China Sea, and the southwestern subbasin is the youngest. The spreading period of the eastern subbasin is longest of all.

ACKNOWLEDGMENTS

I gratefully acknowledge Dr. Kudrass' and Dr. Roeser's help during the investigation of cruises So49, So58 and the data process at BGR.

REFERENCES

- Ben-Avraham, Z. and S. Uyeda, 1973: The evolution of the China basin and Mesozoic paleogeography of Borneo. *Earth and Plan. Sci. Letters*, 18, 365–378.
- He Lishang *et al.*: Geological and geophysical maps of the South China Sea. Chinese Maps Pub-

lishing House.

Li Pinlu *et al.*, 1989: Tectonic feature and evolution of the Zhujiangkou basin. Gas and Oil in the China Sea, 3 (1) .

Lu Wenzheng *et al.*, 1987: Characteristics of magnetic lineations and tectonic evolution of the South China Sea Basin. Acta Oceanologica Sinica, 6 (4) .

Pautot, G. *et al.*, 1986: Spreading direction in the Central South China Sea. Nature, 321, 6060.

Taylor, B. and D.E. Hayes, 1980: The tectonic evolution of the South China Sea Basin. The Tectonic and Geologic Evolution of Southeast Asian Seas and Islands, Geophs. Monogr. Ser. D.E. Hayes (ed.), AGU, Washington, D.C., 23, 89-104.

Taylor, B. and D.E. Hayes, 1983: Origin and history of the South China Sea Basin. The Tectonic and Geologic Evolution of Southeast Asian Seas and Islands, Part 2, American Geophysical Union, Geophysical Monograph, 27.

FEATURES OF SEISMIC STRATIGRAPHY AND DEVELOPMENT OF SEDIMENTARY SEQUENCE IN THE CENTRAL BASIN OF THE SOUTH CHINA SEA *

KE CHANGZHI

Second Institute of Oceanography, SOA, Hangzhou, China

ABSTRACT

Nine 48-channel seismic profiles obtained from cruise Sonne-49 in 1987 have made up a defect in our understanding of the distribution of sedimentary sequences in the South China Sea. The seismic reflection succession in the northern shelf is suitably divided into five reflection strata, the Quaternary and Pliocene series above T_1 , the upper Miocene series between T_1 and T_2 , the middle and lower Miocene series between T_2 and T_4 , the Oligocene series between T_4 and T_6 , the pre-Oligocene series between T_6 and T_g , and the acoustic basement (the sedimentary basement) below T_g . There are differences of reflection events among the Northwestern subbasin, Eastern subbasin and Southwestern subbasin. Four reflection interfaces as T_1 , T_2 , T_4 and T_g are distinguished in the Northwestern subbasin. The interface T_6 is found along the SO49-17, SO49-18 profiles in the section of continental slope. In the Eastern subbasin, the interfaces are mainly T_1 , T_2 and T_g , and T_4 is found locally in its margin. There are only T_1 , T_2 and T_g in the Southwestern subbasin, and T_2 is in random appearance. The appearances of seismic reflections demonstrate the distribution of sedimentary strata in this region and its relation to formation and development of the basin. The process of formation of the central basin follows such a order, the Northwestern subbasin, the Eastern subbasin, and the Southwestern subbasin.

INTRODUCTION

The joint investigation of cruise Sonne-49 carried out by the SOA of China and the BGR of Germany in 1987 has obtained profiles of 48-channel seismic reflection in the South China Sea (SCS), four of which from the northern continental slope of SCS, across the Central Basin and the Zhongsha-Xisha terrain, reach to the northern edge of the Nansha terrain (Fig. 1). These seismic profiles are highly important for us to learn the seismic stratigraphy and the sedimentary development of the central basin of SCS. Now there have still been no drilling data in the central basin, it is difficult to divide the seismic stratigraphy directly. But there are a lot of drilling data on the continental shelf and slope in the south and north of SCS, and the SO49-17, 18 profiles beginning in the Zhu'er depression of the Pearl River Mouth basin, end almost on the northern edge of the Reed Bank. These two conditions above provide the possibilities of indirectly extrapolating the seismic stratigraphy of the central basin.

* Project supported by National Natural Science Foundation of China.

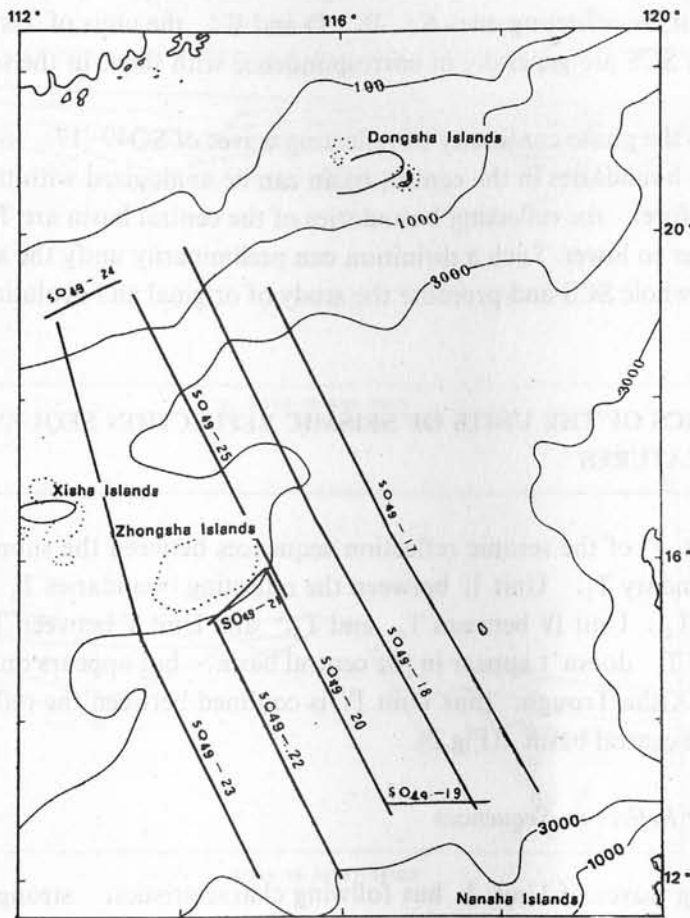


Fig.1 Location of seismic profiles of cruise Sonne-49.

UNITS OF SEISMIC REFLECTION STRATA

On the basis of its numerous data acquired recently, Guangzhou Marine Geological Survey, the MGMR of China has determined that there are five units of seismic reflection strata in the Pearl River Mouth basin of the northern SCS. The reflecting boundaries dividing these five reflection strata are named T_1 , T_2 , T_4 , T_6 and T_g from upper to lower. Nanhai West Oil Corporation of CNOOC has classified the sequence of seismic reflection strata into nine units, among which the reflecting boundaries are T_1 , T_2 , T_3 , T_4 , T_5 , T_6 , T_g and T_{g1} from upper to lower. These two divisions are very much the same, just the latter gives three subboundaries below the boundary T_6 .

ASCOPE (1981) has marked the reflecting boundaries in the Reed Bank basin as six interfaces: A, B, C, D, E, G from upper to lower. Hinz (1985) has determined the reflecting boundaries in the northwestern Palawan Shelf as seven interfaces: A, B, C, D, E, F' and F from upper to lower, which are symbolized by the following colours: yellow, pink, red, light blue, blue, green and purple, respectively. These two divisions on the reflecting boundaries of the southern SCS are almost the same.

If the geologic implications of the reflecting boundaries T_1 , T_2 , T_4 , and T_g are compared with those of the reflecting ones A, B, D and E, the units of seismic reflection strata in the northern SCS are generally in correspondence with those in the southern SCS as to their times.

According to the phase continuity of reflecting waves of SO49-17, 18 profiles, the features of reflecting boundaries in the central basin can be analogized with those in the Zhu'er depression. Therefore, the reflecting boundaries of the central basin are T_1 , T_2 , T_4 , T_6 and T_g from upper to lower. Such a definition can preliminarily unify the sequences of reflection strata of the whole SCS and promote the study of original and evolutionary mechanism of the SCS basins.

CHARACTERISTICS OF THE UNITS OF SEISMIC REFLECTION SEQUENCES AND THEIR GEOLOGICAL FEATURES

There is Unit I of the seismic reflection sequences between the submarine surface and the reflecting boundary T_1 , Unit II between the reflecting boundaries T_1 and T_2 , Unit III between T_2 and T_4 , Unit IV between T_4 and T_6 , and Unit V between T_6 and T_g . The reflecting boundary T_6 doesn't appear in the central basin, but appears only on the continental slope and the Xisha Trough, thus Unit IV is confined between the reflecting boundaries T_4 and T_g in the central basin (Fig.2).

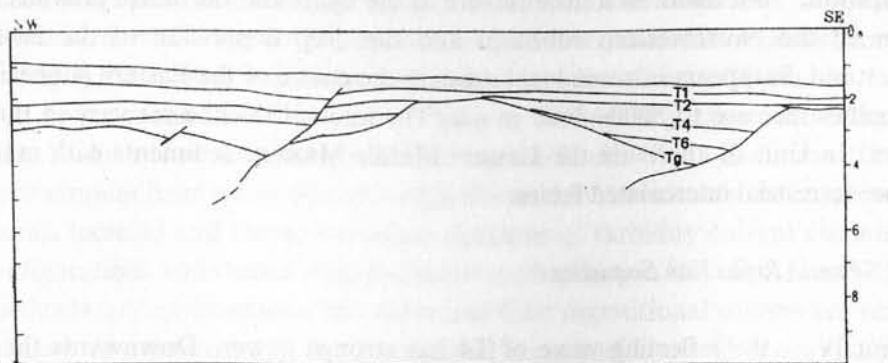
Unit I of Seismic Reflection Sequences

The reflecting waves of Unit I has following characteristics, stronger power, better continuity of phase, denser stratifications, higher apparent frequency and parallel configuration which is like a bed-cover unfolding in the sea areas with gentle submarine and undulates with the relief form of seaknolls and uplifts. The interval velocities of reflecting waves are 1730-2000 m/s. The interval thicknesses are generally 300-500 m, 400-500 m in the Northwestern subbasin and can reach 600 m in few areas, but lower down to about 200 m near seaknolls or seamounts. In the deep sea plain, the interval thickness tends to thin from north to south, but near the northern edge of the Reed Bank basin increases to 300 m again. The interval thickness is usually 200-300 m in the Southwestern subbasin. There are the Quaternary and Pliocene sediments with marine facies in Unit I of the reflection sequences.

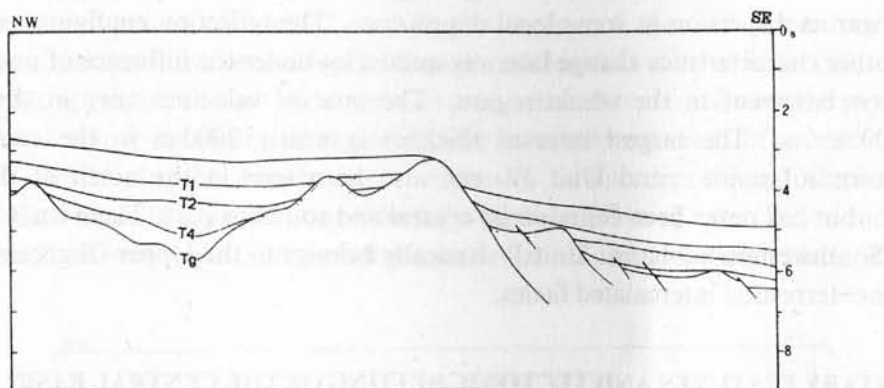
Unit II of Seismic Reflection Sequences

Unit II between the reflecting boundaries T_1 and T_2 is the second unit widespread in the abyssal plain. Its reflecting waves possess stronger power, denser stratifications, good continuity of phase, and nearly parallel configuration. From top to bottom in Unit II, the phase decay is weaker and the apparent frequency is higher. The interval velocities are 2100-2600 m/s. The interval thicknesses are generally 300-500 m and change in agreement with that of Unit I except for the Northwestern subbasin. In the centre of the Southwestern subbasin, the interval thickness of the deep depression increases to 400 m, but is lower than 200 m on its two flanks. There is the Upper Miocene sediment with marine

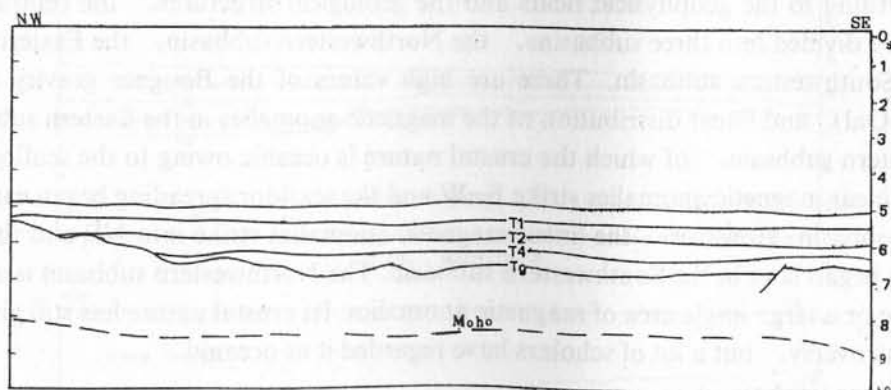
facies.



a. SO49-18 548-1843



b. SO49-18 13367-14183



c. SO49-18 3982-4998

Fig.2 The units of seismic reflection sequences of SO49-18 profile.

Unit III of Seismic Reflection Sequences

The reflecting waves of T_2 and T_4 demonstrate the double-stronger phases with stability and continuity. Inside Unit III there are also the reflecting waves of double-stronge phases

with smaller decay from upper to lower. They have denser stratifications and nearly parallel configuration, but manifest a little flexure at the uplift and the active provinces. Unit III appears in all the Northwestern subbasin and the deep depression of the Southwestern subbasin, and disappears in some local areas in the centre of the Eastern subbasin. The interval velocities increase to 3000–3600 m/s. The interval thicknesses vary in the range of 100–500 m. In Unit III there are the Lower–Middle Miocene sediments with marine facies and marine–terrestrial intercalated facies.

Unit IV of Seismic Reflection Sequences

In Unit IV, the reflecting wave of T4 has strong power. Downwards the reflection power becomes weaker, and the reflection phase is not only obviously malformed but also utterly confused so that the reflection trajectory is discontinuous laterally. The reflecting waves appear as dispersion in some local depressions. The reflection configuration, thickness and other characteristics change laterally quite a lot under the influence of undulation of the acoustic basement in the whole region. The interval velocities vary in the range of 3600–4700 m/s. The largest interval thickness is nearly 2000 m in the centre of the Northwestern subbasin, and Unit IV can also be seen in the north of the Eastern subbasin, but has never been found in its central and southern part. There isn't Unit IV at all in the Southwestern subbasin. Unit IV basically belongs to the Upper Oligocene sediment with marine–terrestrial intercalated facies.

SEDIMENTARY FEATURES AND TECTONIC SETTING OF THE CENTRAL BASIN

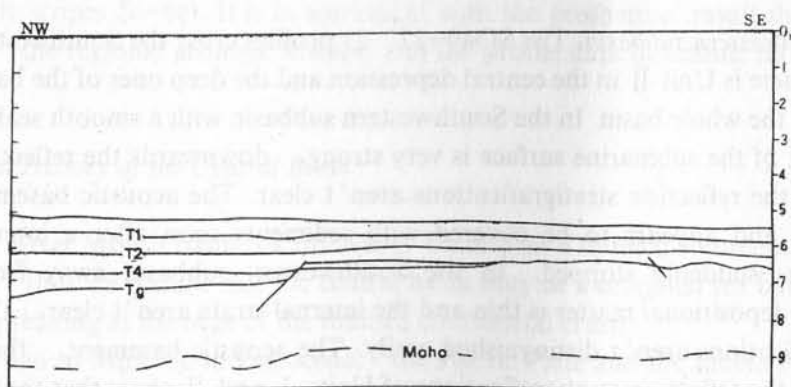
According to the geophysical fields and the geological structures, the central basin of SCS can be divided into three subbasins, the Northwestern subbasin, the Eastern subbasin and the Southwestern subbasin. There are high values of the Bouguer gravity anomalies (> 200 mGal) and linear distribution of the magnetic anomalies in the Eastern subbasin and Southwestern subbasin, of which the crustal nature is oceanic owing to the seafloor spreading. The linear magnetic anomalies strike E–W and the seafloor spreading began earlier in the Eastern subbasin. However, the linear magnetic anomalies strike into NE and the seafloor spreading began later in the Southwestern subbasin. The Northwestern subbasin is a magnetic quiet zone or a large single area of magnetic anomalies. Its crustal nature has still given rise to much controversy, but a lot of scholars have regarded it as oceanic.

Basic Features of Sedimentation in Basins

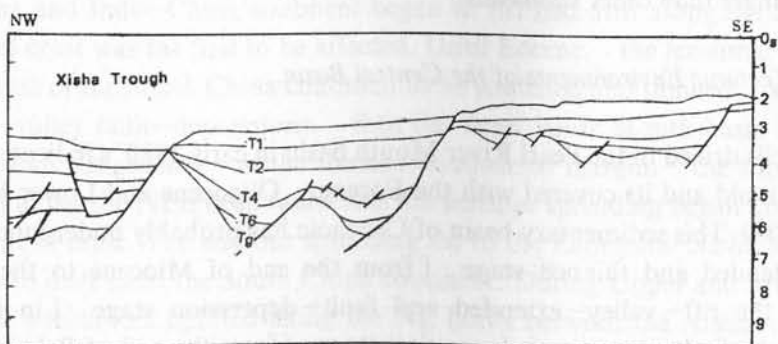
The whole basin of SCS would be divided into 40 sedimentary basins. As to their evolutions, these sedimentary basins have some distinct specialities different from the sedimentary basins of Mesozoic and Cenozoic around SCS. The sedimentary basins of Mesozoic and Cenozoic in the South China continent cannot be generally younger than Early Paleogene, and their depositional time in Cenozoic is shorter. Meanwhile, in the sedimentary basins of Mesozoic on the Indo–China Peninsula west of SCS sedimentation has already stopped due to uplifting in Cenozoic. However, sedimentation occurs in SCS only in Cenozoic, and on

its continental slope the largest thickness of depositional layer can reach over 10000 m. Sedimentation takes place in the central basin of SCS after Later Oligocene.

The Northwestern subbasin. All the units of reflection sequences exist in the Northwestern subbasin (Fig.3). According to the core and dredge samples of cruise SO49, in the surficial layer (the upper section of Unit I) there is mainly silty clay containing a lot of foraminifera, which is some clastics coming from the South China continent. The analytic result of core samples from the continental edge shows that downwards the contents of heavy sandy minerals increase and the accumulative horizons of turbidity current are intercalated. Parallel configurations and denser stratifications of reflection in Units I and II indicate that their sedimentary environments are stable and their depositional sources are very simple. The sedimentary environment and the depositional texture of Unit III is obviously different from Units I and II because its reflection configuration slightly undulates laterally and its continuity of phase becomes weaker. Much more different from three units above, the sedimentary development of Unit IV at the beginning of the SCS spreading with the marine-terrestrial transition caused by the intensive movements of crust is not only controlled by the tectonic movements of sea-bottom basement, but also marked with the sophisticated components of matter consisting of slope, alluvial and silted materials of marine-terrestrial intercalated facies. In the Northwestern subbasin, the depositional thicknesses are 2500-3500 m, there is a parallel unconformity between Units I and II, and between Units II and III respectively, and there is an angular unconformity between Units III and IV.



a. SO49-17 6994-11002



b. SO49-23 12431-13455

Fig.3 The units of seismic reflection sequences of the Northwestern subbasin.

The Eastern subbasin. There are only Units I and II in most areas of the Eastern subbasin except that there is Unit III on its southern and northern edges. The sedimentary environment and the depositional texture of each unit are similar to those of the same unit in the Northwestern subbasin, but its volcanic stuff is abundant. Near the Zhongsha terrain depositional samples are most composed of the semi-consolidated tuff. At the northern end of SO49-18 profile (Fig.4), the reflection phase of Unit II seems onlap and the interval thickness becomes thinner from south to north. It can be explained with the fact that a large scale of volcanic eruptions in the Reed Bank basin has produced huge amounts of pyroclastic grains gravity-slide-depositing on its slope. The sedimentary thickness is generally less than 2000 m in the Eastern subbasin.

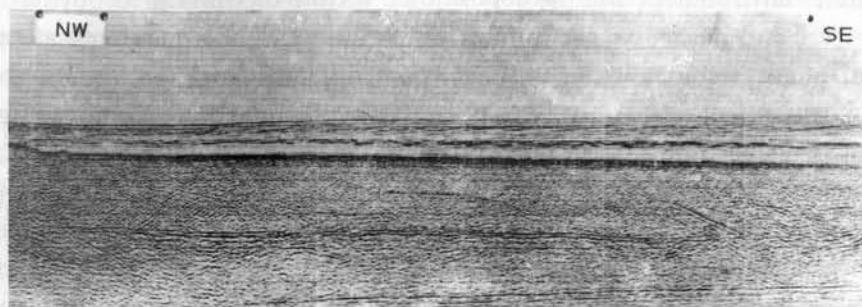


Fig.4 The units of seismic reflection sequences of the northern end of SO49-18 profile.

The Southwestern subbasin. The SO49-22, 23 profiles cross the Southwestern subbasin. Besides that there is Unit II in the central depression and the deep ones of the basin, Unit I can be seen in the whole basin. In the Southwestern subbasin with a smooth seafloor, the reflection power of the submarine surface is very strong, downwards the reflection power decays fast and the reflection stratifications aren't clear. The acoustic basement is rugged and rough, and appears to be covered with sediments soon after a intensive tectonic movement has suddenly stopped. In the Southwestern subbasin away from substance sources, the depositional matter is thin and the internal strata aren't clear, thus the reflection stratifications aren't distinguished easily. The acoustic basement, the sedimentary thickness and the reflection stratifications of Units I and II show that the Southwestern subbasin is younger than other subbasins.

The Regional Tectonic Environments of the Central Basin.

Several wells drilled in the Pearl River Mouth basin in early 1980's indicate that the granite is 90-70 Ma old and its covered with the Eocene, Oligocene and Lower Miocene strata (Jin *et al.*, 1989). This sedimentary basin of Cenozoic has probably undergone four stages, the crustal extended and thinned stage (from the end of Miocene to the beginning of Paleogene), the rift-valley-extended and fault-depression stage (in the middle of Paleogene), the fault-downward depression stage (from the end of Paleogene to the beginning of Neogene) and the downward depression stage (since Neogene). There are the marine-terrestrial intercalated facies of Paleogene sediments and the neritic facies of Neogene sediments in the central basin.

Within the Xiyong Well No.1 at the Zhongsha-Xisha terrain in the west of the central basin, below the depth of 1251 m there are granite gneiss and biotite-plagioclase and -orthoclase gneiss with the isotope age 627 Ma, and above the depth of 1251 m there are reef limestone and bioclast since Neogene. The Zhongsha-Xisha terrain always maintained in a uplifted state and wasn't covered with sediments until it has just changed into a neritic environment with the crust subsiding for over 1000 m since Paleogene.

The Sampaguita Well No.1 at the Reed Bank basin south of the central basin has revealed that the Cenozoic strata of the basin are discordant over the coal-bearing clastic rocks and the pyroclastic rocks with the marginal sea facies of Early Cretaceous, and the Reed Bank was a bathyal environment in Early and Middle Oligocene and has belonged to a littoral and neritic environment up to now.

More than ten years ago, any scholars were sceptical about the linear magnetic anomalies existing in the central basin, then these suspicions have gradually been dispelled. Now various identifications and interpretations on the linear magnetic anomalies with nearly E-W trending in the Eastern subbasin are reaching the same conclusion that these linear magnetic anomalies resulted from the seafloor spreading from Later Oligocene to Early Miocene. But there are different identifications and interpretations on the linear magnetic anomalies in the Northwestern subbasin. These different understandings in the linear magnetic anomalies are concerned in different conclusions on the original mechanism of the SCS basins. Our renewed comparisons and analyses on the linear magnetic anomalies in the Southwestern subbasin indicate that the seafloor spreading took place during Early-Middle Miocene (the timescale No of magnetic stripes 5c-6c). It is in agreement with the geothermal result that the crustal age is 15 Ma, the regional geologic features and the profile data of seismic reflection in this area.

The Evolutional History of the Central Basin

The Pearl River Mouth basin is a rift-valley basin with a thinned continental crust (Jin *et al.*, 1989), thus we deduce that the central basin may be a marginal sea basin originated from rifting-spreading at the edge of the thinned continental crust.

From the end of Miocene to Paleocene, the Pacific Plate and the Indian Plate subducted towards the Eurasian Plate from the east and north directions respectively. Thereafter, the South China and Indo-China continent began to rift and drift along the N-S direction and its marginal crust was the first to be affected. Until Eocene, the tensional faulting made the marginal crust of the South China continent to be stretched and thinned, and resulted in a series of rift-valley fault-depressions, thus the Pearl River Mouth basin began to take shape. During Late Oligocene, at the thinned continental margin, the super-basic substances uplifted along the NEE deep faults and the seafloor spreading began due to the intensive rift and drift of crust. The seafloor spreading led to the Zhongsha-Xisha terrain and the Nansha terrain to drift from the South China continent. During Upper and Middle Miocene the super-basic substances uplifted along the NE faults between the Xisha terrain and the Nansha terrain because of the rift-valley spreading, and the seafloor spreading of the Southwestern subbasin finally occurred. Since the end of Middle Miocene, the seafloor spreading has stopped and the central basin has subsided, and the intensive magmatism has brought about a series of sea-mounts to rebuild the submarine topography.

REFERENCES

- ASCOPE, 1981: Tertiary sedimentary basins of the Gulf of Thailand and South China Sea, stratigraphy, structure and hydrocarbon occurrence.
- Hinz, K., 1985: The southern Palawan-Balabac, an accreted or nonaccreted terraine? Third Conference Papers.
- Jin Qinhuan *et al.*, 1989: Geology and petroleum resources of the South China Sea. Geology Publishing House of China.
- South China Sea Institute of Oceanology, Academia Sinia, 1988: Geologic structure of South China Sea and spreading of continental margin.

THE AGE OF THE SOUTH CHINA SEA TERRAINS RIFT-DEPARTING FROM SOUTH CHINA CONTINENT*

LI QUANXING & WU SHENGDI

Second Institute of Oceanography, SOA, Hangzhou, China

ABSTRACT

The terrains in the South China Sea were a part of the Southeast China continent, and their rift-departing process dominated the formation and evolution of the South China Sea. The survey results of topography and paleoenvironment of the northern South China Sea during SO-49 cruise demonstrate that the terrains rift-departed from the South China continent before early Eocene.

INTRODUCTION

Some geologists considered that the Nansha Islands were a part of the Southeast China continent, but they held different viewpoints about the time of the terrains rift-departing from the South China continent. Jin (1989) considered that the basement of the Xisha, Zhongsha, Nansha terrains and the South China continent all consist of the Proterozoic formation. In Cretaceous the Nansha terrain was connected with the South China continent, and the South China Sea Basin was formed with the first sea-floor spreading from Late Cretaceous to Eocene.

During SO-49 cruise in 1987, topography data and manganese crust samples had been obtained from the northern slope of the South China Sea. Comparison of the depth of break points on the slope with net subsidence curve from wells in the Pearl River Mouth Basin and paleoenvironment information contained in manganese crust show that the terrains rift-departed from the South China continent before early Eocene.

THE FEATURES OF THE NORTHERN SLOPE OF THE SOUTH CHINA SEA

A topographic, geological and tectonic synthetical profile of the northern slope of the South China Sea is shown in Fig.1. This profile is located between the continental margin and the deep sea basin and perpendicular to isobath with the length of 198 km, height difference of 3555 m, average slope of 18 / 1000.

The sea-floor relief on this profile is gentle at upper and steep at lower and consists of 9 steps. The data of their steps are shown in Table 1. The seismic profile shows that the southeastward tilting basement was rifted and slid down along the faults and a series of skip basins were formed. The sediment layers in the basins slope southeastward indicate that the

* Project supported by National Natural Science Foundation of China.

steps on the slope were formed by southeastward extension and depression while sediment was deposited. According to the paleomagnetic data, Emery (1983) considered that the East Asia has drifted about 400 km southward since Paleocene. Therefore, topographic features and tectonic structures on the northern slope of the South China Sea resulted from extension, thinning and depression of the South China continent induced by its southeastward creep diffusion. The break points on these steps, especially those with larger gradient, maybe recorded the crust depressional process. Comparing the topographic profile with the net subsidence curve from wells in the Pearl River Mouth Basin (Ru, 1987) (Fig.2), we

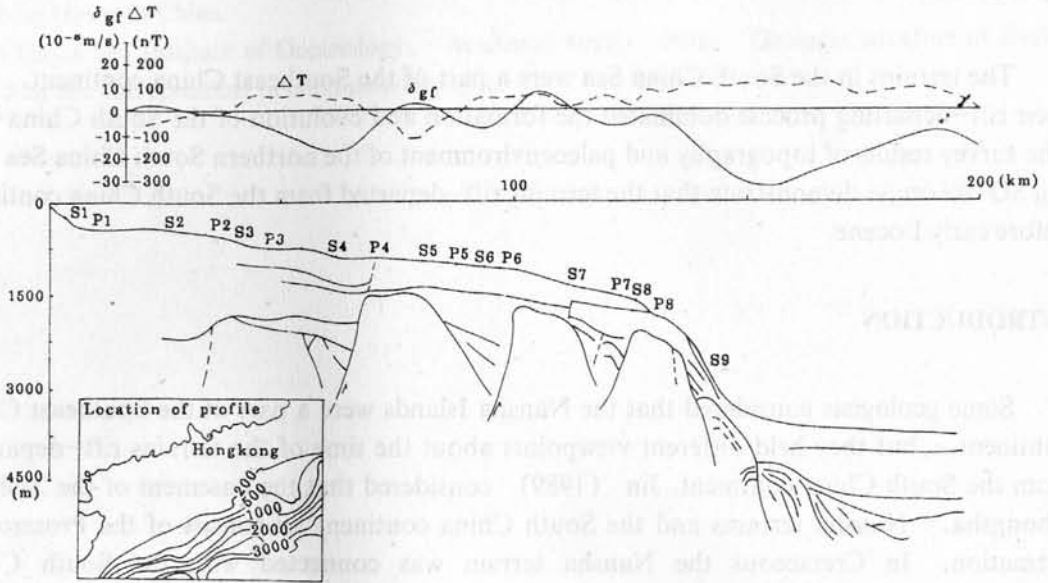


Fig.1 Topographic, geophysical and tectonic profile of northern continental slope.

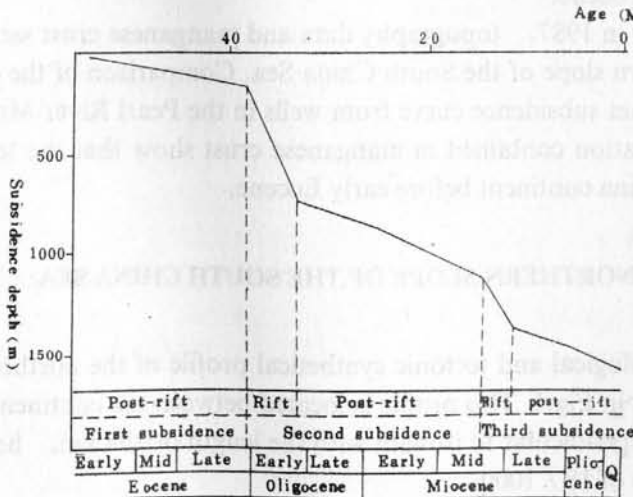


Fig.2 Net subsidence curve from well in the Pearl River Mouth Basin.

discover that depth of turning points on the subsidence curve corresponds to that of break points S1, S4, S7 and S8, respectively. In view of the well data, these turning points indicate the post-rift and rift stage of the first subsidence, the post-rift stage of the second subsidence and the post-rift stage of the third subsidence, respectively. These subsidences

occurred in Eocene, from Oligocene to middle Miocene and after middle Miocene. Thus these times are also the forming ages of the northern slope of the South China Sea.

Table 1 The data of topographic profile of northern slope of the South China Sea

Features		Location		Depth (m)	Distance (km)	Depth range (m)	Gradient
		Lat.	Long.				
Shelf	Break						
Step	Steep 1	20 ° 03.03'	114 ° 02.56'	170			
					5.36	250	2 ° 40.35'
1	Flat 1	20 ° 00.34'	114 ° 03.69'	420			
					15.37	5	1 ° 12'
Step	Steep 2	19 ° 52.62'	114 ° 06.95'	425			
					13.16	100	26.12'
2	Flat 2	19 ° 46.01'	114 ° 09.73'	525			
					3.17	2	2.17'
Step	Steep 3	19 ° 44.42'	114 ° 10.40'	527			
					4.82	183	2 ° 10.46'
3	Flat 3	19 ° 43.00'	114 ° 11.42'	710			
					12.05	10	2.85'
Step	Steep 4	19 ° 35.95'	114 ° 13.97'	720			
					7.37	180	1 ° 10.46'
4	Flat 4	19 ° 32.25'	114 ° 15.53'	900			
					17.12	80	16.06'
Step	Steep 5	19 ° 23.66'	114 ° 19.15'	980			
					6.99	58	28.52'
5	Flat 5	19 ° 20.15'	114 ° 20.62'	1038			
					1.63	9	18.98'
Step	Steep 6	19 ° 19.34'	114 ° 20.97'	1047			
					8.34	71	29.27'
6	Flat 6	19 ° 15.15'	114 ° 22.73'	1118			
					1.10	2	6.25'
Step	Steep 7	19 ° 14.60'	114 ° 22.96'	1120			
					27.11	407	57.57'
7	Flat 7	19 ° 01.00'	114 ° 28.69'	1527			
					1.95	5	8.81'
Step	Steep 8	19 ° 00.02'	114 ° 29.10'	1532			
					4.85	288	3 ° 26.02'
8	Flat 8	18 ° 57.62'	114 ° 30.12'	1820			
					1.56	20	44.07'
Step	Steep 9	18 ° 56.84'	114 ° 30.45'	1840			
9		18 ° 31.04'	114 ° 41.31'	3630	51.43	1790	1 ° 59.60'

PALEOENVIRONMENTAL INFORMATION CONTAINED IN MANGANESE CRUST FROM THE LOWER SLOPE

At the seamount located on the northern slope with a water depth of 2470 m, the manganese crust with thickness up to 8.5 cm was sampled. It grew on the surface of submarine rock. The material content variation of its every layer maybe reflects the evolution of its paleoenvironment. For this reason, according to its growth bedding, we divided it into 10 layers from surface to interiority and analysed samples from its every layer. The element con-

tent and trace element content are shown in Table 2.

In order to discuss the sedimentary environment, it is necessary to determine the growth rate of manganese crust. Because the manganese crust has undergone such a long growth process, it is difficult to determine the earliest time by using direct dating methods. The calculated result based on the empirical formula by Huh and Ku (1984) corresponds to the dating data of manganese nodules sampled from Pacific Ocean and the South China Sea (Mangini and Kudrass *et al.*, 1986). So we Calculated the growth rate of manganese crust using the following empirical formula by Huh and Ku (1984):

$$S \text{ (mm / ma)} = 13.39 \times (\text{Mn} / \text{Fe}^2) + 0.75$$

and obtained the growth rate ranging from 1.5 to 1.2 mm / ma. If the growth discontinuance can be neglected, it is possible that the earliest manganese crust was formed 52 Ma B.P., i.e. early Eocene.

In order to verify the growth age of manganese crust, we have drawn the growth rate and age, chlorine content, $\text{Fe}^{3+} / \text{Fe}^{2+} \delta\text{O}^{18}$, P_2O_5 and CaO in Fig.3.

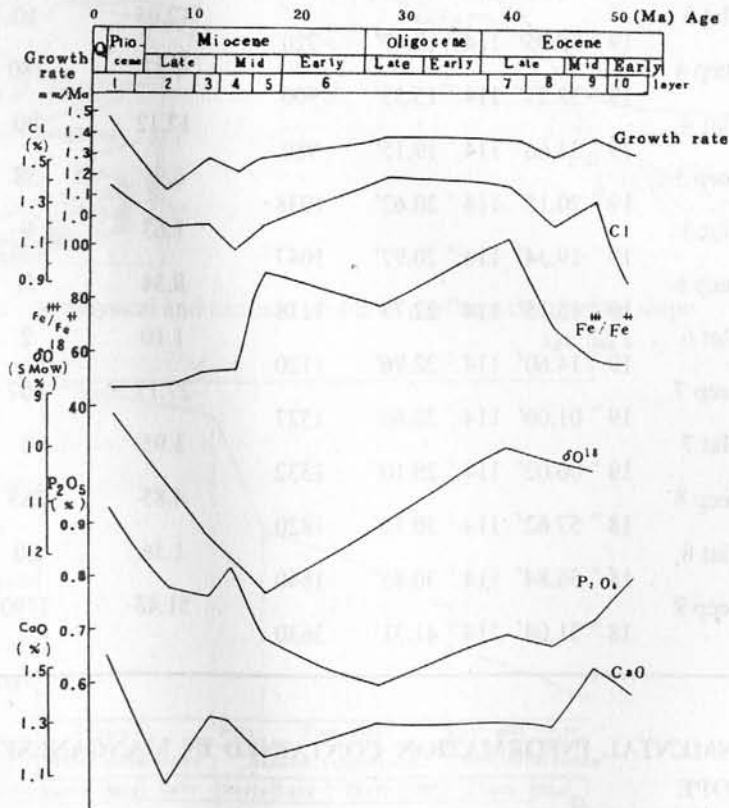


Fig.3 Variation of growth rate, chlorine, $\text{Fe}^{3+} / \text{Fe}^{2+}$, δO^{18} , P_2O_5 and CaO content in manganese crust.

The variation of chlorine content in manganese crust may reflect the variation of salinity in sea water. In early Eocene, the sea basin may be at its initial stage; and the chlorine content was only 0.907%. From late Eocene to early Miocene, the chlorine content increased up

Table 2-1 The element content of manganese crust (%)

Layer	MnO ₂	Fe ₂ O ₃	SiO ₂	Al ₂ O ₃	TiO ₂	CaO	MgO	Na ₂ O	K ₂ O	P ₂ O ₅	Ni	Cu	SrO	Combustible	Σ	H ₂ O	Cl	SO ₃
1	25.968	25.557	10.309	2.981	0.704	1.567	1.420	2.042	0.314	0.922	0.259	0.331	0.339	27.26	99.973	12.55	1.396	0.540
2	16.579	25.553	24.005	4.007	0.491	1.074	1.434	1.710	0.445	0.776	0.113	0.344	0.140	23.43	100.101	10.27	1.171	0.420
3	25.367	28.403	9.605	3.041	0.574	1.337	1.200	1.857	0.290	0.753	0.074	0.084	0.152	26.57	99.307	11.33	1.194	0.385
4	20.554	29.747	15.463	3.352	0.575	1.317	1.344	1.684	0.265	0.815	0.285	0.434	0.109	25.42	101.364	13.18	1.080	0.472
5	23.108	30.826	12.135	2.850	0.547	1.174	1.161	1.514	0.223	0.685	0.182	0.608	0.339	25.58	100.932	11.42	1.184	0.385
6	18.992	25.109	23.354	3.608	0.505	1.315	1.269	1.849	0.313	0.596	0.258	0.090	0.292	21.72	99.270	9.22	1.1407	0.1435
7	25.304	28.737	10.490	2.349	0.441	1.294	1.331	1.461	0.020	0.698	0.162	0.163	0.356	26.68	99.486	12.13	1.387	0.425
8	22.988	28.362	12.813	1.932	0.401	1.281	1.320	1.629	0.214	0.664	0.179	0.216	0.409	26.03	98.438	10.73	1.119	0.437
9	24.894	28.524	12.718	1.222	0.421	1.504	1.235	1.620	0.210	0.701	0.117	0.130	0.315	25.71	99.321	10.60	1.323	0.588
10	23.769	24.162	8.598	2.224	0.436	1.410	1.261	1.522	0.211	0.774	0.143	0.084	0.315	25.50	100.41	10.96	0.907	0.510

Table 2-2 The trace-element content of manganese crust (ppm)

Layer	Cd	Sr	Bi	Pb	Ba	Co	Be	Cr	V	B	Ga	In	Zn	Sn	W	As	Mo	Ag	Rb ₂ O (%)
1	<1	1419	34	2100	1207	2500	<1	19	441	95	4	<1	132	3	52	<30	320	<1	0.0025
2	<1	1118	24	1800	907	1500	<1	20	500	140	2	<1	185	3	44	<30	400	<1	0.0020
3	<1	1462	30	2050	1354	1550	<1	15	519	113	<2	<1	153	3	57	<30	380	<1	0.0020
4	<1	1376	35	2100	1251	1280	<1	15	456	126	2	<1	187	3	56	<30	360	<1	0.0025
5	<1	1500	34	2000	1402	1400	<1	18	475	112	<2	<1	125	3	500	<30	460	<1	0.0025
6	<1	1200	28	1250	1112	1100	<1	27	429	103	4	<1	117	3	52	<30	500	<1	0.0025
7	<1	1634	39	1700	1382	980	<1	12	472	108	4	<1	195	3	62	<30	500	<1	0.0020
8	<1	1677	26	1650	1569	900	<1	12	551	138	3	<1	210	3	68	<30	500	<1	0.0020
9	<1	1750	32	1700	1337	950	<1	11	573	173	4	<1	415	3	72	<30	500	<1	0.0020
10	<1	1634	35	1700	1489	1000	<1	12	604	120	2	<1	260	3	68	<30	500	<1	0.0025

to 1.407% ; in middle Miocene it was 1.080% ; after late Miocene it increased to 1.217%. The variation of salinity may be related to the basin evolution. Karig (1973) considered that there was a transform fault connecting trench with trench between the Luzon Arc and Taiwan in early Tertiary when the South China Sea was opened as an extensional marginal sea. During 32–17 Ma B.P., the South China Sea Basin was enlarged and its salinity increased with the sea–floor spreading (Taylor and Hayes, 1980). In mid–late Miocene and early Pliocene, because the northern extended part of the Luzon volcanic arc collided with Taiwan, the Huo–Shao Tao island and the Babuyan ridge were formed, which impeded water exchange between the Philippine Sea and the South China Sea and made the salinity decrease. Since Pliocene, the central water of the Northwest Pacific Ocean has ever passed through the Bashi Channel and filled into the bottom of the South China Sea Basin (about 1500–4000 m deep), therefore, the chlorine content in the manganese crust was up to 1.396%.

The variation of δO^{18} content in the manganese crust may reflect paleotemperature variation. From late Eocene to middle Miocene, an increase of δO^{18} content indicates a drop in water temperature. It is identical with the variation of paleotemperature in the northern Pacific Ocean.

The Fe^{3+} / Fe^{2+} ratio reflects the oxidizing milieu of sea water. From late Eocene to early Miocene, Fe^{3+} / Fe^{2+} ratio was up to 91–104, indicating that the basin was opened and the water was renewed continuously. After middle Miocene, the oxidizing milieu became weak because the Bashi Channel was formed. However, the South China Sea Basin keeps on opening and is in the stronger oxidizing milieu.

CONCLUSION

The growth rate calculated from the manganese crust and the paleoceanographic variation contained in the manganese crust conforms to tectonic evolution and paleoceanographic variation from the surrounding area, which indicates that calculated age is desirable. Well No.1 in Sampaguita shows that the Read Bank was marginal sea facies in late Cretaceous, deltaic facies in Paleocene, bythyal facies in late Oligocene, bathyal facies in mid–Miocene and marginal facies after mid–Miocene. The coincidence between the paleoceanographic variation contained in the manganese crust and the variation of surrounding tectonics maybe indicates the evolution between northern and southern margins of the South China Sea Basin has internal connection. Along with evolution of slope topography, these conclusions suggest that the terrains rift–departed from South China continent before Eocene. The paleogeographical chart by Jin (1989) expresses the same opinion.

REFERENCES

- Emery, K. O., 1983: Tectonic evolution of East China Sea. International Symposium on Sedimentation on the Continental Shelf, with Special Reference to the East China Sea, 1, 80–90, China Ocean Press.

- Huh, C.A. and T.L. Ku, 1984: Radiochemical observations on manganese nodules from their sedimentary environment in the North Pacific. *Geochim. Cosmochim. Acta*, 48, 951-963.
- Jin Qinghuan, 1989: *Geology and Petroleum Resource of South China Sea*. Geological Publishing House (in Chinese).
- Karig, D. E. , 1973: Plate covergence between the Philippines and Ryukyu Islands. *Marine Geology*, 14, 3, 153-168.
- Mangini, A. and H. Kudrass *et al.* , 1986: Diffusion and supply rates of ^{10}Be and ^{230}Th radiotopes in two manganese encrustations from the South China Sea. *Geochim. Cosmochim. Acta*, 50 (1), 149-156.
- Ru Ke, 1987: The plate tectonic analysis of marginal basin in northern South China Sea. International Symposium on Petroleum Geology of Northern Continental Shelf in South China Sea, 632-641. The Chinese Petroleum Society (in Chinese).
- Taylor, B. and D. Hayes, 1980: The tectonic and geologic evolution of Southeast Asian seas and islands. *Geophysical Monograph*, 23, 89-104.

TECTONIC MOVEMENT OF MARIANA TRENCH-ARC-TROUGH SYSTEM*

LIN CHANGSONG¹⁾ & WANG GUANRONG²⁾

1) *Second Institute of Oceanography, SOA, Hangzhou, China*

2) *First Institute of Oceanography, SOA, Qingdao, China*

ABSTRACT

In the West Pacific the Mariana trench-arc-trough system was cut along a long narrow oceanic belt which is an isostress belt. Under the combined action of both horizontal and vertical stresses, the Mariana trench-arc-trough system controlled by a double-subduction zone underwent both the differential rotation in the westward level and the revolving-tensional tilt toward the trench axis. Such two kinds of movement built the new moon-shaped trough and the island-arc bowed to the ocean. Actually, the Mariana trough has been a part of the Mariana island-arc system ever since its beginning of evolution.

RESEARCH CONDITION AND PROBLEMS

On the cruise SO-57 in 1988, scientists from China and Germany carried out a joint investigation of marine geology in the Mariana trough and its forearc, as well as the Philippine Sea basin. Having combined our investigation results with previous knowledge we put forward some new ideas on the formation and tectonization of the Mariana trench-arc-trough system.

The Mariana trench-arc-trough system (Fig.1) lies in the West Pacific. The trough is a new moon-shaped interarc basin, on average 4000 m in water depth with thin sediment or exposed basalt basement. Both on its east and west flanks there are fault scarps (Fig.2). Its wave velocity structure and thickness are similar to those of the oceanic basin (Bibee *et al.*, 1980; Hussong, 1987). It was figured out that the trough began to develop about 5 Ma B.P. and its spreading rate was 10 cm/a (Karig, 1971), 8 cm/a (Karig *et al.*, 1978), or 3cm/a (Bibee *et al.*, 1980). Having analysed the magnetic anomaly profiles across the so-called spreading center axis, we found no anomalies of which the feature is analogous to that of the magnetic lineations. They vary very gently with low amplitude (Fig.3). Because of the complexity of tectonic movement in the trench-arc-basin, there are many geological factors which affect the interpretation of magnetic anomalies, so there is still a large room to explore on the interpretation of magnetic anomalies in the back-arc region including some old oceanic basins.

The Mariana arc is a volcanic arc. It has undergone a successive volcanic action since Eocene (Hussong and Uyeda, 1981). Its forearc was dominated by subsidence and

* Project supported by National Natural Science Foundation of China.

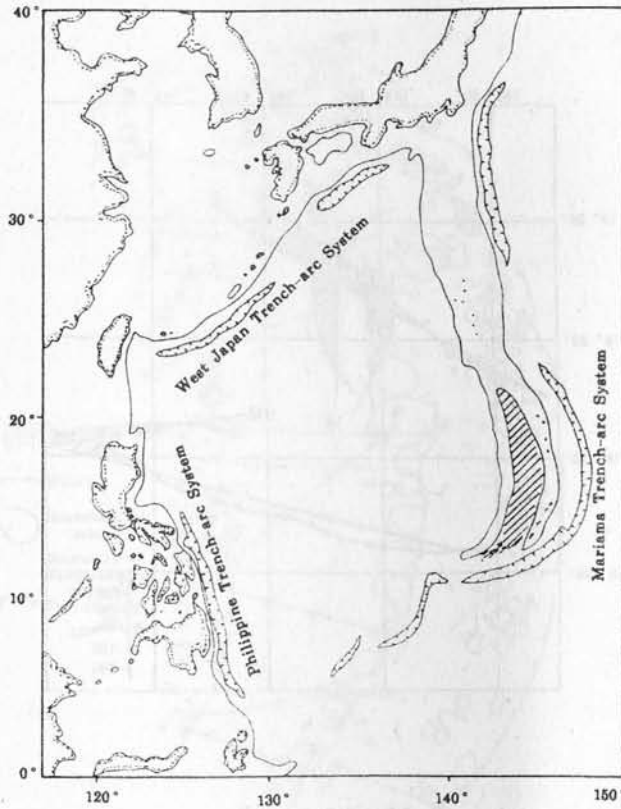


Fig.1 Tectonic position of the Mariana trench-arc-trough system. The Mariana trough is indicated by the oblique lines.

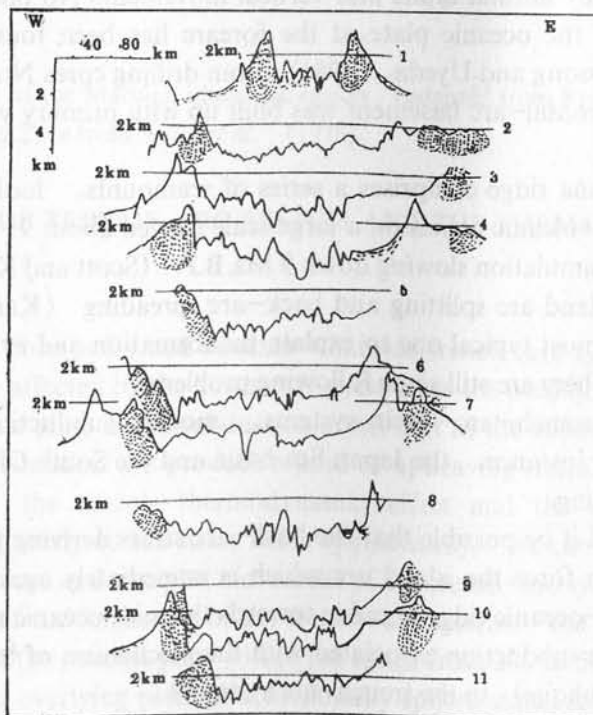


Fig.2 Profiles across the Mariana trough (their locations shown in Fig.4). The dot pattern indicates areas thought to be underlain by frontal-arc basement (from Karig *et al.*, 1978).

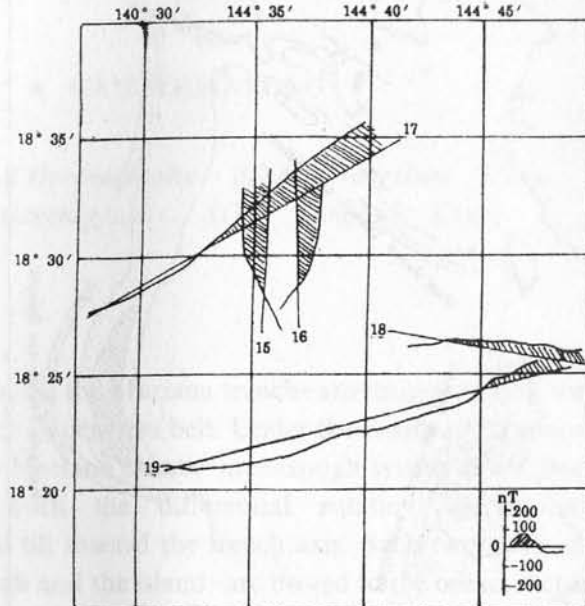


Fig.3 Profiles of magnetic anomaly in the Mariana trough.

destroyed obviously by normal faults and vertical movement. No phenomenon of compression or accretion of the oceanic plate at the forearc has been found (Von Huene and Uyeda, 1981; Hussong and Uyeda, 1981). From drilling cores No. 458 and 459, it was discovered that the frontal-arc basement was built up with primary volcanic rocks (Uyeda *et al.*, 1983).

The West Mariana ridge comprises a series of seamounts, looking like an arc on the whole (Fig.4). The volcanic action on a large scale started about 9–20 Ma B.P. and ended with the volcanic accumulation slowing down 9 Ma B.P. (Scott and Kroenke, 1981).

The model of island arc splitting and back-arc spreading (Karig, 1971, 1972 and 1974) is so far the most typical one to explain the formation and evolution of back-arc or interarc basin, but there are still some following problems.

(1) In many trench-arc-basin systems, modern subduction still exists while the back-arc basin, for instance, the Japan Sea basin and the South China Sea basin, has already stopped spreading.

(2) How could it be possible that the back-arc stress deriving from the subduction of the oceanic plate can force the island arc which is immediately against the stress from the spreading of the mid-oceanic ridge to move towards the mid-oceanic ridge on a large scale?

(3) How is the subduction associated with the mechanism of back-arc spreading axis perpendicular (or oblique) to the trench-arc system?

(4) While the island arc under the stress from the subduction of the oceanic plate can move towards ocean, why does the back-arc spreading appear symmetrically?

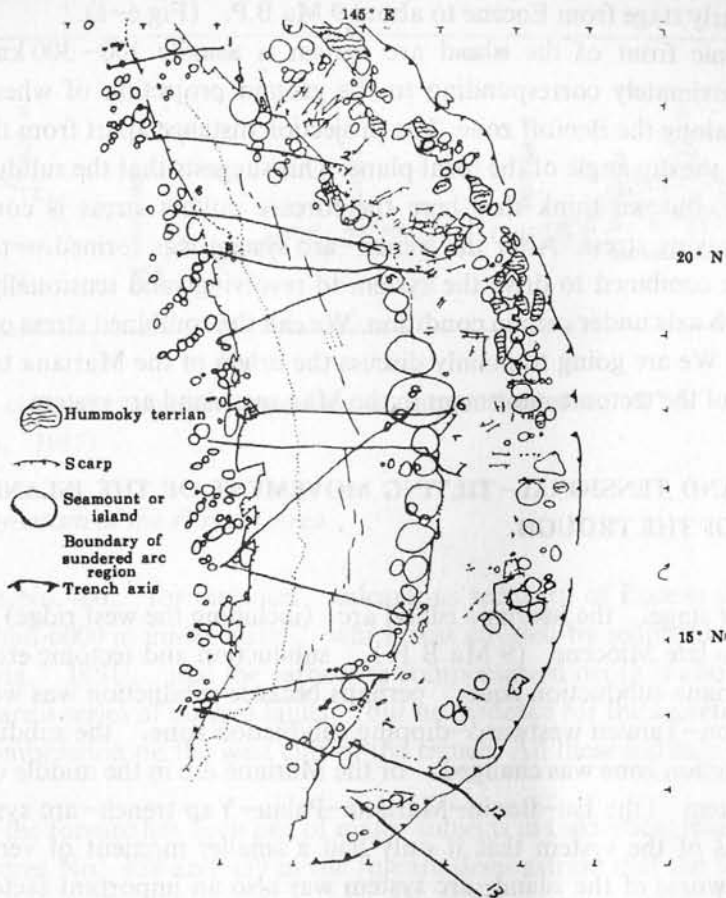


Fig.4 Geological sketch of the Mariana island arc region (adapted from Fryer *et al.*, 1985). Locations of the profiles in Fig.2 are from Karig *et al.* (1978).

THE STRESS FIELD OF TRENCH-ARC SYSTEM AND THE FORMATION OF EARLY ISLAND ARC

After the Benioff zone is formed beneath whatever trench-arc systems the island-arc system will not only be affected by the horizontal stress from the oceanic plate but also be pulled down by the oceanic plate in the subduction zone. But as the subduction plate reaches a certain depth, the subduction will produce a kind of upheaving stress, which results from the frictional heat, the mantle thermodynamic effect and the crust-mantle density difference. Only having analysed the stress fields synthetically, we can make out completely the features of both intense and complex movement of the trench-arc system.

At the beginning of the formation of the trench-arc system, the upheaving stress produced by subduction of the oceanic plate within the range from 300 to 500 km near the trench axis, would make the overlying plate in a tensionally splited state. As a result, substance and energy from subduction would be relieved, and faults, magmation and volcanism occurred along the island arc. The accumulation of substance led to formation and rise of the early island arc. The Mariana arc, including the West Mariana ridge, went through such a

process at its early stage from Eocene to about 9 Ma B.P. (Fig.6-1).

The volcanic front of the island arc system is usually 150-300 km apart from the trench, approximately corresponding to the ground projection of where seismic activity stops abruptly along the Benioff zone. The projection distance apart from the trench has a direct bearing on the dip angle of the focal plane. This suggests that the subduction plate begins to melt here, but we think that here the forearc pulling stress is confronted with the back-arc upheaving stress. After the trench-arc system was formed, these two kinds of stress would be combined to drive the system to revolvingly and tensionally tilt vertically towards the trench axis under certain condition. We call the combined stress of them the vertical rotation stress. We are going to mainly discuss the origin of the Mariana trough and a series of phenomena of the tectonic movement in the Mariana island arc system.

REVOLVING AND TENSIONAL-TILTING MOVEMENT OF THE ISLAND ARC AND THE FORMATION OF THE TROUGH

At its early stage, the Mariana island arc (including the west ridge) had appeared as a whole. Before late Miocene (9 Ma B.P.), subduction and tectonic erosion were intensified in the Mariana subduction zone, perhaps because subduction was weakened and stopped in the Luzon-Taiwan westward-dipping subduction zone, the subducting angle of the Mariana subduction zone was changed, or the Mariana arc in the middle of the big Mariana trench-arc system (the Izu-Bonin-Mariana-Palau-Yap trench-arc system) was so far from both ends of the system that it only had a smaller moment of vertical rotation. Of course, the newness of the island-arc system was also an important factor. More possibly there are many factors simultaneously acting on the system. While the Mariana island arc system was rising on the whole, it revolvingly and tensionally tilted towards the trench axis under the influence of the vertical rotation stress and splitted into both the east and the west part, and the Mariana interarc basin was formed (Fig. 6-2). Meanwhile, the main magmatic activity region migrated from west to east so that magmatism was much weakened at the west ridge. With the enlargement of its space, and the eruption and intrusion of a large amount of magma, the present Mariana trough was gradually formed (Fig.6-3).

Chemical components of the rock from drilling hole No. 453 in the trough is similar to that from No.451 in the west ridge and No.460 and 461 in the forearc (Hussong and Uyeda, 1981). Therefore, with the revolving and tensional-tilting movement, its part of the early island arc was splitted, and plunged into the trough. Both Fig.2 and Fig.5 have displayed the tensional basement with scarps developed on the east and the west flanks of the trough and structural regime steep in the east and gentle in the west due to the eastward revolving and tensional-tilting movement of the whole island arc system.

Noticeably, such an enlargement of the interarc basin resulted from the revolving and tensional-tilting eastward movement of the surface of the island arc under the influence of the vertical rotation stress, and naturally belongs to the tensional-splitting movement of the island arc, not the symmetrical spreading one in the back-arc basin on a large scale.

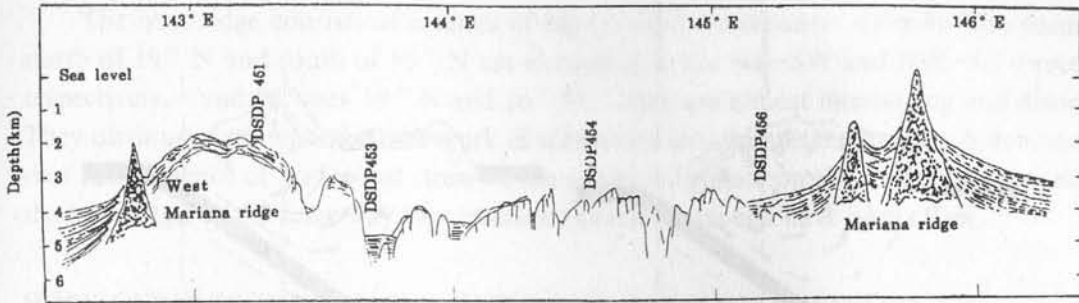


Fig. 5 Profile of the composite interpretation of several airgun lines along 18° N (adapted from Londale and Hawkins, 1985)

Subsidence and Magmatism of the Forearc Area

At drilling core No. 460, for instance, calcareous sediment of Eocene and Oligocene was located more than 6000 m under water, which was covered by sediment of Pleistocene (Hussong and Uyeda, 1981), and the carbonate compensation depth is about 3500 m. In the forearc, there are a series of normal faults, but no evidence for the accretion of oceanic plate and for the compression on the west cliff of the trench. All these indicate subsidence of the forearc.

Magmatism of the forearc has been one of major subjects in theoretical research of the island arc. Drilling cores No. 458 and 459 in the forearc demonstrate that the basement consists of primary volcanic rock relative with the island arc (Hussong, 1987; Uyeda *et al.*, 1983). Besides this, two volcanic seamounts lie 140 km east of the modern active volcanic chain, 30 to 60 km from the trench axis and less than 20 km from the Benioff zone (Jongma and Barber, 1981). Their origin seems unimaginable.

The reasonable explanation, we think, is that after the island arc system was splitted under the influence of the vertical rotation stress, the east ridge started to rotate tensionally and tilt towards the trench axis; at the same time, tectonic erosion caused by subduction made the surface of the island arc be in the tensional state and the early island arc continuously move towards the trench axis, subside or partially subduct (Fig. 6). It also can be reasonably explained in the same way that the nearer it is to the trench axis, the older the basement sediment is at the Mariana forearc (Hussong and Uyeda, 1981).

Fossiles of the late Cretaceous and the late Jurassic have been found in the metamorphic rock from drilling cores No. 460 and 461 (Hussong and Uyeda, 1981). This suggests that the original oceanic basement of the island arc should be formed in late Mesozoic, and in the developing process of the island-arc system, be completely destroyed, be deeply buried or be migrated towards the trench axis by intensive tectonization and magmatism, as well as disappear with tectonic erosion.

Tectonization of Back-arc Region

We are mainly to discuss something about the trough and west ridge which lie behind the volcanic front.

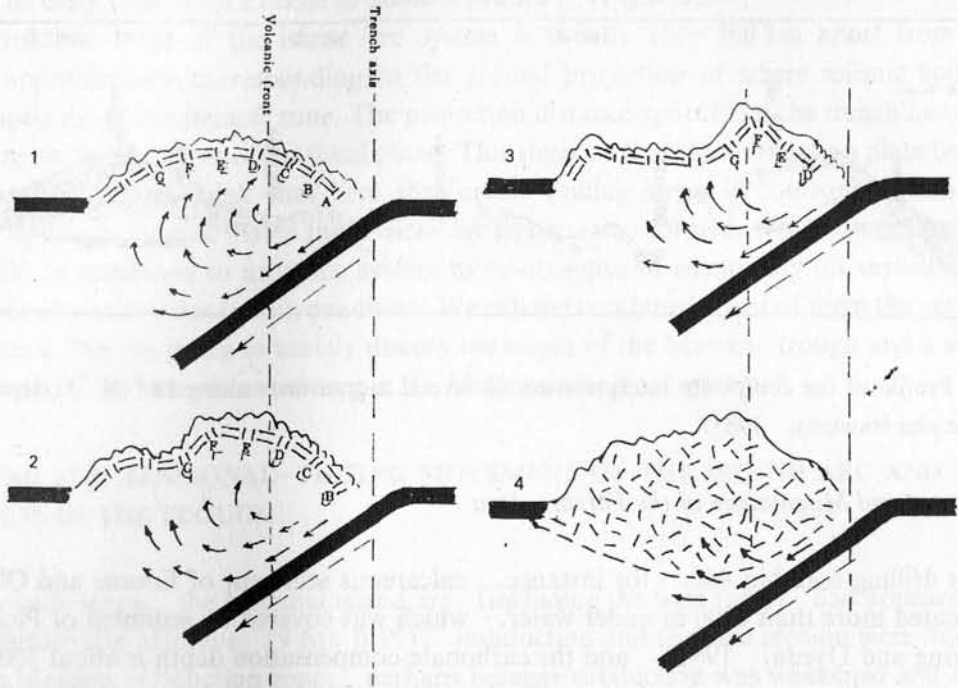


Fig.6 Sketch of the evolution of the Mariana arc and trough. (1) Island arc system formed at early stage; (2) Trough beginning to develop in the vertical rotation stress field; (3) Mariana arc further moving to the trench axis with the revolving and tensional-tilting movement and the trough formed; (4) Island arc (including west ridge) and trough combined into a continental island arc system in the end.

Tectonization of the Mariana trough is intensive and its basement consists of young tholeiite. Such rocks were sampled during cruise SO-57. Rocks at deep sea drilling hole No. 453 had been pyritized by hydrothermal activity which was also found at No.456 near the frontal-arc (Jongma and Barber, 1981). During cruise SO-57 huge number of hydrothermal sulfidic sediment was also discovered in the middle of the trough, overlying the present inactive fissure for eruption of basalt and generally being of low content of metal, some even being brown or white silicide. Thus, it can be concluded that from west to east in the trough under the influence of the tensional stress field, there is a wide range of hydrothermal activity different from that of the oceanic mid-ridge. The eastward revolving and tensional-tilting movement of the east ridge would be beneficial to matter and energy rising from the subduction plate and mantle in the back-arc region. Such kind of rising is for magma to extrude and intrude with multi-axes and migrating pattern along faults caused by the revolving and tensional-tilting movement, but not along the only central ridge. Therefore, what is so-called the spreading center of the trough is nothing but a modern active fault zone. Of the character of magnetic anomalies, there is a sharp difference between the trough and the oceanic mid-ridge, which indicates that their tectonic settings are quite different from each other. The magnetic anomalies with low amplitude and gentle variation suggests that the magnetism of basalt in the trough has been greatly weakened by dynamic and

thermal process.

The west ridge consists of a series of big or small seamounts (Fig.4). The seamounts north of 19° N and south of 16° N are elongated in the NE-SW and NW-SE direction, respectively, and between 19° N and 16° N, they are almost intersecting and disorderly. They obviously correspond to the mark of transverse structure in the forearc. It demonstrates that the influence of horizontal stress of the subducting plate on the forearc has extended to the west ridge. In the same way the structure lines in the trough have been offset.

HORIZONTAL TECTONIC MOVEMENT OF THE TRENCH-ARC SYSTEM

Many models have been proposed to explain why the island arcs are bowed to the ocean. Isacks *et al.* (1968), Toksoz and Hsui (1978) pointed out that the rising of magma in the back-arc basin is the main cause of formation of the convex arc.

As the unequilibrium of divergence and convergence of matter and stress was intensified between the subduction along the Japan-Taiwan-Philippine trench-arc system and the spreading of the Pacific mid-ridge, Lin (1987) thought, the oceanic plate would be finally cut off along an isostress belt and it was developed into a new site, the big Mariana trench-arc system, absorbing both matter and stress that the old trench-arc system failed to absorb. This new subduction zone and the old one lying to the west comprised a fan-like double-subduction zone in a mosaic pattern. Thus a new equilibrium between subduction and spreading was built up. This was the original pattern of the Mariana trench-arc system bowing to the ocean (indicated by the dotted line in Fig.7).

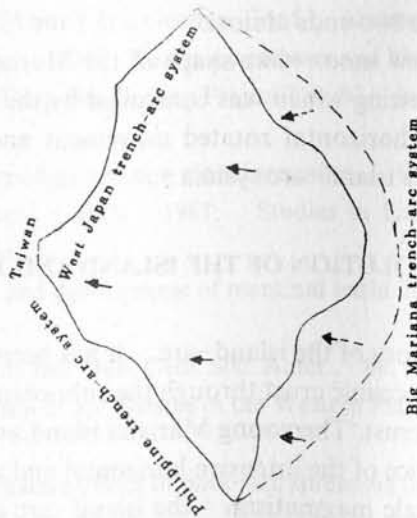


Fig.7 Sketch of the movement of the big Mariana trench-arc system in the horizontal direction (from Lin, 1987).

After the double-subduction zone was formed, the old subduction zone still unequally absorbed matter and stress from the Philippine Sea, therefore, as an isostress belt, the big Mariana trench-arc system under the influence of the horizontal stress from the spreading of

the oceanic mid-ridge must be restricted to move and would rotate differentially in the westward horizontal direction (Fig. 7). The Izu-Bonin trench-arc system and the Yap-Palau trench-arc system rotated round a fulcrum respectively, and the two flanks of the Mariana trench-arc system displayed the sinistral and dextral movement respectively (as showing in Fig. 7). At the same time, the east ridge differentially, revolving and tensionally tilted to the trench axis (mentioning back). Therefore, the Mariana island-arc system has evolved into the present one.

THE FORMATION MECHANISM OF THE NEW MOON-LIKE SHAPE OF THE MARIANA TROUGH

The early Mariana trough could be ever connected with the interarc basin on the Izu-Bonin island arc. They were separated by the westward differential rotation of the big Mariana trench-arc system. The rotatory movement also made the early equilibrium between subduction of the big Mariana trench-arc system and spreading of the oceanic mid-ridge broke up. The angle between the straight lines from the middle of the Mariana trench-arc system to its two flanks and the direction of spreading stress of the oceanic mid-ridge would come to decrease (or increase) with the change of the Mariana trench-arc curvature, and it will get more and more difficult for the plate to subduct, so that the horizontal stress acting on the island arc becomes bigger and bigger from the middle of the system to its two flanks. Obviously, such changes of both the curvature of the trench-arc system and the horizontal stress acting on the island arc led to the eastward revolving and tensional-tilting movement of the island arc to decrease more and more from the middle of the system to its two flanks and to disappear at its two ends almost.

Thus we can see that the new moon-like shape of the Mariana trough has been developed in such a special tectonic setting which was controlled by the double-subduction zone, and results from the westward horizontal rotated movement and eastward revolving and tensional-tilting movement of the island-arc system.

DISCUSSION OF TECTONIC EVOLUTION OF THE ISLAND AND TROUGH

Through research of the history of the island-arc, it has been known that the island arc crust generally evolves from the oceanic crust through the suboceanic crust (or subcontinental crust), then to the continental crust. The young Mariana island arc will certainly go through such a process. Under the influence of the intensive horizontal and vertical tectonic movement and the long period of large-scale magmatism, the island-arc crust will continuously become thick, be denuded and covered with deposits, and at last be developed into continental crust. During the long geological period, the revolving and tensional-tilting movement of the island arc will make some old crust above the surface of water subside at the forearc region with a series of geological phenomena such as stratigraphic unconformity and strata tilting or overturning at the forearc of the Japan Islands.

However, the change of subducting angle, rate and direction, and the maturity and senescence of the island arc probably will retard, restrict or even stop the further develop-

ment of the revolving and tensional-tilting movement of the island arc, but make uplift, denudation and horizontal movement of the island arc strong accordingly. Oscillation possible happens to the vertical movement of the forearc region. Stripping substance of the subduction plate possible will accumulated at the Sava forearc. If the vertical-rotating stress field still exists, subsidence will dominate the forearc tectonization.

The Mariana trough will not be transversely enlarged on a larger scale. But as a negative structure of the island arc system, the trough will act as an active region of tensional stress field, and intensely active region of faulting and magmatism, a region to receive sediments from the island arc within a long geological period. It will undergo development and evolution of the multi-axes geosyncline similar to that of Hanshu, Japan (in the old mid tectonic period), that is, there will occur such a kind of tectonic movement which is dominated by a tensional stress field in the wide region of compressional stress field.

To sum up, the Mariana trough will at last emerge above the water to be one part of Mariana island arc system, and the whole system will rise high in the West Pacific (Fig.6-4).

REFERENCES

- Bibee, L.D. *et al.*, 1980: Inter-arc spreading in the Mariana trough. *Marine Geology*, 35, 183-197.
- Fryer, P. *et al.*, 1985: Origin and emplacement of Mariana forearc seamounts. *Geology*, 13, 774-777.
- Hussong, D.M., 1987: Tectonic implications of the crustal structure of the Mariana island arc system near 18° N Latitude (Abstr.). *Int. Geodyn. Conf., Abstracts of Papers, Tokyo*, 60-61.
- Hussong, D.M. and S. Uyeda., 1981: Tectonic processes and history of the Mariana arc: A Synthesis of the Results of the Deep Sea Drilling Project Leg 60, Initial Rep. *Deep Sea Drill. Proj.*, 60, 909-929.
- Isacks, B. *et al.*, 1968: Seismology and new global tectonics. *J. Geophys. Res.*, 73, 5855-5899.
- Jongma, D. and A. J. Barber (eds.), 1981: *Studies in East Asian tectonics and resources. CCOP-10C, Second Edition.*
- Karig, D.E., 1971: Origin and development of marginal basin in the Western Pacific. *J. Geophys. Res.*, 76, 2542-2561.
- Karig, D.E., 1972: Remnant arcs. *Bull. Geol. Soc. Amer.*, 83, 1057-1068.
- Karig, D.E., 1974: Evolution of arc systems in the Western Pacific. *Ann. Rev. Earth Planet. Sci.*, 2, 51-57.
- Karig, D.E. *et al.*, 1978: Characteristics of back-arc spreading in the Mariana trough. *J. Geophys. Res.*, 83, 1213-1226.
- Lin, C.S., 1987: Plate stress field and tectonization of the double-subduction Zone—Studing on the origin and development of the Big Mariana trench-arc system. *Bull. Marine Sci.*, 4 (6), 80-86 (in Chinese).
- Londale, P. and J. Hawkins., 1985: Silicic volcanism at an off-axis geothermal field in the Mariana trough back-arc basin. *Bull. Geol. Sol. Amer.*, 96, 940-951.
- Scott, R.B. and L. Kroenke, 1981: Periodicity of remnant arcs and back-arc basin of the South Philippine Sea. *Proc. 26th IGC. Geology of Continental Margins, Paris.*

- Toksoz, M.N. and A.T. Hsui, 1978: Numerical studies of back-arc convection and the formation of marginal basins. *Tectonophysics*, 50, 177-196.
- Uyeda, S., 1977: Some basic problems in the trench-arc-back arc system. M. Talwani and W.C. Pitman III (eds.), *Island Arcs, Deep Sea Trenches and Back-arc Basins*, Maurice Ewing Ser., 1, Am. Geophys, Washington, D.C., 1-14.
- Uyeda, S. *et al.*, 1983: The structure of the eastern edge of the Philippine Sea-Mariana and Bonin Arc. *Sci.*, 7 (53), 439-447 (in Japanese).
- Von Huene, R. and S. Uyeda, 1981: A summary of results from the IPOD transects across the Japan, Mariana and Middle America convergent margins. *Proc. 26th IGC Geology of Continental Margins*, Paris.

THE EARLY MESOZOIC OROGENY IN THE NORTHERN SHELF OF THE SOUTH CHINA SEA AND ITS ADJACENT LANDS

ZHOU ZUYI

Department of Marine Geology, Tongji University, Shanghai, China

ABSTRACT

Paleomagnetic data showed that an early Triassic continental collision was taking place in southeast China as the related continents drifted northward. This collision marks the beginning of an early Mesozoic orogeny in the region, which has a close genetic relationship with the evolution of western Fujian—eastern Guangdong foreland basin. As the orogeny ended in late Jurassic, Borneo began its rifting away from South China margin, creating the proto—South China Sea Basin. The present South China Sea has evolved following the drifting away from South China margin of continental fragments such as northern Palawan, Reed Bank, Xisha Islands, Zhongsha Islands and others.

INTRODUCTION

Regional studies in Southeast Asia and South China in the last decade have culminated in the recognition of several continental blocks which were pieced mainly from late Paleozoic to early Mesozoic (e.g. Sengor, 1984, and many others). The middle and late Triassic collision between South China block and Indo—China block along Black River suture and Red River suture is well documented, yet little was discussed about the possible suture zones eastwards. The similarity of Cambrian sedimentary sequence, ore deposits and trilobites between Hainan Island and Australia, and the discovery of late Paleozoic glacio—marine deposit (Yang *et al.*, 1989) similar to those from North Tibet, West Yunnan and Southeast Asia suggest that Hainan Island is a fragment rifted away from Gondwana—Land after or at the end of Paleozoic. Wang (1986) suggested that the suture zone be located at the Reiqiong Strait which separates Hainan Island from mainland China. Zhu (1987) proposed that a pre—Cretaceous active margin, along the northern shelf of South China Sea, links up with Red River suture and passes through the southern part of Hainan Island. Others (Yan, Zhen, 1989, oral communication) argued that it is located at some places in the northern part of the island. The case in the eastern part of northern shelf of South China Sea and Southeast China continental margin is poorly known, due to the covering of sea water, the wide distribution of Mesozoic granites and the well—developed Jurassic and early Cretaceous volcanics. In this paper, the author will first put forward the paleomagnetic obtained from Permian—Triassic rocks in western Fujian in order to illustrate the position of the region during that time. More emphases will be then laid on the geological characteristics of western Fujian—eastern Guangdong Mesozoic foreland basin. Based on these information and other available geophysical and regional geological information, the author will discuss the early Mesozoic orogeny in the region and its geological implication, including the forma-

tion and evolution of South China Sea.

PALEOMAGNETISM STUDY OF PERMIAN-TRIASSIC ROCKS FROM WESTERN FUJIAN

Three formations were chosen (Fig. 1) and altogether 182 samples were collected for the paleomagnetism study. After the measurement of their NRM, synthetic demagnetization have been carried out for all the samples except for those samples which exhibit too weak an intensity to accomplish further measurement. Thereafter, stereographic projections,

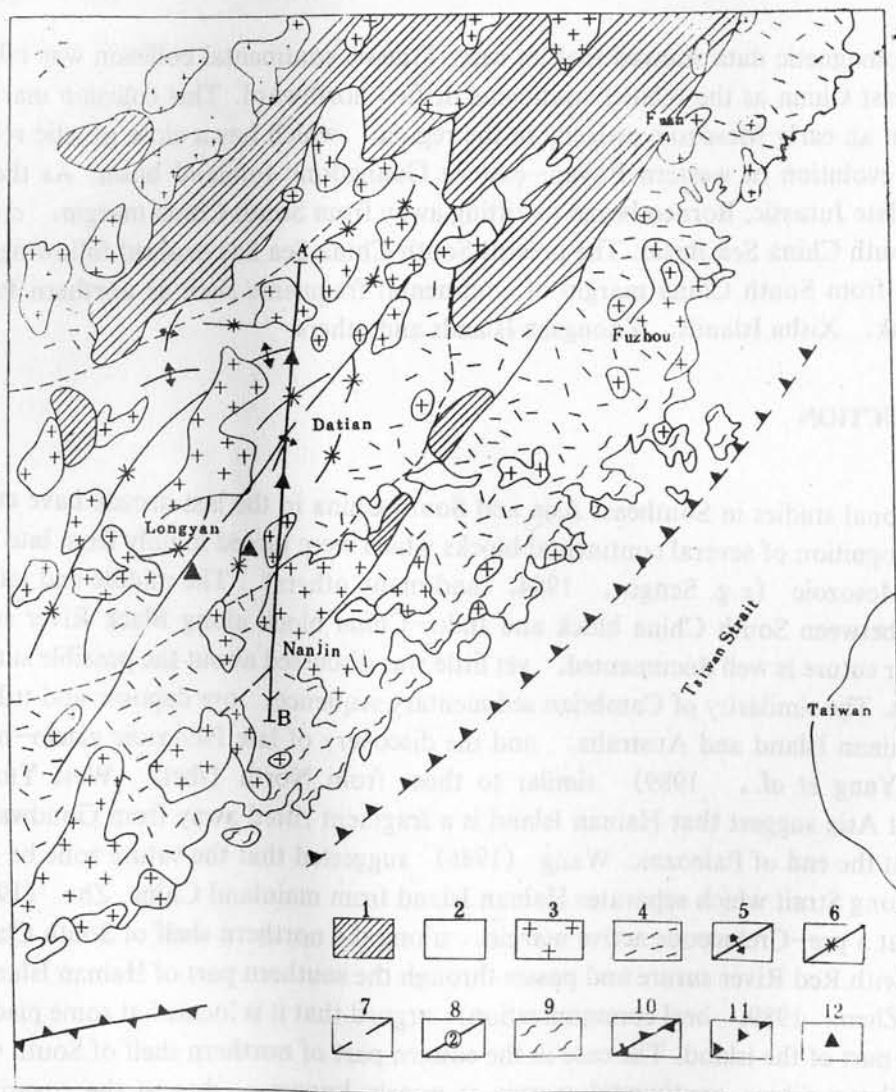


Fig.1 Tectonic map of Southeast China. Dashed lines mark the boundary of western Fujian-eastern Guangdong foreland basin. Legend: 1—Pre-Cambrian rocks; 2—Paleozoic-Mesozoic rocks; 3—granites; 4—volcanic rocks; 5—anticlines; 6—synclines; 7—Fuan-Nanjin fracture; 8—Zhenhe-Dapu fracture; 9—East Fujian tectonic zone; 10—continental collision zone; 11—subduction zone; 12—paleomagnetism sampling sites.

normalized intensity curves, Zijderveld diagrams, principle component analysis (PCA) and linear spectrum analysis (LSA) were applied in the presentation and processing of data. For most of the samples, two or three components can be successfully identified. Based on these analysis various parameters as shown in Table 1 were obtained. The result shows that the studied region has a paleolatitude of 13–19° N around Permian–Triassic boundary. A comparison of this result with those of Yangtze block and the northern part of Southeast China block for the same period shows that their corresponding pole positions were very close to each other. This suggests that Yangtze block and Southeast China block (including the studied region in this paper) had already united by the end of Permian. Both of them moved rapidly northward in early Triassic and had almost reached their present positions by the end of Jurassic (Fig.2). The paleolatitude and declination of different ages for the reference point (16° N, 103° E) for South China (including Yangtze block and Southeast China block) and Indo–China show that the difference of paleolatitude decreased from Triassic to Jurassic. This means that Indo–China had undergone a more rapid movement and, as a result, convergence between South China and Indo–China took place from Triassic to Jurassic.

Table 1 Site–mean paleomagnetic directions from West Fujian

Site	Age	N	I	D	Plg	Plt	A95	K	Dp	Dm	Lp
Lantian Formation											
LTO	Pu	5	55.80	26.50	207.90	36.60	42.60	9.46	25.00	46.10	
LT1	Tl	5	36.80	46.60	193.80	57.00	17.10	52.85	14.20	22.00	
LT2	Tl	4	31.40	35.00	211.90	60.40	4.70	24.30	3.10	5.40	
LT3	Tl	7	44.10	31.00	209.70	48.20	22.20	18.13	13.80	24.80	
Me	an	21	42.60	35.10	206.40	50.30	4.10	43.40	9.40	16.30	19.40
Yanshi Formation											
YSO	Pu	5	21.40	31.50	225.80	68.40	20.60	1.42	12.94	23.20	17.08
Xikou Formation											
XKO	Tl	8	11.30	31.10	168.00	76.00	17.50	3.30	10.90	19.60	
XK1	Tl	10	23.40	24.00	180.20	64.20	25.40	10.00	14.50	27.10	
XK2	Tl	10	12.40	26.30	163.40	73.20	12.00	40.00	7.00	13.00	
XK3	Tl	3	22.10	29.20	140.10	66.90					
XK4	Tl	2	25.40	19.40	178.10	61.10					
Mean		33	20.10	26.30	178.30	67.60	6.70	133.33	3.90	7.30	13.90

Note: Pu—late Permian; Tl—early Triassic; N—number of samples averaged; D—declination in degrees; I—inclination in degrees; Plt, Plg—latitude and east longitude of virtual geomagnetic poles in degrees; A95—radius 95% confidence in degrees; K—precision parameter; Dp, Dm—semiaxes of oval of 95% confidence about poles; Lp—paleolatitude.

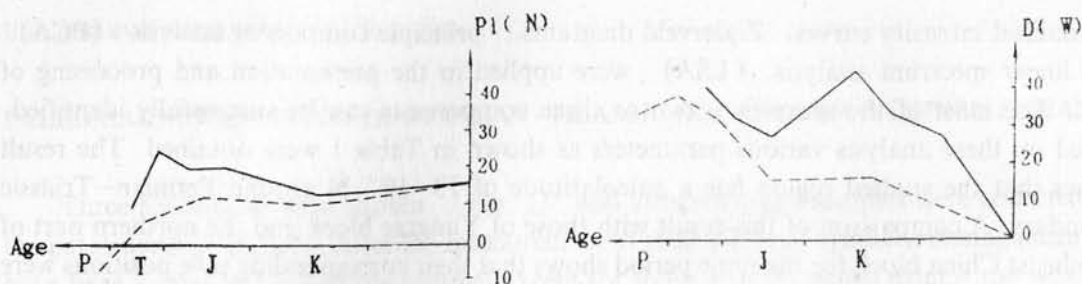


Fig. 2 Comparison of paleolatitudes and declinations computed at the point 16° N, 103° E for Indo-China (heavy line) and South China (dashed line). The data of Indo-China are from Achache *et al.* (1985).

WESTERN FUJIAN-EASTERN GUANGDONG MESOZOIC FORELAND BASIN

The basin is usually called Yongmei depression and is believed to be either a Hercynian fold zone or a Hercynian-Indosinian fold zone or even a Calidonian fold zone. The author's previous study showed that it had evolved from the late Paleozoic passive continental margin to the early Mesozoic foreland basin, which has a close genetic relationship with an early Mesozoic continental collision in the south.

The Mesozoic sedimentary sequence of West Fujian had evolved from the early Triassic flysch deposits to the coal-bearing mollasse deposits of late Triassic to late Jurassic, which constitutes a typical foreland basin sedimentary sequence. This foreland basin stretched out in an ENE direction with its scope changing through later development. In early Triassic, the foredeep of the basin was in Central Fujian's Datian county where deep water fine turbidites were deposited. Then, as the scope of the basin getting larger and larger, the depth of the water got shallower and shallower. This process culminated from late Triassic to late Jurassic when the extremely thick mollasse were rapidly deposited and the scope of the basin reached its uttermost.

The radiometric ages of Permian-Triassic granites in West Fujian foreland basin range from 201 Ma to 248 Ma. The diagenetic minerals of the granites show a preferential orientation and evidences of stress. Their well-documented radiometric data show high values of $(\text{Sr}^{87} / \text{Sr}^{86})$ ratio. They are chemically rich in alkalis, $\text{K}^{+} / \text{Na}^{+}$ ratio, SiO_2 and Al_2O_3 , and poor in $\text{Fe}^{2+} / (\text{Fe}^{2+} + \text{Fe}^{3+})$. Their LREE / HREE ratio are relatively high. The plots of trace elements such as Rb / Zr against SiO_2 , Nd, Y, Yb against SiO_2 respectively, Nb against Y, and Rb against Y + Nb suggest a syn-collision or post-collision origin for these granites. All the above features show that these granites correspond to the S-type granites of White (1977). These Permian-Triassic granites may be related to the partial melting of the partly subducted continental crust or voluminous sediments accumulated between the two continents before the final closure of the intervening ocean.

DISCUSSION

From the latest Paleozoic to the earliest Mesozoic, the Cimmerian continent rifted

away from the northern margin of Gondwana—Land. This continent further disintegrated as it moved across the Tethys domain. Paleomagnetic and paleontologic evidences show the possible Gondwana—Land provenance for blocks such as Yangtze, South China and Hainan Island. The early Mesozoic collision in Southeast China and the paleomagnetic results obtained in this paper suggest that, before the Cimmerian continent united with Eurasia from late Triassic to middle Jurassic, some of the blocks had already collided as they moved northward. The collisions of continental blocks that constitute the Cimmerides therefore took place diachronically along the Tethysides of Sengor (1984).

The evolution of western Fujian—eastern Guangdong foreland basin has proved to be in close genetic relationship with a continent—continent collision which took place to the south of the basin in early Triassic. This collision marks the beginning of the early Mesozoic orogeny in the region. The orogeny, however, did not stop as the collision ended. The continuing uplift of continental blocks in the collision zone, which resulted in the deposition of thick molasse of T_3 — J_3 in the related foreland basin. The difficulty in identifying the evidences of the suture zone was to a great degree due to the massive magmatic activity from late Jurassic to early Cretaceous, the extremely deformed and overprinted structures and the covering of the sea—water of South China Sea. However, geophysical data in the region still exhibit some evidences of the existence of a ENE trending tectonic zone. The trend of Bouguer anomaly gradient zone in Southeast Fujian changes from NE to ENE when it reaches the southern border of the foreland basin. After an upward—continuing of 30 km, the Bouguer anomaly in East Guangdong stretches out in E—W direction. The ENE trending Hongkong—Nanao tectonic zone is characterized by the relatively low aeromagnetic anomaly and the Bouguer anomaly gradient zone. It has a width of 60—70 km and a length of more than 400 km. In the eastern part of the Pearl River Mouth basin, there are three negative anomaly zones striking W—E, with anomaly values of -227 , -150 and $-200 \times 10^{-5} \text{ m/s}^2$ (mgal), respectively. These anomaly zones can be attributed to the positive magnetization of deep buried basic rock.

To the north of Zhu 3 and Zhu 2 sags in Pearl River Mouth basin, there are occurrences of metamorphic quartz sandstone and schist, corresponding to the Paleozoic metamorphic rock in the continental area. In Xisha—Zhongsha area, the magnetic basement is buried at depth of 1.0—1.5 km, while the crust is of 24—27 km thick. From the southwest of the Pearl River Mouth basin to the Xisha Islands, there is a wide and flat negative anomaly zone trending approximately W—E, which probably represents the granite gneiss with an isotopic age of 627—1465 Ma that was encountered in Xiyong I well. This shows that the Xisha Islands and the Zhongsha Islands in the northern part of the central basin of South China Sea could enigmatically be relic continents. Southward, it is evident from geophysical data and rocks dredged from these areas that a continental fragment underlies the Dangerous Grounds and Reed Bank (Kudrass *et al.*, 1986). Another continental fragment in the south includes the northern Palawan Island and the southwestern Mindoro Island. The affinities of basement rocks in Borneo and South China made Ben—Avraham and Uyeda (1973) suggest that during the early Mesozoic, Borneo was adjacent to the China margin. That is, Borneo, northern Palawan, Reed Bank, Xisha Islands and Zhongsha Islands were part of South China continental margin. They collaged to South China in early Triassic. The ending of deposition of molasse in the related western Fujian—eastern Guangdong foreland basin in late Jurassic suggests that, the rifting of collaged continental blocks away from South China

margin happened after late Jurassic. This is in agreement with what Ben-Avraham (1989) put forward that the opening of the proto-South China Sea basin had occurred by the early Cretaceous, due to the rifting of Borneo and perhaps the Philippines from South China. At that time, the other continental fragments, including the northern Palawan, Reed Bank, Xisha Islands and Zhongsha Islands, were part of the South China margin of proto-South China Sea basin. Along with the subduction of oceanic crust of proto-South China Sea basin beneath Borneo, these fragments gradually rifted away from the South China margin to creat the present South China Sea (Fig.3).

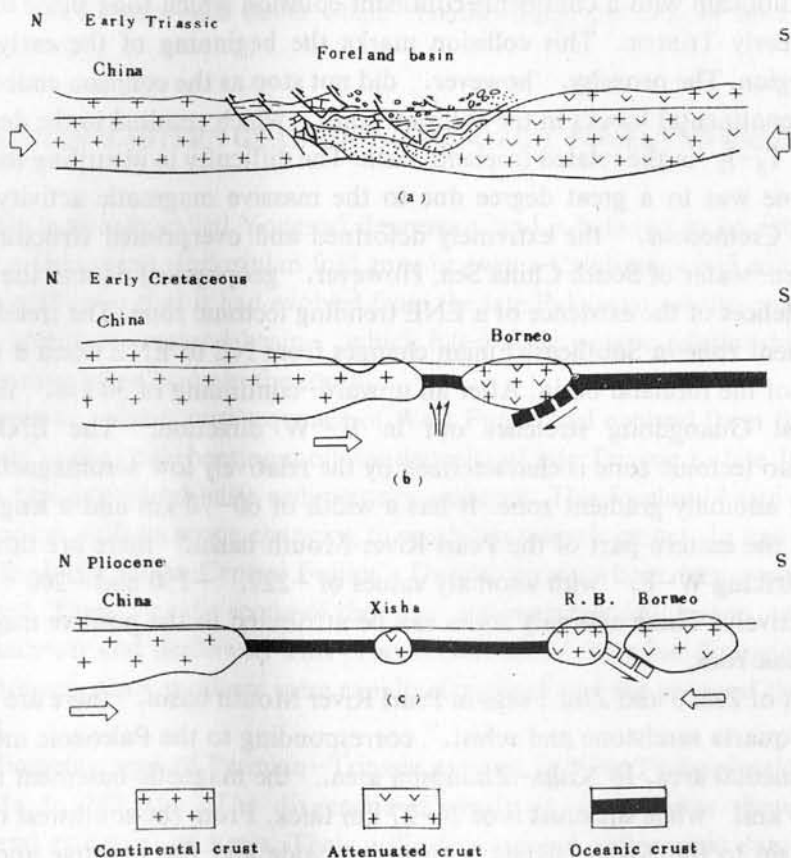


Fig.3 The schematic cross sections to show the evolution of South China and the South China Sea. (b) and (c) are adapted from Ben-Avraham (1989).

CONCLUSIONS

1. A continental collision took place in early Triassic to the south of western Fujian-eastern Guangdong foreland basin, which marked the beginning of early Mesozoic orogeny in the region. The southern continent may includes fragments of Hainan, Xisha Islands, Zhongsha Islands, Reed Bank, northern Palawan, Borneo and others.
2. Paleomagnetic results from western Fujian suggest that the collision was taking place as the two related continental blocks drifted northward, indicating that the collage of colli-

sion blocks that constitute Cimmerides took place diachronically.

3. The drifting of Borneo from the South China margin occurred following the ending of the orogeny at the end of Jurassic, resulting in the formation of proto-South China Sea basin.

4. The present South China Sea was probably created by the rifting of the other continental fragments away from the present South China margin. These fragments now are distributed separately in South China Sea.

REFERENCES

- Ben-Avraham, Z. and S. Uyeda, 1973: The evolution of the China basin and the Mesozoic paleogeography of Borneo. *Earth Planet. Sci. Lett.*, 18, 365-376.
- Ben-Avraham, Z., 1989: Multiple opening and closing of the eastern Mediterranean and South China basins. *Tectonics*, 8 (2), 351-362.
- Chen, Y.A. and P.Z. Wang, 1982: A study on the regional geophysical and geochemical characteristics of Fujian Province. *Geology of Fujian*, 1 (2), 69-82 (in Chinese).
- Kudrass, H.R., M. Weidicke, P. Cepek, H. Kreuzer and P. Muller, 1986: Mesozoic and Cenozoic rocks dredged from the South China Sea (Reed Bank area) and Sulu Sea and their significance for plate-tectonic reconstructions. *Mar. Pet. Geol.*, 3, 19-30.
- Ren, J.S., C.F. Jiang, Z.K. Zhang and D.Y. Qing, 1980: Geotectonics of China and its evolution. Science Press, Beijing (in Chinese).
- Sengor, A.M.C., 1984: The Cimmeride orogenic system and tectonics of Eurasia. *Geol. Soc. Am. Sp. Paper*, 195, 82.
- Wang, D.Z. and C.S. Liu, 1986: Distribution regularities and genetic series of granites of Hercynian-Indosinian cycle in SE China. *Acta Petrologica Sinica*, 2 (4), 1-13 (in Chinese).
- Wang, H.Z., 1986: Geotectonic development of China. *The Geology of China*, T. Yang (ed), Oxford, England, Clarendon Press, 363.
- Yang, S.F., Z.Y. Yu, L.Z. Guo and Y.S. Shi, 1989: The division and paleomagnetism of the Hainan Island and plate tectonic significance. *Journal of Nanjing University (Earth Science Edition)*, 1-2, 38-46 (in Chinese).
- Zhou, Z.Y. and Q.Y. Lao, 1990: Mesozoic evolution of eastern Fujian and its adjacent areas. *Terrane Analysis of China and the Pacific Rim*, Circum-Pacific Council for Energy and Mineral Resources, T.J. Wiley *et al.*, (eds), Earth Science Series, 13, 185-187.
- Zhu, X., 1987: On the evolution of continental margins of China. *Marine Geology and Quaternary Geology*, 7 (3), 115-119 (in Chinese).

CRUSTAL ISOSTASY AND MANTLE ANOMALY IN THE SOUTH CHINA SEA*

JIANG JIAZHEN

Second Institute of Oceanography, SOA, Hangzhou, China

ABSTRACT

The flexure model of the crustal isostasy contributes a major method to study the oceanic crustal structure with the free-air gravity anomalies. Using this technique, we have proved existence of the thermal mantle anomaly under the northwestern basin of the South China Sea.

INTRODUCTION

The concept of isostasy describes the manner in which topographic features on the earth's surface are compensated at depth. The two most commonly used models were those developed by Airy (1855) and Pratt (1855). In the Airy model the crust is of constant density but is thicker beneath mountain ranges than lowlands. For the Pratt model the average crustal density is smaller beneath mountain ranges than lowlands. These models satisfied the early requirements of physical geodesy but initially were only of limited interest to geologists and geophysicists. Subsequent seismic studies showed that the Airy model, in particular, satisfactorily explained variations in crustal structure associated with such features as mountain ranges and continental margins (Heiskanen and Vening Meinesz, 1958).

The Airy model, however, implies a crust that cannot support vertical shear stresses or their equivalent gravity anomalies. Barrell (1914) argued that isostatic equilibrium in the form envisaged by Airy could not exist everywhere on the earth's surface because of the finite strength of the crust. He defined this strong rigid upper layer of the earth as the lithosphere.

A number of studies (Vening Meinesz, 1914; Walcott, 1970; Watts *et al.*, 1980) have subsequently investigated the response of the lithosphere to surface loads such as seamounts and oceanic islands. These studies indicate that in a number of cases the response of the lithosphere to surface loads can be modeled as that of a thin elastic plate overlying a weak fluid. This model of isostasy, referred to as the flexure model, is similar to the Airy model in which surface loads are supported by crustal thickening, but differs by including the lateral strength of the crust. A useful parameter in the flexure model, which characterizes the response of lithosphere to these loads, is the effective flexural rigidity of oceanic lithosphere which ranges from 7×10^{26} to 1×10^{31} dyn-cm and is a strong function of crustal age and temperature. A number of studies (Sleep, 1971; Watts and Ryan, 1976; Steckler and Watts, 1978) have shown that the post-rift tectonic subsidence of margins can be explained in terms of simple thermal cooling models. These observations suggest that

* Project supported by National Natural Science Foundation of China.

the effective flexural rigidity, and therefore the state of isostasy, may vary during the evolution to the margin.

The objective of this paper is to analyse information on the isostatic state in the South China Sea. The procedures we use are (1) to determine the relationship between observed free-air gravity anomalies and topography in the South China Sea, (2) to interpret this relationship in terms of different models of crustal isostasy and (3) to use the preferred models of isostasy to better understand the crustal character of the South China Sea.

GEOLOGICAL SETTING

The South China Sea basin is a small 'Atlantic-type' basin with water depths of more than 4000 m. It is bounded by rifted continental margins comprising some prominent submarine plateaus, namely, the shoaly Dangerous Grounds (Nansha Islands) and Reed Bank to the south and the Paracel Islands (Xisha Islands) and Maceles Field Bank (Zhongsha Islands) to the north. The eastern boundary forms an active subduction zone west of Luzon, whereas the western boundary is presumed to be primarily a sheared, transform margin (Taylor & Hayes, 1980; Fig. 5).

According to Taylor & Hayes (1983), normal seafloor spreading processes created the South China Sea basin beginning about 32 Ma B.P. and terminating about 17 Ma B.P.. Taylor & Hayes (1983) determined half-spreading rates between 2.2 and 3.0 cm/a and a north-south spreading direction. The east-trending magnetic anomalies identified by them as anomalies No. 5d-11 are only recognizable in the eastern subbasins, i.e., east of 115° E. The deep oceanic basin in the western half of the South China Sea is much narrower than that of the eastern half. On the basis of recent data Chinese researchers believe that the northeast-trending magnetic anomalies in the western subbasin resulted from pre-Oligocene seafloor spreading. The anomalies have been interpreted as magnetic lineation No. 27-32 (74-63 Ma B.P.). But Taylor & Hayes (1983) assumed that the southwestern basin of the South China Sea as developed contemporaneously with the younger oceanic portions of the eastern central subbasins and that much less oceanic crust was generated at the inferred southwestern spreading centre than at the eastern spreading centre, because the crust was more intensively stretched in the west than west that in the east.

DATA REDUCTION

In this study we have used surface-ship gravity, bathymetry and sediment profiles obtained from cruise So-49, 1987. Gravity measurements at sea were carried out with two sea gravimeters operated independently. The sea gravimeter GSS3 No. 53 served on cruise So-49 only as a redundancy system for the new sea gravimeter KSS31 No. 22 in case of trouble. From the comparison between the two gravity curves one can justify if there is a bias in the free-air anomalies due to inaccurate Eotvos correction when GPS was used. The normal gravity was calculated according to the 1967 Geodetic Reference System Formula (ATG, 1967).

METHOD OF ANALYSIS

It has been recognized for some time that gravity anomalies at sea mainly reflect the effect of sea floor topography and the manner in which it is compensated. Gravity and bathymetry generally correlate closely at short wavelengths (less than a few tens of kilometers) and poorly at longer wavelengths (greater than a few hundred kilometers). The change is due to isostatic compensation. Thus in the absence of noise and other effects such as changes in the mean depth of the water, the relationship between gravity and topography as a function of wavelength provides information on isostatic compensation.

First, using the cross-spectral techniques, we obtain a transfer function of filter which can convert an observed bathymetry profile into a series which resembles the observed gravity anomaly profile. In order to emphasize regional crustal character, we have subdivided a few long profiles into some relatively short profiles.

Then, with different isostatic characters (crustal thickness and effective elastic thickness) about the Airy model and flexure model, we obtain standard and theoretical admittance which can be calculated from theoretical formula. As pointed out by McKenzie and Bowin (1976), the observed filter or complex admittance can be easily compared with isostatic models based on different hypotheses for the manner in which sea floor topography is supported, and the isostatic characters (crustal thickness and effective elastic thickness) of different regions can be obtained.

Thus we make the transfer function convert the observed bathymetry profile into the theoretical gravity anomaly profile. The observed gravity anomaly minus this gravity anomaly is considered as that caused from sedimentary noise and non-isostatic factor. Therefore, in a certain extent we can evaluate isostatic anomaly.

This study utilizes time series techniques to analyse gravity and bathymetry as Lewis and Dorman (1970), Dorman and Lewis (1970), and McKenzie and Bowin (1976).

In the space domain the gravity anomaly consists of convolving an impulse response (or Green's function) $f(x)$ with the bathymetric profile $b(x)$:

$$g(x) = f(x) * b(x) \quad (1)$$

In the wave number domain this is equivalent to a simple multiplication:

$$G(k_n) = Z(k_n) \times B(k_n) \quad (2)$$

where $Z(k_n)$ is similar to the form of the transfer function used by Dorman and Lewis (1970) and Lewis and Dorman (1970). In the presence of noise a better estimate of $Z(k_n)$ is given by McKenzie and Bowin (1976):

$$Z(k_n) = [G(k_n) \times B(k_n)^*] / [B(k_n) \times B(k_n)^*] \quad (3)$$

where * indicates the complex conjugate. In this case, the admittance is given only by using all complex function form for spectrum of gravity and bathymetry.

The required filter can then be obtained by using inverse Fourier transform for the admittance. In order to reduce the noise from sediment in the estimate of the admittance,

sediment density correction is required. There are most of the profiles for cruise So-49 which are long enough to cross the regions of various geological features. So according to crustal feature we have subdivided these long profiles into a number of shorter profiles.

The basic computational steps are similar to those outlined by McKenzie and Bowin (1976). After subdividing long profiles into a number of shorter profiles, the discrete Fourier series is obtained by using the fast Fourier transform.

ISOSTATIC MODELS AND THEORETICAL ADMITTANCE

The method which was developed by Dorman and Lewis (1970) is used to determine quantitatively the state of isostasy for a geological feature. The free-air gravity anomalies are caused by topography and its compensation.

The admittance for an Airy model of compensation is given by the sum of the Fourier transforms of two sinusoidal density layers, one representing the sea floor topography and one representing the base of the compensating mass (McKenzie and Bowin, 1976). The resulting admittance is

$$Z(K_n) = 2\pi G (\rho_2 - 1.03) e^{-K_n d} (1 - e^{-k_n t}) \quad (4)$$

where ρ_2 is the density of the crustal layer, d is the mean water depth and t is the average Airy crustal thickness.

A similar procedure is used to determine an expression for the admittance when a plate model of compensation is assumed, although the computations are more involved since the deflection due to the load must be calculated as part of the computation of the gravity effect of the compensation. McKenzie and Bowin (1976) outlined a procedure for this derivation. The expression is improved by Cochran (1979). The resulting admittance is:

$$Z(K_n) = 2\pi G (\rho_2 - 1.03) e^{-k_n d} \left\{ 1 - [e^{-k_n t_2} (\rho_3 - \rho_2) + e^{-k_n t_c} (\rho_m - \rho_3)] / [(\rho_m - \rho_2) + 4(\rho_m - 1.03) M k'^2 A B^{-1}] \right\} \quad (5)$$

where t_2 is the thickness of layer 2; t_c is the mean thickness of the upper mantle; ρ_3 is the density of layer 3, taken to be 2.87 g/cm^3 ; ρ_m is the density of the upper mantle, taken to be 3.3 g/cm^3 ; $M = E / 3 g h (\rho_m - 1.03)$, where E is Young's modulus and the plate thickness is $2h$; $k' = kh$; $A = [\sinh(2k') / 2k']^2 - 1$ and $B = [\sinh(4k') / 4k']^2 + 1$.

Calculated admittance curves for the Airy model and the plate model of compensation are superimposed on the observed admittance values in Fig.1, Fig.2 and Fig.3.

RESULTS

By applying the admittance function approach to the analysis of observed gravity anomaly and topography profiles, it is possible to investigate isostatic mechanism. The interpretation of the observed admittance function in terms of an isostatic model involves assumptions concerning the rheology and density structure of the margin.

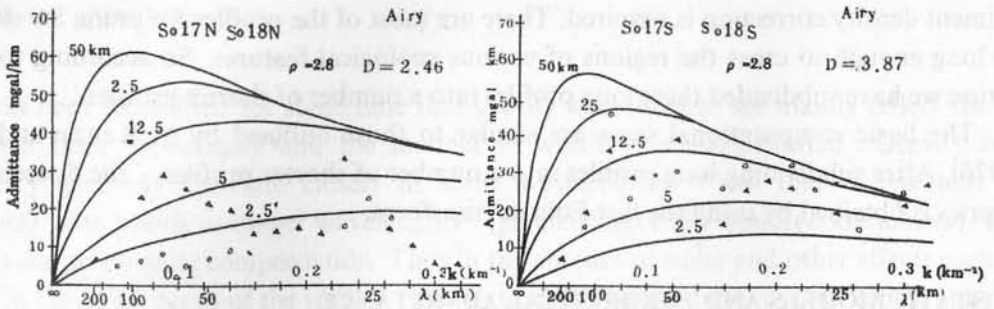


Fig.1 Observed admittance values for profiles So17 (open dots) and So18 (solid triangles) compared with Airy's models.

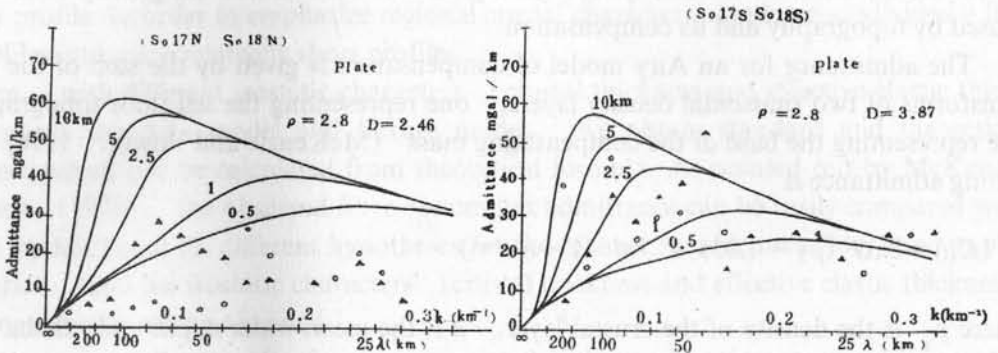


Fig.2 Observed admittance values for profiles So17 (open dots) and So18 (solid triangles) compared with plate models.

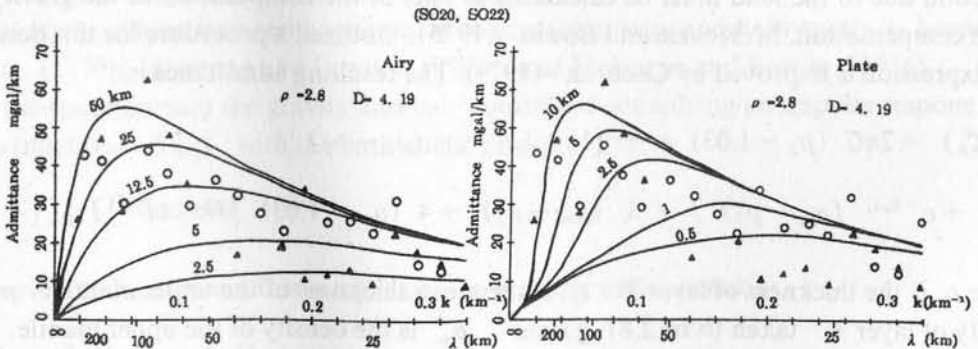


Fig.3 Observed admittance values for profiles So20 (open dots) and So22 (solid triangles) compared with Airy's and plate models.

Profiles So17S and 18S are in the spreading centre of the eastern subbasin. Figs.1 and 2 shows $T_c = 5-25$ km, $T_e = 1-10$ km for So17S and $T_c = 2.5-15$ km, $T_e = 0.5-2.5$ km for So18S. T_c is crustal thickness for the Airy model, and T_e is effective elastic thickness for the plate model. Comparing theoretical gravity with observed gravity, we can find $T_c = 10-15$ km, $T_e = 5$ km for So17S and $T_c = 10-13$ km, $T_e = 3-8$ km for So18S (Fig.4). The above results are based mainly on the admittance for long wavelength, but not for uncompensated short wave lengths ($\lambda < 100$ km)

Profiles So17N and So18N are in the northern continental shelf and the northwestern subbasin of the South China Sea. Figs.1 and 2 shows $T_c < 5$ km, $T_e < 1$ km for So17N and $T_c < 10$ km, $T_e < 2$ km for So18N. And there are stronger isostasy gravity anomalies, high value for the northwestern subbasin and low value for the continental shelf (Fig.6).

Profiles So22 and So20 are in the southwestern subbasin and its edge, respectively. Their T_c and T_e are higher, $T_c = 20-40$ km, $T_e < 25$ km for So20 and $T_c = 10-30$ km, $T_e < 20$ km for So22 (Fig.3).

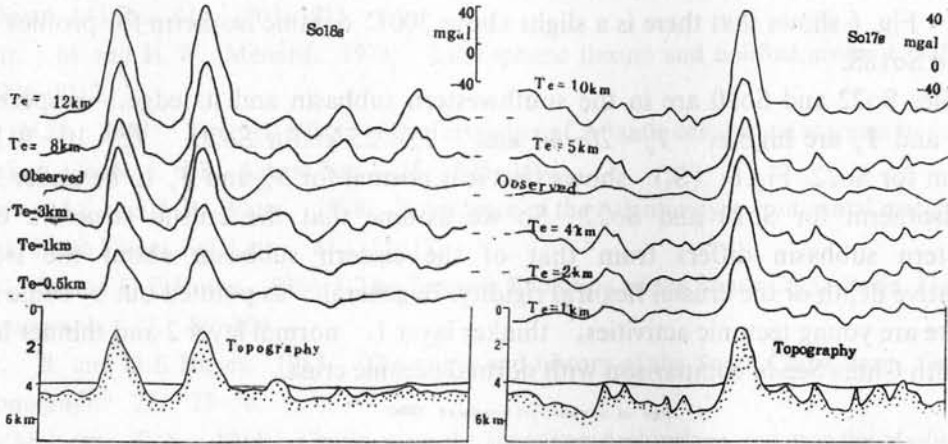


Fig.4 Comparison of observed and computed free-air gravity anomalies of So17S and 18S.

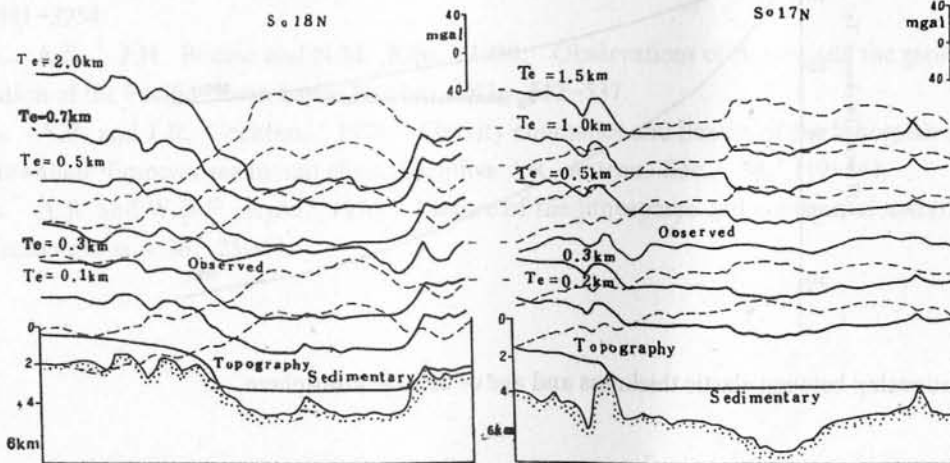


Fig.5 Comparison of observed and computed free-air gravity anomalies of So17N and 18N.

DISCUSSION

Fig.6 shows that the elastic thickness estimates determined from different surface loads on the oceanic lithosphere can be reasonably well fitted by the 450 ± 500 °C oceanic isotherm, based on simple thermal models for the cooling lithosphere (Watts, 1980). But except profiles So20 and So22 (S_3) our results (S_1, S_2) are obviously above 300°C oceanic isotherm. Especially, the effective elastic thickness for profiles So17N and So18N

which cross the northern continental shelf and the northwestern subbasin, are only less than 2 km. These values would not be caused by the noise or calculated error. The profiles both in the northern continental shelf and the northwestern subbasin (Fig. 5) display the stronger isostasy gravity anomalies. It is convenient that there are stronger low (minus) isostasy gravity anomalies in the continental shelf, but stronger high isostasy anomalies and small T_c or T_e in the northwestern subbasin. So we assume that there are thermal mantle anomalies in the northwestern basin. Just this thermal mantle anomaly has changed the oceanic lithosphere flexural rigidity and the effect elastic plate thickness since the floor spreading. In addition, Fig. 6 shows that there is a slight above 300°C oceanic isotherm for profiles (S_1) So17S and So18S.

Profiles So22 and So20 are in the southwestern subbasin and its edge, respectively. Their T_c and T_e are higher, $T_c = 20-40$ km, $T_e < 25$ km for So20, $T_c = 10-30$ km, $T_e < 20$ km for So22. Fig. 6 (S_3) shows that it is normal for T_c and T_e to be under 300°C oceanic isotherm for So20 and So22. So we assume that the crustal structure of the southwestern subbasin differs from that of the eastern subbasin about the isostasy compensative depth or the crustal flexural rigidity. In general, as pointed out by some scholars, there are young tectonic activities, thicker layer 1, normal layer 2 and thinner layer 3 in the South China Sea in comparison with normal oceanic crust.

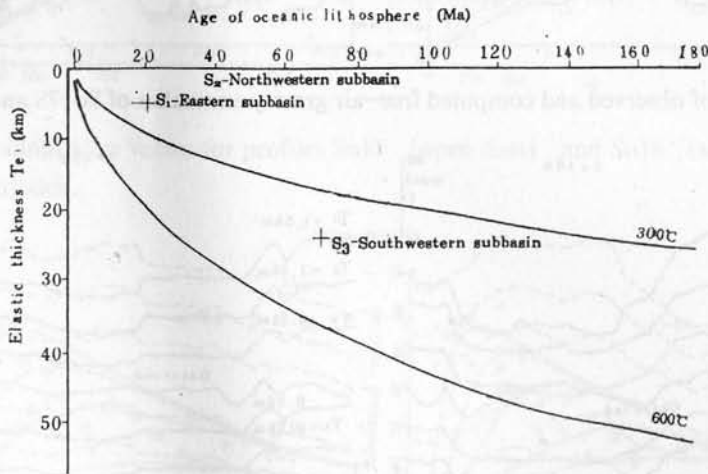


Fig.6 Relationship between elastic thickness and age of oceanic lithosphere

REFERENCES

- Airy, G.B., 1855: On the computation of the effect of the attraction of mountain-masses as disturbing the apparent astronomical latitude of stations of geodetic surveys. *Phil. Trans. R. Soc.*, 145, 101-104.
- Barrell, S., 1914: The strength of the earth's crust 8, physical conditions controlling the nature of lithosphere and asthenosphere. *J. Geol.*, 22, 425-443.
- Cochran, J.R., 1979: Analysis of isostasy in the world's oceans, 2, Mid-ocean ridge crests. *J.G.R.*, 84, 4713-4729.
- Dorman, L.M. and B.T.R. Lewis, 1970: Experimental isostasy 1, Theory of the determination of the earth's isostatic response to a concentrated load. *J.G.R.*, 75, 3357-3365.

- Heiskanen, W. A. and F. A. Vening Meinesz, 1958: *The Earth and its Gravity Field*. McGraw-Hill, New York.
- Jin Qinghuan, 1989: *Geology and Source of Oil & Gas in South China Sea*. China Geology Press.
- Karner, G.D. and A.B. Watts, 1982: On isostasy at Atlantic-type continental margins. *J.G.R.*, 87, 2923-2948.
- Lewis, B. T. R. and L. M. Dorman, 1970: Experimental isostasy 2, An isostatic model for the U.S.A. derived from gravity and topography data. *J.G.R.*, 75, 3367-3386.
- McKenzie, D.P. and C. Bowin, 1976: The relationship between bathymetry and gravity in Atlantic Ocean. *J.G.R.*, 81, 1903-1915.
- McNutt, M. and H. W. Menard, 1978: Lithospheric flexure and uplifted atolls. *J.G.R.*, 83, 1206-1212.
- Sleep, N.H., 1971: Thermal effects of the formation of Atlantic continental margins by continental breakup. *Geophys. J.R. Astron. Soc.*, 24, 325-350.
- Steckler, M.S. and A.B. Watts, 1978: Subsidence of the Atlantic-type continental margin off New York. *Earth Planet. Sci. Lett.*, 41, 11-13.
- Taylor, B. and D.E. Hayes, 1980: The Tectonic Evolution of the South China Basin. *Geophysical Monograph*, 23, 89-104.
- Taylor, B. and D.E. Hayes, 1983: The origin and history of the South China Basin. *Geophysical Monograph*, 27, 23-56.
- Vening Meinesz, F.A., 1914: Gravity over the Hawaiian Archipelago and over the Madiera area: Conclusions about the Earth's crust. *Proc. K. Ned. Akad. Wet.*, 44, 1-41.
- Walcott, R.I., 1970: Flexural rigidity, thickness and viscosity of the lithosphere. *J.G.R.*, 75, 3941-3954.
- Watts, A.B., J.H. Bodine and N.M. Ribe, 1980: Observations of flexure and the geological evolution of the Pacific Ocean basin. *Nature*, 283, 532-537.
- Watts, A.B. and J.R. Cochran, 1974: Gravity anomalies and flexure of the lithosphere along the Hawaiian-Emperor sea mount chain. *Geophys. J.R. Astron. Soc.*, 38, 119-141.
- Watts, A.B. and W.B.F. Ryan, 1976: Flexure of the lithosphere and continental margin basins, *Tectonophysics*. 36, 25-44.

PALEOCEANOGRAPHY AND SEDIMENTATION

The study of the paleoceanography and sedimentation of the Tethyan region during the Tertiary period is of great importance for the study of the evolution of the Tethyan region and the evolution of the Tethyan region. The study of the paleoceanography and sedimentation of the Tethyan region during the Tertiary period is of great importance for the study of the evolution of the Tethyan region and the evolution of the Tethyan region. The study of the paleoceanography and sedimentation of the Tethyan region during the Tertiary period is of great importance for the study of the evolution of the Tethyan region and the evolution of the Tethyan region.

The paleoceanography and sedimentation of the Tethyan region during the Tertiary period is of great importance for the study of the evolution of the Tethyan region and the evolution of the Tethyan region. The study of the paleoceanography and sedimentation of the Tethyan region during the Tertiary period is of great importance for the study of the evolution of the Tethyan region and the evolution of the Tethyan region. The study of the paleoceanography and sedimentation of the Tethyan region during the Tertiary period is of great importance for the study of the evolution of the Tethyan region and the evolution of the Tethyan region.

REFERENCES

The paleoceanography and sedimentation of the Tethyan region during the Tertiary period is of great importance for the study of the evolution of the Tethyan region and the evolution of the Tethyan region. The study of the paleoceanography and sedimentation of the Tethyan region during the Tertiary period is of great importance for the study of the evolution of the Tethyan region and the evolution of the Tethyan region. The study of the paleoceanography and sedimentation of the Tethyan region during the Tertiary period is of great importance for the study of the evolution of the Tethyan region and the evolution of the Tethyan region.

EROSION AND SEDIMENTATION IN THE XISHA TROUGH AT THE CONTINENTAL MARGIN OF SOUTHERN CHINA

H.R.KUDRASS¹⁾, X.L. JIN²⁾, H.BEIERSDORF¹⁾ & P.CEPEK¹⁾

1) *Federal Institute for Geosciences and Natural Resources, Hannover, Germany*

2) *Second Institute of Oceanography, SOA, Hangzhou, China*

ABSTRACT

The E-W trending Xisha Trough begins southeast of Hainan Island, runs parallel to the foot of the South China continental slope and ends in the 4400 m deep abyssal plain of the South China Sea. Two sections of the trough were surveyed by using multibeam echosounder, 3.5 kHz profiler, deep-towed side-scan sonar, TV and photcamera, and piston corer.

The 7 km broad floor of the U-shaped channel exhibits a rough microtopography along horizontal sections and a smooth surface on the flat cone-shaped wedges which protrude onto the channel floor from its margins. The wedges consist of Late Pleistocene hemipelagic mud with intercalated sand turbidites. The horizontal areas of the channel floor are underlain by highly contorted stiff to firm hemipelagic mud of Late to Early Pleistocene age and are dissected by numerous channel-parallel furrows. Individual furrows are 100 m to 300 m broad, a few metres deep, and up to 5 km long. The ridges between the furrows have very steep, sometimes overhanging striated walls which are occasionally interrupted by meter-sized potholes.

According to these observations, the channel has been eroded by more than 200m into Pleistocene and Tertiary hemipelagic sediments. Pleistocene sediments slumped in from the flanks and covered most parts of the channel floor. Turbidity currents have meandered over the channel floor probably forming helical flows which have eroded the furrows.

The hemipelagic sediment exposed at a slump scarp indicates that the area was deeply submerged in the Middle to Late Oligocene, hence dating the failed rift of the Xisha Trough.

INTRODUCTION

The continental rise of southern China is incised by a broad trough separating the continental margin from the continental block of Xisha Islands. This so-called Xisha Trough starts with a broad depression in about 1800 m (or 1000 fm.) water depth southeast of Hainan. Along its transition to the 4400 m deep abyssal plain of the South China Sea the bottom of the trough is incised by a channel (Fig.1). We discuss the results of multibeam echosounding, 3.5 kHz subbottom profiling, side-scan sonar recording, bottom photography, heat flow measurements, and sediment sampling on two sections across the channel obtained in 1987, 1988 during SO49 / SO58 cruises with R.V. Sonne.

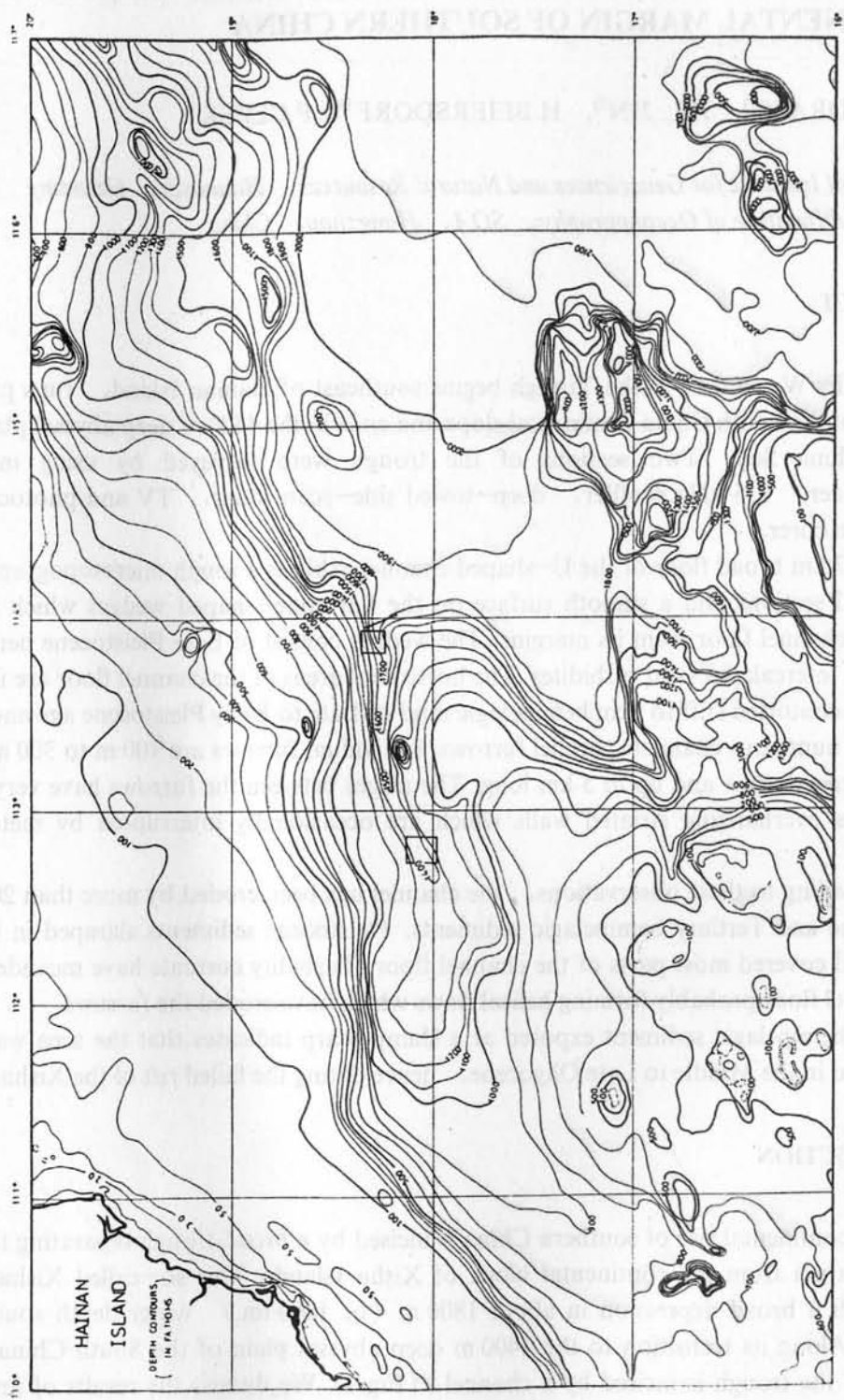


Fig.1 Bathymetric map. slightly modified from Defense Mapping Agency, Hydrographic Center, Washington, D.C. Map No. 93036 (1969), showing location of profile (SO49-25) and detailed survey areas (quadrangles, see also Figs. 2 & 3), depth contours in fathoms.

CHANNEL MORPHOLOGY

The width of the channel is about 7 km at both surveyed sections. The channel floor dips gently eastwards from a water depth of 2765 m for 120 km to 3365 m in the eastern section (average dip 0.30° or 5 m per km). This gradient corresponds well with the slope of other fan channels dissecting the upper continental slope (Indus Fan > 2 m / 1000 m: Kolla & Coumes, 1987; Congo Canyon 4 m / 1000 m: Heezen *et al.*, 1964; Amazonas Fan 5–11 m / 1000 m: Damuth & Flood, 1984).

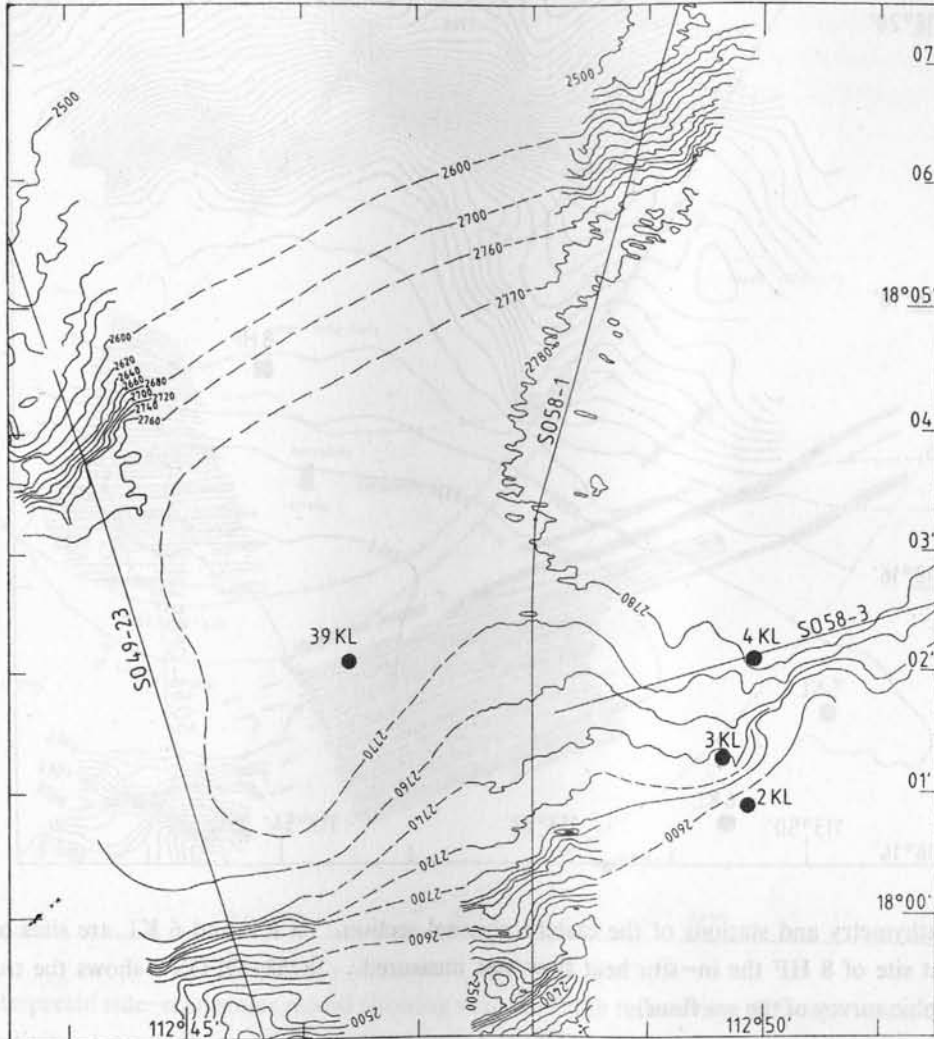


Fig. 2 Bathymetry and sites of core samples (KL) of the western channel section near profiles SO49–23, SO58–1, and SO58–3. (Profile SO58–1 shows a more detailed morphology as data were plotted directly from the Seabeam track map) Core 1KL is outside of this map. For graphical reasons the map was not extended to its longitude.

In general, the channel has a U-shaped cross profile with steep northern and southern flanks. The steepest flank with an inclination of 25° was observed at the southern end of the

SO58-OFOS 9 track (Fig.3). The channel floor is mostly flat (Fig.4, profile SO49-23), but cone-shaped wedges extend from the southern flank (Fig.2, SO58-1, 2770 m contour) or the northern flank (Fig.4, profile SO49-25) reducing the width of the flat part of the channel floor. The surface of these wedges appears to be smooth. The horizontal channel floor is dissected by numerous about 10 m deep furrows running parallel to the channel axis (Seabeam profile SO58-1, Fig.2).

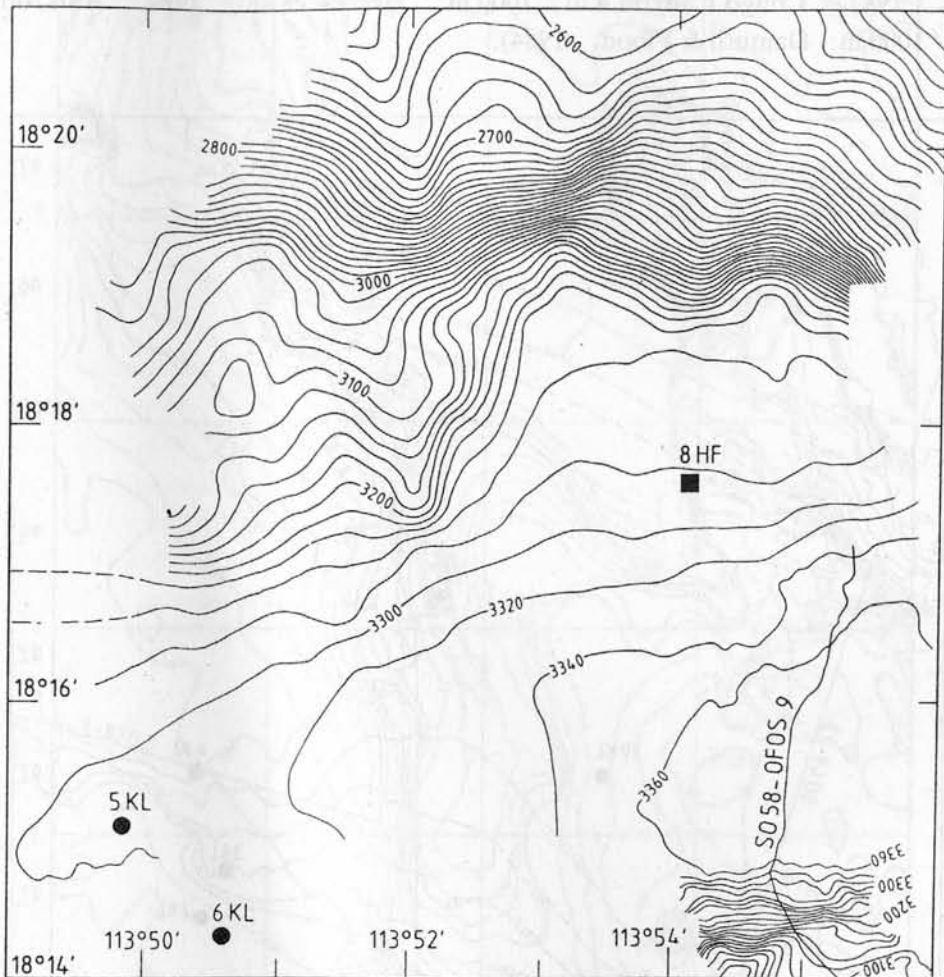


Fig.3 Bathymetry and stations of the eastern channel section, 5 KL and 6 KL are sites of piston cores, at site of 8 HF the in-situ heat flow was measured, SO58-OFOS 9 shows the track of a photographic survey of the sea floor.

A deep-towed side-scan sonar (HSES), predecessor of the SeaMark I instrument, was used to obtain more information on the areal extent of such fine-scale features. The HSES was towed 1000 m above the sea floor and, hence was able to survey a strip of 4 km width. A profile was run parallel to the channel axis in the eastern survey area and then on the continental slope to detect possible outcrops along the channel axis (Fig.4). In the central part of the channel floor black and white stripes show the ridge-and-furrow morphology already detected by the Seabeam. The ridges and furrows run parallel to the channel axis and

individual forms can be traced over a distance of more than 5 km. Furrows and ridges seem to have the same cross-sectional width, being 100–300 m broad with a height difference of some meters. This type of relief is mostly described from erosional areas in shallow-water environments with cohesive sediment (e.g., Strait of Malacca: Kudrass & Schluter, 1983). From the deep-sea environment this relief is rarely known and mostly correlated with boundary currents (Blake Plateau: Flood, 1983; Newfoundland Rise: Cochon et al., 1989).

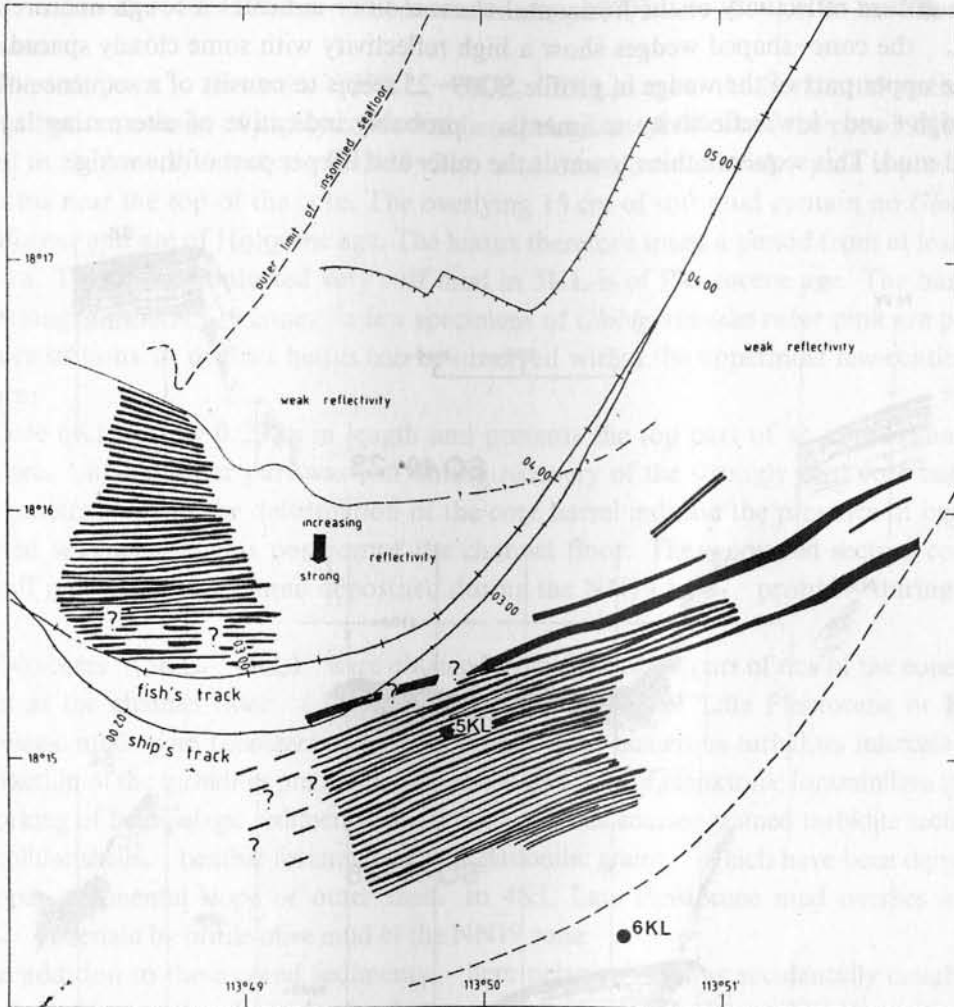


Fig.4 Interpreted side-scan sonar record showing stripes of high reflectivity (black), areas of diffuse high reflectivity (stippled) and sites of piston coring (5KL, 6KL).

The photographic survey in combination with a television camera revealed that the flanks of the ridges are dissected by smaller furrows, small terraces with steep, sometimes overhanging flanks and numerous potholes. In parts erosion seems to have been active very recently, as erosional surfaces are not covered by recent mud and show no signs of boring by benthic organisms. The numerous meter-sized potholes indicate a rather fast, turbulent bottom water flow.

EVALUATION OF 3.5 KHZ PROFILES

On both sides of the channel, the 3.5 kHz records exhibit numerous closely spaced parallel reflectors separated by acoustically transparent layers. On the continental slope, the transparent layers are thicker than those on the continental block of Xisha Islands (Fig.5, profile SO49-35).

The diffuse reflectivity of the horizontal channel floor indicates a rough microrelief. In contrast, the cone-shaped wedges show a high reflectivity with some closely spaced reflectors. The upper part of the wedge in profile SO49-25 seems to consist of a sequence of alternating high- and-low reflectivity sediments, probably indicative of alternating layers of sand and mud. This sequence thins towards the outer and deeper part of the wedge.

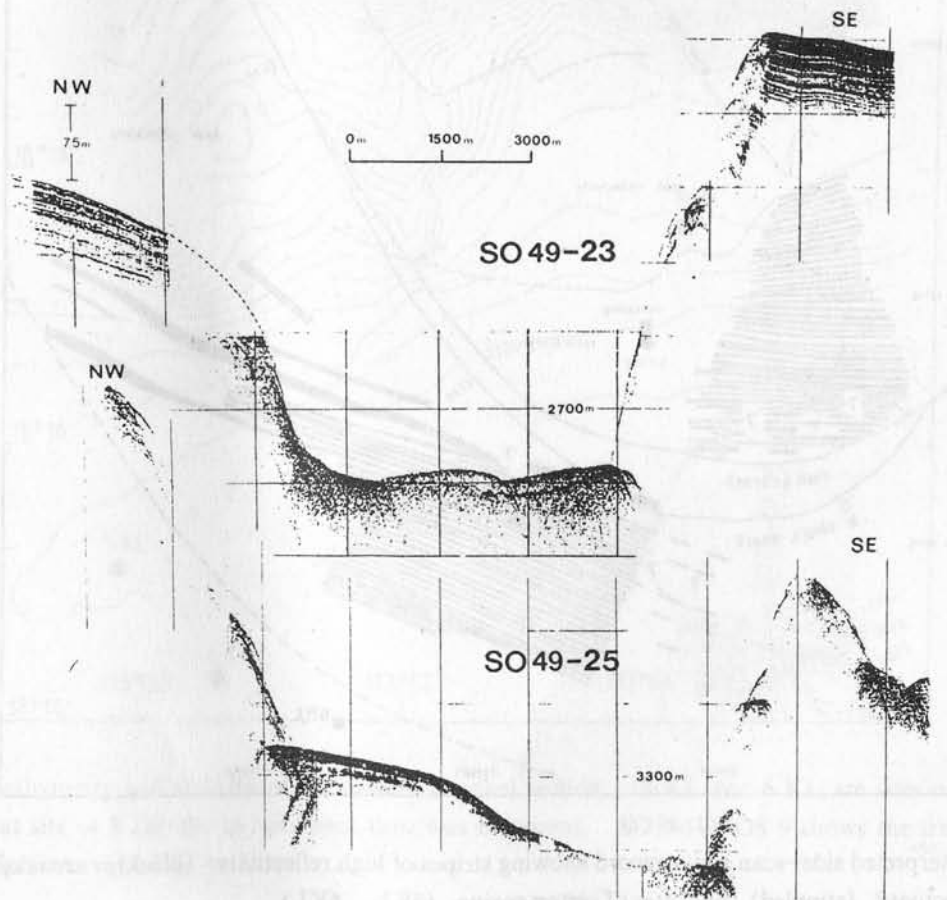


Fig.5 3.5 kHz profile SO49-23 (see Fig. 2 for location) and 3.5 kHz profile SO49-25 (see Fig. 1 for location).

SEDIMENTOLOGY AND STRATIGRAPHY OF SEDIMENTS

Seven piston cores were taken from the floor of the channel and its southern flank (Ta-

ble 1, for location see Figs. 2 & 3). Highly bioturbated hemipelagic mud with different stages of consolidation was cored at the southern flank of the channel (1KL and 2KL). The lower part of both cores consists of very stiff, grey hemipelagic mud of early Pleistocene age (NN19) containing some contorted layers or spots of very fine terrigenous sand (Fig. 6). (The stratigraphic NN / NP zonation of Martini & Mueller (1986) is used). Their upper part is free of sand layers and slowly grades from stiff to soft hemipelagic mud. The marked discontinuity of consolidation in both cores indicates a hiatus within the Pleistocene. As *Globigerinoides ruber* pink is not found in the mud overlying the hiatus, the sediments of the "pink" interval (400–120 ka, Thompson *et al.*, 1979) are thought to have been lost at the hiatus.

The sediments in the cores (39KL, 5KL, 6KL) from the horizontal section of the channel bottom consist of highly contorted hemipelagic mud. Most of the core 39KL was deposited in the Late Pleistocene (NN20–21) and *Globigerinoides ruber* pink is present up to the hiatus near the top of the core. The overlying 15 cm of soft mud contain no *Globorotalia crassaformis* and are of Holocene age. The hiatus therefore spans a period from at least 120 ka to 18 ka. The highly contorted very stiff mud in 5KL is of Pleistocene age. The base of this core belongs to the NN19 zone, a few specimens of *Globigerinoides ruber* pink are present in two core sections. A distinct hiatus can be observed within the uppermost few centimeters of the core.

Core 6KL is only 0.23 m in length and presents the top part of an approximately 6 m long core, whose lower part was lost during recovery of the strongly bent core barrel. The small penetration and the deformation of the core barrel indicate the presence of highly consolidated sediments at this position of the channel floor. The recovered section consists of very stiff grey hemipelagic mud deposited during the NN19 zone, probably during its early time.

Two cores (3KL, 4KL) were obtained from the eastern part of one of the cone-shaped wedges at the channel floor (Fig. 2). Both cores consist of Late Pleistocene or Holocene hemipelagic mud (no *Globigerinoides ruber* pink) with numerous turbidites intercalated. The sand fraction of the turbidites predominantly consists of tests of planktonic foraminifera indicating a reworking of hemipelagic sediments. In addition, some coarse-grained turbidite sections contain mollusc shells, benthic foraminifera and glauconitic grains, which have been derived from the upper continental slope or outer shelf. In 4KL Late Pleistocene mud overlies a marked hiatus, underlain by brittle olive mud of the NN19 zone.

In addition to these cored sediments, hemipelagic mud was accidentally caught by the photosledge during the photographic bottom survey OFOS 9 when it hit steep scarps at the southern flank of the channel. Gray hemipelagic mud yielded coccoliths of the NN19 zone. Stiff olive mud, however, contained a much older assemblage of the NP16–NP25 zone (Middle Eocene to Late Oligocene: *Cyclicargolithus floridanus* (Roth & Hay), *Dictyococcites bisectus* (Hay, Mohler & Wade)) with very few coccoliths (possible *Discoaster cf. druggii*, Bramlette & Wilcoxon) indicating a Lower Miocene to lower Middle Miocene admixture. The foraminiferal assemblage is dominated by foraminifera of Middle Oligocene to lower Late Oligocene. (*Globigerina angustumbilicata* (Bolli), *Globigerina ciproensis* (Bolli), *Catapsydrax dissimilis* (Cushman & Bermudez), *Globorotalia obesa* (Bolli), *Globorotalia opima nana* (Bolli), *Globorotalia siakensis* (Leroy), *Globigerinella aequilateralis* (Brady), *Globigerinoides sacculifer* (Brady), *Globorotalia tosaensis*

(Takayanagi & Saito)). Some few other foraminifera are due to contamination by Miocene or Plio-Pleistocene sediments.

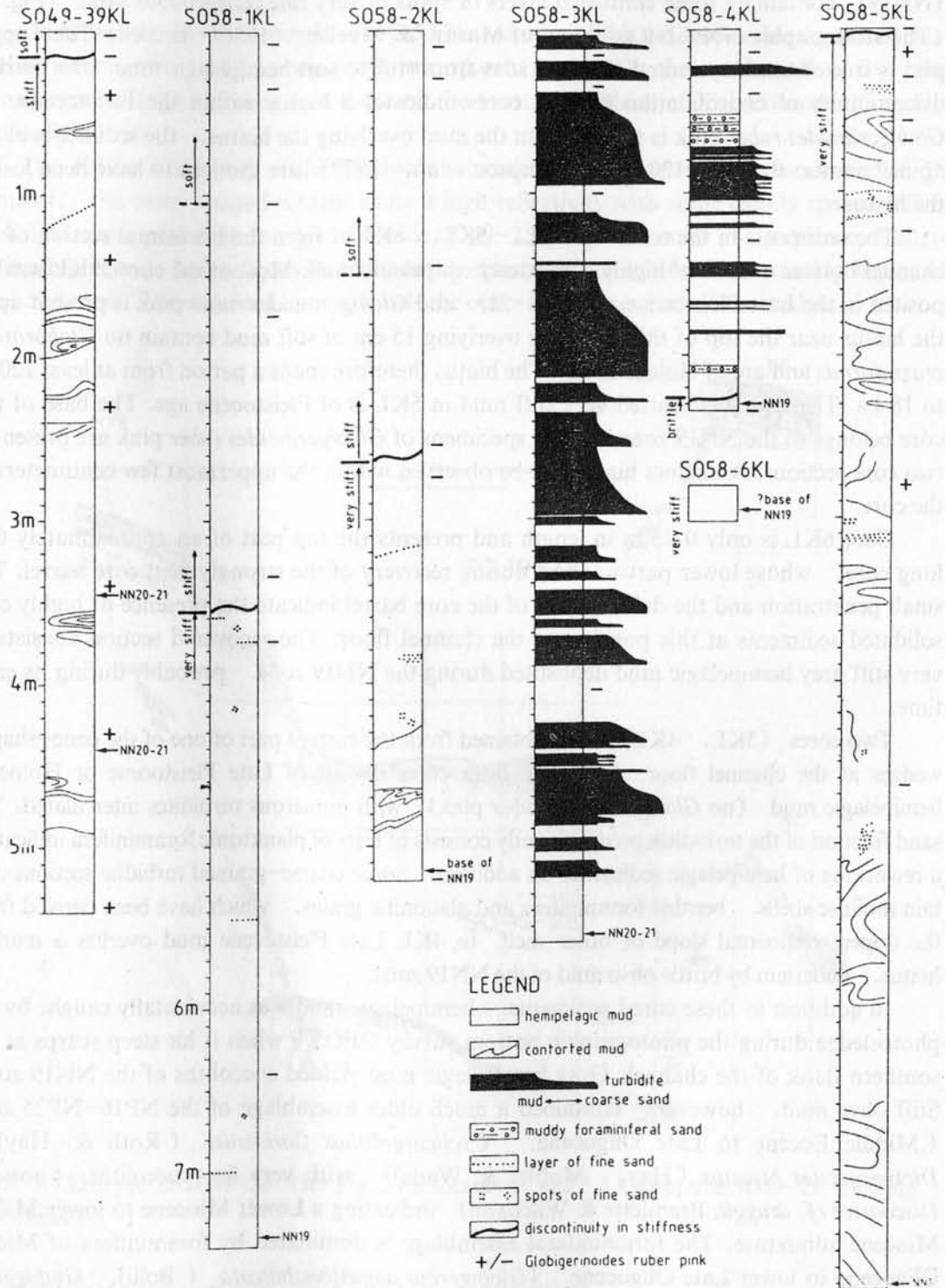


Fig.6 Lithology and stratigraphy of piston cores.

Table 1 Coordinates, water depth, core length, and location of sampling sites. A short description of recovered sediment and its maximum age is given. Water depth is based on echosounding during coring procedure, difference to water depths as seen in the maps (Figs. 2 and 3) are due to positioning errors.

Station No.	Coordinates	Water depth (m)	Core length (m)	Location	Sediment	Age
SO49-39KL	18 ° 02.10' N 112 ° 46.33' E	2757	5.40	Trough wedge or thalweg	Hemipelagic mud	NN20-21 Pleistocene
SO58-1KL	18 ° 00.22' N 112 ° 42.65' E	2354	7.46	Southern trough wall	Hemipelagic mud	NN19 Pleistocene
SO58-2KL	18 ° 00.90' N 112 ° 49.85' E	2511	5.21	Southern trough wall	Hemipelagic mud	NN19 Pleistocene
SO58-3KL	18 ° 01.27' N 112 ° 49.57' E	2710	5.60	Trough wedge	Hemipelagic mud with sandy turbidites	NN19-20 Pleistocene
SO58-4KL	18 ° 02.06' N 112 ° 49.87' E	2748	2.41	Trough wedge	Hemipelagic mud with sandy turbidites	NN19 Pleistocene
SO58-5KL	18 ° 15.12' N 113 ° 49.85' E	3298	7.73	Trough wedge or thalweg	Hemipelagic mud (distorted structure)	NN19 Pleistocene
SO58-6KL	18 ° 14.29' N 113 ° 50.58' E	3296	0.23	Trough wedge or thalweg	Hemipelagic mud (very stiff)	NN19 Pleistocene
SO59-9 OFOS	18 ° 14.30' N 113 ° 50.90' E	3150	Dredged sample	Southern trough wall	Hemipelagic mud (gray)	NN19 Pleistocene
SO58-9 OFOS	18 ° 14.80' N 113 ° 54.70' E	3550	Dredged sample	Southern trough wall	Hemipelagic mud (yellowish)	Middle Oligocene to Late Oligocene

HEAT-FLOW MEASUREMENT

Due to the stiffness of the sediments exposed in the channel in-situ heat flow could be measured only at position 8 HF. The conductivity with 2.48×10^3 (cal/cm sec °C) is relatively high for hemipelagic mud probably due to its high consolidation. The heat flow at the channel bottom of 2.23 mW/m^2 is comparable to previous measurements from the neighbouring abyssal plain (Taylor & Hayes, 1983; Block & Steinmann, 1987).

CONCLUSION

Undeformed sediments are rarely found in the channel and at its flank. The recovered sediments mostly consist of intensively contorted, stiff to very stiff hemipelagic mud. Slumping has obviously caused this deformation affecting complex sections of mud, and even deforming barely plastic muds (5KL). The age of these allochthonous sediments ranges from Late Pleistocene (39KL 120–400 ka in the NN20–21 zone) to Early Pleistocene (2KL, base of NN19, approximately 1.7 ma). The hiatus found on top or near the upper end of the cores indicates that a considerable part of Late Pleistocene sediments was removed by mass wasting or erosion.

As observed in the records of the deep-towed side-scan sonar and in the photographs of the sea floor, the horizontal parts of channel are presently subjected to erosion producing a channel-parallel ridge-and-furrow relief. This type of erosion proven in the eastern survey area seems to prevail also in the western area, as indicated by the rugged topography in the Seabeam records.

In contrast, cone-shaped wedges are of depositional features, their upper parts being composed of Late Pleistocene to Holocene hemipelagic mud with intercalated turbidites.

Turbidity currents may have eroded the some km-long furrows into overconsolidated, highly contorted hemipelagic sediments which slumped in from the channel flanks. At the time of the photographic survey, erosion was not active, it rather has occurred maybe only some months ago, since signs of erosion look rather fresh and no boring of the sediment surface by animals is visible. However, the observed ridge-and-furrow relief is usually referred to be caused by helical flow patterns (Flood, 1983), which are not expected in case of turbidity currents. As similar patterns of ridge-and-furrows are observed by deep-towed side-scan sonar in channels attributed to turbidity currents (Malinverno *et al.*, 1988), it might be necessary to modify the model of turbulent flow of turbidity currents.

The oldest sediment was not recovered from the channel floor, as one would expect, but dredged from the flank of the channel, where it was exposed at a slump scarp. The Middle to Late Oligocene age of this bathyal sediment proves that deep open-marine conditions prevailed at that time and consequently seafloor spreading or rifting in combination with subsidence must have started before this time. This period fits to the age interpretation of magnetic lineations which indicate that spreading started in the central South China Sea at the beginning of the Late Oligocene (Taylor & Hayes, 1983). The relatively low heat flow also corresponds to an early opening. The failed rift of the Xisha Trough therefore documents some of the earliest periods of seafloor spreading in the South China Sea.

ACKNOWLEDGEMENTS

We thank Dr. W. Weiss for the analysis of planktonic foraminifera and D. Hansen for transferring side-scan sonar records into a map.

REFERENCES

- Block, M. & D. Steinmann, 1987: Geothermal studies. Hinz, K. & Kudrass, H.R. (eds.), Geophysical, Geological and Geochemical Studies in the South China Sea (S049). BGR Rep. 101466, Part. 2, 81-97.
- Cochonat, P., G. Ollier & J.L. Michel, 1989: Evidence for slope instability and current-induced sediment transport, the RMS Titanic wreck search area, Newfoundland Rise. *Geo. Mar. Letts.*, 9, 145-152.
- Damuth, J.E. & R.D. Flood, 1983/1984: Morphology, sedimentation processes, and growth pattern of the Amazon Deep-Sea Fan. *Geo. Mar. Letts.*, 3, 109-117.
- Martini, E. & C. Mueller, 1986: Current Tertiary and Quaternary calcareous nannoplankton stratigraphy and correlations. *Newsl. Stratigr.*, 16 (2), 99-112.
- Flood, R.D., 1983: Classification of sedimentary furrows and a model for furrow initiation and evolution. *Bull. Geol. Soc. Amer.*, 94, 630-639.
- Heezen, B.C., R.J. Menzies, E.D. Schneider, W.M. Ewing & N.C.L. Granelli, 1964: Congo submarine canyon. *Bull. Amer. Ass. Petrol. Geol.*, 48 (7), 1126-1149.
- Kolla, V. & F. Coumes, 1987: Morphology, internal structure, seismic stratigraphy, and sedimentation of Indus Fan. *Bull. Amer. Ass. Petrol. Geol.*, 71 (6), 650-677.
- Kudrass, H.R. & H.U. Schluter, 1983: Report on geophysical and geological offshore surveys in Malacca Strait (1976). CCOP, Techn. Report 12, Exploration for offshore placers and construction materials, 115-154.
- Malinverno, A., W.B.F. Ryan, G. Auffret & G. Pautot, 1988: Sonar images of the path of recent failure events on the continental slope off Nice, France. *Geol. Soc. Am. Spec. Pap.*, 229, 59-75.
- Taylor, B. & D.E. Hayes, 1980: The tectonic evolution of the South China Sea Basin. D.E. Hayes (ed.), *The Tectonic and Geologic Evolution of the Southeast Asian Seas and Islands*. Amer. Geophys. Union, *Geophys. Monogr.*, 23, 89-104.
- Taylor, B. & D.E. Hayes, 1983: Origin and history of the South China Sea Basin. D.E. Hayes (ed.), *The Tectonic and Geologic Evolution of Southeast Asian Seas and Islands*, part 2. Amer. Geophys. Union, *Geophys. Monogr.*, 27, 23-56.
- Thompson, P.R., A.W.H. Be, I.C. Duplessy & N.J. Shackleton, 1979: Disappearance of pink-pigmented *Globigerinoides ruber* at 120000 yr B.P. in the Indian and Pacific Oceans. *Nature*, London, 280, 554-558.

A PRELIMINARY STUDY OF THE ORIGIN OF TAIWAN SHOAL

CAI AIZHI, LI YUANMI, CAI YUE'E, ZHU XIAONIN & LE YUZAN

Xiamen University, Xiamen, China

ABSTRACT

A zone of underwater basalt hills from South Fujian to Penghu Is. and the coast of southwest Taiwan is an important foundation for the development of the Taiwan Shoal. The sediments of Taiwan Shoal are mainly made up of mid-coarse sands with 5-10% of shells and some gravels of basalt and beach rocks. The numerous mesobedforms such as sand waves (dunes) and ridges are controlled by currents and waves in the whole shoal. At present, the bedforms of Taiwan Shoal are changing and migrating because of the action of wave and current; especially when the storm comes up, sands and shells on the shoal are transported from the north and the south to the center part of the shoal.

INTRODUCTION

Taiwan Shoal is an individual unit with wonderful forms and mystical origin in marine geology, which has been fascinating many geologists and oceanologists. In the past, only foreign scholars did some normal sampling and laboratory analysis. Niino and Emery (1961) have proposed that the sediments of Taiwan Shoal are relict continental shelf sediments. Chinese scholars in Taiwan province or in the continent have investigated the shoal for several times in past twenty years. Boggs, Wang and Chen (1974), Zhou (1971) had studied the sediments in the east of Taiwan Shoal. Qing and Zhen (1982), Zhang (1989) had studied bottom morphology, sedimentary type and mineral in the west of Taiwan Shoal. This paper is based on the past work, in which some new methods is used for the study of change of underwater sand waves (dunes), composition and transportation of sediments, distribution of basalt relict hill and beach rock in the sea bottom. We discussed the recent dynamics and conditions of the shoal formation by means of numerous scientific documents.

INVESTIGATING METHODS AND ANALYSIS RESULTS

The morphological observation of sand waves on Taiwan Shoal was accomplished by using Che-III type of echosounder at the marine expeditionary vessel, "Dongfanghong" with satellite position system. The total length of sounding profiles on two cruises is 650 km. The position and direction of sounding lines are shown in Fig. 1. Fifteen surficial sediment samples were obtained by the oceanic type of grab sampler. In stations which depth is smaller than 80 m, the sea bed has been observed and recorded by the Sea-Beer-I type of underwater TV. We have observed only when the ship is at anchor, because the least sailing speed is six miles an hour.

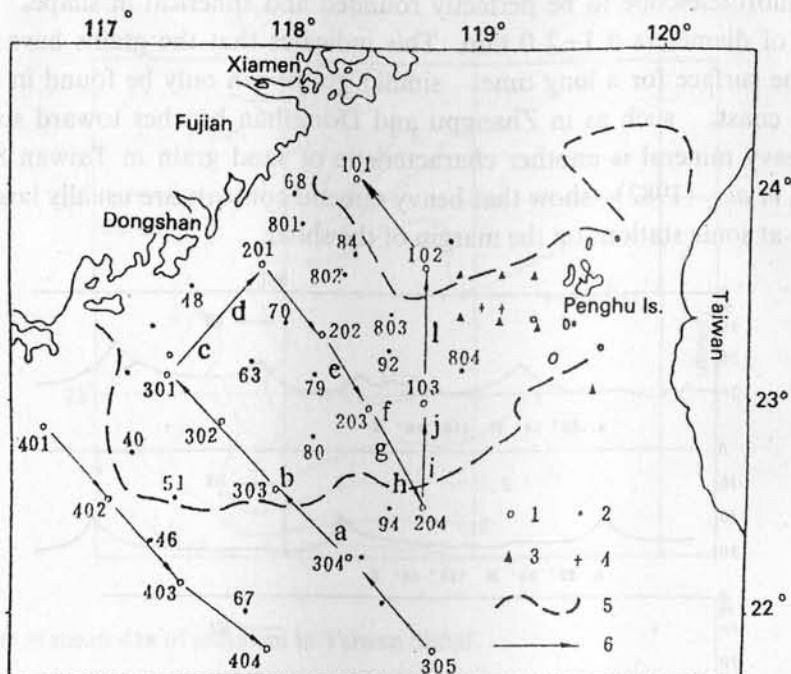


Fig. 1 The boundary of Taiwan Shoal and working map. Legends: 1. Investigated station at this time; 2. Zhang *et al.*, 1976 & 1982; 3. Zhou J.T., 1971; 4. Boggs, Wang & Chen, 1974; 5. Boundary line of the shoal; 6. Echosounding line at this time.

Some typical sounding profiles are selected and from a vast record of echosounding, length (L) and high (H) of sand wave were calculated. The results obtained by analyzing the above data indicate the following features (Fig. 2).

1) L of sand waves is 0.5–2.0 km and H of sand wave is 15–22 m in the central part of Taiwan Shoal. On the deeper margin of the shoal L of sand waves is 100–300 m and H is 5–10 m (Fig. 2c, d, i). The relationship plot (Fig. 3) obtained from statistic result shows that the average height of sand wave minus its average depth is negative.

2) The asymmetry of sand wave is caused by the combined actions of waves and currents. When waves and currents push the sediments on the bottom forward, the gentle front slope and the steep lee slope will be formed.

3) The trends of sand wave change with the change of direction of currents and incoming wave. Owing to the regimes of frequent hydrodynamic change, characteristics of sand wave morphology such as kurtosis and asymmetry in Taiwan Shoal is highly changeable. The comparison of our echosounding record with those taken by Zhang (1989) in the same region shows that the bipeak type of sand wave seldom appears.

4) The regular sounding record of sand wave may disappear suddenly because of appearance of basalt and beach rock on the bottom.

Grain-size analysis of sediment in Taiwan Shoal has been made. Grain-size parameters in Table 1 have been calculated according to C.K. Wentworth's grain criterion system. The mean size of sediments is about 1Φ in the central part of Taiwan Shoal and 1.5–2.0 Φ on the margin of the shoal (Fig. 3). The grain particles in the middle of Taiwan Shoal are discov-

ered by the microtelescope to be perfectly rounded and spherical in shape, especially for quartz sands of diameters 0.1–2.0 mm. This indicates that the grains have suffered wave abrasion in the surface for a long time, similar grains can only be found in the beaches of South Fujian coast, such as in Zhangpu and Dongshan beaches toward southeast. High content of heavy mineral is another characteristic of sand grain in Taiwan Shoal. Results drawn by Sen *et al.* (1982) show that heavy mineral contents are usually larger than 2%, and up to 4% at some stations on the margin of the shoal.

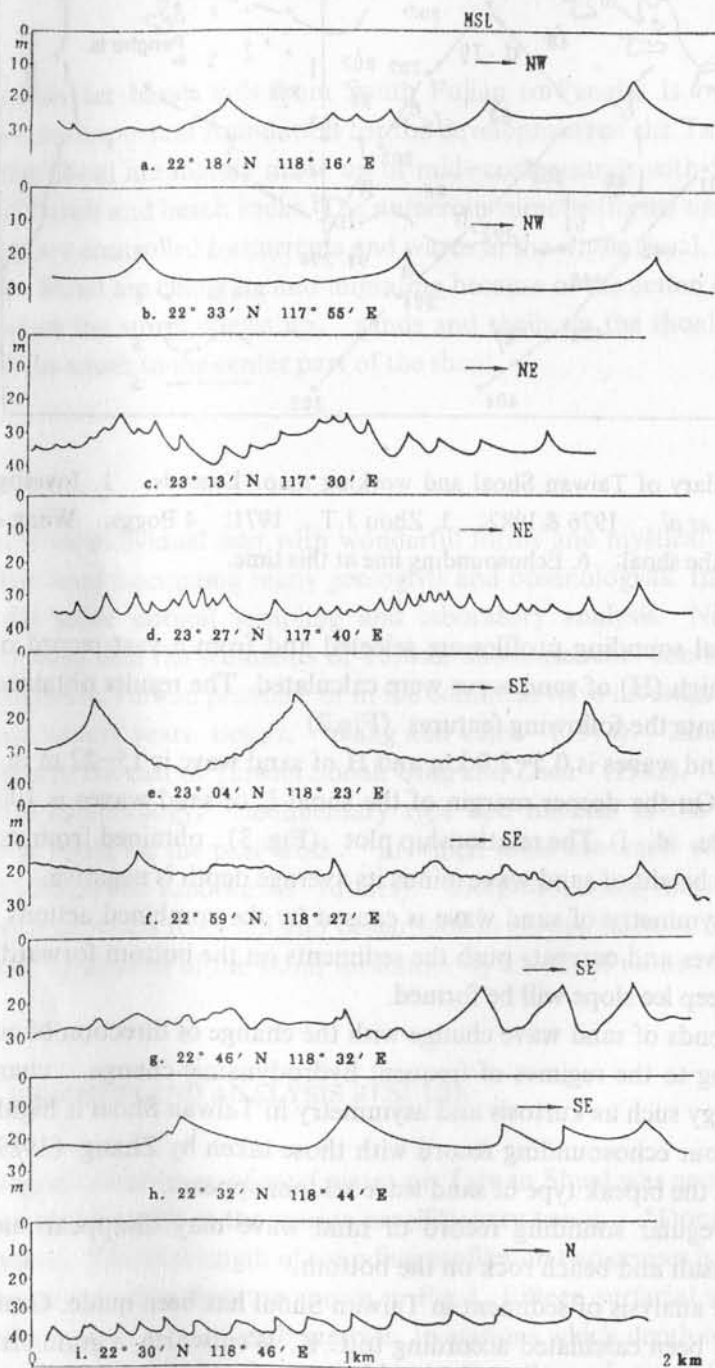


Fig.2 Some typical profiles of sand wave in Taiwan Shoal

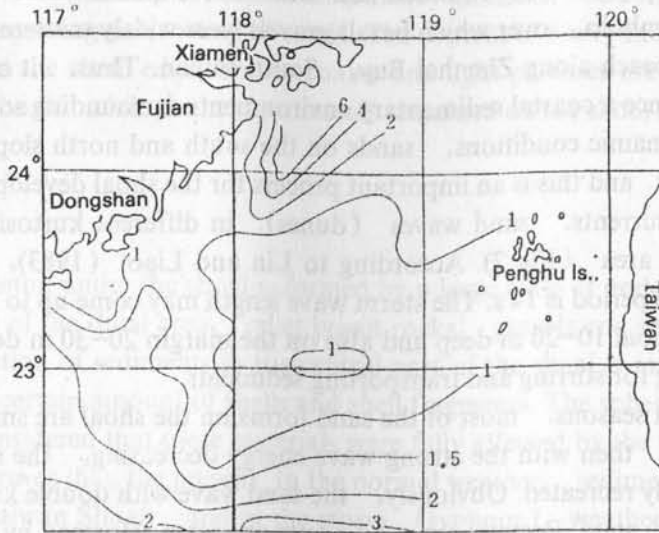


Fig.3 The isoline of mean size of sediment in Taiwan Shoal.

The underwater TV system has been used to observe the shoal relief which water depth is smaller than 80m, especially at the hydrographic survey stations, T103, T201, T204, T302, and T304. Thus, we have induced the following results. (1) Sea bed deposits are composed of sands, silt-sands, shells and gravels of basalt and beach rock; (2) There are many kinds of micro-bedforms such as ripples and biological burrows etc.; (3) Sand of different size move under the action of currents in which steady currents flow and sands move in straight line, and when turbulent flows exist, sands move in clouds which direction and magnitude change every now and then; (4) Suspended sands obtained by the sand trap which was fixed in the scope of the television screen were 1-2.5 Φ in diameter, including some shell fragments. It can be deduced that sand movement will be very strong during storms in Taiwan Shoal. When the current velocity surpassed 80 cm / s in Taiwan Shoal, the anchored ship could be moved. Because the storm speed can reach 30-40 cm / s at this time, we corrected the position data by satellite.

DISCUSSION ON THE FORMATION OF TAIWAN SHOAL

The origin of Taiwan Shoal was seldom discussed before, only a tentative idea had been advanced by Zhen and Zhang (1982). Far more efforts have been paid on characteristics and resources of its sands (Qing and Zhen, 1982; Zhang, 1989). In Penghu Islands and the coastal zone of Zhangpu, South Fujian, basalt rocks and volcanoes are widely distributed, and in the central part of the shoal around station T202, relict basalt hills and many basalt gravels are discovered by the underwater TV. It can be considered that a basalt hill chain which is the existing fundament of the shoal lies across the south of Taiwan Shoal. During lower sea level, there were a series of basalt islands from Penghu Is. to South Fujian coast. Otherwise, when the sea level was 20-30 m in Early Holocene lower than at present, beach rocks were formed on this region of coastal zone. During the lower sea level, the posi-

tion covered by the present well-rounded and mid-coarse quartz sands was coastal beach such as barrier or tombolo, over which basalt gravels were widely scattered, in the same as the present barrier beach along Zhenhai Bay, South Fujian. Thus, it can be proved that Taiwan Shoal was once a coastal sedimentary environments surrounding some islands. Under the present hydrodynamic conditions, sands on the south and north slope of the shoal are moved to the center, and this is an important process for the shoal development. Effected by storms and strong currents, sand waves (dunes) in different kurtosis and scales are formed in the shoal area (Fig.2). According to Lin and Liao (1983), the wave height reaches 16 m and the period is 14 s. The storm wave length may come up to 100-110 m. In the central part of the shoal 10-20 m deep and also on the margin 20-30 m deep, the wave influence is very strong for stirring and transporting sediments.

During typhoon seasons, most of the sand forms on the shoal are smoothed by violent waves and currents, then with the strong wave energy decreasing, the sand waves (and dunes) are gradually recreated. Obviously, the sand wave with double kurtosis is an "interim" or "temporal" state. Because the sand waves are often reformed by storms, benthos can't live and propagate in this area. Nevertheless, we have collected present shells and shell fragments in this area. They are transported by current and wave from other places in which sediments must contain some clay (15%) for shell propagation.

Data in Table 1 show that sediments of the central part of the shoal rarely contain clay, so the benthos can't live. Observation of the underwater TV and use of the sand trap collecting the tract load made us find that the diameter of sand transported by the current is about 1-2.5 Φ , and the bed-current velocity is 80 cm/s at station T202. Therefore, kurtosis and skewness of the sand wave are controlled not only by the current velocity and direction but also by the storm intensity.

Table 1 Grain parameters of sediment in Taiwan Shoal

Stations		Content of size groups (%)					Mean size	Standard deviation	Name of sediments
No.	G	CS	MS	FS	T	MZ			
T801	8.5	80.5	10.6	0.4		0.03	0.82	CS	
T303		61.2	30.3	8.2	0.3	0.92	0.74	MCS	
T103	18.2	77.4	4.1	0.3		-0.27	0.80	CS	
5-B	1.3	55.0	31.1	12.6		0.82	0.90	MCS	
6-B	2.8	31.1	58.8	6.6	0.7	1.40	1.05	CMS	
M-38	10.6	58.2	22.8	6.8	1.3	0.43	1.19	MCS	
M-43	18.4	65.6	13.2	1.9	0.9	-0.07	1.10	CS	
M-48	0.7	35.9	56.7	3.7	3.0	1.20	0.63	CMS	
M-51		2.6	19.2	76.7	1.5	2.23	0.44	FS	
M-54	19.4	72.2	5.0	0.7	2.7	-0.20	0.92	CS	
M-67	1.6	46.6	45.9	4.0	2.1	1.03	0.78	CMS	
M-80	27.2	44.6	26.3	2.0		0.20	1.53	MCS	
M-84	0.5	67.6	31.2	0.7		0.73	0.66	MCS	

The sediments in Taiwan Shoal contain more heavy minerals, and it is another evidence for the present transporting and sorting of sands. The content of heavy minerals is the highest at a few stations on the shoal edge. So the coarse and light particles are transported to the central part of the shoal, while the heavy minerals remained on the shoal edge.

CONCLUSIONS

The stable skeleton under the shoal is formed by a large scale of underwater relict basalt hills. On the seabed of the shoal area, relict basalt rocks, gravels and solid beach rocks are universal. Composition of sediments in the central part of the shoal is mainly coarse to medium sands with uncertain amount of shells and shell fragments. The sphericity of sediment is very well. It was considered that these materials were fully affected by the wave when the sea-level was 20–30 m lower than the present. In the normal weather, sediments are transported by the current in Taiwan Shoal, and in the storm (typhoon) weather, the underwater sand such as sand waves, dunes and ridges are recreated violently by wave and current.

REFERENCES

- Boggs, Huaqing Wang and Ruqin Chen, 1974: Structure and composition of sediment model in the continental shelf of Taiwan. *Acta Oceanographical Taiwan*, 4, 13–56.
- Cai Aizhi, 1989: Beach cycle and coastal engineering. *The Ocean Engineering*, 7 (3), 57–64 (in Chinese).
- Lin Yulian and Kangming Liao, 1983: The wave study in the Taiwan Strait. *Taiwan Strait*, 2 (1), 20–26.
- Niino, H. and O.K. Emery, 1961: The sediment of shallow portion of East China Sea and South China Sea. *Geol. Soc. Amer. Bull.*, 75 (5), 731–762.
- Qing Yuesun and Temin Zhen, 1982: A preliminary study on the characteristics of sediment distribution in East China Sea continental shelf. *Geology of Yellow China Sea and East China Sea*, Science Press, Beijing, China, 39–51 (in Chinese).
- Sen Suanxi, Wenpuan Shu and Liron Chen, 1982: The feature of composition and distribution of heavy mineral in continental shelf of South Fujian–Taiwan Shoal. *ibid.*, 98–104.
- Wentworth, C.K., 1922: A scale of grade and class terms for classic sediments. *Jour. Geol.*, 30 (5), 377–392.
- Zhang Junyuan, 1989: Preliminary study on the topography and sediment characteristics of the Taiwan Strait and adjacent area. *Studia Marine Science*, 30, Science Press, Beijing, China, 1–17 (in Chinese).
- Zhen Temin and Junyuan Zhang, 1982: A preliminary study on the characteristic of bed form and sediment of Taiwan Shoal and adjacent continental shelf. *ibid.*, 52–66.
- Zhou, J.T., 1971: Sediment of Taiwan Strait and South Taiwan basin. *Technical Bulletin CCCP*, 6, 75–97.

OXYGEN / CARBON ISOTOPES AND PALEOPRODUCTIVITY IN THE SOUTH CHINA SEA DURING THE PAST 110 000 YEARS

KYAW WINN¹⁾, LIANFU ZHENG²⁾, HELMUT ERLLENKEUSER³⁾ & PETER STOFFERS¹⁾

1) *Geol.- Palaont. Inst., Christian-Albrechts University, Kiel, Germany*

2) *Second Institute of Oceanography, SOA, Hangzhou, China*

3) *C-14 Lab., Inst. of Pure & Applied Nuclear Physics, CAU, Kiel, Germany*

ABSTRACT

Stable isotope measurements on both planktonic and benthic foraminifera in two deep sea sediment cores from the South China Sea allow a detailed stratigraphy for the past 110000 years. The isotope stratigraphy is based on the benthic foraminifera *Cibicidoides wuellerstorfi*, which reveals the more consistent and stable $\delta^{18}\text{O}$ -profile. For the last Glacial and Holocene, ages were derived by comparison with AMS- ^{14}C -dated $\delta^{18}\text{O}$ -curves of other cores, with appropriate U-Th-corrections applied to the conventional ^{14}C -dates. Sedimentation rates are generally higher in glacial than in interglacial time. The higher rates during Stages 4 and 5 in the deeper core are caused by turbidites.

The $\delta^{13}\text{C}$ niveau $< -22\text{‰}$ of total organic carbon in the sediment indicates an increased terrigenous supply during the Interglacials, while marine organic matter $> -20\text{‰}$ is dominating during the Glacial.

The estimated (marine carbon) paleoproductivity which is calculated by means of an empirical equation based on the organic carbon accumulation rates show a pronounced contrast between the last Glacial and the penultimate and present Interglacial, with the glacial productivity being higher by a factor of up to 4.

The $\delta^{13}\text{C}$ values of the epibenthic *C. wuellerstorfi* in the South China Sea conforms with the regional decrease in the western Pacific observed from west of New Zealand to the Ontong Java Plateau. The Last Glacial $\delta^{13}\text{C}$ levels are generally 0.3‰ lighter than in the Holocene and indicate bottom water renewal mainly through the deep Bashi Channel (threshold at ~ 2600 m) in the northeast.

INTRODUCTION

The primary productivity of the surface ocean is estimated to have been more than 3 to 4 times the present level in the coastal and shelf regions and major upwelling areas of the oceans during the last Glacial (Reimers and Suess, 1983; Muller *et al.*, 1983; Sarnthein *et al.*, 1988; Sarnthein and Winn, 1990), leading to a drawdown of atmospheric CO_2 as evidenced by ice core studies (Neftel *et al.*, 1982; Barnola *et al.*, 1987). The higher productivity was accompanied by higher nitrogen / carbon ratios during the glacials (Hartmann *et al.*, 1976; Muller *et al.*, 1983). This implies a reconsideration of the proportion of organic carbon to phosphate in the Redfield ratio, enabling a much higher productivity in the tropical oceans from a limited phosphate budget during the ice ages.

In order to estimate the extent of the fluctuations in the ocean carbon reservoir which constitutes about 98% of available total carbon, and to quantify the associated changes in atmospheric $p\text{CO}_2$, it is necessary to determine in detail the paleoproductivity of the different parts of the world's oceans. As part of an ongoing project within the framework of the German national climate programme, the nutrient budgets of various tropical and subtropical regions in glacial and interglacial periods were analysed (Sarnthein and Winn, 1990). Here, we present further results of detailed paleoproductivity studies supported by stable isotope stratigraphy in two deep sea sediment cores, Sonne 50-29KL (N18.4°, E115.7°, 3766 m) and Sonne 50-37KL (N18.9°, E115.8°, 2695 m). The cores were raised from the continental slope off South China in the northern part of the South China Sea.

METHODS

All cores were sampled at 10 cm intervals, and after determination of the water content, were wet-sieved through a 100 μm mesh. The planktonic foraminifera *Globigerinotdes trilobus sacculifer* (Brady) and *G. ruber* (d'Orbigny) as well as the benthic foraminifera *Cibicidoides wuellerstorfi* (Schwager) were picked from the 315-400 μm size fraction for oxygen and carbon stable isotope measurements. The runs were made with a Finnigan MAT-251 mass spectrometer coupled to the automated CARBO-KIEL sample preparation device. Samples were reacted by individual acid addition. The isotope results are given on the usual δ -scale and have a standard deviation of $\pm 0.07\%$ for oxygen and $\pm 0.04\%$ for the carbon isotope ratio. Organic carbon contents (weight %) were determined with the LECO instrument (accuracy $\pm 0.5\%$).

Due to the proximity of our core locations to land, the sediments may contain appreciable amounts of land derived organic matter. Therefore, we have also measured the stable isotope composition of the total organic matter in the sediment, a parameter which is dependent upon the terrigenous carbon input (Erlenkeuser, 1978). For organic carbon analysis CO_2 gases were prepared from sediment samples by dry combustion after carbonates were gently removed by warm 2% HCl.

RESULTS AND DISCUSSION

Oxygen Isotopes

The oxygen isotope events have been identified by comparison with the standard reference section of the graphic correlation composite $\delta^{18}\text{O}$ record for sediments of the Brunhes Chron. (Prell *et al.*, 1986). For the Holocene and the Last Glacial, we have converted to calendar dates following Bard *et al.* (1990) (Table 1). The older $\delta^{18}\text{O}$ events were dated by correlation with the high resolution chronostratigraphy of Martinson *et al.* (1987). The stage boundaries from the plankton oxygen isotope curves do not necessarily coincide with those from the benthic curve. This phenomenon has been observed in a large number of cores from other marine regions, and may be due to species-specific fractionation as well as

to the influence of different water masses and microhabitats ("vital effects"). In addition, carbonate dissolution has occurred in some horizons, with the thinner shelled planktonic foraminifera being more affected than the thicker shelled benthos. For our chronostratigraphy, we have selected the more stable benthic $\delta^{18}\text{O}$ -curve (Table 1, Figs.1 and 2).

Table 1 $\delta^{18}\text{O}$ stratigraphy and chronology of cores 29KL and 37KL.

$\delta^{18}\text{O}$ -event	Core 29KL	Core 37KL	Conventional	Corrected
	(depth, cm)		^{14}C -age (in 1000 yrs)	age*
Present	0.0	0.0	0.0	0.0
End termination I	61.0	91.0	9.1	9.8*
Begin termination I	126.0	161.0	14.8	18.3*
$\delta^{18}\text{O}$ -event 3	321.0	316.0	26.0	29.3*
$\delta^{18}\text{O}$ -event 3.31	546.0	561.0		55.5**
$\delta^{18}\text{O}$ -event 4.24	631.0	641.0		71.1**
$\delta^{18}\text{O}$ -event 5.1	811.0	721.0		79.3**
$\delta^{18}\text{O}$ -event 5.2	861.0			90.9**
$\delta^{18}\text{O}$ -event 5.31	921.0			96.2**
$\delta^{18}\text{O}$ -event 5.33		831.0		103.3**
$\delta^{18}\text{O}$ -event 5.4	992.5			110.8**

* Converted to $^{238}\text{U} / ^{230}\text{Th}$ age scale after Bard *et al.* (1990).

** Chronology after Martinson *et al.* (1987).

For the upper part of the cores which represents the time interval from the Last Glacial maximum to the present, the AMS-stratigraphy of the South China Sea core V35-5 and the East Pacific core TR163-31 were used as guides (Broecker, 1988a, b). The chronology determined by Bard *et al.* (1990) applying the Uranium-Thorium method (calendar dates) shows significant offsets of the calendric time scale from the AMS ^{14}C -ages, especially during the Termination I and the Late Glacial. According to the new, but still tentative time scale, the $\delta^{18}\text{O}$ Stage 2 / 3 boundary is dated at 29.3 ka, the beginning of Termination I at about 18.3 ka, the Younger Dryas event between 12.8 ka and 12.2 ka, and the end of Termination I at around 9.8 ka. The 2 cm thick volcanic ash layer encountered at 302-304 cm in core 29KL has an interpolated age of 28.3 ka.

The planktonic and benthic $\delta^{18}\text{O}$ -records show last glacial to interglacial differences of 1.4-1.6‰. In general, the oxygen isotope stratigraphy of both planktonic and benthic species show comparable results down to the base of oxygen isotope Stage 4, which is remarkably well pronounced in both cores. Below Stage 4, the plankton oxygen isotope curve deviates considerably from the benthic profile in both cores. The $\delta^{18}\text{O}$ minima are not identifiable as such but appear as rather broad plateaus. A detailed intercore comparison of the isotope curves of *G. ruber*, *G. sacculifer* and *C. wuellerstorfi*, however, suggests that only the upper parts of Stage 5 (5a, 5b) are identifiable in core 37KL, while the lowest horizon in core 29KL could be assigned to Stage 5c (5d?). The $\delta^{18}\text{O}$ -values did not reach the typical light levels of Stage 5e, and this substage is certainly not cored. The comparatively heavy

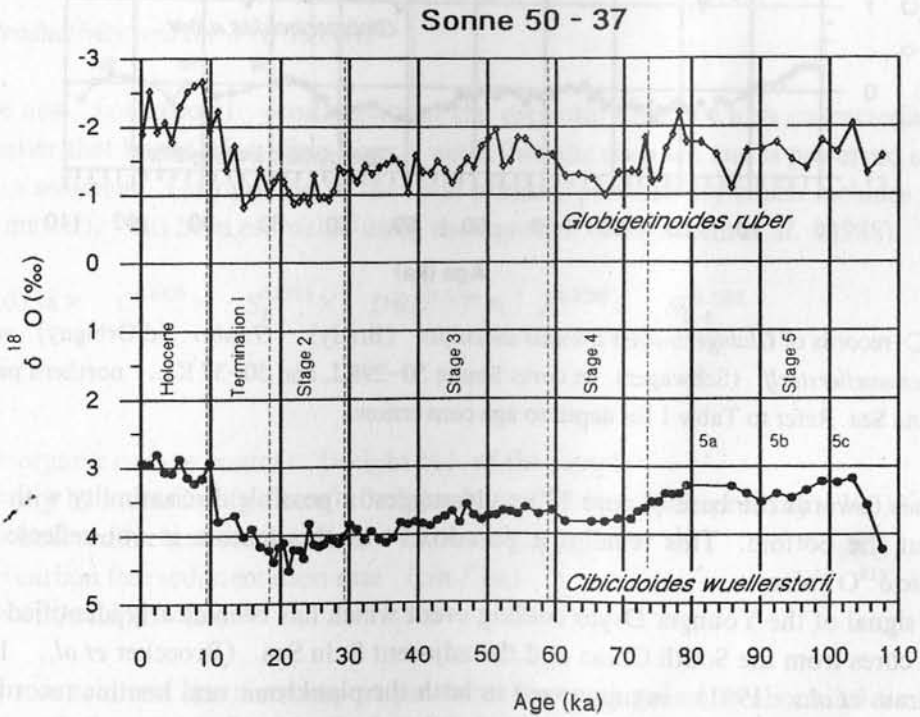
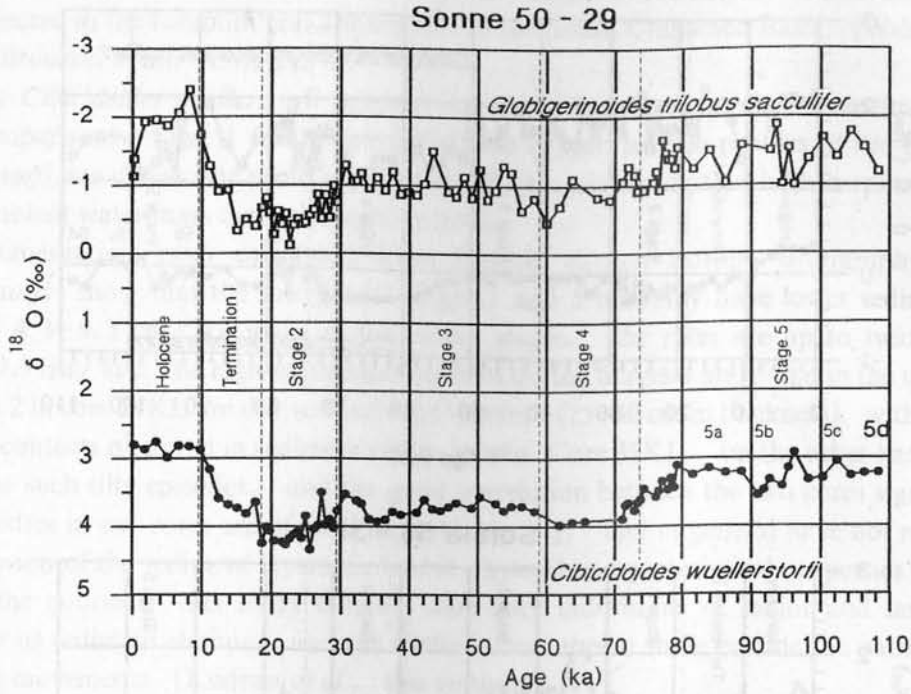


Fig.1 $\delta^{18}\text{O}$ -records of *Globigerinoides trilobus sacculifer* (Brady), *G. ruber* (d'Orbigny) white and *Cibicides wuellerstorfi* (Schwager) in cores Sonne 50-29 KL and 50-37 KL, northern part of the South China Sea. Refer to Table 1 for depth to age conversions.

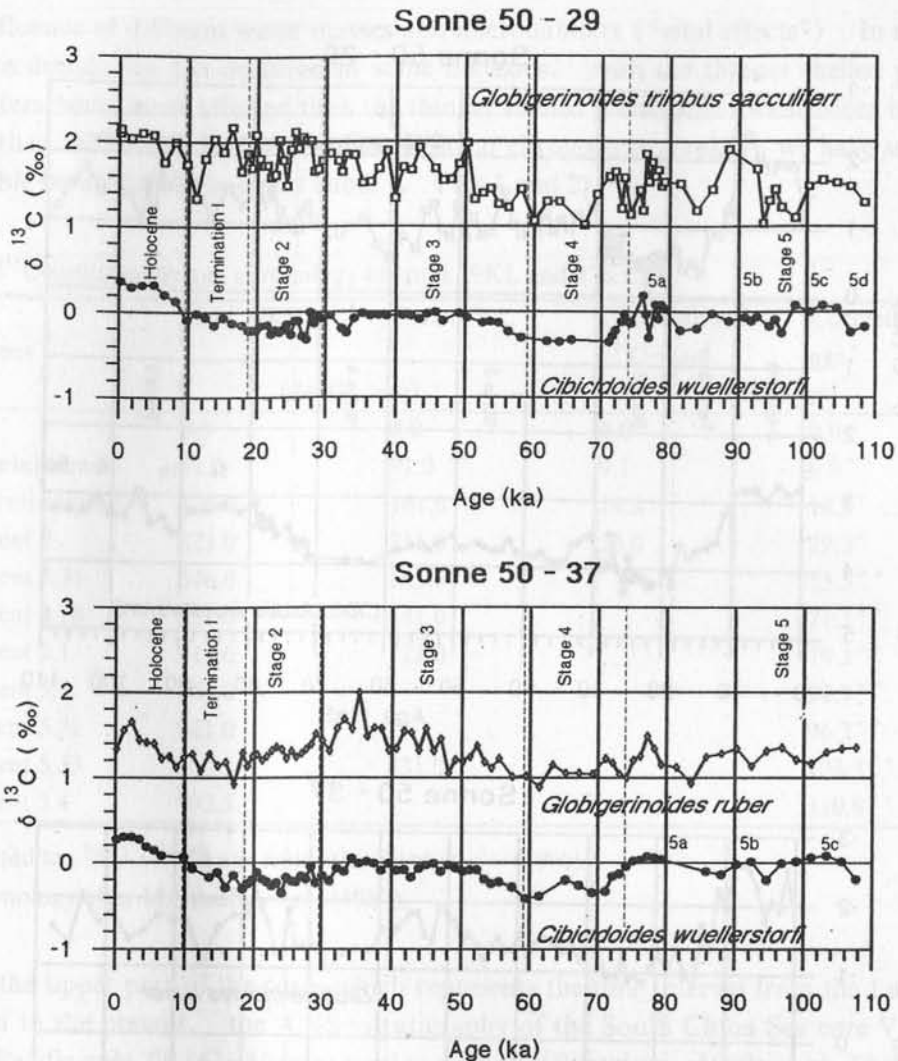


Fig.2 $\delta^{13}\text{C}$ -records of *Globigerinoides trilobus sacculifer* (Brady), *G. ruber* (d'Orbigny) white and *Cibicidoides wuellerstorfi* (Schwager) in cores Sonne 50-29KL and 50-37 KL, northern part of the South China Sea. Refer to Table 1 for depth to age conversions.

$\delta^{18}\text{O}$ values towards the base of core 37 would suggest a possible discontinuity with parts of Stage 6 at the bottom. This remains a paradox, as this feature is not reflected in the planktonic $\delta^{18}\text{O}$ values.

The signal of the Younger Dryas cooling event which has been clearly identified in other sediment cores from the South China and the adjacent Sulu Sea (Broecker *et al.*, 1988 a & b, Kudrass *et al.*, 1991) is suppressed in both the planktonic and benthic records of our cores. On the other hand, the Bolling/ Allerod climatic changes and the associated meltwater events (e.g., Sarnthein *et al.*, 1991) are fairly well recognised in the planktonic $\delta^{18}\text{O}$ -records of the cores. A temporary halt or slight reversion of the deglacial $\delta^{18}\text{O}$ trend may either be caused by a subsequent climatic deterioration or large fluctuations in the fluvial discharge. In the benthic $\delta^{18}\text{O}$ profile, the Bolling/ Allerod event is also recognisable, with the second phase of the termination (Termination Ib) as a well pro-

nounced feature. These records of rapid climatic changes at the end of the Last Glacial were also reflected in the foraminiferal abundances in the South China Sea Basin (Wang *et al.*, 1986; Broecker *et al.*, 1988 a & b).

The *Cibicidoides wuellerstorfi* oxygen isotope in both cores (shown on time axes for easy comparison, Figs. 1 & 2) reveal that the oxygen isotope profiles of the benthic *C. wuellerstorfi* are closely the same for the past 88 ka, signifying that both cores were in the same ambient water mass throughout this period.

Sedimentation rates calculated from benthic oxygen isotope stratigraphy of *C. wuellerstorfi* show that the interglacial stages 1 and 5 normally have lower sedimentation rates of 4.3–9.3 cm/ka while in the colder stages, the rates are up to twice as high (13.9–17.5 cm/ka). The high sedimentation rates during Stages 4 and 5 and in the upper part of Stage 2 in core 29KL are due to "turbidite" cycles (25–30 cm in thickness) with irregular bottom contacts observed in sediment radio-graphs. Core 37KL, on the other hand, does not show such silty episodes, and the good correlation between the two cores signifies that the turbidites in our cores are of local importance only, and in general have not resulted in deep erosion of the sediment layers. Sediment physical and geotechnical properties measured during the course of this study did not show any indications of major and large-scale subaqueous sediment slumps, and the studied cores appear to lie outside the path of major turbidite movements (Kudrass *et al.*, this volume).

Paleo Productivity and the $\delta^{13}C$ Record

The new (or export) productivity of the euphotic zone, which characterizes the organic matter that leaves the surface layer, sinks into the deep sea and is preserved as organic carbon in sediment (as opposed to the total primary productivity which includes reutilized organic matter), has been estimated using the equation of Sarnthein *et al.* (1988).

$$P_{\text{exp}} = 0.0238 \times C^{0.6429} \times S_B^{0.8575} \times DBD^{0.5364} \times Z^{0.8292} \times S_{B-c}^{-0.2392} \quad (1)$$

where

C = organic carbon content (weight %) of the sample

DBD = dry bulk density (g/ccm) (solid particle density \times (1-porosity/100))

S_B = bulk sedimentation rate (cm/ka)

S_{B-c} = carbon free sedimentation rate (cm/ka)

Z = water depth (m)

The results reveal that total export productivities were generally about 2.5 times higher during the glacial than during the interglacials. However, these estimates incorporate not only the marine production, but also a possible fraction of terrigenous organic carbon. The primary $\delta^{13}C$ signatures of these two organic fractions are usually well distinguished, amounting to about -19.5‰ (vs. PDB) for marine organic matter from equatorial oceans, and to about -26.5‰ for the terrigenous component (Erlenkeuser, 1978; Muller *et al.*, 1983; Westerhausen *et al.*, 1991). Within the bounds of these source isotope

compositions, a simple two source mixing model has been applied to differentiate between the contributions of these organic fractions. The $\delta^{13}\text{C}$ -profile and the distribution of the organic carbon content down the core run closely in parallel and clearly show that the relative proportion as well as the absolute amount of the total marine organic matter culminates in the glacial $\delta^{18}\text{O}$ Stage 2, while in the interglacial Stages 1 and 5, the relative abundance of marine matter is on a pronouncedly lower level (Tables 2 and 3). The sample at 940–942 cm in core 29KL possibly indicates that an even higher supply of terrigenous organic matter occurs in the older interglacial deposits. It thus appears that the glacial climates are not conducive for large belts of vegetation as found today in the neighbouring continental area. These results are in harmony with the findings of Adams *et al.* (1990) showing extended desert terraced deserts and decreased vegetation, and hence reduced terrestrial organic carbon production on the Chinese mainland during the Last Glacial Maximum, 18000 year ago.

Table 2 $\delta^{13}\text{C}$ measurements on total organic carbon in sediment

Core No. SO50–29KL		Core No. SO50–37KL	
Interval measured	$\delta^{13}\text{C}$	Interval measured	$\delta^{13}\text{C}$
(cm)	‰vs. PDB	(cm)	‰vs. PDB
20–22	-21.23 ± 0.02	20–22	-21.21 ± 0.04
30–32	-21.33 ± 0.04	40–42	-21.24 ± 0.02
50–52	-21.54 ± 0.02	60–62	-21.21 ± 0.04
150–152	-20.76 ± 0.03	80–82	-21.39 ± 0.04
180–182	-20.41 ± 0.03	200–202	-20.34 ± 0.04
200–202	-20.28 ± 0.02	210–212	-21.48 ± 0.03
220–222	-20.24 ± 0.03	230–232	-24.42 ± 0.02
250–252	-20.02 ± 0.02	250–252	-20.29 ± 0.06
350–352	-20.25 ± 0.02	307–309	-19.82 ± 0.02
400–402	-20.31 ± 0.02	347–349	-19.72 ± 0.02
500–502	-21.12 ± 0.03	397–399	-20.14 ± 0.02
620–622	-21.16 ± 0.04	447–449	-19.92 ± 0.01
710–712	-22.90 ± 0.03	500–502	-20.64 ± 0.02
760–762	-21.89 ± 0.03	550–552	-20.74 ± 0.01
850–852	-21.79 ± 0.03	600–602	-20.85 ± 0.01
880–882	-22.49 ± 0.03	650–652	-21.46 ± 0.03
920–922	-22.09 ± 0.02	710–712	-21.53 ± 0.03
940–942	-23.54 ± 0.02	750–752	22.93 ± 0.03
960–962	-22.19 ± 0.01	800–802	-21.87 ± 0.04

Correcting for the allochthonous contribution of organic matter from land, the dissimilarities between the paleoproductivities during the cold and the warm periods become even more accentuated. The glacial / interglacial difference for both cores increases to a factor of up to 4, compared to a factor of 2.5 before correcting for the terrigenous fraction. Correcting for the terrigenous contribution could have far reaching implications for the global paleoproductivity and reconstructed carbon budgets, as our previous estimates (Sarnthein and Winn, 1990) did not adequately correct for terrestrial carbon because appropriate supporting data is lacking. The role of the oceans as a reservoir for carbon may have to be

further upgraded. The difference between the paleoproductivity during the last Interglacial and from Stage 4 to the lower part of Stage 3 in core 37KL is small, but is appreciable in the deeper water core 29KL (Fig. 3). This is probably an artifact of the very high sedimentation rates during Stage 4 in the latter core, and is due to the higher clastic flux and to the possibly associated amounts of allochthonous organic material. In both cores the paleoproductivities are high in Stage 2, and declined during the Holocene to present day levels. This decrease of productivity towards the end of the Last Glacial preceded the $\delta^{18}\text{O}$ signals of both plankton and benthos in both cores by 800–1000 years.

Table 3 Terrigenous fraction of total organic carbon from the carbon isotope levels

Time period	$\delta^{13}\text{C}$ (‰ vs. PDB)	Terrigenous material (%)*
Holocene	-21.2 to -20.5	20–25
$\delta^{18}\text{O}$ Stage 2	-19.8 to -20.5	0–8
$\delta^{18}\text{O}$ Stage 3	-19.7 to -21.1	0–18
$\delta^{18}\text{O}$ Stage 4	-20.9 to -21.2	15–20
$\delta^{18}\text{O}$ Stage 4–5.1	-21.5 to -22.9	25–48
$\delta^{18}\text{O}$ Stage 5.1–5.2	-21.8 to -21.9	30–48
$\delta^{18}\text{O}$ Stage 5.3	-20.0	0–2
$\delta^{18}\text{O}$ Stage 5.4	-22.2 to -23.5	37–58

* Calculated using the end values of -19.5‰ for full marine and -26‰ for terrestrial organic material.

The $\delta^{13}\text{C}$ records plotted vs. age (Fig. 2) of the benthic foraminifera *C. Wuellerstorfi* in cores 29KL and 37KL, are almost identical for the past 88 ka. The response of $\delta^{13}\text{C}$ of this species to the surface productivity—with the higher productivity being reflected by the lighter $\delta^{13}\text{C}$ values—is clearly seen from a glacial–interglacial difference in $\delta^{13}\text{C}$ of 0.45–0.5‰ (Figs. 2 and 3). The $\delta^{13}\text{C}$ record of the planktonic species *G. ruber* in core 37KL reveals a similar response to the higher glacial productivity, corresponding with findings in other oceanic regions (Sarnthein and Winn, 1990). On the other hand, the $\delta^{13}\text{C}$ record of *G. trilobus sacculifer* in core 29 KL shows only a general gradual trend towards heavier $\delta^{13}\text{C}$ levels during the past 60 ka, without any distinct response to the higher glacial productivity. Since both cores lie in similar oceanographic and geographic settings, this phenomenon might be attributed to a species-specific characteristic.

Deep Water Distribution

The Geosecs sections illustrating the distribution of total CO_2 in the western Pacific (Craig *et al.*, 1981) show a water mass spreading northward between 2000 m and 3000 m water depth (Fig. 4). A transect of the Holocene $\delta^{13}\text{C}$ levels of the benthic species *C. wuellerstorfi* which measures the carbon isotope composition of the deep water mass show a gradual trend towards lighter values from New Zealand (cores DSDP 594 and Q208, $\delta^{13}\text{C}$ between 0.94‰ and 0.47‰) through the Fiji Islands (0.54‰ to 0.32‰, Winn *et al.*, 1990) to $\delta^{13}\text{C}$ of 0.32‰ to 0.25‰ on the Ontong Java Plateau (Vincent *et al.*, 1981) and $\delta^{13}\text{C}$ levels between 0.27‰ and 0.22‰ in the South China Sea (this study). The glacial

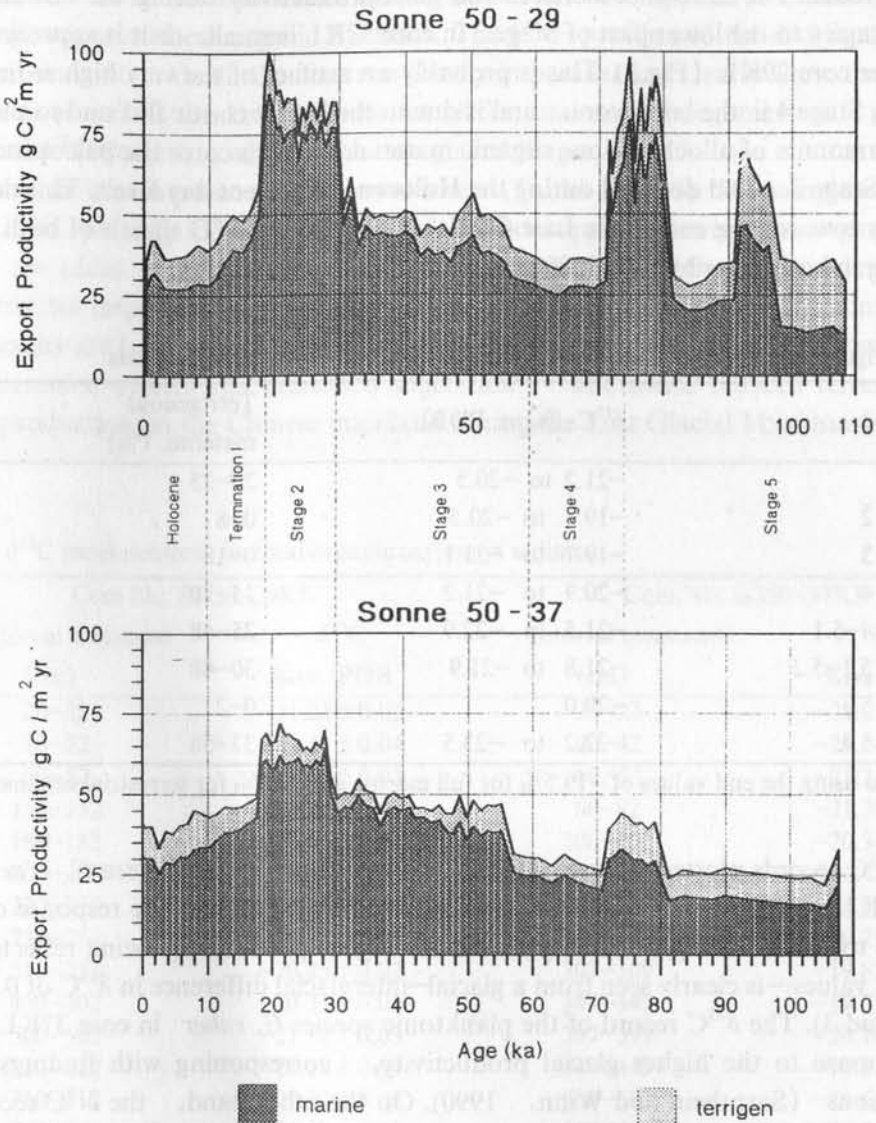


Fig.3 Estimates of total export productivity and net export productivity of marine provenance (dark hatched area) in the South China Sea cores Sonne 50-29 KL and 50-37 KL. Note that the apparent high productivity around 75 ka in core SO50-29 KL is an artifact of high sedimentation rates due to turbidites.

transect shows a similar trend towards lighter $\delta^{13}\text{C}$ levels with values between 0.34‰ and 0.19‰ off New Zealand to figures of 0.21‰ to -0.05‰ in the Fiji-Lau basins, to -0.24‰ in the Ontong Java region, to values of -0.19‰ to -0.23‰ in the South China Sea. For both time slices, however, core V35-05 from the southern part of the basin (Broecker *et al.*, 1988 a and b) reveals much lighter values (by 0.2‰) (Fig.4). In general, glacial $\delta^{13}\text{C}$ values are about 0.3‰ lighter than in the Holocene. During the glacial, the South China Sea is an enclosed inland sea of limited extent having its main connection to the West Pacific through the Bashi Channel with a threshold depth of around 2500 m, and through the

Balabac and Mindoro Straits to the Sulu Sea (Wang, 1990). The regional $\delta^{13}\text{C}$ trends are thus in accordance with this paleogeographical setting, with major deep water renewal / ventilation only through the north-east sector of the basin.

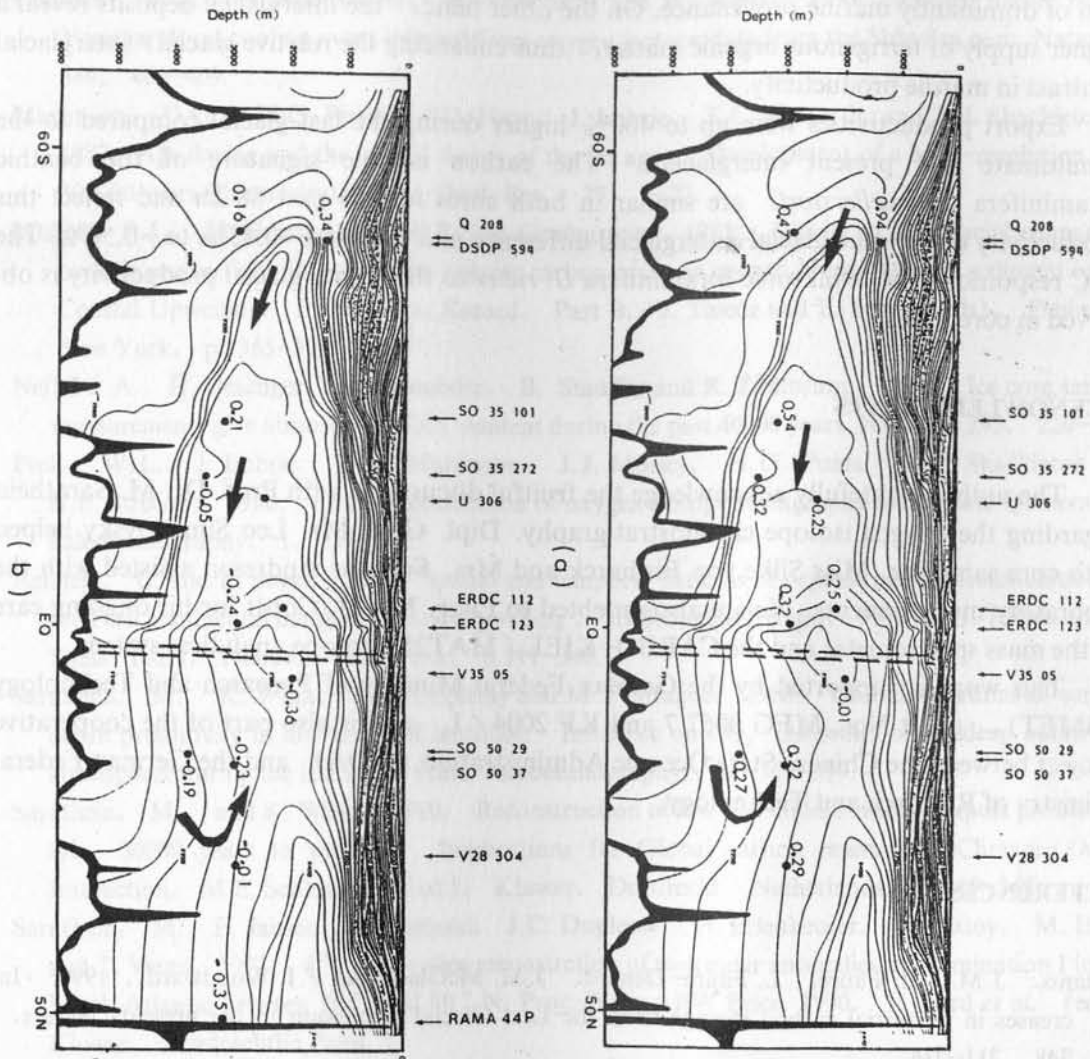


Fig.4 $\delta^{13}\text{C}$ transects across the western Pacific contours show total carbon dioxide in sea water after Craig *et al.* (1981). (a) Holocene; (b) Last Glacial.

CONCLUSIONS

High resolution oxygen isotope stratigraphy based on planktonic and benthic foraminifera in two deep sea sediment cores from the northern flank of the South China basin show that the major global isotope signature is also well documented in this area. Both cores penetrated down to isotope Stage 5. The glacial-interglacial $\delta^{18}\text{O}$ shift amounts to about 1.6‰ for the planktonic species *G. trilobus sacculifer* and *G. ruber*, and is about 1.4‰ for the

benthic *C. wuellerstorfi*. Sedimentation rates were up to twice as high during the glacial stages than during the interglacials. Coarse turbidites were not encountered. The silty "turbidite" cycles below Stage 3 in core 29KL have only local significance. The volcanic ash layer in core 29 KL has an interpolated age of 28.4 ka.

$\delta^{13}\text{C}$ values of total organic fraction indicate that the glacial sediments have organic carbon of dominantly marine provenance. On the other hand, the interglacial deposits reveal a higher supply of terrigenous organic matter, thus enhancing the relative glacial / interglacial contrast in marine productivity.

Export productivities were up to 400% higher during the last glacial compared to the penultimate and present interglacials. The carbon isotope signature of the benthic foraminifera *C. wuellerstorfi* are similar in both cores for the past 88 ka and reflect this productivity effect—the glacial–interglacial difference in $\delta^{13}\text{C}$ being -0.45‰ to -0.50‰ . The $\delta^{13}\text{C}$ response of the planktonic foraminifera *G. ruber* to the higher glacial productivity is observed in core 37KL.

ACKNOWLEDGMENTS

The authors gratefully acknowledge the fruitful discussions with Prof. Dr. M. Sarnthein regarding the oxygen isotope chronostratigraphy. Dipl. Geol. Mr. Leo Simanovsky helped with core sampling. Miss Silke von Bismarck and Mrs. Susanne Andresen assisted with the laboratory measurements. We are also indebted to Engg. Mr. H. Cordt for his ongoing care of the mass spectrometer and the CARBO–KIEL / MAT251 isotope analytical system.

This work is supported by the German Federal Ministry of Research and Technology (BMET), grant Nos. MFG 0057 7 and KF 2004 / 1, and is also part of the cooperative project between the Chinese State Oceanic Administration (SOA) and the German Federal Ministry of Research and Technology.

REFERENCES

- Adams, J.M., H. Faure, L. Faure–Denard, J.M. McGlade and F.I. Woodward, 1990: Increases in terrestrial carbon storage from the Last Glacial Maximum to the present. *Nature*, 348, 711–714.
- Barnola, J.M., D. Raynaud, Y.S. Korotkevich and C. Lorius, 1987: Vostok ice core provides 160000–year record of atmospheric CO_2 . *Nature*, 329, 408–414.
- Broecker, W.S., M. Andree, M. Klas, G. Bonani, W. Wolfli and H. Oeschger, 1988a: New evidence from the South China Sea for an abrupt termination of the last glacial period. *Nature*, 333, 156–158.
- Broecker, W.S., M. Andree, G. Bonani, W. Wolfli, M. Klas, A. Mix and H. Oeschger, 1988b: Comparison between radiocarbon ages obtained on coexisting planktonic foraminifera. *Paleoceanography*, 3, 647–657.
- Craig, H., W.S. Broecker and Derek Spencer, 1981: Geosecs Pacific expedition, Volume 4, Sections and profiles. U.S. Govt. Printing Office, Washington, 251 p.
- Erlenkeuser, H., 1978: The use of radiocarbon in estuarine research. *The Biogeochemistry of*

- Estuarine Sediments, Proceedings of a UNESCO / SCOR Workshop, Melreux, Belgium, 1976. UNESCO, Paris, France, p. 140–153.
- Hartmann, M., P.J. Muller, E. Suess, and C.H. van der Weijden, 1976: Chemistry of Late Quaternary sediments and their interstitial waters from the Northwest African continental margin. "Meteor" Forschungsergebn. Reihe C, 24, 1–67.
- Kudrass, H.R., H. Erlenkeuser, R. Vollbrecht and W. Weiss, 1991: Global nature of the Younger dryas cooling event inferred from oxygen isotope data from the Sulu Sea core. *Nature*, 349, 406–409.
- Martinson, D.G., N.G. Pisias, J.D. Hays, J. Imbrie, T.C. Moore Jr. and N.J. Shackleton, 1987: Age dating and the orbital theory of the ice ages: Development of a high-resolution 0 to 300000 years Chronostratigraphy. *Quat. Res.*, 27, 1–27.
- Muller, P.J., H. Erlenkeuser and R. von Grafenstein, 1983: Glacial to interglacial changes in oceanic productivity inferred from organic carbon cycles in eastern North Atlantic sediment cores. *Coastal Upwelling, Its Sediment Record, Part B*, J. Thiede and E. Suess (eds), Plenum, New York, p. 365–398.
- Neftel, A., H. Oeschger, J. Schwander, B. Stauffer and R. Zumbunn, 1982: Ice core sample measurements give atmospheric CO₂ content during the past 40000 years. *Nature*, 295, 220–223.
- Prell, W.L., J. Imbrie, D.G. Martinson, J.J. Morley, N.G. Pisias, N.J. Shackleton and H.F. Streeter, 1986: Graphic correlation of oxygen isotope stratigraphy to the Late Quaternary. *Paleoceanography*, 1, 137–162.
- Reimers, C. and E. Suess, 1983: Spatial and temporal patterns of organic matter accumulation on the Peru continental margin. *Coastal Upwelling, Its Sediment Record, Part B*, J. Thiede and E. Suess (eds), Plenum, New York, p.311–346.
- Sarnthein, M., K. Winn, J.C. Duplessy and M. Fontugne, 1988: Global variations of surface ocean productivity in low and mid latitudes: Influence on CO₂ reservoirs of the deep ocean and atmosphere during the last 21000 years. *Paleoceanography*, 3, 361–399.
- Sarnthein, M., and K. Winn, 1990: Reconstruction of low and middle latitude export productivity, 30000 years to present: Implications for Global carbon reservoirs. *Climate–Ocean Interaction*, M.E. Schlesinger (ed.), Kluwer, Dordrecht, Netherlands, p. 319–342.
- Sarnthein, M., E. Jansen, M. Arnold, J.C. Duplessy, H. Erlenkeuser, A. Flatoy, M. Hahn and T. Veum, 1991: δ^{18} time-slice reconstruction of meltwater anomalies at Termination I in the North Atlantic between 50° and 80° N. *Proc. Naro ARW Erice, 1990*, E. Bard *et al.* (eds.). Kluwer, Dordrechtlin Press.
- Sarnthein, M., M. Hahn, E. Vogelsang, H. Erlenkeuser, J.C. Duplessy and M. Arnold, 1991: Meltwater spreading from the Barents shelf ice sheet records, an estuarine North Atlantic 13.6 ka ago. *Nature* (in press).
- Vincent, E., J.S. Killingley and W.H. Berger, 1981: Stable isotopes in benthic foraminifera from Ontong–Java Plateau, box cores ERDC 112 and 113. *Palaeogeogr., Palaeoclimatol., Palaeoecol.*, 33, 221–230.
- Wang, C.H., M.P. Chen, S.C. Lo and J.C. Wu, 1986: Stable isotope records of the Late Pleistocene sediments from the South China Sea. *Bull. Inst. Earth Sciences, Academia Sinica*, 6, 188–195.
- Wang, P., 1990: The Ice–Age China Sea — Research results and problems. *Proc. Ist Int. Conf. on Asian Marine Geology*, Shanghai, 1988, China Ocean Press, Beijing, p. 181–197.
- Wang, P., M. Qiubao, B. Yunhua and F. Wenke, 1986: Planktonic foraminifera in the conti-

mental slope of the northern South China Sea during the last 130000 years and their paleo-oceanographic implications. *Acta Geologica Sinica*, 60 (3), 215-225.

Westerhausen, L., J. Poynter, G. Eglinton, H. Erlenkeuser and M. Sarnthein, 1991: Marine and terrigenous origin of organic matter in modern sediments of the equatorial East Atlantic: Molecular and $\delta^{13}\text{C}$ evidence. *Deep Sea Research* (in press).

Winn, K., M. Wiedicke and H. Erlenkeuser, 1990: Stable isotope stratigraphy, paleoproductivity and sedimentation rates in the South Lau and North Fiji basins, western Pacific. *Geological Evolution and Hydrothermal Activity in the Lau and North Fiji Basins* (Southwest Pacific, Sonne Cruise SO-35), U. von Stackelberg and U. von Rad. *Geol. Jahrbuch* (eds.), D 92, 231-253, Hannover.

STRATIGRAPHY AND SEDIMENTARY EVENTS IN THE PHILIPPINE SEA

WU SHIYING

First Institute of Oceanography, SOA, Qingdao, China

ABSTRACT

Stratigraphical sequences, sedimentary events and history of the Mariana Trough and the West Philippine Basin were studied based on biostratigraphy, magnetic stratigraphy and isotopic stratigraphy of 5 representative sediment cores. It is thought that, the sedimentary hiatus from the Middle Miocene to the Early Pleistocene found in the core 77KG is the reflection of the global important lacuna events. It is of great significance for a global comparison in the studies of event sedimentology and paleoceanography.

INTRODUCTION

Problems on marine sedimentology in the studied areas were explored by Bouma (1975). Since DADP and ODP were carried out, Klein & Lee (1984), and Hussong & Uyeda (1981) have studied sediment cover deposited since the Early Tertiary.

This study involves two box cores and three gravity cores collected in the SO-57 cruise and is aimed at the investigation of stratigraphy and sedimentary events. Their geographical positions and general characteristics are shown in Fig.1 and Table 1.

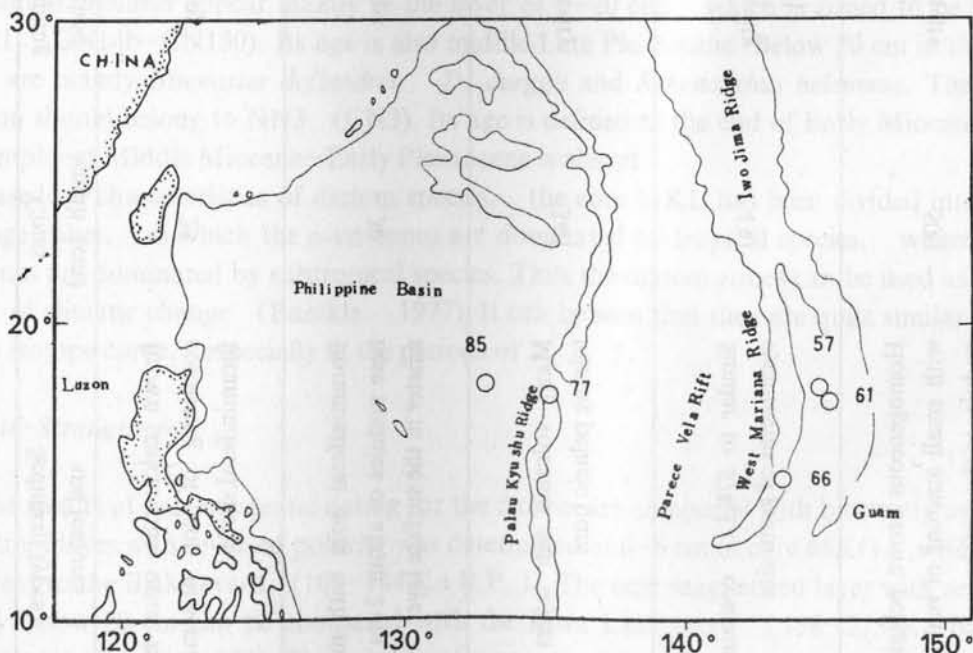


Fig.1 Sampling positions and tectonic features in the Mariana Trough and the Philippine Basin.

Table 1 Basic parameters and characteristics of five cores

Station No.	Station location	Water depth (m)	Tectonic position	Sampling method	Cores length (cm)	Sediment types and features
66KG	14° 29.89' N 143° 05.15' E	2040	West Mariana Ridge	Box	25	Brown calcareous ooze mainly consisting of iron disseminated foraminiferal shells
77KG	17° 38.03' N 135° 01.50' E	2820	Palau-Kyushu Ridge	Box	30	Foraminiferal ooze with manganese nodules of about 2 cm in diameter in the surface layer
57KL	17° 54.31' N 144° 44.05' E	3860	Eastern flank of the small spreading ridge of the Mariana Trough	Gravity	340	Many volcanic ash layers containing pelagic ooze
61KL	12° 28.13' N 144° 48.45' E	4690	South of the Mariana Trough	Gravity	430	Similar to 57KL, containing 5 cyclothem of grain size
85KL	17° 49.71' N 132° 58.46' E	5900	Deep-sea plain of the West Philippine Basin	Gravity	500	Homogeneous brown pelagic clay with small amount of manganese nodules in the surface layer

DIVISION OF STRATIGRAPHIC SEQUENCES

The five cores involved in the paper will be studied. However, because of the limitation in lithology and research methods, the information on stratigraphy is obtained confinedly.

Biostratigraphy

66KG and 77KG contain abundant planktonic foraminifera. The content of pink shells of *Globigerinoides ruber* decreases distinctly from the bottom to the top and vanishes at 6 cm below the surface. According to Thompson *et al.* (1979), who studied 11 cores from the Pacific to Indian ocean, the extinct age of the pink shells of *Gs. ruber* is the 5e subperiod of oxygen isotope (about 120 Ka B.P.). In addition, a lot of *Gr. truncatulinoides* occurs at 66KG and the upper section of 77KG. But, no *Gr. tosaensis* is found. Such a kind of foraminifera is considered vanishing in Early Pleistocene. Thus, the age of this section is Middle–Late Pleistocene.

There is a pronounced difference in lithology between the layers below and above 20 cm in core 77KG. The species of *Gs. sacculifer* began to appear in Early Miocene (N6 zone), whereas *Gs. altiapertura* vanished at this time (N7 zone). The species assemblages defined that the age of this buried fauna should be the middle Early Miocene, that is, the N6 zone.

According to the analysis of calcareous nannofossils, in the core 66KG there are dominantly *Gephyrocapsa oceanica* and *Emiliania huxleyi*, which should belong to NN21 in the fossil zonation (Martini, 1971) and are equivalent to CN15 in the zonation table of Okada and Bukry (1980). Thus the stratigraphic age should be middle Late Pleistocene (Okada *et al.*, 1980).

Abundant calcareous nannofossils exist also in core 77KG. *Emiliania huxleyi* and *Ceratolithus cristatus* appear mainly in the layer of 0–20 cm, which is zoned to be NN20–NN21 (CN14b–CN150). Its age is also middle Late Pleistocene. Below 20 cm in the core 77KG are mainly *Bischoferia deflandrei*, *D. durggii* and *Sphenolithus belemnos*. The fossil zonation should belong to NN3 (CN3). Its age is defined as the end of Early Miocene. The stratigraphy of Middle Miocene–Early Pleistocene is absent.

Based on characteristics of diatom species, the core 61KL has been divided into 6 assemblage zones, in which the even zones are dominated by tropical species, whereas the odd zones are dominated by subtropical species. Thus the diatom zones can be used as an indicator of climatic change (Burckle, 1977). It can be seen that they are quite similar to the oxygen isotope curve, especially at the periods of 1, 2, 5.

Magnetic Stratigraphy

The results of paleomagnetic dating for the 5 cores are compared with biostratigraphy. A magnetized layer with reversed polarity was determined at 0–6 cm in core 66KG, which was equivalent to the Blake event (108–144 Ka B.P.). The next magnetized layer with reversed polarity below 20 cm can be compared with the Biwa Lake event (198–215 Ka B.P.) named by Yasukawa (1973). The polarity of magnetized layer is positive in cores 77 KG and 57KL, therefore, they have no significance in the stratigraphic discrimination.

From the magnetic survey, it can be seen that two magnetized layers with reversed polarity are located at 81–95 cm and 109–127 cm in core 61KL. The magnetized layer with reversed polarity at 81–85 cm was temporarily named as the Gotobarg event (10.8–14.0 Ka B.P.) according to Morner (1977). Based on diatom data, we inferred that the depth of near 100 cm might be the boundary between the climatic periods of 2 and 3, and its age might be about 30 Ka B.P.. Thus another magnetized layer with reversed polarity (109–127 cm) could be compared with the Mungo event (30780 ± 520 a B.P.) named by McEthinnny (1972). In addition, at 299–333 cm there is also a magnetized layer with reversed polarity, but it is not normalized. According to Burckle (1977), the lower limit of this layer would be 125 Ka B.P. equivalent to the Blake event.

85KL is monolithologic, but the paleogeomagnetic survey is encouraging. According to the table of geomagnetic age, two polarity periods, the Brunhes normal epoch and the Matuyama reversed epoch can be separated at 333 cm. In the Matuyama reversed epoch there is also a positive event at 400–420 cm, which is equivalent to the Jamarillo event (900–970 Ka B.P.).

Carbon and Oxygen Stable Isotope Stratigraphy

Carbon and oxygen isotope age was determined only in box cores 66KG and 77KG because of the limitation in lithology. The determined specimens were planktonic foraminifera, *Globigerinoides sacculifer*. $\delta^{13}\text{C}$ and $\delta^{18}\text{O}$ were measured on MAT251 mass spectrometer.

The layers containing the pink shells of *Gs. ruber* and the shape of oxygen isotope curve indicated that the oxygen isotope stages were 5e–7 in core 66KG and in the upper 20 cm in core 77KG. They should undergo an alternation, one cold stage (6) between two warm stages (5e, 7). Their ages ranged from 200 to 120 Ka B.P. (Shackleton *et al.*, 1976). In the sediment layer below 20 cm in core 77KG isotope data can not be compared with others in the time sequence because of the long period of sediment gap.

SEDIMENTARY EVENTS AND HISTORY

Of the 5 sediment cores with different length, the oldest sediments occurred in the layer below 20 cm in core 77KG. According to the abundant data of biostratigraphy, especially the data of calcareous nannofossils, the layer is dated at the end of Early Miocene. Thus the Middle Miocene–Early Pleistocene strata are absent (Fig. 2).

This hiatus after Middle Miocene has been discussed by many scientists. Ujiie (1984) considered that the Middle Miocene hiatus in the Pacific Ocean began 13 Ma B.P. and lasted at least 1 Ma. The reason for this hiatus was discussed by van Gersel *et al.* (1981). They thought that because of the cooling climate occurred during the Middle Miocene time, the Antarctic ice sheet was formed, and the temperature gradient between the pole and the equator increased to enhance the atmospheric convection. Thus the increase of Antarctic bottom current not only caused a wide bottom erosion, but also led to the increase of ocean currents and upwelling currents, and the turbidity current was aroused further to enlarge the area and the strength of submarine erosion.

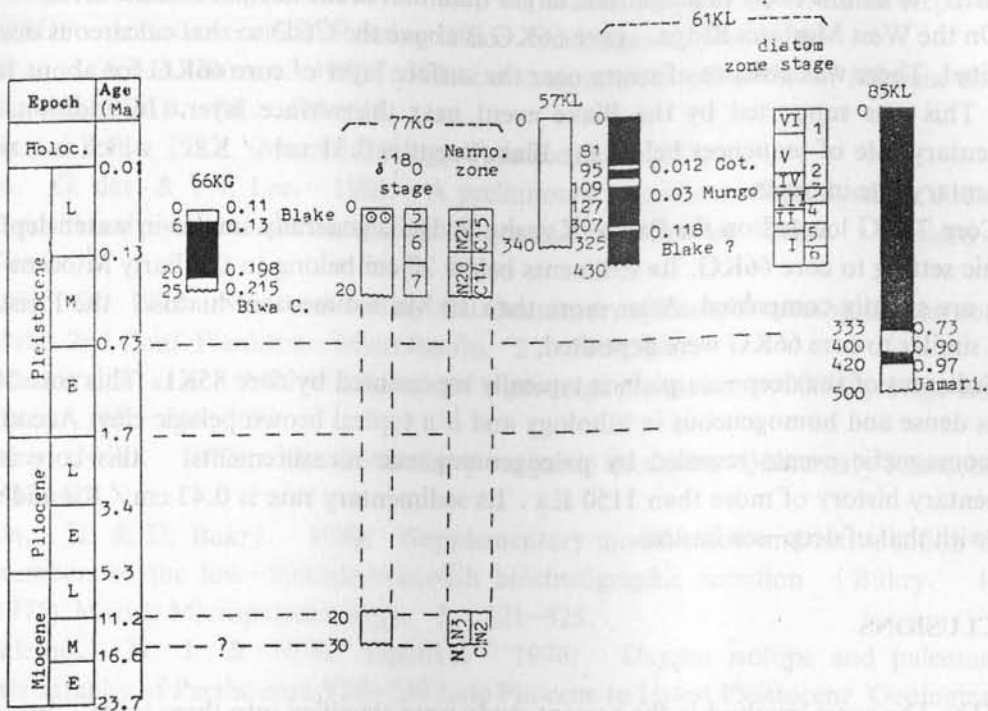


Fig.2 Sedimentary events and age comparison of 5 cores.

The development of the Antarctic ice sheet leads to a global lowering of sea level at the end of Miocene. Thus the Japan Sea might be isolated from the Pacific and changed into a fresh water lake at that time (Kennett, 1982). Particularly, drying of the Mediterranean Sea happened at that time attracted much attention in geology (Hsu, 1982).

As to the geodynamic reason for this important lacuna event, Keller *et al.* (1983), from the Oligocene–Pliocene hiatus in the Pacific, inferred that collision between the Australian plate and the Indonesian plate in Miocene might close the channel between the Pacific and Indian Ocean so that the bottom currents flowed northwards round along the West Pacific margin. Erosion and solution of carbonate were enhanced in the West Pacific. Such a process can be verified by the persistence of erosional surface and the solution of foraminifera present in the lower strata of the core 77KG.

It can be seen from the above that the long depositional hiatus in 77KG located on the Palau–Kyushu Ridge is not an occasional event. It is a reflection of the global important lacuna events after the Middle Miocene time. It will be of significance for the global comparison in the studies on event sedimentology and paleoceanology.

The discussion mentioned above has, in fact, revealed the evolutionary history of the studied areas from different points of view. The discussion below will be restricted to three different tectonic locations, the depressions on the small spreading ridge in the Mariana Trough, the relict and present oceanic ridge and the deep-sea plain. At the depressions of the small spreading ridge in the Mariana Trough frequent volcanic activities caused by the high spreading rate made the sediment cores rich in more volcanic ash layers and led to several sediment cycles of turbiditic sedimentation. The sedimentary rate in such areas (2.82

cm / Ka) to be one order in magnitude larger than that in the normal oceanic areas.

On the West Mariana Ridge, core 66KG is above the CCD so that calcareous ooze was deposited. There was absence of strata near the surface layer of core 66KG for about 100 Ka long. This was supported by the Blake event near the surface layer. In addition, the sedimentary rate of sequences below the Blake event is 0.31 cm / Ka, which is a normal sedimentary rate in ocean.

Core 77KG located on the Palau-Kyushu Ridge is generally similar in water depth and tectonic setting to core 66KG. Its sediments below 20 cm belong to the Early Miocene strata which are slightly compacted. After more than 10 Ma sedimentary hiatus, the Pleistocene strata similar to core 66KG were deposited.

Sediment of the deep-sea plain is typically represented by core 85KL. This core 500 cm long is dense and homogeneous in lithology and is a typical brown pelagic clay. According to the geomagnetic events revealed by paleogeomagnetic measurements, this core is of a sedimentary history of more than 1150 Ka. Its sedimentary rate is 0.43 cm / Ka and agreement with that of deep-sea basins.

CONCLUSIONS

(1) The cores involved in the present study were classified into three types, calcareous ooze, brown ooze containing many volcanic ash layers and homogeneous brown pelagic clay. They are so typical that they can be used to study tectonic setting, geomorphological features and sediment types.

(2) The division of stratigraphical sequences was mainly based on the studies of biostratigraphy, magnetic stratigraphy and isotope stratigraphy. The oldest stratum in the areas is the Early Miocene.

(3) The absence of Middle Miocene - Early Pleistocene strata is an ubiquitous phenomenon in the Pacific Ocean. The sedimentary hiatus at least 10 Ma long is a reflection of the global important lacuna events after the Middle Miocene time. It will be of significance for the global comparison in the studies on event sedimentology and paleoceanology.

REFERENCES

- Berggren, W.A., 1980: Towards a Quaternary time scale. *Quaternary Research*, 13, 1980, 277-302.
- Bouma, A.H., 1975: Structural and textural characteristics of debrites from the Philippine Sea. D.E. Karig, J.C. Ingle, Jr., *et al.* (eds), *Initial Reports of the DSDP*, U. S. Government Printing Office, Washington, D.C., 497-506.
- Burckle, L.H., 1977: Pliocene and Pleistocene diatom zone from the eastern equatorial Pacific. *Quaternary Research*, 7, 330-340.
- Carison, R.L. & K. Kobayashi (eds.), *Geodynamics of back-arc regions*, *Tectonophysics*, 102, 119-152.
- Hsu, K.J., 1982: Thirteen years of deep-sea drilling. *Ann. Rev. Earth Planet. Sci.*, 10, 109-128.

- Hussong, D.M. & S. Uyeda, 1981: Deep sea drilling project Leg 60. Initial Reports of the DSDP, U.S. Government Printing Office. Washington, D.C., 60.
- Keller, G. & J.A. Barron, 1983: Paleooceanographic implications of Miocene deep-sea hiatuses. *GSAB*, 94, 590-613.
- Kennett, J.P., 1982: *Marine Geology*. Prentice Hall, 813.
- Klein, G. dev. & Y.I. Lee, 1984: A preliminary assessment of geodynamic controls on depositional systems and sandstone diagenesis in back-arc basins, Western Pacific Ocean.
- Martini, E., 1971: Standard Tertiary and Quaternary calcareous nannoplankton zonation. *Proc. 2nd Conf. Planktonic Microfossils*, 2, 739-786.
- McEthinny, B. *et al.*, 1972: Evidence of a geomagnetic excursion 30000 yrs ago B.P.. *Nature*, 163, 565-567.
- Morner, N.A., 1977: The Gothenbury magnetic excursion. *Quaternary Research*, 7, 413-427.
- Okada, H. & D. Bukry, 1980: Supplementary modification and introduction of code numbers to the low-latitude coccolith biostratigraphic zonation (Bukry, 1973, 1975). *Marine Micropaleontology*, 5, 321-325.
- Shackleton, N. J. & N. D. Opduke, 1976: Oxygen isotope and paleomagnetic stratigraphy of Pacific core V28-239 Late Pliocene to Latest Pleistocene. *Geological Society of America, Memoir*, 145, 449-464.
- Thompson, P.R. *et al.*, 1979: Disappearance of pink-pigmented *Globigerinoides ruber* at 120000 yr B.P. in the Indian and Pacific Oceans. *Nature*, 280, 554-558.
- Ujiie, H., 1984: A middle Miocene hiatus in the Pacific region: Its stratigraphic and paleooceanographic significance. *Palaeogeography, Palaeoclimatology, Palaeoecology*, 46, 143-164.
- van Gersel, J. T. & S. R. Troelstra, 1981: Late Neogene planktonic foraminiferal biostratigraphy and climostratigraphy of the Solo River section (Java, Indonesia). *Marine Micropaleontology*, 6, 183-209.
- Yasukawa, K., J. Nakajima, M. Torth, M. Natsunata & S. Horle, 1973: Paleomagnetism of a core from Lake Biwa (1). *J. Geomagn. Geoelect.*, 25, 447-474.

A STUDY OF VOLCANIC GLASS IN NORTHERN SOUTH CHINA SEA DURING THE LAST 100KA

CHEN WENBIN¹⁾ & ZHOU FUGEN²⁾

1) *Second Institute of Oceanography, SOA, Hangzhou, China*

2) *Tongji University, Shanghai, China*

ABSTRACT

The volcanic glass in the calcium-dissolved particles with the size of larger than 0.038 mm in total 281 samples of three cores (SO50-37KL, SO50-29KL and SO50-91KL) from northern South China Sea has been studied. The volcanic glass can be divided into three basic types: the brown glass, the achromate "silk" glass and the achromate "plate" glass. The volcanic glass increases in abundance from south (SO50-91KL) to north (SO50-29KL and SO50-37KL). If the sediment bed containing more than 30% of volcanic glass is regarded as volcanic ash bed, the upper, middle and lower volcanic ash bed can be defined and compared with each other in the cores. The upper, middle and lower ones correspond to the stages 1, 3 and 5 of the oxygen isotope curves, respectively. The top boundary of the middle one accords with that of the stage 3, and the top boundary of the lower one is similar to that of the stage 5. These three beds, especially the middle one, are the good index beds for a stratigraphic correlation in northern South China Sea.

INTRODUCTION

Total 281 samples were taken out from three cores (SO50-37KL, 18° 54.60' N, 115° 45.78' E, 2695 m deep, 863 cm long; SO50-29KL, 18° 20.08' N, 115° 59.22' E, 3766 m, 1023 cm; and SO50-91KL, 14° 38.3' N, 115° 07.33' E, 4282 m, 788 cm) in northern South China Sea. The sediment samples were decalcified with hydrochloric acid and sieved through 0.038 mm mesh. The particles with the size of larger than 0.038 mm were dried and examined under a microscope. The abundance of various volcanic glass in the particles has been identified and counted for every sample. The optical characters of various volcanic glasses were examined by Dr. Wu Yunxin and Dr. Xia Anning.

CHARACTERS OF THE VOLCANIC GLASS

The volcanic glass has been found in most samples. According to the color and form, they can be divided into the following three basic types.

Brown Volcanic Glass

There are generally light brown, brown and transparent, but semitransparent in a minority of grains with dark brown. Their forms appear as banding fragment or irregular

grain, with irregular arc rims and highly concentrated, regularly arranged banding or fibrous cracks. There are generally some elliptical gaseous inclusion (or vesicular) within glass grains and sometimes inclusion of small columnar crystals of apatite. The grains of glass are mostly possessed of isotropism and rarely devitrified between crossed polars. The relief of most grains is convex, and their refraction index is usually larger, but sometimes less than balsam.

Achromatic Banding ("Silk") Volcanic Glass.

The form appears as achromatic, transparent and irregular banding or "silk" fragment. There are a lot of irregular arc edges and a few ground corners. There are irregular arc cracks within the grains. And there are also a lot of elliptical gaseous inclusions with distinct dark margins. The index of refraction is lower than balsam, and most of them are usually possessed of isotropism and a few are devitrified between crossed polars.

Achromatic "Plate" Volcanic Glass

It is achromatic and transparent. Its surface is as clear and smooth as water. Such a very thin plate fragment belongs to irregular polygon with straight margins. There are no or fewer cracks. Its appearance is very similar to broken cover glass. The index of refraction is lower than balsam and all of the glass is possessed of isotropism between crossed polars.

Electron microprobe analysis and refractive index measurement for the volcanic glass from surface sediments in the South China Sea have been done by Li Zhizhen (SOA, 1988). The analysing result is shown in Table 1.

Table 1 Result of electron microprobe analysis for the volcanic glass

Stat.	Name	SiO ₂	TiO ₂	Al ₂ O ₃	Cr ₂ O ₃	FeO	MnO	MgO	CaO	Na ₂ O	K ₂ O.
8347	achro.	66.7	0.74	12.6	0.05	6.05	0.19	0.59	2.27	2.39	4.05
8336	brown	60.7	1.11	14.6	0.00	9.27	0.26	2.32	5.37	1.92	1.88

The refractive index of brown glass is equal to 1.5565–1.5637, and that of achromatic glass is equal to 1.4980. The features of above three types of volcanic glass suggest that brown glass belongs to basic effusive mass with many vesiculars, achromatic banding glass belongs to intermediate and intermediate–acid effusive mass which has ever undergone roll and drift and achromatic "plate" glass belongs to intermediate–acid and acid effusive mass.

DISTRIBUTION OF THE VOLCANIC ASH BEDS AND THEIR STRATIGRAPHIC IMPLICATIONS

The distribution of volcanic glass in cores SO50–37KL, SO50–29KL and SO50–91KL is shown in Fig. 1.

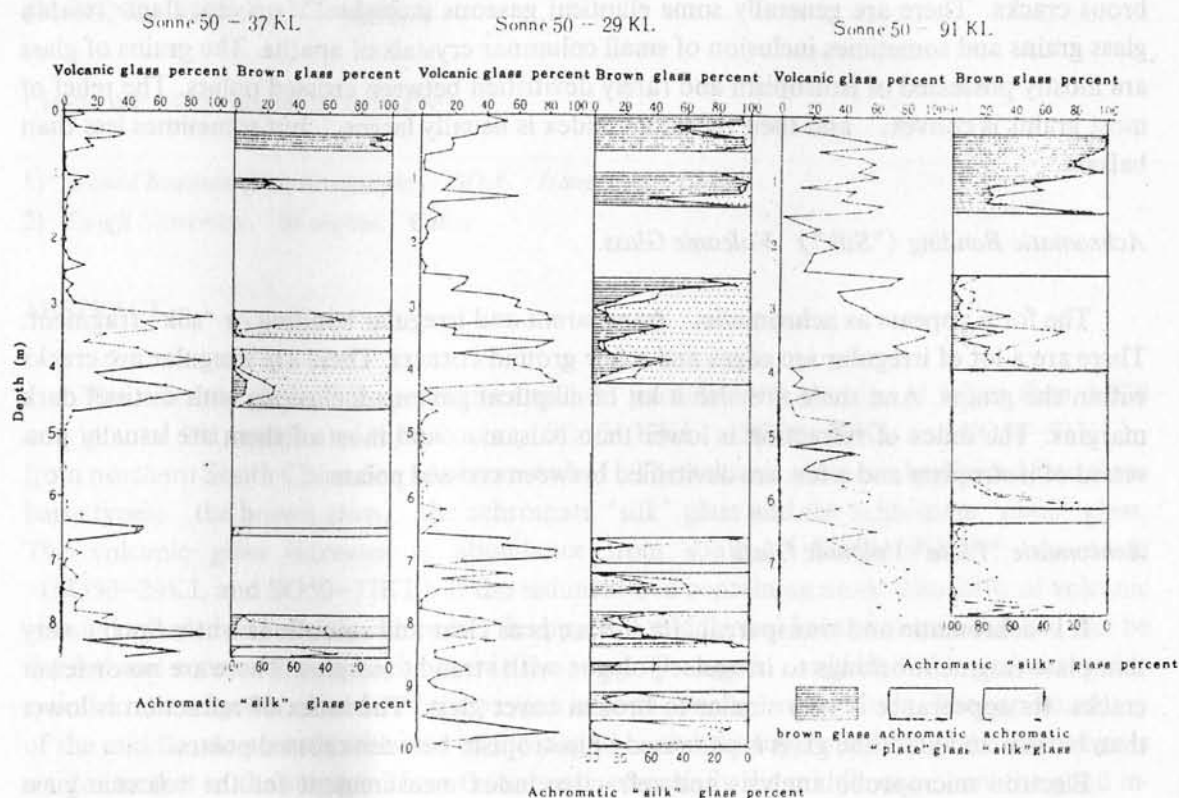


Fig. 1 Distribution of volcanic glass.

The Fig.1 Shows that the abundance of volcanic glass decreases distinctly from south to north, i.e. from SO50-91KL to SO50-29KL and SO50-37KL. The abundance of volcanic glass in most samples of the core SO50-91KL is more than 20%, but in SO50-29KL and SO50-37KL, it is about 10%.

If the sediment beds with more than 30% of volcanic glass are regarded as volcanic ash beds, three ash beds (upper, middle and lower) can be distinguished in all of above three cores. The volcanic ash bed with 4 cm thickness at the depth of 303 cm in the core SO 50-29KL is as white as milk and consists of achromatic volcanic glass dominantly and other crystal minerals. The composition and grain size of the ash bed are analyzed at Tongji University with the powder X-ray diffraction (Table 2). The analysis result shows that crystal minerals make up 10.14% of the total ash in which there are 5.10% of albite (high temperature), 3.16% of anorthite (low temperature) and 1.93% of quartz. The probability cumulative curve (Fig.2) does not reflect the influence of water dynamics on the ash with $Md = 4.22 \phi$, but the curve of size distribution reflects this influence (Fig. 3). The grain size concentrates at about 9ϕ , but weight percentage concentrates at about 4ϕ .

The main characters of vertical distribution of the volcanic ash beds in three cores (Table 3) shows that the upper, middle and lower ash beds can be compared with each other respectively.

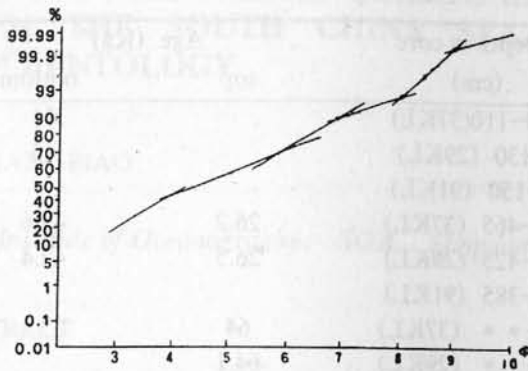


Fig. 2 Probability cumulative curve of the volcanic ash bed at depth 303 cm from the core SO50-29KL.

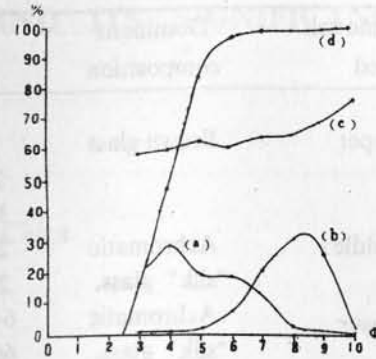


Fig. 3 The curve of size distribution of the volcanic ash bed at depth 303 cm from the core SO50-29KL. (a) Weight percentage; (b) Distribution of the size; (c) Cumulative frequency curve of weight percentage; (d) Roundness $R = 2\sqrt{4\pi s/p}$, s - area, p - perimeter.

Table 2 Minerals in the volcanic ash beds from core SO50-29KL (in order of abundance)

Volcanic ash bed	Mineral analysis	X-ray diffraction analysis
Upper	0-15 cm: calcite, quartz, muscovite, pseudowollastonite; 100-115 cm: calcite, orthoferrosilite, fayalite, Fe-Mn-oxides	31-46 cm: calcite, quartz, orthofe., Mn-Fe-oxides; 100-110 cm: calcite, quartz, gehlenite
Middle	300-313 cm: calcite, quartz, orthofe., albite, anorthose, muscovite, Mn-Fe-oxides	395-409 cm: calcite, quartz, orthofe., fayalite, muscovite, gehlenite, Fe-Mn-oxides
Lower	815-965 cm: calcite, quartz, orthofe., pyrochrotite, fayalite, albite, anorthose, Mn-Fe-oxides, gehlenite, muscovite	757-800 cm: calcite, quartz, arthofe., fayalite, gehlenite, muscovite, Fe-Mn-oxides

The upper volcanic ash bed is dominated by the brown glass. According to the oxygen isotope curves (Fig. 4), the ages of bottom boundaries of the upper bed are 4.45 Ka and 4.57Ka in the SO50-37KL and SO50-29KL, respectively, and the average of them is 4.5 Ka. The age of the bottom boundary of the upper ash bed is 15 Ka in SO50-29 KL.

The middle volcanic ash bed is characterized by the high abundance of volcanic glass which is dominated by achromatic "silk" volcanic glass, and has clear top and bottom boundaries. The ages of the top and bottom boundaries are 26.2 Ka and 43.6 Ka in SO50-37KL, and 26.5Ka and 42.4Ka in SO50-29KL, respectively. The average ages of the top and bottom boundaries of the middle volcanic ash beds are 26.4 Ka and 43 Ka, respectively.

Table 3 Main characters of volcanic ash beds

Volcanic ash bed	Dominant composition	Depth in core (cm)	Age (Ka)*	
			top	bottom
Upper	Brown glass	30-110(37KL)		11
		0-130 (29KL)		15
		25-150 (91KL)		
Middle	Achromatic "silk" glass,	310-465 (37KL)	26.2	43.6
		275-425 (29KL)	26.5	42.4
Lower	Achromatic "silk" glass,	645- * * (37KL)	64	
		"silk" glass,	660- * * (29KL)	64.1
		"plate" glass	560- * * (91KL)	

* The ages are on the basis of the oxygen isotope curves.

* * The bottom was not drilled.

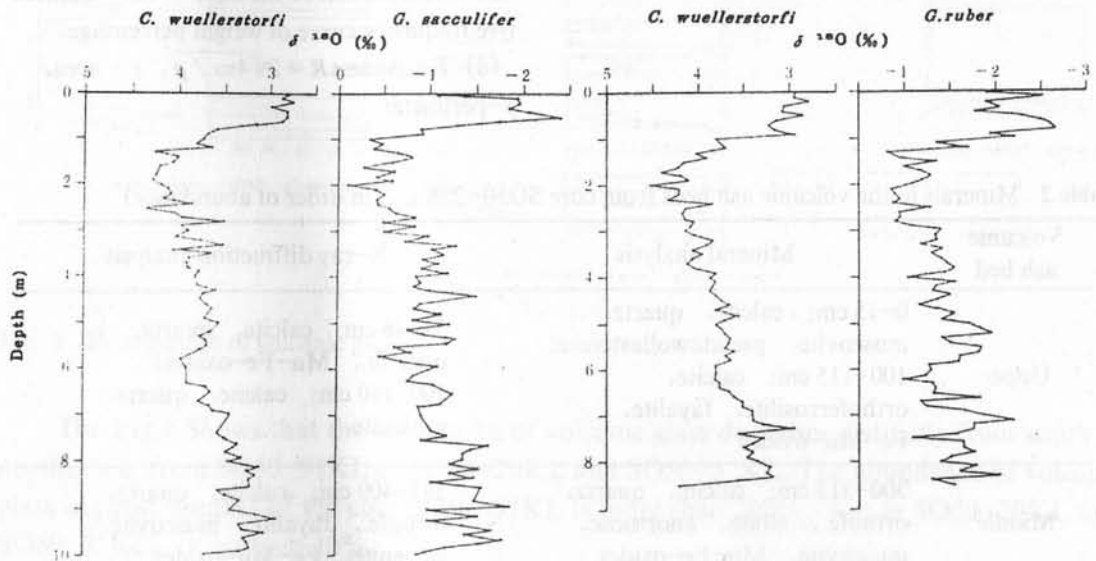


Fig.4 Oxygen isotope curves of the cores SO50-29KL (Left) and SO50-37KL (Right).

The lower volcanic ash bed is characterized by the increase of achromatic "plate" glass. Its top boundary ages are 64 Ka in SO50-37KL and 61.1 Ka in SO50-29KL, respectively.

All of the volcanic ash beds are the good index beds for a stratigraphic correlation in northern South China Sea. Especially, the middle volcanic ash bed is a very ideal index bed, because it possesses very high abundance of volcanic glass, clear top and bottom boundary as well as exact ages. A comparison of the depth of the volcanic ash beds to the curves of oxygen isotope in the cores SO 50-37KL and SO 50-29KL shows that the volcanic ash beds located in the warm stages of the oxygen isotope curves, and the upper, middle and lower volcanic ash beds correspond to the stage 1, 3 and 5, respectively. The top boundary of the middle volcanic ash bed accords with the top boundary of the stage 3 of the oxygen isotope curves, and the top boundary of the lower volcanic ash bed is similar to the top boundary of the stage 5 in the above two cores.

SURFACE TEXTURES OF QUARTZ GRAINS IN CORES KL37 AND KL29 FROM THE SOUTH CHINA SEA AND ITS SIGNIFICANCE OF SEDIMENTOLOGY

HE LIANGBIAO

First Institute of Oceanography, SOA, Qingdao, China

ABSTRACT

Quartz in the cores KL37 and KL29 are characterized by lower content, finer grain size (70–300 μ), lower value of roundness (<0.7), and subangular outlines, well-developed chemical features and common mechanical features, so that the area is a tropic and subtropic environment of deposition with low–middle energy and polysource of sediments since Middle Pleistocene.

INTRODUCTION

Shapes and surface textures of quartz grains can be analysed with semi-quantitative method owing to the following facts. (1) Quartz grains occur widely in marine sediments because they are separated from the rocks weathered mechanically and chemically and carried into sea by river, wind, glacier and others. (2) Quartz grains are so hardy broken that their surfaces preserve their messages in the transportational and depositional process. (3) Scanning electron microscope with high resolution can be used to observe the surface features of quartz grains accurately.

Cores KL37 and KL29 analysed in the paper were sampled from the South China Sea during cruise 50 of R/V Sonne, 1987. The purpose of the paper is to provide the informations in the depositional environment and its change around the cores since Middle Pleistocene. The locations and lithology of KL37 and KL29 are shown in Table 1.

Table 1 Locations and lithology of KL37 and KL29

Core	Location	Depth of water (m)	Lithology
KL37	18° 55'N, 115° 46'E	2695	Muddy silt and silty mud foraminifera and ash
KL29	18° 26'N, 115° 59'E	3766	Muddy silt and silty mud, foraminifera and ash at its upper

METHODS

Sample Preparation

About 20 g of each sample was disaggregated by appropriate mechanical and chemical

techniques and wet-sieved to isolate coarse silt fraction (0.032–0.063 m). One split of the coarse silt fraction was bathed in dilute HCl or HF for 3–10 min in order to etch or dissolve nonquartzose detritus. The split was finally dried.

15 quartz grains in the dried sample were selected with a binocular microscope and observed under a scanning electron microscope.

Analysis of Shape of Quartz Grains

Analysis of shape of quartz grains is a kind of classification of their closed form through the Fourier series. 200 quartz grains in each sample were selected, and they were divided into 23 standard shape components (harmonics 2 through 24) by a standard closed form with evenly spaced nodes at which the harmonic number is. Finally the relative contribution (amplitude) of each harmonic is calculated. This method is of effect on the study of sediment sources because the grain shape and distribution in sediments vary with sediment sources. However, this method costs in time and effort for selection and statistics of a large number of samples, and it needs a lot of samples. For these the method was not adopted in the paper.

A comparative method of Rittenhouse's sphericity and Krumbein's roundness was adopted in the paper. But this method has a lower accuracy. Fig.1 (Table 2) shows the spectra of sphericity of quartz grains and Fig.2 (Table 3) shows the roundness of quartz grains.

Table 2 S-sphericity values of quartz grains

Code	S	Code	S	Code	S
1	0.45	10	0.63	19	0.81
2	0.47	11	0.65	20	0.83
3	0.49	12	0.67	21	0.85
4	0.51	13	0.69	22	0.87
5	0.53	14	0.71	23	0.89
6	0.55	15	0.73	24	0.91
7	0.57	16	0.75	25	0.93
8	0.59	17	0.77	26	0.95
9	0.61	18	0.79	27	0.97

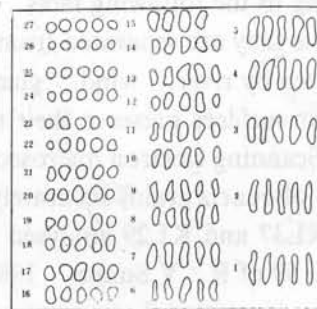


Fig.1 Rittenhouse's sphericity of quartz grains.

Table 3 Roundness

Code	Roundness values
1	0.1
2	0.2
3	0.3
4	0.4
5	0.5
6	0.6
7	0.7
8	0.8
9	0.9

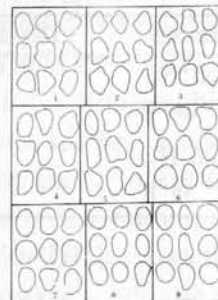


Fig.2 Krumbein's roundness of quartz grains.

Analysis of Surface Texture of Quartz Grains

15 grains were mounted on an aluminium plug coated with gold-palladium alloy, and examined under a scanning electron microscope and photographed for surface textures of quartz grain.

(1) The surface textures of quartz grains were divided into 2 classes and 15 species (Table 4). The surface textures in 15 grains of each sample were sorted out.

Table 4 Surface textures of quartz grains

Class	Species	Code
Mechanical features	Mechanical V-shaped	1
	Mechanical pits	2
	Conchoidal fractures	3
	Upturned plates	4
	Dish shaped concavities	5
	Straight and curved grooves	6
	Meandering ridges	7
Chemical features	Etched V-shaped (oriented)	8
	Solution crevasses	9
	Solution precipitation	10
	Solution etching	11
	Adhering particles	12
	Flaking and scaling	13
	Surface cracks	14
	Smooth precipitation surface	15

(2) Percentage of each surface texture of quartz grains in each sample was calculated.

(3) The sediment environments were interpreted based on the association of surface textures of quartz grains.

The association of surface textures of quartz grains in some of common marine environments is shown in Fig.3.

SURFACE TEXTURES AND SHAPES OF QUARTZ GRAINS IN KL37 AND KL29

Core KL37

The core was divided into 5 strata based on the stratigraphic data. Characteristics of shape and surface texture of quartz grains in each stratum are as follows.

Stratum I, 8.63–6.85 m. Quartz grains have size of 80–350 μ , sphericity of 0.53–0.71, roundness of 0.3–0.5. The surface of quartz grains exhibits well-developed mechanical pits, conchoidal fractures and upturned plates (Plate IV, c). Solution crevasses and solution precipitation can also be found, particularly in the lowest part (Plate IV, d).

Stratum II, 6.85–5.81 m. Quartz grains mostly have size of 100–160 μ , sphericity of 0.75–0.89, and roundness of 0.5–0.7. Two classes of quartz grains were all found. One class shows well-developed mechanical features, meandering ridges, straight and curved

grooves (Plate IV, b). The other shows well-developed chemical features, solution crevasses (Plate IV, a).

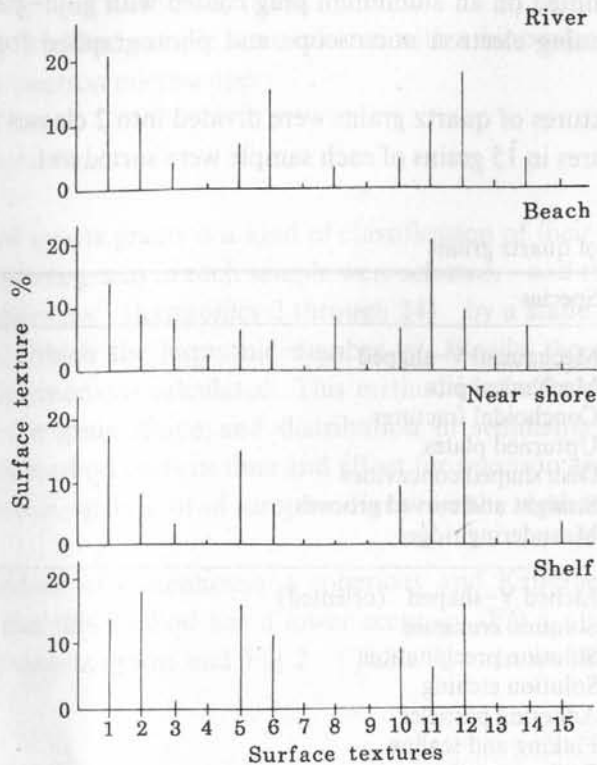


Fig.3 The association of surface textures of quartz grains in different marine environments.

Stratum III, 5.81–3.21 m. Quartz grains have size of 70–100 μ , sphericity of 0.75–0.93 and roundness of 0.6. The surface textures of meandering ridges, mechanical pits, solution crevasses and solution precipitation are well developed (Plate III, d).

Stratum IV, 3.21–1.70 m. Quartz grains have smaller size of about 90 μ , sphericity of 0.69–0.83 and roundness of 0.5–0.7. Curved grooves, conchoidal fractures, solution crevasses and solution precipitation were found on their surface (Plate III, c).

Stratum V, 1.7–0.0 m. Size of quartz grains changes from 70 μ to 900 μ . Smaller quartz grains with sphericity of 0.75 and roundness of 0.5 occur in the layer of 1.70–1.00 m, and larger quartz grains with sphericity of 0.81–0.93 and roundness of 0.7–0.8 occur in the layer of 1.00–0.0 m. In the former chemical feature is well developed and in the latter mechanical feature is well developed (Plate III, a and b).

Additionally, the content of quartz varies with different stratum and the content in stratum I, III and V is more than that in stratum II and IV.

Core KL29

The core was divided into 5 strata, too. The shapes and surface textures of quartz in each stratum are as follows.

Stratum I, 10.23–7.21 m. Size of quartz grains is commonly 270 μ . Their sphericity is 0.65–0.79 and their roundness is 0.5–0.7. The surface textures of quartz grains are character-

ized by well-developed mechanical features such as mechanical spits, conchoidal fractures, straight and curved grooves, and meandering ridges (Plate II, d). The surface textures of chemical feature can also be found in the stratum (Plate II, c and d).

Stratum II, 7.21–5.16 m. Quartz grains have size of $80\ \mu$ with sphericity of 0.75 and roundness of 0.5. Their surface textures are characterized by solution crevasses, solution precipitation and adhering particles of chemical features, and meandering ridges of mechanical features (Plate II, b).

Stratum III, 5.16–2.81 m. Quartz grains have size of about $90\ \mu$ with sphericity of 0.75–0.81 and roundness of 0.5–0.6. The surface textures of quartz grains are meandering ridges, curved grooves, conchoidal fractures and mechanical pits of mechanical features, and solution crevasses, solution precipitation and adhering particles of chemical features (Plate II, a), and generally mechanical features are well developed.

Stratum IV, 2.81–0.84 m. Quartz grains with size of $100\text{--}200\ \mu$, sphericity of 0.75–0.85 and roundness of 0.5–0.7 are mostly characterized by the surface textures of chemical feature such as solution crevasses and etched V-shaped, and minorly by those of mechanical features such as meandering ridges, straight and curved grooves and mechanical pits (Plate I, c).

Stratum V, 0.84–0.0 m. The stratum can be partitioned into two layers. The lower layer is characterized by such quartz grains with size of about $300\ \mu$, sphericity of 0.75 and roundness of 0.6, and well-developed mechanical surface textures such as curved grooves, conchoidal fractures and meandering ridges (Plate I, b). The upper layer is characterized by such quartz grains with size of $100\ \mu$, sphericity of 0.85–0.93 and roundness of 0.7, and well-developed chemical surface features such as solution crevasses and solution precipitation (Plate I, a). Meandering ridges of mechanical features occur in the upper layer, too.

The content of quartz in stratum I and V is the highest, and that in stratum III and IV is next and that in stratum II is the lowest.

The characteristics and change of shapes and surface textures of quartz grains in cores KL37 and KL29 are shown in Fig.4.

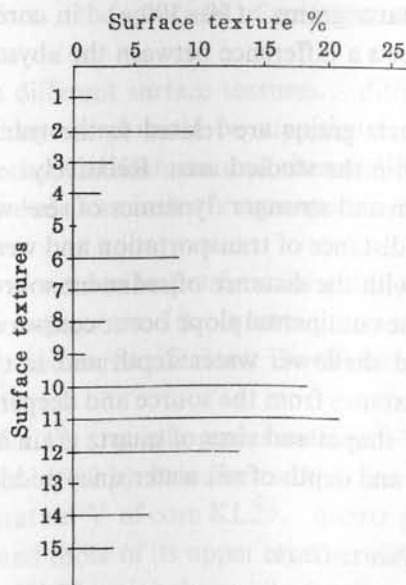


Fig.4 Change of shapes and surface textures of quartz grains in cores KL37 and KL29.

DISCUSSION

Cores KL37 and KL29 were sampled from the north continental slope edge with water depth of 2695 m and the abyssal plain with water depth of 3766 m. The cores consist of grey muddy silt and silty mud rich in foraminifera and ash, so that they are bathyal sediments with polysources consisting of mainly terrigenous material.

Selection of quartz grains from the samples is difficult because sediments in the cores consist of about 50% clays, 50% fine silt and few fractions of 0.063 mm. Therefore, though the fractions of 0.032 mm in the samples were used, few samples were satisfactory to our demand (select 15 quartz grains in each sample). It is an important character for the sediments in the cores that the content of quartz is less and the grain size of quartz is finer (about 70–300 μ), and this character is controlled by the geological occurrences of the cores. However, the shapes, sizes and surface textures of quartz grains in the cores vary with different layers (Fig.4). The details of the cores are described as follows.

Change of Shapes of Quartz Grains

As it is seen from Fig. 4, the quartz grains in stratum I of KL37 have size of 80–300 μ , roundness of 0.3–0.5 and subangular outlines; those in stratum II have size of 100–160 μ , roundness of 0.5–0.7 and rounded outlines; those in stratum III have size of 70–100 μ ; those in stratum IV are 900 μ with rounded outlines and roundness of 0.6. Stratum V was divided into two layers and the lower one containing 70 μ quartz grains with rounded or subangular outlines and the upper one containing 900 μ quartz grains with roundness of 0.8 and rounded outlines (Plate III, a and b).

Core KL29 is similar to core KL37 in the change law of shapes of quartz grains, but in its stratum V the lower layer contains coarser quartz grains (300 μ) with roundness of 0.7 and the upper layer contains finer quartz grains (100 μ) with roundness of 0.5–0.6. Additionally, the fact that quartz grains (80–300 μ) in core KL29 are finer than those (70–900 μ) in core KL37 reflects a difference between the abyssal plain and the continental slope (Plate I and III).

Generally, shapes of quartz grains are related to the transport distance of sediments and the dynamics of sea–water in the studied area. Relatively, rounded grains result from longer distance of transportation and stronger dynamics of sea–water. On the contrary, angular grains result from shorter distance of transportation and weaker dynamics of sea–water. The grain size of quartz varies with the distance of sediment source and the depth of water in depositional area, so that in the continental slope occur coarser quartz grains owing to nearer distance from the source and shallower water depth and in the abyssal plain occur finer quartz grains owing to longer distance from the source and deeper water depth.

Therefore, the changes of shapes and sizes of quartz grain in cores KL37 and KL29 implicate the changes of dynamics and depth of sea water since middle Pleistocene in the area.

Change of Surface Textures of Quartz Grain

Core KL37 was taken as example. In stratum I the quartz grains with well–developed

mechanical features were more than those with well-developed chemical features; in stratum II the quartz grains with chemical features were more than those with mechanical features; in stratum III the quartz grains with mechanical features were as many as those with chemical features; in stratum IV the quartz grains with chemical features were more than those with mechanical features; in stratum V the quartz grains of its lower layer have well-developed chemical features and those of its upper layer have well-developed mechanical features (Plate III, a and b).

The change law of surface textures of quartz grains in core KL29 is nearly similar to that in KL37, except for its stratum V. The lower layer of stratum V contains quartz grains with well-developed mechanical features and the upper layer contains quartz grains with well-developed chemical features (Plate I, a and b).

Surface textures of quartz grains are controlled by sources of sediments, dynamics of sea water and geochemical environments of deposition in the studied area. The mechanical features are related to stronger dynamics of sea water, and the chemical features are related to weaker dynamics of sea water and environments with higher temperature and salinity. The changes of surface textures of quartz grains in cores KL37 and KL29 should indicate that depositional dynamics and geochemical environments in the studied area have changed during their depositional process.

1) The dynamics of water in the area has undergone the changes of stronger-weaker-stronger-weaker-stronger since middle Pleistocene. Stratum I, III, V in cores KL37 and KL29 is rich in volcanic ash and stratum II, IV is poor in ash, so that the content change of volcanic ash in the cores shows a law of rich-poor-rich-poor-rich through stratum I-V, and the change of the dynamics of water in the area could be influenced by oceanic volcanic activity.

2) Compared with shallow water area, the surface textures of quartz grains in the area are characterized by well-developed chemical features (Fig. 3 and 4). It is consistent with a lower-energy, bathyal, tropical and subtropical (higher temperature), and higher salinity environment. Therefore, the spectrum of surface textures of quartz in a bathyal area could be set up (Fig.5).

3) Quartz grains with different surface textures, different shapes and different sizes could be found in the same layer and could be supposed to come from polysource of sediments in the area. Both mechanical features and chemical features are found on the same quartz grain and can be regarded as a result of retransportation and redeposition of sediments in the area.

There are two problems to need to be put forward as follows.

In the bottom of the cores (stratum I), quartz grains with lower roundness (0.3-0.5), have varieties of shape, size and surface feature. Do these result from turbidity current? Is stratum I a turbidite?

In stratum V of core KL37, quartz grains with well-developed mechanical features and rounded outline are large (900 μ). It indicates there is a stronger dynamics of sea water in the area recently. But in stratum V of core KL29, quartz grains of its lower layer are similar to those in core KL37, and those of its upper layer are different from those in core KL37. That is, stratum V of core KL29 mainly has well-developed chemical features. Could core KL37 be incomplete in the upper Holocene?

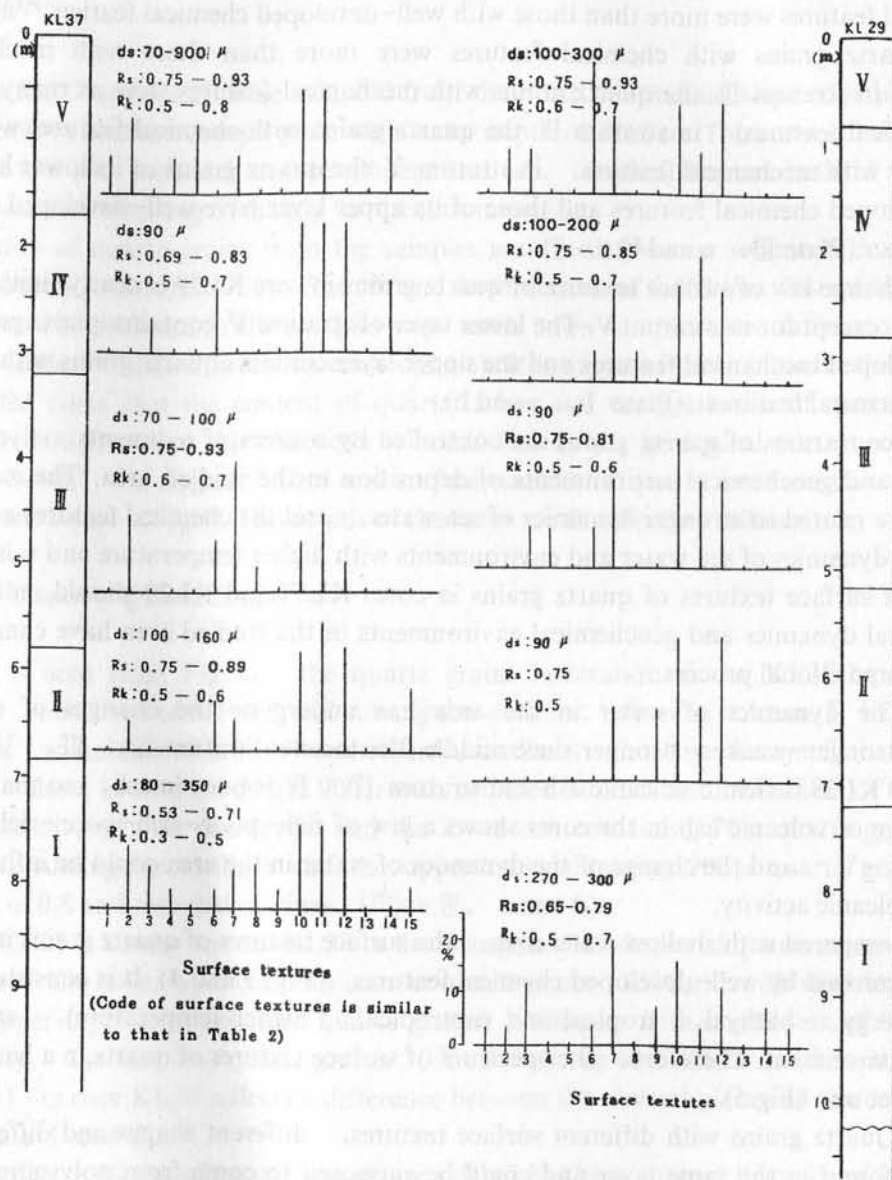


Fig.5 The spectrum of surface textures of quartz grains in a bathyal area.

CONCLUSIONS

Based on analysis of shapes and surface textures of quartz grains in cores KL37 and KL29, we come to following conclusions of the sediment environments and their changes on the abyssal plain and the continental slope in the middle South China Sea since middle Pleistocene.

1) Content of quartz grains in sediments is lower, and quartz grains ($>0.063 \text{ mm}$) in each fresh sample weighing 20 g are less than 15 or nothing. Sizes of quartz grain are mostly less than 200μ , and in a few layers are more than 300μ . Roundness of quartz with subangular outline is less than 0.7. All these indicate a sediment environment with a low-middle energy, bathyal sea in the area.

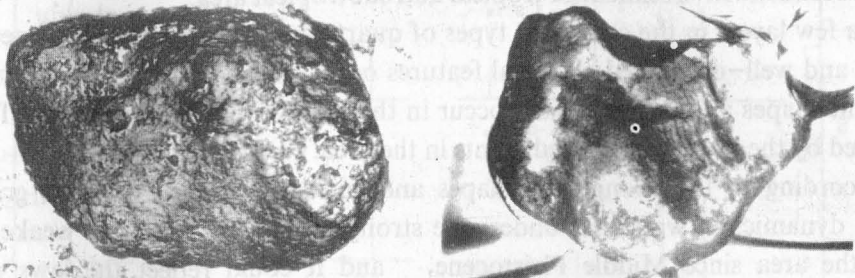
2) Surface textures of quartz grains are characterized by well-developed chemical features, such as very common and typical solution crevasses and solution precipitation, related with a sediment environment of tropical and subtropical area.

3) In a few layers in the cores two types of quartz grains with well-developed mechanical features and well-developed chemical features occur simultaneously, and quartz grains with different shapes and different sizes occur in the same layer simultaneously. These could be interpreted by the polysource of sediments in the area.

4) According to the changes of shapes and surface textures of quartz grains in the cores, the dynamics of water has undergone stronger-weaker-stronger-weaker-stronger change in the area since Middle Pleistocene, and it could reflect the laws of tectonic movement and volcanic activity in the bottom of the area.

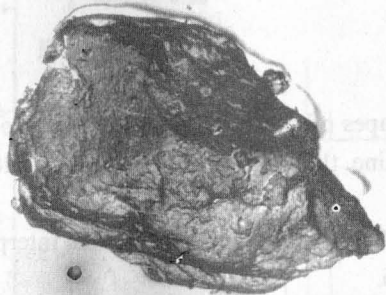
REFERENCES

- Haines, J. and J. Mazzullo, 1988: The original shapes of quartz silt grains: A test of validity of the use of quartz grain shape analysis to determine the sources of terrigenous silt in marine sedimentary deposits. *Mar. Geol.*, 78, 227-240.
- Frihy, O.E. and D.J. Stanley, 1987: Quartz grain surface textures and depositional interpretations, Nile Delta region. *Egypt. Mar. Geol.*, 77, 247-255.

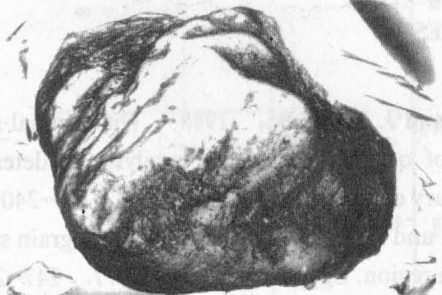


A 1 8.0KV 10MM 15.086

B

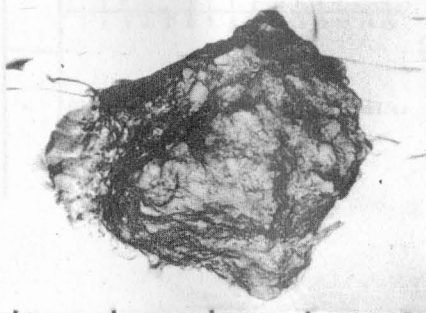


C 1 8.0KV 30MM 16.091

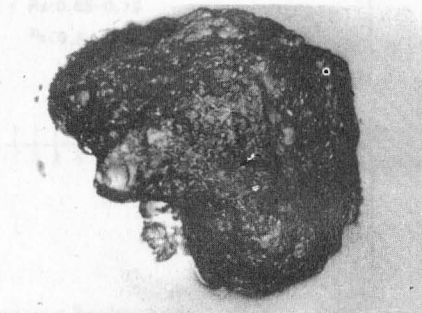


D 1 8.0KV 30MM 02.003

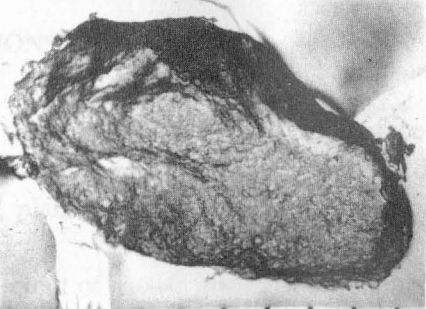
Plate I



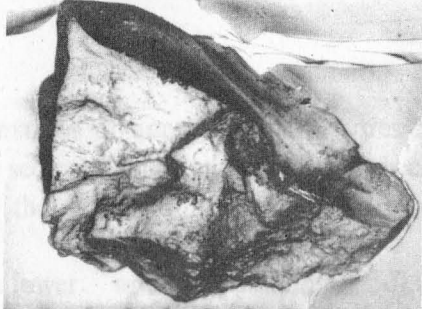
A 1 8.0KV 30MM 03.008



B 1 8.0KV 30MM 18.103



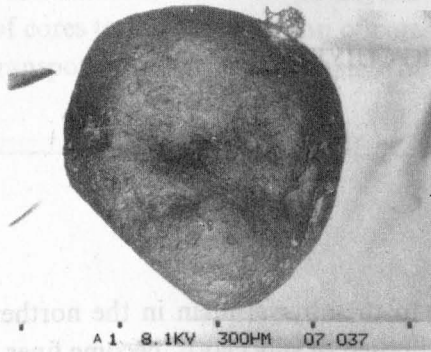
C 1 8.0KV 30MM 04.019



D 1 8.0KV 30MM 05.024

Plate I

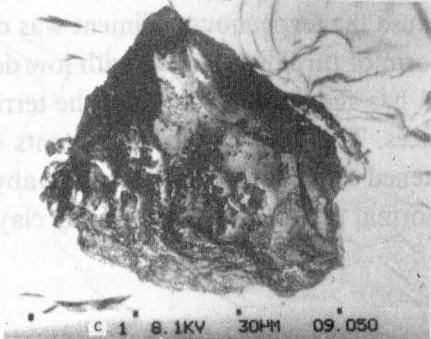
DEPOSITION PROCESS AND CHARACTER OF THE DEEP WATER SEDIMENT IN THE NORTHERN SOUTH CHINA SEA



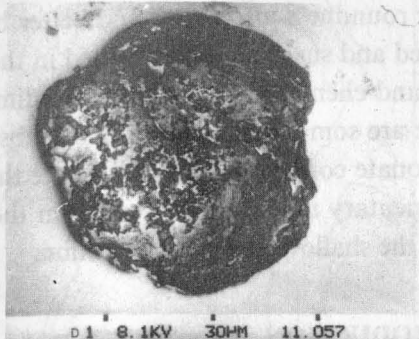
A 1 8.1KV 300µM 07.037



B 1 8.1KV 10µM 07.040



C 1 8.1KV 30µM 09.050



D 1 8.1KV 30µM 11.057

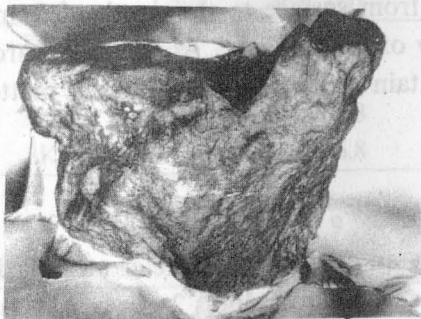
Plate II



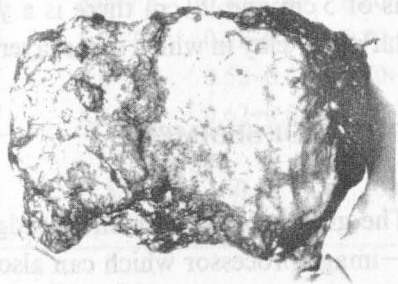
A 1 8.1KV 30µM 12.062



B 1 8.1KV 30µM 12.064



C 1 8.1KV 100µM 13.075



D 1 8.1KV 30µM 13.079

Plate III

relationship between grain size and bed thickness (Table I). The grain of sediment which is fine and less varied (average grain size: 6-9 φ, Md=6-8 φ) seem nearly to be silt. In which some samples are calcareous ooze. The distribution curve of grain size of soft

DEPOSITION PROCESS AND CHARACTER OF THE DEEP- WATER SEDIMENT IN THE NORTHERN SOUTH CHINA SEA

ZHOU FUGEN, YUN ZHIQIANG, FENG CUIYING & GUO LIQUN

Tongji University, Shanghai, China

ABSTRACT

From the continental slope and rise to the abyssal plain in the northern South China Sea, grains of the sediment (mainly composed of silty clay) become finer and finer, and their roundness also better and better because the terrigenous sediment was diffusively transported and suspendedly deposited in the form of turbidity current with low density. The mineral and chemical composition of sediment has shown that, besides the terrigenous matter, there are some biotic and volcanic substances. The clay and tephra contents increase and the carbonate content decreases with the thickened sediment layer toward the abyssal plain. This sedimentary model is different from the normal sedimentary one of silty clay and carbonate with the shallow-deep sea transition.

INTRODUCTION

In cruise 50 of R/V Sonne, both Chinese and German scientists have obtained four cores (Fig.1), 29KL (length: 990 cm, water depth: 3766 m) on the abyssal plain, 37KL (830 cm, 2695 m) on the continental rise, 33KG (33 cm, 3240 m) on the basin edge and 8KL (993 cm, 1040 m) on the upper continental slope off the Zhujiang River Mouth. We have analysed grain size and mineral, chemical composition of sediments in these four cores, and discussed sediment characteristics, sedimentary processes and settings in the northern South China Sea. The surface sediments around 29KL, 33KG and 37KL are composed of foram-radiolarian silty clay, and the surface sediments around 8KL of foram silty clay (Luo *et al.*, 1985). In our cores there is no clear bedding construction and biotic trace. The floating mud exists from surface to the depth of 5 cm. Between the depths of 5 cm and 20 cm there is a yellow oxidation layer. Again downwards there is grey and dark grey clay in which some layers contain higher content of organic matter.

GRAIN SIZE OF SEDIMENT

The grain size of sediment is judged by an equivalent diameter measured by the microscope-image processor which can also measure the roundness $2\sqrt{4\pi s/p}$, (s — area, p — perimeter). The measured result can reduce the disturbance of thin piece of mineral to the relationship between grain size and hydrodynamics (Table 1). The grains of sediment which are fine and less varied (average grain size: 6–9 ϕ , $Md = 6-8 \phi$) seem nearly to be silty clay in which some samples are calcareous ooze. The distribution curve of grain size of sedi-

ment is a positive deviation with a single peak. The probability curves consisting of two sections of straight line (Fig.2a, b) are arranged in order of water depth. The angle between these two lines is increased both from the abyssal plain to the continental slope and from the lower section of cores to the upper section of cores. The sediments of four cores belong to the same kind of transportation-deposition system of turbidity current with low density.

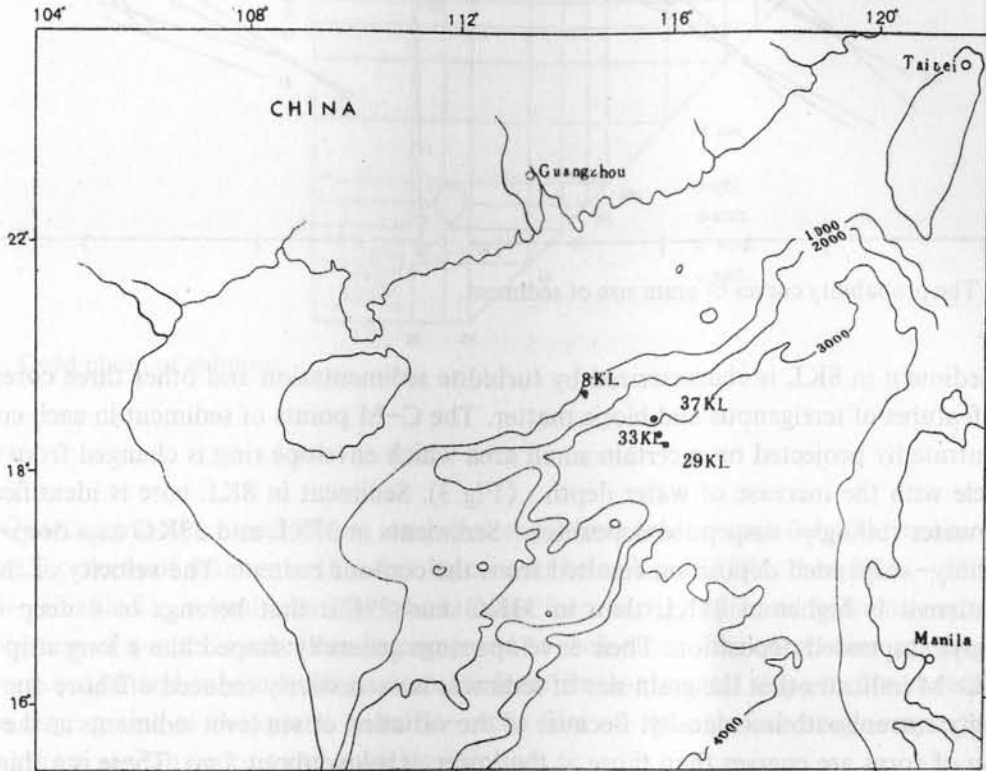


Fig.1 The map of sampled station.

Table 1 Grain size of deep-water sediment

Sediment name	Core	Sample No.	Mean size (ϕ)	Md (ϕ)	Mean size (wt%)	Roundness	
						6 ϕ	9 ϕ
Mud	29KL	22	8.0-8.5	7-8	6.0-7.6	0.46-0.67	0.80-0.84
	33KG	14	8.0-8.5	7-8	6.0-7.6	0.55-0.68	0.79-0.83
	37KL	23	6.0-6.8	6-7	4.8-6.5	0.52-0.68	0.70-0.82
	8KL	25	6.0-6.8	6-7	4.5-6.0	0.62-0.68	0.70-0.80
Volcanic ash	29KL	1	7.9	5.6	5.2	0.49	0.64
Suspended matter	29-33-37	9	8.0-9.0	7-8	7.4-7.6	0.65-0.68	0.80-0.84

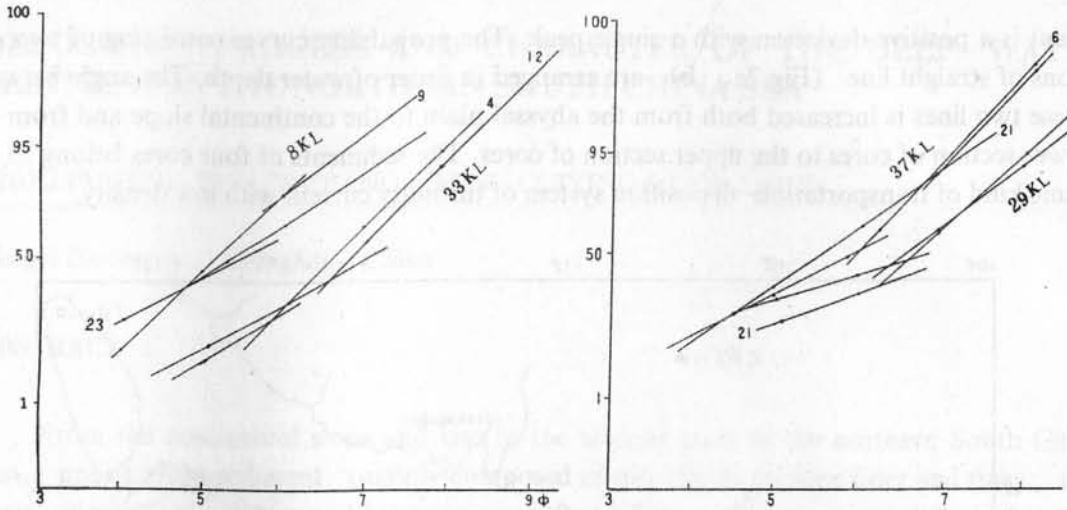


Fig.2 The probability curves of grain size of sediment.

Sediment in 8KL is characterized by turbidite sedimentation and other three cores have grain features of terrigenous and biotic matter. The C-M points of sediment in each core are concentratedly projected on a certain small area which envelope ring is changed from ellipse to circle with the increase of water depth (Fig. 3). Sediment in 8KL core is identified as a deep-water rollingly-suspended deposition. Sediments in 37KL and 33KL as a deep-water uniformly-suspended deposition resulted from the contour current. The velocity of the contour current is higher in 37KL than in 33KL and 29KL that belongs to a deep-water stillingly-suspended deposition. Their envelope rings generally shaped like a long strip parallel to C-M indicates that the grain size of sediment is successively reduced offshore due to the turbidity current with low density. Because of the variation of sea level sediments at the upper section of cores are coarser than those at the lower (below about 5 m). There is a thin layer of volcanic ash at 3.3 m in 29KL which grains are coarser than those of other sediments. The roundness of sediments becomes better with the fineness of grains on $R = 0.70-0.84$ (9ϕ), but otherwise on $R = 0.46-0.68$ (6ϕ). The sediments are basically subround while the volcanic ash is subhorned.

Sediments in these four cores are mainly composed of biotic bodies and fragments, terrigenous debris, volcanic ash, clay mineral and Fe-Mn oxide. Forams, volcanic glass, Fe-Mn oxide and few quartz grains are coarse while clay and coccolith are fine.

MINERAL COMPOSITION

The complicated compositions of mineral are mainly calcite, quartz, clay, a little plagioclase, albite (high temperature), anorthite, muscovite orthoferrosilite, haptite, fayalite, forsterite, tschermakite, pyrochroite, natrophosphate, jacobsonite etc. and are indicated by the X-ray diffractogram. Basic minerals in the upper are more than those in the lower, but light-colored minerals are on the contrary.

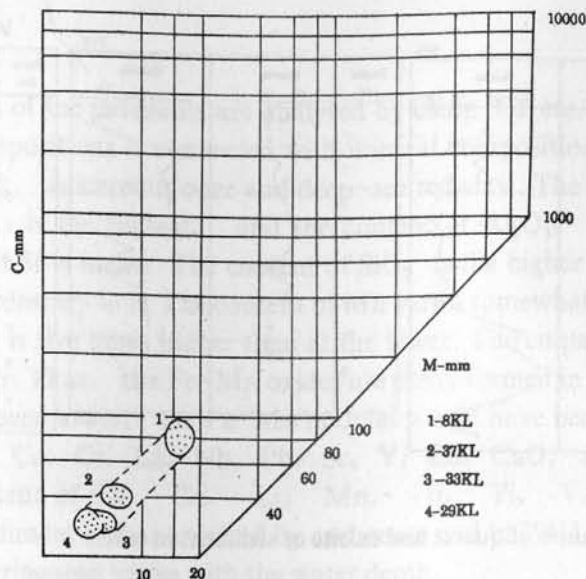


Fig.3 C-M photo of sediment.

Quartz

Quartz grains are usually fine, and even some sizes are less than 2μ . Quartz amounts to about 20 percent of sediment (Fig.4a). Its content being less in 37KL than 8KL, 33KG and 29KL (Table 2) reveals that the quartz came from terrigenous and volcanic matter. The distribution of quartz in cores can be compared to each other. The correlation of distribution between quartz and calcite tends to decrease from the continental slope to the abyssal plain. Some large grains of the quartz have Fe-oxide film on their surface or gloomy edge, resulting from atolian deposit and volcanic eruption.

Table 2 Average content of quartz and calcite of sediment in cores (%)

Core	Quartz	Calcite	Highmagnesian
8KL (25)	23.37	24.36	2.90
37KL (23)	16.19	22.90	1.34
(33KG) (14)	(19.11)	(20.67)	(0.53)
29KL (22)	19.33	7.38	0.82

Carbonate is mainly composed of low-magnesian calcite and little high-magnesian calcite ($< 3\%$, Table 2) which are a kind of calcite containing different content of $MgCO_3$. The average content of calcite in cores are reduced (24.36–7.58 %, Table 2) from the upper slope to the abyssal plain. The calcite basically consists of foram and coccolith (Fig.4a), and its content is higher about at 1 m, 5 m and 8 m layers in cores and coincident with the changing tendency of $\delta^{18}O$ of foram (Fig. 4b). The pulsation of terrigenous supplies, thus, shows that CCD is located at the depth of 3500 m. The average rate of deposition in 8KL, 37KL and 29KL is 5.57 cm/ka, 7.68 cm/ka and 9.62 cm/ka, respectively, that is, the depositional rate and thickness increase from the continental slope to the abyssal plain.

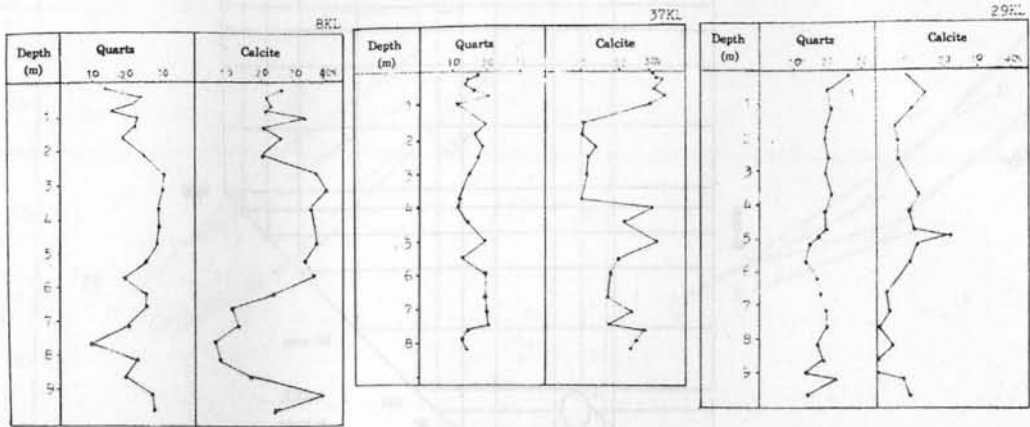


Fig.4 The distribution of quartz and calcite of sediment in cores.

Volcanic Ash

There is a thin layer of volcanic ash at 3.3 m in 29KL, but in other cores volcanic ash is scattered only at 1 m, 4 m and 8 m (Fig.4c). In 29KL the white and grey volcanic ash is mainly composed of volcanic glass, with a little albite (high temperature), plagioclase, anorthite, quartz etc.. In 8KL, 37KL and 33KG there is mainly brown volcanic glass at the upper and white volcanic glass at the lower, with a little olivine, pyroxene, amphibole, quartz, feldspar, mica etc..

The volcanic ejecta may be originated from the Taiwan Island and the Philippine Islands. According to the distribution of carbonate and the $\delta^{18}O$ curve, the volcanic ejecta not only affected the transportation and deposition of terrigenous matter, but also affected the reproductivity and deposition of biotic matter.

Clay Mineral

Grains of size less than 2μ occupy about 30% of sediments in the studied cores. Besides clay mineral, there are quartz, carbonate (mainly coccolith) and organism. In order of their relative percents, the clay mineral consists of illite, chlorite, smectite and kaolinite. With the increase of water depth in each core, there is much illite but less chlorite. The contents of smectite and kaolinite are the highest in 37KL (Table 3). From the continental shelf to the abyssal plain the content of illite increases a little, and the content of smectite increases little; kaolinite decreases a little and chlorite doesn't change obviously. The distribution change of clay mineral shows that the contents of illite and smectite change less than that of chlorite and kaolinite. Smectite is mainly 21.5 nm crystalline grain, and montmorillonite (17.5 nm grain, treated by ethylene glycol) is less, and is usually mixed with chlorite and doesn't change into illite obviously. The change of contents of clay minerals is concerned with composition, transporting distance and depositional rate of terrigenous matter.

CHEMICAL COMPOSITION

Chemical compositions of the sediments are analysed by using ICP etc. (Table 4). The complexity of chemical compositions is connected with mineral compositions which are different from normal mudrock, calcareous ooze and deep-sea red clay. The content of SiO_2 (containing biotic silicon) is the highest, and the content of Al_2O_3 , CaO , K_2O , MgO , Fe_2O_3 , Ti , P and Sr is higher. The content of SiO_2 is the higher in 29KL than in 37KL, but Ca and Sr are contrary to it. The content of Mn varies somewhat great in the sediments, and at the surface is five times higher than at the lower. The content of Mn is also higher in the mesopore water. Thus, the Fe-Mn oxides are easily formed in the sediments. If the sedimentation rate had been lower, the Fe-Mn nodules would have been easily formed. In 37KL the content of Ba , Ce , Cr , La , Nb , Pb , Sc , Y , Zn , CaO , and Al_2O_3 higher, but in 29KL the content of Cu , Ga , Li , Mn , Ni , Ti , V , Zr is higher. Therefore, in 37KL the sediment is characterized by carbonate and in 29KL by volcanic ash. The basic character to be terrigenous varies with the water depth.

Table 3 Average content of clay mineral in cores (in relative percent)

Station	Illite	Chlorite	Smectite	Kaolinite
8KL (25)	60.76	25.27	8.22	5.75
37KL (23)	60.78	15.63	15.47	8.12
(33KG) (14)	(61.02)	(19.96)	(14.53)	(4.17)
29KL (22)	61.62	18.54	14.06	5.78
Shelf	49.70	20.70	12.20	17.40

Table 4 The chemical composition of sediment in 37KL and 29KL

Station	Sample No.	The content of elements (%)							
		SiO_2	Al_2O_3	Fe_2O_3	CaO	MgO	Na_2O		
37KL	23	40.7	13.45	5.73	11.53	2.38	3.03		
29KL	23	51.53	12.58	5.87	4.44	2.88	2.45		
		(ppm)							
		Ba	Be	Ce	Co	Cr	Cu	Ga	La
		944	3	63	21	142	59	29	31
		736	2	53	20	110	61	34	24
		Li	Mn	Nb	Ni	P	Pb	Sc	Sr
		66	1756	12	59	501	80	15	453
		69	1809	11	63	487	49	13	215
		Th	Ti	V	Y	Yb	Zn	Zr	
		13	3327	120	19	4	640	78	
		14	3425	124	15	4	582	92	

CONCLUSIONS

To sum up, the grains of sediment of the four deep-water cores from the northern

South China Sea are somewhat fine and less varied, and belong to silty clay of which part has become calcareous ooze. The grain size of sediment becomes less and its roundness becomes better toward the deep sea. Probably due to the change of sea level, the grains of sediment in cores are bigger at the upper than at the lower. Both the probability curves and the C-M pictures reveal the change of suspended deposition of seaward diffusive matter: the rollingly-suspended deposition at 8KL on the upper slope, the uniformly-suspended deposition at 37KL and 33KG on the continental rise and the basin edge where the contour current existed, and the deep-water stillingly-suspended deposition at 29KL on the abyssal plain. The probability curves of the cores except 8KL are characterized by the terrigenous and biotic matter. Their envelope rings shaped like a long strip parallel to C-M can be attributed to the long-period sedimentation of the same transporting and depositional system (turbidity current with low density).

The mineral and chemical compositions of sediment are mainly calcite, quartz, clay and volcanic ash. The contents of quartz in 8KL, 29KL and 33KG are higher than that in 37KL. Clay mineral is mainly composed of illite, chlorite, smectite and kaolinite. Illite increases and chlorite decreases toward the deep-sea. The contents of smectite and kaolinite, basically similar to the distributional change of quartz, are higher in 37KL.

The content of kaolinite changes more obviously than other clay minerals in these four cores. Smectite is mainly 21.5 nm clay mineral, and less montmorillonite only mixed with chlorite doesn't change into illite. The clay mineral came from terrigenous matter and volcanic ejecta. Carbonate is mainly biotic sediment, that is, foram and coccolith. The mineral compounds of carbonate are mainly calcite and little high-magnesian calcite which are controlled obviously by CCD (about 3500 m of water depth). Judging from $\delta^{18}\text{O}$, the sedimentation rate increased (5.57–9.62 cm/ka) from the continental slope to the abyssal plain. The contents of clay and volcanic ash increase and the contents of terrigenous matter and carbonate (calcite) decrease with the thickening of sediment layer toward the abyssal plain.

REFERENCES

- Betzer., P.R. *et al.*, 1988: Long-range transport of giant mineral aerosol particles. *Nature*, 336 (8).
- Feng Wenks *et al.*, 1988: The geological environment of Late Quaternary in the northern South Chian Sea. Quandong Science and Technology Publishing House (in Chinese).
- Kenneth Pye, 1987: *Aeolian Dust and Dust Deposits*. Cambridge University Press.
- Li Gaogong, 1990: The composition and distribution of clay mineral of surface sediment in shallow China Sea. *Acta Oceanologica Sinica*, 12 (4) (in Chinese).
- Luo Youlang *et al.*, 1985: A preliminary study on the surface sediment types and their grain size characteristics of the northern part of the South China Sea. *Tropic Oceanology*, 4 (1) (in Chinese).
- Marine Department, Tongji University, 1989: *Introduction to Paleooceanography*. Tongji University Publishing House (in Chinese).
- Yang Yubao and Fan Shiqing, 1990: Approaching the origin of volcanic sediment of Late Quaternary in the South China Sea. *Tropic Oceanology*, 9 (1) (in Chinese).

HYDROCARBON GASES IN SURFACE SEDIMENTS OF THE SOUTH CHINA SEA

WOLFGANG BEHRENS* & RICHARD FABER**

Geobot. Ztg., 3033 Hannover 71, Germany

*Geobot. Ztg., 3033 Hannover 71, Germany
Federal Institute for Hydrogeology and Natural Resources, 30169eg 2, 3033 Hannover 71, Germany*

GEOCHEMISTRY, MINERALOGY AND PETROLEUM GEOLOGY

Gas-bearing South China Sea sediments contain in all gases of surface sediments methane and propane and small amounts of ethane and butane. These gases point to a bacterial origin of methane which is produced from the reduction of carbon dioxide. These gases are related to a recent "in situ" production of bacterial methane in high methane concentrations together with low sulfate concentrations. It was observed that a slight concentration decrease of methane in the sulfate zone with increasing sediment depth is accompanied by a decrease of the light carbon isotope of methane to point to a secondary oxidation of methane under anaerobic conditions. Although deep-diffusion of the methane is obviously mature, no thermogenic hydrocarbons were detected in the surface sediments. This might be due to the migration barrier of the hydrates.

On the continental shelf of the South China gas content of hydrocarbons methane to ethane, nitrogen composition and carbon isotope ratios of methane point to a thermogenic origin. Two groups of geotectonically different gases can be distinguished. Samples from the offshore regions of the shelf are likely to be related to source rocks of organic matter corresponding to the end of oil-window. The sediment of the two basins above a sedimentary sequence up the slope of the Xisha Trough contain gases which show a molecular composition and carbon ratios which are typical for light hydrocarbons generated from an organic matter of a lower maturation level. Maturities predicted from the hydrocarbon gases on the continental shelf correspond to the calculated maturity of the source rocks which exceeds the upper boundary of the organic-rich Oligocene sequence defined in other areas.

INTRODUCTION

The purpose of our geochemical investigations on surface sediments is to obtain information on the nature and origin of gaseous hydrocarbons absorbed in these sediments. From this information we try to estimate the hydrocarbon potential of the specific area. This type of sediment geochemistry for hydrocarbons has been applied by the DGR geochemistry group for more than 20 years. A data base of more than 30 case studies has been established from different continental shelves all around the world.

In the present study (see also (Fig. 1)) with different structural series we will compare Diding two cruises of the German vessel R/V "Albatros" (SO-49 and SO-19) in the South China Sea off Sabah (East Malaysia) and off South China in 1977 and 1978 period.

HYDROCARBON GASES IN SURFACE SEDIMENTS OF THE SOUTH CHINA SEA

ULRICH BERNER¹⁾ & ECKHARD FABER²⁾

1) *Gollstr. 12a, 3000 Hannover 71, Germany*

2) *Federal Institute for Geosciences and Natural Resources, Stilleweg 2, 3000 Hannover 51, Germany*

ABSTRACT

Offshore Sabah (East Malaysia) methane is the dominant component in all gases of the surface sediments. Ethane and propane are present only in small amounts. Gas ratios and isotopic composition point to a bacterial origin of methane which is produced from the reduction of carbon dioxide. These gases are related to a recent 'in situ' production of bacterial hydrocarbons as high methane concentrations coincide with low sulfate concentrations. It was also observed that a rapid concentration decrease of methane in the sulfate zone with decreasing sediment depth is accompanied by a decrease of the light carbon isotope of methane. This points to a secondary oxidation of methane under anaerobic conditions. Although deep sediments of the accretion are thermally mature, no thermogenic hydrocarbons were detected in the surface sediments. This might be due to the migration barrier of the hydrates.

On the continental shelf of the South China gases consist of hydrocarbons methane to butanes. Molecular composition and carbon isotope ratios of methane point to a thermogenic origin. Two groups of genetically different gases can be distinguished. Samples from the northern region of the shelf are likely to be related to source rocks of organic maturities corresponding to the end of oil-window. The sediments of the two locations above a sedimentary basin close to the slope of the Xisha Trough contain gases which show a molecular composition and isotope ratios which are typical for light hydrocarbons generated from an organic source of a lower maturation level. Maturities predicted from the hydrocarbon gases on the continental shelf correspond to the calculated maturities of the seismic reflector which stands for the upper boundary of the organic rich Oligocene sequence drilled in other areas.

INTRODUCTION

The purpose of our geochemical investigations on surface sediments is to obtain information on the nature and origin of gaseous hydrocarbons absorbed in these sediments. From this information we try to estimate the hydrocarbon potential of the specific area. This type of surface prospecting for hydrocarbons has been applied by the BGR geochemistry group for more than a decade. A data base of more than 30 case studies has been established from offshore and onshore surveys all around the world.

In the present study two areas (Fig.1) with different structural settings will be compared. During two cruises of the German vessel R.V. 'Sonne' (SO-49 and SO-58) in the South China Sea off Sabah (East Malaysia) and off South China in 1987 and 1988 piston

cores of surface sediments have been sampled for geochemical purposes.

On the outer accretionary zone offshore Sabah we tested the effect of hydrates on hydrocarbon migration. For this purpose sampling of sediments was carried out in an area where seismic profiles show bottom simulating reflectors (BSR) which trace the lower boundary of gas hydrates.

On the continental shelf of South China we intended to obtain information on the hydrocarbon potential of three rift basins which have been identified on the seismic record.

In our studies molecular composition, gas concentrations and stable isotope analysis, including both carbon and hydrogen measurements, are used to characterize light hydrocarbons in marine surface sediments.

GEOLOGICAL SETTING

Offshore Sabah

The Palawan Trough, the 2800 m deep depression bordering the western continental slope of Sabah, is underlain by subsided continental crust, which dips towards the east and disappears below the accretionary wedge forming the continental margin (Fig. 2). The seismic data indicate that the system of imbricate thrust-sheets forming the outer accretionary wedge, is still active and that the surface of the down-going continental plate forms a major detachment plane.

The morphology of the westernmost part of the accretion is characterized by a ridge and swale topography, which is created by deformation along imbricate thrust sheets.

Bottom simulating reflectors occur in the accretionary wedge at water depths between 1500 m and 2800 m. The reflectors which are only recognizable below the ridges (Fig. 2) range from 0.3 to 0.6 sec below the sea floor, corresponding to a subbottom depth of 300 to 600 m.

The BSR is a strong indication that ice-like structures of gas hydrates (for detailed information see Hedberg, 1980) occur in the subsurface (Hinz *et al.*, 1987). The bottom simulating reflectors indicate the lower boundary of the hydrate zone. The interface between hydrates and the free gas below provide a velocity contrast responsible for the BSR. After our calculations (based on heatflow and temperature measurements in this area) the upper boundary of the temperature and pressure field for hydrates reaches to the sea floor. Although, BSR's are only detectable below the ridges, hydrates can occur in the whole area of investigation. The large amounts of methane required for the formation of gas hydrates are normally provided through bacterial decay and thermal alteration of organic matter (Brooks *et al.*, 1986).

The coastal area of Sabah is known for its hydrocarbon occurrences, either oil or gas. Maturity calculations using the model of Houbolt and Wells (1980) in combination with the time independent maturity model of Price (1989) show that not only in the shelf area close to the coast mature sediments occur but also in the area where BSR's have been detected and also below the abyssal plain in front of the accretion.

Offshore Sabah

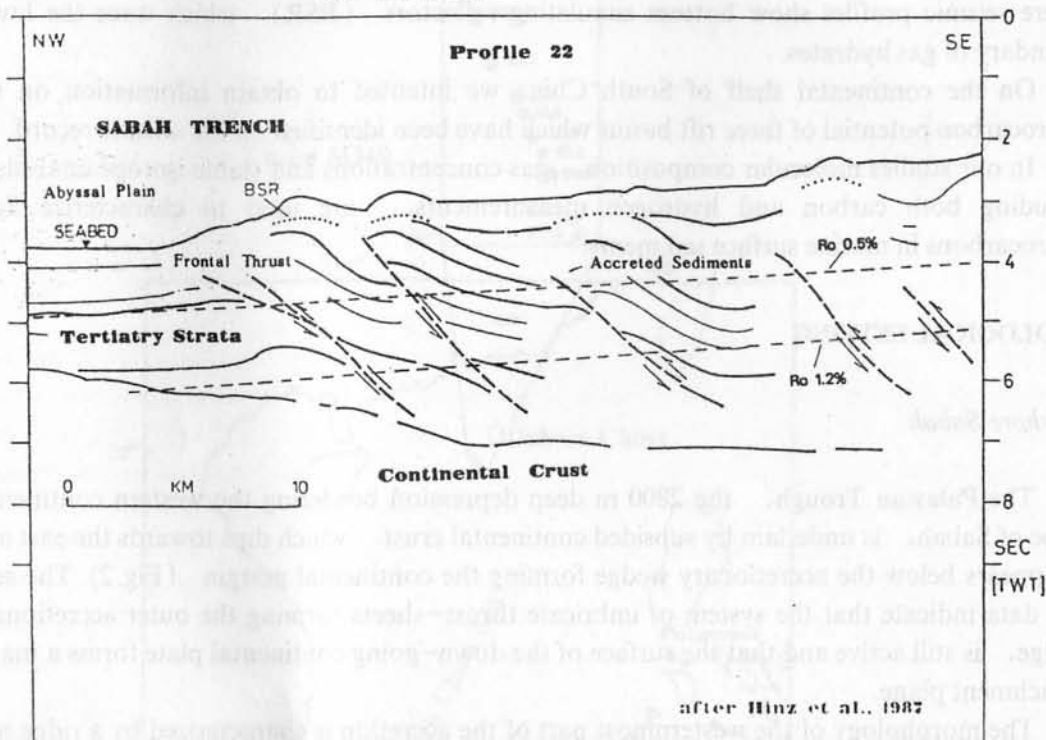


Fig.2 Interpreted seismic section offshore Sabah. Superimposed are calculated present-day maturities (vitrinite reflectance equivalent: R_0) of organic matter. Bottom simulating reflectors (BSR) occur below the ridges.

Offshore China

Distinctively planated basement blocks, split by a series of half-grabens, underlie the Chinese outer shelf and slope (Fig. 3). The sedimentary troughs have a characteristic V-shape configuration. The transition to the adjacent Xisha Trough is narrow and fault-controlled.

According to the seismic stratigraphy of Gaedicke (this volume) a seismic reflector T6 can be identified in all half-grabens on the Chinese shelf. The reflector T6 most likely represents the upper boundary of Oligocene sediments containing organic-rich source rocks of mostly terrestrial origin. These sediments have been drilled in adjacent areas.

A model of the vertical maturity distribution along the seismic profile is based on heatflow measurements in combination with the time independent maturity model of Price (1989). According to this model the presumed Oligocene source rocks are well within the mature zone of the "oil and gas window" (Fig.3).

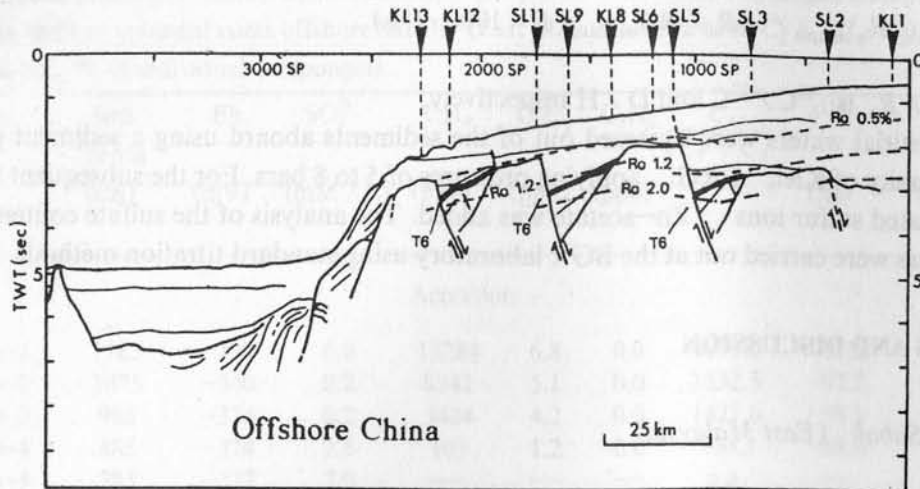


Fig.3 Interpreted seismic section offshore China. Superimposed are calculated present-day maturities (vitrinite reflectance equivalent: R_0) of organic matter. Reflector T6 marks most likely to the upper boundary of the Oligocene organic rich sequence.

METHODS

Cores of surface sediments have been sampled using piston corers. Up to five sediment samples of about 300 gr each were taken from each core.

The redox potential was measured 'in situ' using a calibrated Eh probe and is given in mV.

The samples were subsequently degassed on board in a blender apparatus by a vacuum-acid treatment described by Faber and Stahl (1983). Desorbed hydrocarbon gases for isotopic analysis at the BGR laboratory were expanded into glass bulbs. Gaschromatographic Flame-Ionization-detector (FID) analyses were carried out on board using a Packard 430 gaschromatograph provided with a 2 m long steel column filled with Porapak-Q. The gases were injected with a syringe of 1000 μl volume. For the calibration of the measurements a Matheson standard gas was used containing hydrocarbon components methane through pentane. Gas concentrations are given in ngr gas per gr wet sediment (ppb).

At the BGR laboratory a selection of gas samples from both areas was analysed for their carbon and hydrogen isotope ratios. The individual gas components were separated chromatographically and subsequently combusted to CO_2 and H_2O using the preparation line described by Dumke *et al.* (1989). The combustion product H_2O is reduced to H_2 by reaction with zinc in sealed glass tubes at 450°C.

The stable isotope measurements on the combustion product CO_2 were carried on a Finnigan MAT 250 mass spectrometer. For the D/H analysis a Finnigan Delta mass spectrometer was used. Isotope ratios are reported in the usual d-notation relative to the PDB (Pee Dee Belemnite) standard for carbon and SMOW (Standard Mean Ocean Water) standard for hydrogen:

$$dr = [(R_a / R_b)_{\text{sample}} / (R_a / R_b)_{\text{standard}} - 1] \times 1000 \quad (\text{‰})$$

where R_a / R_b is $^{13}\text{C} / ^{12}\text{C}$ and D / H respectively.

Interstitial waters were squeezed out of the sediments aboard using a sediment press of the University of Kiel, FRG, applying pressures of 5 to 8 bars. For the subsequent fixation of dissociated sulfur ions, Zn-acetate was added. The analysis of the sulfate content of the pore waters were carried out at the BGR laboratory using standard titration methods.

RESULTS AND DISCUSSION

Offshore Sabah (East Malaysia)

Highly variable methane concentrations from over 15000 to 4 ngr / gr were observed in the cores from offshore Sabah. Hydrocarbons ethane and propane are only present in small amounts and do not exceed background concentrations (Table 1).

Methane shows systematic variations from low concentrations in the upper parts of the cores to high concentrations in the sulfate free zone. The observation that sulfate concentrations (Table 1) decrease from 28 mM / L (sea water concentration) in the upper part of the cores to 0 mM / L in the methane zone indicates bacterial sulfate reduction and decomposition of organic matter which leads to formation of H_2S and CO_2 . This process causes the changes of the negative redox potential values. The Eh changes with depth from values around -100 mV in the upper part to values of lower than -300 mV in the zone where free hydrogen sulfide is present (detected by smell). In the bottom part of the cores, where no free H_2S was observed, Eh-values rise again to about -200 mV. These systematic changes of methane, sulfate and hydrogen sulfite concentrations in combination with the changes of Eh point to a bacterial origin of the methane (Claypool and Kvenvolden, 1983).

The bacterial origin of methane is confirmed by carbon and hydrogen isotopic compositions which show (Table 1) that the gases were generated through bacterial CO_2 reduction typical for a marine environment (Whiticar *et al.*, 1986). Carbon isotope ratios and molecular composition (Table 1) also classify the gases as bacterial hydrocarbons. It is observed that with decreasing methane concentrations the light carbon isotope content decreases. This can be explained by methane migration from the methane generation zone into the sulfate zone and a subsequent bacterial methane consumption via sulfate reduction (Whiticar and Faber, 1986). The methane oxidation causes an isotope fractionation by which the heavy carbon isotopes become enriched in the residual methane. The fractionation factor for the oxidation process offshore Sabah is $\alpha_c = 1.003$ (calculated after Whiticar and Faber, 1986) which is close to the fractionation factor $\alpha_c = 1.004$ postulated by Whiticar and Faber (1986) for the residual methane model for methane oxidation.

Only small amounts of ethane and propane were detected in the surface sediments. The low concentrations of these components can be generated through bacterial decay (Oremland *et al.*, 1988).

There is no evidence in this area that thermal hydrocarbons migrated from deeply buried rocks, although deeper sediments of the accretion are thermally mature (compare Fig. 2).

Table 1 Redox potential, sulfate concentrations, gas yields, carbon and hydrogen isotope ratios of methane in shallow sediment cores offshore Sabah (East Malaysia). The ratio $C_1 / (C_2 + C_3)$ is calculated from vol.-% of individual components.

Sample	Sed. depth (cm)	Eh (mV)	SO ₄ ²⁻ (mM / L)	CH ₄ (ppb)	C ₂ H ₆ (ppb)	C ₃ H ₈ (ppb)	$\frac{C_1}{C_2 + C_3}$	$\delta^{13}C_1$ (‰)	δD (‰)
Accretion									
KL110-1	1185	-197	0.0	15284	6.8	0.0	4999.0	-95.5	-230
KL110-2	1075	-340	0.2	8342	5.1	0.0	3332.3	-97.2	-208
KL110-3	985	-374	0.2	3424	4.2	0.0	1427.6	-98.9	-193
KL110-4	885	-374	2.5	103	1.2	0.0	160.3	-88.0	—
KL110-5	785	-327	7.0	—	—	—	n.a.	—	—
KL110-6	685	-152	12.3	—	—	—	n.a.	—	—
KL110-11	185	-149	—	8	0.0	0.0	n.a.	—	—
KL114-1	1295	-137	0.6	7671	1.4	0.7	9999.0	-100.0	-213
KL114-2	1195	-348	0.0	4602	0.8	0.0	9999.0	-100.8	-199
KL114-3	1095	-363	1.6	195	0.7	0.4	356.1	-96.7	—
KL114-5	895	-132	13.0	12	0.0	0.0	n.a.	—	—
KL114-12	195	-119	23.5	5	0.0	0.0	n.a.	—	—
Abyssal plain									
KL109-1	1190	-200	0.3	15824	0.0	0.0	n.a.	-91.3	-207
KL109-2	1105	-168	0.2	10087	0.0	0.0	n.a.	-92.9	-204
KL109-3	980	-200	1.4	5380	0.0	0.0	n.a.	-97.6	-207
KL109-4	900	-479	0.9	2529	0.0	0.0	n.a.	-101.7	-208
KL109-5	775	-318	2.5	31	0.3	0.0	168.5	-90.0	—
KL109-6	700	-285	5.6	14	0.6	0.5	12.7	—	—
KL109-12	75	-108	23.2	4	0.0	0.0	n.a.	—	—
KL119-1	1185	-179	0.4	6603	0.0	0.0	n.a.	-89.6	-204
KL119-2	990	-346	0.2	7637	0.0	0.0	n.a.	-98.4	-209
KL119-3	690	-378	12.7	55	1.0	0.8	69.4	-83.3	—
KL119-4	460	-323	24.2	10	0.4	0.2	35.0	—	—
KL119-5	330	-152	26.4	10	0.6	0.5	19.6	—	—
KL120-1	1090	-176	0.3	7174	0.8	0.8	9999.0	-87.1	-206
KL120-2	990	-210	0.7	6719	1.9	1.9	4998.5	94.2	—
KL120-3	690	-392	8.2	297	1.3	1.6	414.9	-95.7	—
KL120-4	490	-343	20.1	21	0.6	0.3	48.5	-71.4	—
KL120-6	390	-246	25.9	9	0.4	0.0	48.3	—	—
KL122-1	1155	-190	0.0	7911	2.0	2.0	4999.0	-88.6	—
KL122-2	955	-396	0.4	11236	2.5	2.5	4999.0	-95.1	-210
KL122-3	725	-396	11.5	584	0.8	0.0	1249.0	-93.6	-198
KL122-4	530	-340	23.2	39	0.6	0.5	75.9	-81.3	—
KL122-5	320	-110	26.2	9	0.4	0.0	45.7	—	—

This observation can be explained in terms of a migration barrier formed by the hydrates.

Continental Shelf of China

In contrast to the observations offshore Sabah, gases from the continental shelf of China contain components: methane, ethane, propane and butanes (Table 2). Furthermore, all gases: components exceed background concentrations. Gases concentrations in cores KL1, SL2, SL3, SL5, SL6, KL8, SL9 and SL11 (shelf) differ from those in core KL12 and KL13 (transition).

Table 2 Gas yields, carbon isotope ratios of methane and redox potential of shallow sediment cores from the continental shelf of China. The ratio $C_1 / (C_2 + C_3)$ is calculated from vol.-% of individual components.

Sample	Sed. depth (cm)	CH ₄ (ppb)	C ₂ H ₆ (ppb)	C ₃ H ₈ (ppb)	iso-C ₄ H ₁₀ (ppb)	n-C ₄ H ₁₀ (ppb)	$\frac{C_1}{C_2 + C_3}$	$\delta^{13}C_1$ (‰)	Eh (mV)
SO49-									
KL1-1	410	94.6	5.0	2.3	0.0	0.0	26.97	-25.2	-90
KL1-3	210	145.7	7.7	3.8	1.2	1.4	26.52	—	-10
SL2-1	115	59.8	4.0	2.1	1.0	0.9	20.59	—	-20
SL2-2	50	90.1	5.9	2.5	1.3	1.1	22.04	—	-90
SL3-1	350	90.1	4.9	2.1	0.8	0.8	26.60	-31.5	-100
SL3-3	150	72.0	3.6	1.4	0.3	0.4	29.54	—	—
SL5-1	387	136.6	7.3	3.5	1.2	1.3	26.37	-33.7	-70
SL5-3	187	177.1	8.7	3.6	1.2	1.4	29.80	—	-20
SL6-1	233	121.5	6.6	3.0	1.1	1.1	26.37	-35.5	-30
KL8-1	950	96.0	5.6	3.2	1.2	1.2	23.18	-34.4	-100
KL8-7	350	144.3	8.1	4.2	1.4	2.2	24.72	—	-70
SL9-1	250	80.7	4.0	2.1	0.7	0.5	27.99	-35.8	-40
SL11-1	207	70.3	3.6	1.8	0.6	0.9	27.42	-33.7	—
KL12-1	894	70.6	9.7	5.8	3.3	2.8	9.71	—	—
KL12-4	294	92.0	14.6	9.5	5.5	3.8	8.20	—	-10
KL13-1	1000	100.2	16.6	10.0	6.1	3.4	8.03	-37.1	-30
KL13-2	920	80.5	38.4	23.8	20.1	8.9	2.76	—	-10
KL13-3	700	100.1	13.8	8.2	4.2	3.0	10.62	—	—

An obviously good correlation of gas concentrations is observed in cores KL1 to SL11. This indicates a single origin of all components. Although there are remarkable variations of gas concentrations within each core (Table 1), the gas ratios remain the same in all

samples. Methane dominates over the other components on average by a factor of about 25.

For gases from cores KL12 and KL13 a good correlation of concentrations is observed for ethane, propane and butanes. Again this indicates a single origin of these components. The concentration ratios are similar in all samples. Methane dominates over the other components by a factor of about 8 only. Generally, concentrations of ethane to butanes from cores KL12 and KL13 are higher than in cores KL1 to SL11.

Thermal Origin

Based on carbon isotope and molecular ratios all gases offshore China are of thermal origin (Fig. 4). Gases from cores SL3 to SL11 seem to be derived from a source of a higher thermal maturity (about 1.2% Ro, vitrinite reflectance equivalent) than gases from cores KL12 and KL13 (0.5% Ro). This is also supported by the butane ratios as gases from KL12 and KL13 have higher ratios than the others. The thermal stability of isobutane is lower than that of normal butane. The result of an increasing maturity is a decrease of the *i*-butane / *n*-butane ratio. The ratio *i*-butane / *n*-butane, although maturation dependent, is also used as an indicator for the type of source rock by Leythaeuser *et al.* (1979). He postulates that ratios below 0.5 are related to marine organic matter, whereas ratios above 0.5 stand for a predominance of a humic source. This is in good accordance with the classification by gas ratios and carbon isotope values. After this classification the gases are likely derived from organic matter that contains a mixture of marine and terrestrial particles with the exception of gases from core KL1 where carbon isotopes point to a terrestrial source. The source rock maturity of gases from KL1 is estimated to be about 0.7 to 0.8% Ro (Fig. 4).

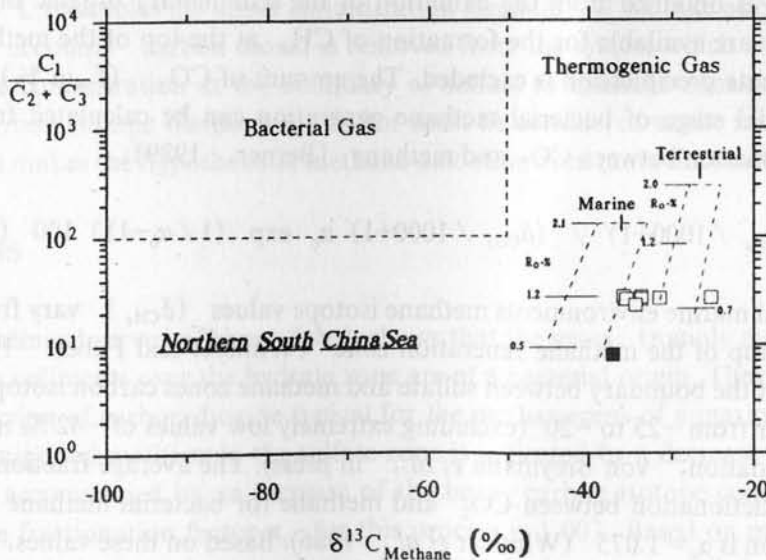


Fig. 4 Carbon isotope ratios of methane and molecular ratios point to a thermal origin of gases offshore China (light squares: KL1 to SL11; dark squares: KL12 and KL13; diagram modified after Berner, 1989).

A comparison between the gas maturities (Fig. 4) and calculated maturities from heatflow measurements (Fig. 3) shows that maturities of the presumed source rock (reflector T6; Gaedicke, this volume) is in very good accordance with the gas maturities. Also the predicted source rock type (marine / terrestrial from the gas data) fits to the drilling results in adjacent areas for sediments resembled by reflector T6. Only at the northern most locations KL1 and SL2 the reflector T6 could not be identified.

Bacterial Methane Generation and Oxidation

A contrasting interpretation to the above would be the assumption that methane offshore China is generated by bacterial CO_2 reduction and subsequently oxidized in the sulfate zone by methane consuming bacteria under anaerobic conditions. To test this hypothesis, we calculated a model for methane generation and oxidation assuming ideal conditions for methane production (validity of stoichiometric relations between sulfate, carbon dioxide and methane concentrations).

The negative redox potential clearly shows the reducing conditions in the sediments collected. In addition pyrite was found in several sediment samples and a slight smell of H_2S was detected. This indicates that samples have been collected from the sulfate reduction zone where anaerobic methane oxidation could occur.

Methane Generation

In this zone 28 mM / L of sulfate (sea water concentration) can be used up (see also Fig. 5a-f) for the bacterial generation of 55 mM / L dissolved CO_2 (Whiticar *et al.*, 1989) which is obtained from the oxidation of the sedimentary organic matter. These 55 mM / L CO_2 are available for the formation of CH_4 at the top of the methane generation zone if carbonate precipitation is excluded. The amount of CO_2 (f in %) which is used up in the initial stage of bacterial methane generation can be calculated from the carbon isotope fractionation between CO_2 and methane (Berner, 1989):

$$f = \left[1 - (\delta_{\text{CH}_4} / 1000 + 1) / (\delta_{\text{CO}_2} / 1000 + 1) \alpha_c \exp(1 / \alpha_c - 1) \right] 100 \text{ (\%)}$$

In natural marine environments methane isotope values (δ_{CH_4}) vary from -100 to -90 (‰) at the top of the methane generation zone (Whiticar and Faber, 1986; Berner *et al.*, 1990). At the boundary between sulfate and methane zones carbon isotope values of CO_2 (δ_{CO_2}) occur from -25 to -20 (excluding extremely low values of -42 ‰ in cases of extensive CH_4 oxidation; von Breymann *et al.*, in press). The average fractionation factor for the isotope fractionation between CO_2 and methane for bacterial methane formation from CO_2 reduction is $\alpha_c = 1.075$ (Whiticar *et al.*, 1986). Based on these values, approximately 7.2 % of the CO_2 theoretically converted into methane at the top of the methane zone which agrees with observations by Whiticar *et al.*, (1989). This corresponds to the generation of 4 mM / L of methane.

Methane Oxidation

A carbon isotope fractionation factor of 1.004 is postulated by Whiticar and Faber (1986) for the residual methane model of anaerobic methane oxidation in natural marine environments. But also higher fractionation factors are reported in the literature which, however, are still well below 1.009 (Whiticar and Faber, 1986 and authors cited therein). From the data available (Whiticar *et al.*, 1986; Berner *et al.*, 1990; gases offshore Sabah, this paper) an average carbon isotope fractionation factor of 1.007 is obtained. Only laboratory experiments with bacterial aerobic oxidation of methane show fractionation factors of up to 1.03 (Whiticar and Faber, 1986).

Two models for the carbon isotope fractionation of methane through anaerobic oxidation are compared to the gas data offshore China. These models are based on the equations given in Whiticar and Faber (1986) and an average fractionation factor of 1.007 (see above). The initial carbon isotope ratios are -90 and -100 ‰ and the initial methane concentration is 4 mM/L (see above) which corresponds to 64000 mgr/gr . The two models deviate from each other through ethane and propane concentrations which are deduced from the average concentrations in gases from KL1 to SL11 ($C_2+C_3=10 \text{ mgr/gr}$, model I) and KL12 and KL13 ($C_2+C_3=26 \text{ mgr/gr}$, model II). The concentrations of these two components remain unaffected through sulfate reduction (Whiticar and Faber, 1986).

Obviously, the gas data offshore China cannot be explained in terms of methane oxidation as the model curves deviate significantly from the measured data. Only carbon isotope fractionation factors of more than 1.009 would explain the gas data. Based on observations in natural systems this seems to be unrealistic. Furthermore, the methane concentration of 4 mM/L resembles the upper concentration boundary. If we take also carbonate precipitation into account, carbon dioxide is removed from the system which results in a lower initial methane concentration at the boundary of sulfate to methane zones. In this case an even higher carbon isotope fractionation factor must be considered as the ratio C_1 / C_2+C_3 decreases. This makes the hypothesis of methane oxidation even more unrealistic.

CONCLUSIONS

The geochemical survey offshore Sabah shows that the gases (mainly methane) found in near surface sediments over the hydrate zone are of a bacterial origin. They were produced from the reduction of carbon dioxide typical for the methanogens of a marine environment. Oxidation of migrated methane in the sulfate zone is indicated by a decrease of the methane concentration accompanied by an increase of the heavy carbon isotope concentration. The carbon isotope fractionation factor α_c for this process is 1.003. Based on maturity calculations a thermogenic hydrocarbon generation below the hydrate zone is likely, although no thermogenic gases were detected in the surface sediments. This might be due to the migration barrier of the gas hydrates.

Molecular composition and carbon isotope ratios of methane offshore China point to a thermogenic origin. Groups of genetically different gases can be distinguished. Samples from the northern region of the shelf are likely to be related to source rocks of organic maturities

corresponding to the end of the oil-window. The sediments of two cores above a sedimentary basin close to the slope of the Xisha Trough contain gases which show a molecular composition and isotope ratios which are typical for light hydrocarbons generated from an organic source of a lower maturation level. Maturities predicted from the hydrocarbon gases in the surface sediments of the continental shelf correspond to the calculated maturities of the seismic reflector T6 which stands for the organic rich Tertiary sequence drilled in other areas. Based on model calculations, methane oxidation under anaerobic conditions in the sulfate zone cannot explain gas data offshore China.

REFERENCES

- Berner, U., 1989: Entwicklung und Anwendung empirischer Modelle für die Kohlenstoffisotopenvariationen in Mischungen thermogener Erdgase. PhD Thesis, TU Clausthal.
- Berner, U., L. Dumke, E. Faber and J. Poggenburg, 1990: Organic geochemistry of surface sediments of the Sulu Trench / Philippines. Rangin, Silver, von Breyman *et al.* (eds.), Proc. ODP, Init. Pets., 124, College Station, Texas.
- Brooks, M. J., H.B. Cox, W.R. Bryant, M.C.II. Kennicut, R.G. Mann & T.J. McDonald, 1986: Association of gas hydrates and oil seepage in the Gulf of Mexico. Leythaeuser & Rullkotter (eds.), Advances in Organic Geochemistry, 1985, Org. Geochem., 10, 221–234.
- Claypool, G.E. & K.A. Kvenvolden, 1983: Methane and other hydrocarbon gases in marine sediments. Ann. Rev. Earth Planet. Sci., 11, 299–327.
- Dumke, I., E. Faber & J. Poggenburg, 1989: Determination of stable carbon and hydrogen isotopes of light hydrocarbons. Anal. Chem., 61, 19, 2149–2154.
- Faber, E. & J.W. Stahl, 1983: Analytical procedure and results of an isotope geochemical surface survey in an area of the British North Sea. Brooks, J. (ed.), Proceedings of the British Isles Geological Congress on the Petroleum Geochemistry Exploration of Europe, September 23–24, 1982, Geol. Society of London, Blackwell Spec. Publ., 11, 51–63.
- Faber, E. & J.W. Stahl, 1984: Geochemical surface exploration in the North Sea. AAPG Bul., 68, 3, 363–386.
- Hedberg, H.D., 1980: Methane generation and petroleum migration. Roberts & Cordell (eds.), Problems of Petroleum Migration, AAPG Studies in Geol., 10.
- Hinz, K., J. Frisch, E.H.K. Kempter, H. Meyer, A.M. Mohammad, D. Mohamed & J.J. Benavides, 1987: Structural elements of the continental margin of Sabah, NW Borneo. Progress Report BGR Hannover, Archiv-Nr. 101 150.
- Leythaeuser, D., R.G. Schaefer, C. Cornford & B. Weiner, 1979: Generation and migration of light hydrocarbons (C₂–C₇) in sedimentary basins. Org. Geochem., 1, 191–204.
- Oremland, R.S., M.J. Whiticar, F.E. Strohmeier & R.P. Kiene, 1988: Bacterial ethane formation from reduced ethylated sulfur compounds in anoxic sediments. Geochim. Cosmochim. Acta, 52, 7, 1859–1904.
- Von Breyman, M.T., P.K. Swart, G.W. Brass & U. Berner: Pore water chemistry of the Sulu and Celebes Seas: Extensive diagenetic reactions at Sites 767 and 768 (in press).
- Whiticar, M.J., E. Faber & M. Schoell, 1986: Biogenic methane formation in marine and freshwater environments, CO₂ reduction vs. acetate fermentation — Isotope evidence. Geochim. Cosmochim. Acta, 50, 693–709.

Whiticar, M.J. & E. Faber, 1986: Methane oxidation in sediment and water column environments - Isotope evidence. *Leythaeuser, D. & J. Rullkotter (eds.), Advances in Organic Geochemistry, 1985, Org. Geochem., 10, 759-768.*

Whiticar, M. J., E. Suess, G. Wefer & P.J. Muller, 1989: Calcium carbonate hexahydrate (Ikaite): History of mineral formation as recorded by stable isotopes. *Earth Planetary Sci. Letters.*

ABSTRACT

In the Yangtze and Qiongzhusi basins, there exists thick marine source rock in Neogene with rich submarine facies. It has been studied as good to excellent source rock. The rock contains abundant and well-preserved limited special mechanisms for generation and migration of hydrocarbons. The Yangtze basin and the Ledong 30-1 gas field has been proved to be stemmed from the Neogene.

The Yangtze and Qiongzhusi basins (Ying-Qiong Basin) are located in the sea area to the southeast and southwest of the Hainan Island (Fig. 1), from 107° 10' E to 112° 30' E and from 19° 03' N to 20° 19' N respectively, with an area of about 92000 km². There is a fault zone, a tectonic boundary fault, to the east of which is the northeast-trend Qiongzhusi basin, to the west of which is the northwest-trend Yangtze basin in the shape of long and narrow stripes. They were separated from each other in Paleogene, and subsided as a whole in Neogene when they received thick marine sediment. In Neogene, the Yangtze basin was characterized by rapid subsidence, high temperature, high pressure and well-developed mud diapir (Zhang et al., 1987).

SOURCE ROCK

The Neogene sedimentary basins in the Yangtze and Qiongzhusi basins are characterized by thick marine source rock. The thickness of the Yangtze and Qiongzhusi basins is about 1000-1500 m, and that of the Hainan Island is about 200-300 m. The maximum thickness of Neogene and Quaternary sediments is about 1000 m with 80% of mudstone and siltstone.

GENERATION AND MIGRATION OF HYDROCARBONS OF NEOGENE IN YINGGEHAI AND QIONGDONGNAN BASINS

ZHANG QIMING, ZHANG QUANXING, HU ZHONGLIANG & WANG ZHENFENG

Scientific Research Institute, Nanhai West Oil Corp., Zhangjiang, Guangdong, China

ABSTRACT

In the Yinggehai and Qiongdongnan Basins, there exists thick marine source rock of Neogene with rich submicroscopic resinite. It can be classified as good to excellent source rock. The rapid thermal subsidence and sedimentation created special mechanisms for generation and migration of hydrocarbons. The Yacheng gasfield and the Ledong 30-1 geopressured gas are believed to be stemmed from the Neogene.

GEOLOGICAL SETTING

The Yinggehai and Qiongdongnan Basins (Ying-Qiong Basins) are located in the sea area to the south-east and south-west of the Hainan Island (Fig. 1), from 107° 10' E to 112° 50' E and from 15° 34' N to 19° 03' N geographically, with an area of about 95000 km². There is Fault No. 1, a regional boundary fault, to the east of which is the northeastward Qiongdongnan Basin, to the west of which is the northwestward Yinggehai Basin in the shape of long and narrow stripe. They were separated from each other in Paleogene, and subsided as a whole in Neogene when they received thick marine sediment. In Neogene, the Yinggehai Basin was characterized by rapid subsidence, high temperature, high pressure and well-developed mud diapirs (Zhang *et al.*, 1987).

SOURCE ROCK

In Neogene, the development of the Ying-Qiong Basins came into a depression stage after a rift splitting stage. According to seismic interpretation, the Neogene sediment of neritic to bathyal was deposited with about 5000-8000 m in thickness. The sediment contains rich organic matter.

Thick Mudstone

In the central part of the Yinggehai Basin, the thickness of the Yinggehai and Huangliu Formations (Ying-Huang Formations) is 3200-4300 m, and that of Meishan Formation is more than 2300 m. The latter is confirmed by Ledong 30-1-1A well (Fig. 2). The maximum thickness of Neogene and Quaternary surpasses 10000 m with 80% of mudstone on an average.

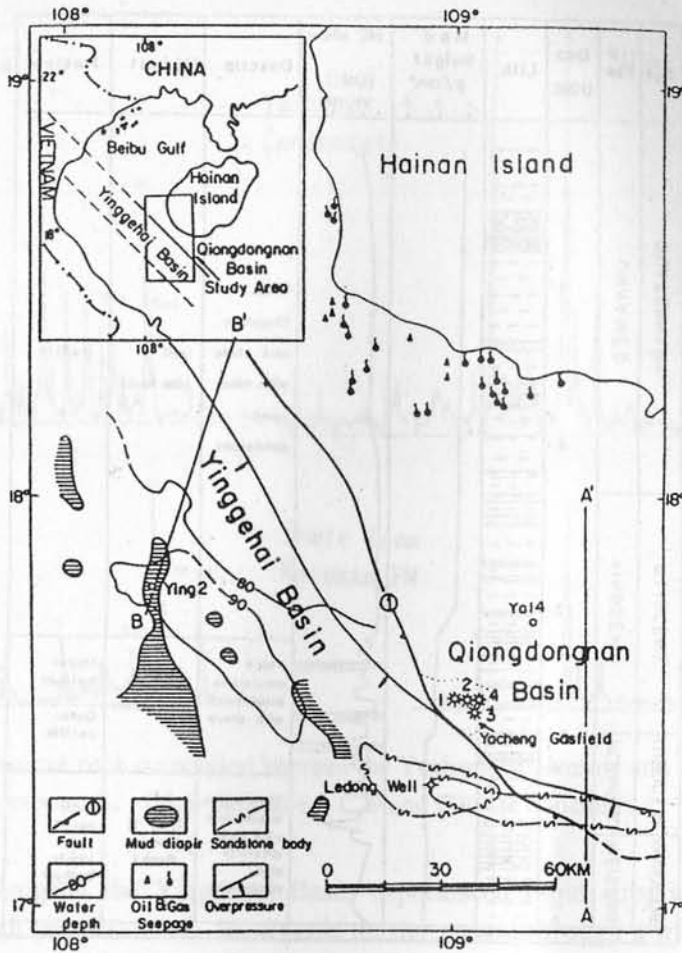


Fig.1 Map of Yinggehai Basin.

Terrestrial Organic Matter with Resinite

The Neogene and Quaternary sediments are neritic to bathyal. The kerogen microscopic examination showed that vitrinite is dominant, with the H/C ratio less than 0.9 and the hydrogen index less than 150 mg/g. The kerogen is classified as Type III. TOC is in the range of 0.4–2.0%, mostly 0.4–0.6%. Only below the depth of 4500 m at Ledong 30–1–1A, TOC is higher, with an average value of 1.17%. Insoluble organic matter is dominated by terrestrial vitrinite, but the soluble part of organic matter is rich in resinite. The resinite compounds of conifer is rich in Ying–Huang Formations and that of dipterocarpaceae is rich in Meishan Formation. The resinite compounds are not originated from thermal cracking of kerogen, but from the evolution of organic matter directly. The resinite compounds of Meishan Formation make up 90% of saturated hydrocarbons, which are the important organic matter. Hydrocarbon yield of Neogene varies in the range of 50–120 mg HC/g TOC. According to the Powell's standard (Powell, 1978), the source rock belongs to good to excellent.

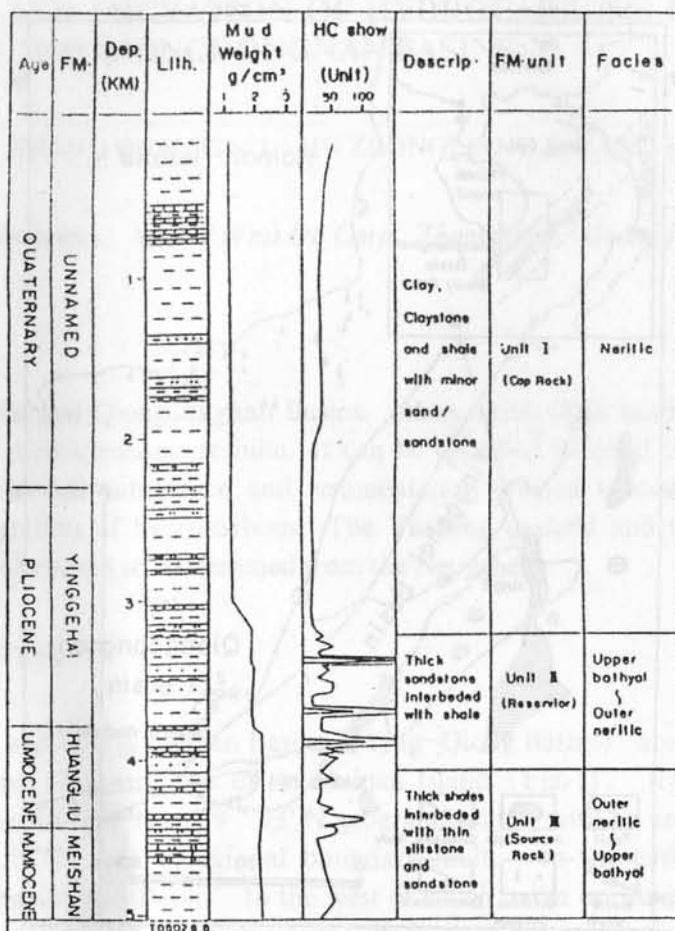


Fig.2 Ledong well formation evaluation.

Oil-Source Rock Correlation

Through steranes and triterpanes the oil-source rock correlation can be established between Meishan Formation and condensate pool of Yacheng gasfield (Fig.3), and between Ying-Huang Formations and gas seepages at Yinggehai Village, also geopressured gas of Ledong 30-1 sandbody.

Evolution of Organic Matter

According to vitrinite reflectance (Ro), drilling gas chromatography, clay mineral diagenesis and sterane structural features, it is determined that the threshold of hydrocarbon generation is at the depth of about 2800 m where Ro is 0.7% and formation temperature is 149°C, that the top limit for wet gas is at about 3800 m where Ro is 1.3% and formation temperature reaches to 195°C, and that the stage for dry gas is at 4600 m where Ro is 2.0% and formation temperature is 232°C.

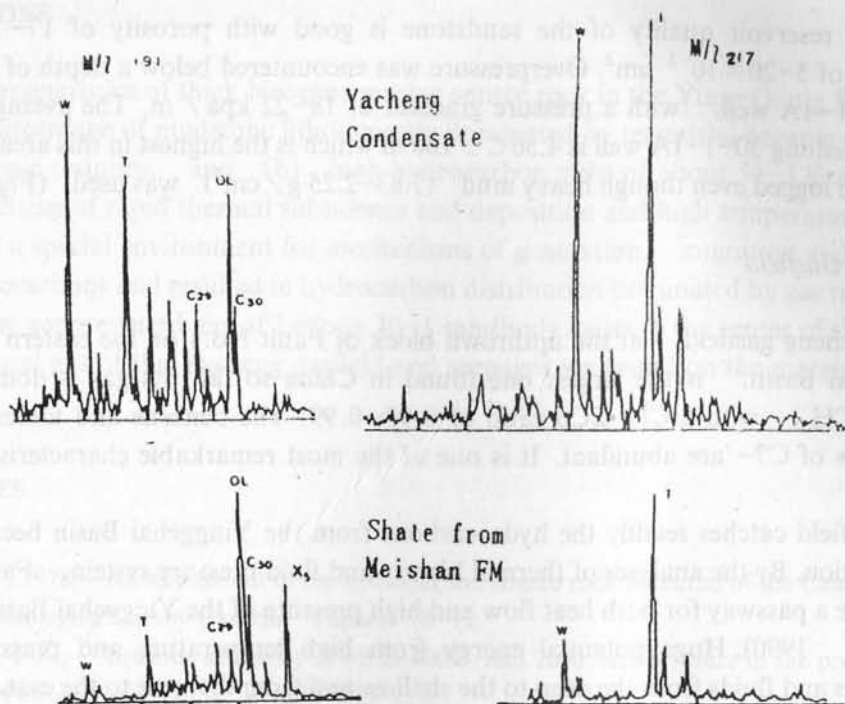


Fig.3 Condensate-source rock correlation between the Yacheng condensate and the Meishan FM. W and T are resinous compounds, OL is oleanane, C29 and C30 are hopanes.

Because in Neogene the Yinggehai Basin experienced rapid subsidence (0.7–0.86 mm/yr) and high temperature, its organic matter passed through a whole course of evolution from immature to highly mature stages in a short period of 2.0–3.5 Ma (Zhang and Huang, 1990). The mature rate of organic matter is so high that hydrocarbons generated earlier were overburied and thermally cracked into natural gas. That is why gas is primary but oil is secondary here.

OCCURRENCE OF HYDROCARBONS

Seepages at Yinggehai Village

Oil and gas seepages along the coast of Yinggehai Village have been noticed for more than one hundred years. As many as 32 seepages were located by the recent surveys (Fig.1). Some oil and gas samples were collected from shallow wells near to the seepages (Zhang and Zhang, 1987).

Geopressed Gas of Ledong 30-1 Sandbody

The Ledong 30-1 turbidite sandbody in Ying-Huang Formations,⁽¹⁾ which is located in the southeastern part of the Yinggehai Basin,⁽¹⁾ is the biggest reservoir sandstone found in this area so far, with an area of 468 km², a maximum thickness of 260 m and a top burial depth range of 3110–3990 m. According to the wireline log interpretation and the conventional core

analysis, the reservoir quality of the sandstone is good with porosity of 17–23% and permeability of $5-20 \times 10^{-3} \mu\text{m}^2$. Overpressure was encountered below a depth of 3000 m in Ledong 30-1-1A well, with a pressure gradient of 18–22 kpa / m. The average thermal gradient of Ledong 30-1-1A well is $4.56^\circ\text{C} / 100 \text{ m}$ which is the highest in this area. High gas readings were logged even though heavy mud ($1.83-2.25 \text{ g/cm}^3$) was used (Fig.2).

The Yacheng Gasfield

The Yacheng gasfield, at the upthrown block of Fault No.1 on the eastern margin of the Yinggehai Basin, is the largest one found in China so far. Its gas is dominated by methane (CH_4) with a $\text{Cl}/\Sigma\text{Cn}$ ratio of 0.93–0.99. The benzene and toluene in light hydrocarbons of C7– are abundant. It is one of the most remarkable characteristics of the gas.

The gasfield catches readily the hydrocarbons from the Yinggehai Basin because of its suitable location. By the analyses of thermal history and fluid pressure system, Fault No.1 is believed to be a passway for both heat flow and high pressure of the Yinggehai Basin (Zhang and Zhang, 1990). Huge potential energy from high temperature and pressure drives hydrocarbons and fluids from the deep to the shallow and from the west to the east, through Fault No.1 and into the Yacheng structure to form the gas reservoir (Fig.4). This is the case of aqueous migration of hydrocarbons as described by Price (1987).

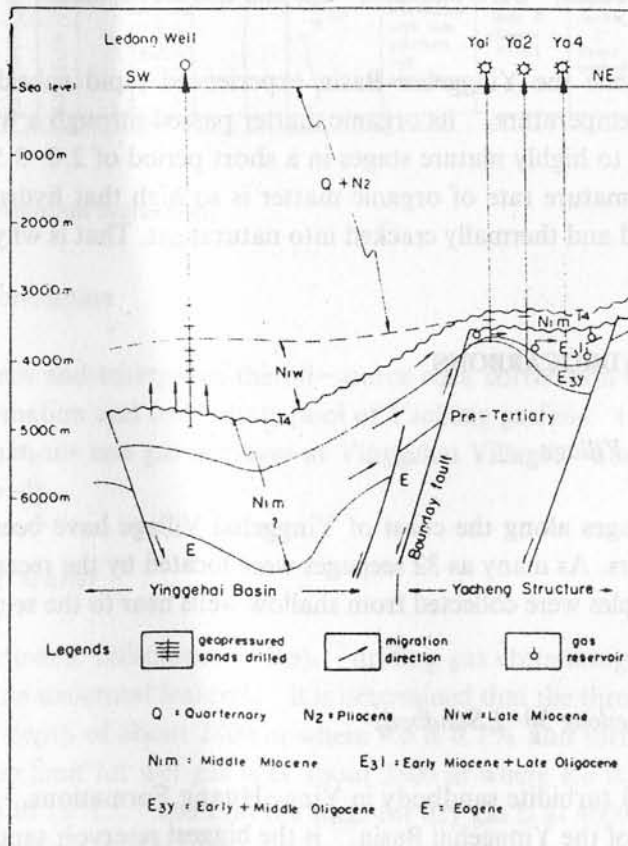


Fig.4 Oil and gas migration direction of the Yacheng gasfield.

CONCLUSIONS

The characteristics of thick Neogene marine source rock in the Ying-Qiong Basins are: (a) high percentage of mudstone lithologically dominated by terrestrial organic matter with submicroscopic resinites, and (b) high hydrocarbon yield of about 50–120 mg/g. The geological setting of rapid thermal subsidence and deposition and high temperature and pressure created a special environment for mechanisms of generation, migration and accumulation of hydrocarbons and resulted in hydrocarbon distribution dominated by gas reservoir. As a result, the geopressured gas of Ledong 30–1 sandbody exists in the center of the basins, and the natural gas of the Yacheng gasfield and seepages are found on the margin of the basins.

REFERENCES

- Powell, J.G., 1978: An assessment of the hydrocarbon source rock potential of the Canadian Arctic Islands. Geological Survey Canada, Paper, 78–12.
- Price, L.C., 1987: Aqueous solubility of oil to 400°C and 2000 bars pressure in the present of gas. *Journal of Petroleum Geology*, 4 (2), 195–223.
- Zhang Qiming and Zhang Quanxing, 1987: A unique petroleum-bearing basin—Yinggehai Basin. *China Offshore Oil and Gas (Geology)*, 1 (1), 11–19 (in Chinese).
- Zhang Quanxing and Zhang Qiming, 1990: Geochemical characterization of petroleum migration of Yacheng gasfield. *Journal of Southeast Asian Earth Sciences*, 4 (3) 1, 89–194.
- Zhang Quanxing and Huang Baojia, 1990: An overview of gases and source rocks from the area around the Hainan Island, offshore South China. *China Offshore Oil and Gas (Geology)*, 4 (1), 5–13 (in Chinese).

THE TECTONIC EVOLUTION OF SOUTH CHINA SEA AND ITS CONTROL OF HYDROCARBONS

WU JINMIN

The Second Marine Geological Investigation Brigade, Guangzhou Marine Geological Survey, Ministry of Geological and Mineral Resources, Guangzhou, China

ABSTRACT

South China Sea had basically undergone four evolving stages: (1) Andean-type continental margin, (2) shearing tensile margin, (3) little Atlantic sea and (4) island arc marginal sea. During Cenozoic, four margins with different characters, eastern, southern, western and northern ones, were formed there, and then five types and ten categories of basin, such as divergent, convergent, shearing, gravity settling and complex basin were generated. The evolution of those basins is obviously controlled by the regional tectonic background. So far, 16 Cenozoic hydrocarbon-bearing basins and 226 oil and gas fields or oil- and gas-bearing structures have been found in South China Sea. The generation and distribution of hydrocarbon are related to subsidence scale and sedimentation rate, sedimentary cycles and facies, geothermal gradient and source rock characters, types and formation time of traps, separated nature and uplift-depression structure of basins, etc. Finally the forming features of oil and gas field in different types of basin are also described in this paper.

INTRODUCTION

South China Sea has increasingly become the focus of the world attention for its important geographic and tectonic location as well as its abundant resources of hydrocarbon. As for the formation and evolution of South China Sea, there are some different views, but it is generally acknowledged that South China Sea was rifted under the action of extensive stress field (Taylor and Hayes, 1980 and 1983). According to the latest information from the Zhujiang Mouth and Zengmu basins, the authors revised some details of the Taylor and Hayes' scheme and elucidated the law of distribution and accumulation of hydrocarbon in South China Sea.

TECTONIC EVOLUTION OF SOUTH CHINA SEA

South China Sea is the most complex margin-sea in western Pacific tectonically. Near the triple junction of Eurasia, Pacific and India-Australia plates, there has been its complex features in geological structure due to the interaction among these plates. As shown in Fig.1, the structural framework of South China Sea and its adjacent sea area are composed of three landmasses of South China, Indo-Sino and Burma-Thai-Malay and each

landmass of many small blocks. Therefore, the tectonic evolution of South China Sea is essentially the history of separation and convergence of these continental fragments.

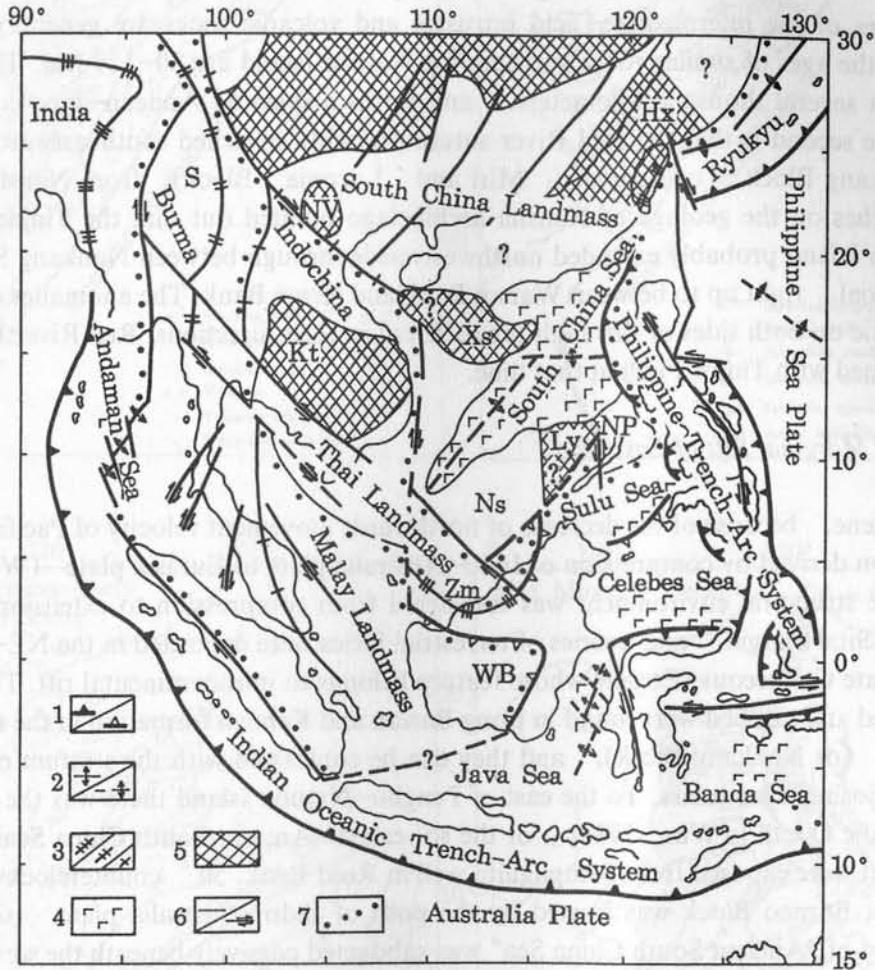


Fig. 1 Tectonic map of South China Sea and neighbouring areas. 1. Active / Inactive subduction zone; 2. Active / Inactive spreading center; 3. Himalayan / Yanshanian / Indosinian stages sutures; 4. oceanic crust; 5. Pre-Cambrian landmass: Yz—Yangzi, Kt—Kuntum, Hx—Huaxia, Xs—Xisha, Nv—North Vietnam; 6. Fault / Strike-slip fault; 7. Tectonic element boundary; Other continental crust block: S—Shan, WB—West Borneo, Zm—Zengmu, NP—North Palawan, Ns—Nansha, Ly—Liyue.

The Formation of Andean-type Continental Margin of East Asia

Before Jurassic Indosinian landmass and Burma-Thai-Malay landmass were sutured up first, then South China landmass came into collision with Indosinian one (Hayashi, 1988). The strong Indosinian movement led to extensive magmatic activity and fold thickened, and the united continent was formed by gradual cratonization in Southeast Asia.

In Jurassic-Cretaceous, the continent of Southeast Asia had two following distinct characteristics. The first is that the East Asia volcanic-arc caused by the successive

submergence of Kula plate had stretched southwards from the eastern part of Zhujiang Mouth Basin, Xisha-Zhongsha Islands, right up to Natuna Island and western Kalimantan Island. The data of drilling in Zhujiang Mouth Basin supported this pattern. The isotopic ages of the intermediate-acid intrusive and volcanic rocks are generally 70-130 Ma, and the ages of similar rocks surrounding Natuna Island are 80-129 Ma. The arc extends about several thousand kilometers, and forms a splendid Andean-type continental margin. The second is that the Red River suture probably stretched southeastwards and divided Nankang Block (or Zengmu, Miri and Luconia Block) from Nansha Block. The researches on the geology of Nansha archipelago pointed out that the Tinjar Fault in Kalimantan Island probably extended northwestwards through between Nankang Shoal and Beikang Shoal, right up to between Wanan Bank and Xiwei Bank. The anomalies of gravity and magnetic on both sides of this fault are different in their directions. Red River Fault was possibly joined with Tinjar Fault at that time.

Continental Marginal Rift of East Asia

In Eocene, because of the decrease of northwards movement velocity of Pacific plate or the extension derived by compression of Indo-Australia plate to Eurasia plate (Wan *et al.*, 1989), the structural environment was transferred from compression to extension on East Asia continental margin, and a series of terrestrial facies were deposited in the NE-trending basins of Late Cretaceous-Eocene whose feature belongs to intracontinental rift. The deposits of red bed and salt bed were found in Long Bawan and Kelalan formation in the eastern of Miri Block (or Nankang Block), and they can be contrasted with the stratum of Khorat basin in Indosinian landmass. To the east of Penghu-Natuna Island there was the marginal part of Pacific Ocean (Wu, 1988), or the so-called "Ancient South China Sea" with its deposits that were exposed from Sampaguita well in Reed Bank. 50° counterclockwise rotation of west Borneo Block was started by the push of Indo-Australia plate, so part of oceanic crust of "Ancient South China Sea" was subducted passively beneath the west Borneo Block. The Lubok Antu ophiolite zone on Kalimantan Island can be considered as the evidence of this event.

Formation of Oceanic Crust of South China Sea

After the movement direction of Pacific plate was transferred from NNW to NWW 40 Ma B.P., nearly NS spreading of South China landmass started 32 Ma B.P.. According to EEN 11-5D alignment magnetic lineations in the central basin of South China Sea, we can be sure that the spreading process lasted right up to early Miocene (17 Ma B.P.). This spreading process and the spread of the southwest basin (Fig. 2) which was developed along the early NE rifting direction 15 Ma B.P., impelled Zengmu block and Nansha block successively to drift southwards. Zengmu block collided with Sibuyan accretionary prism to cause the rising of fold of early Miocene in Balingian area of south margin of Zengmu basin, and in late early-Miocene, Nansha block moved southwards and collided with Zengmu block to cause the rising of the eastern of Zengmu basin, and the forming of Nankang platform.

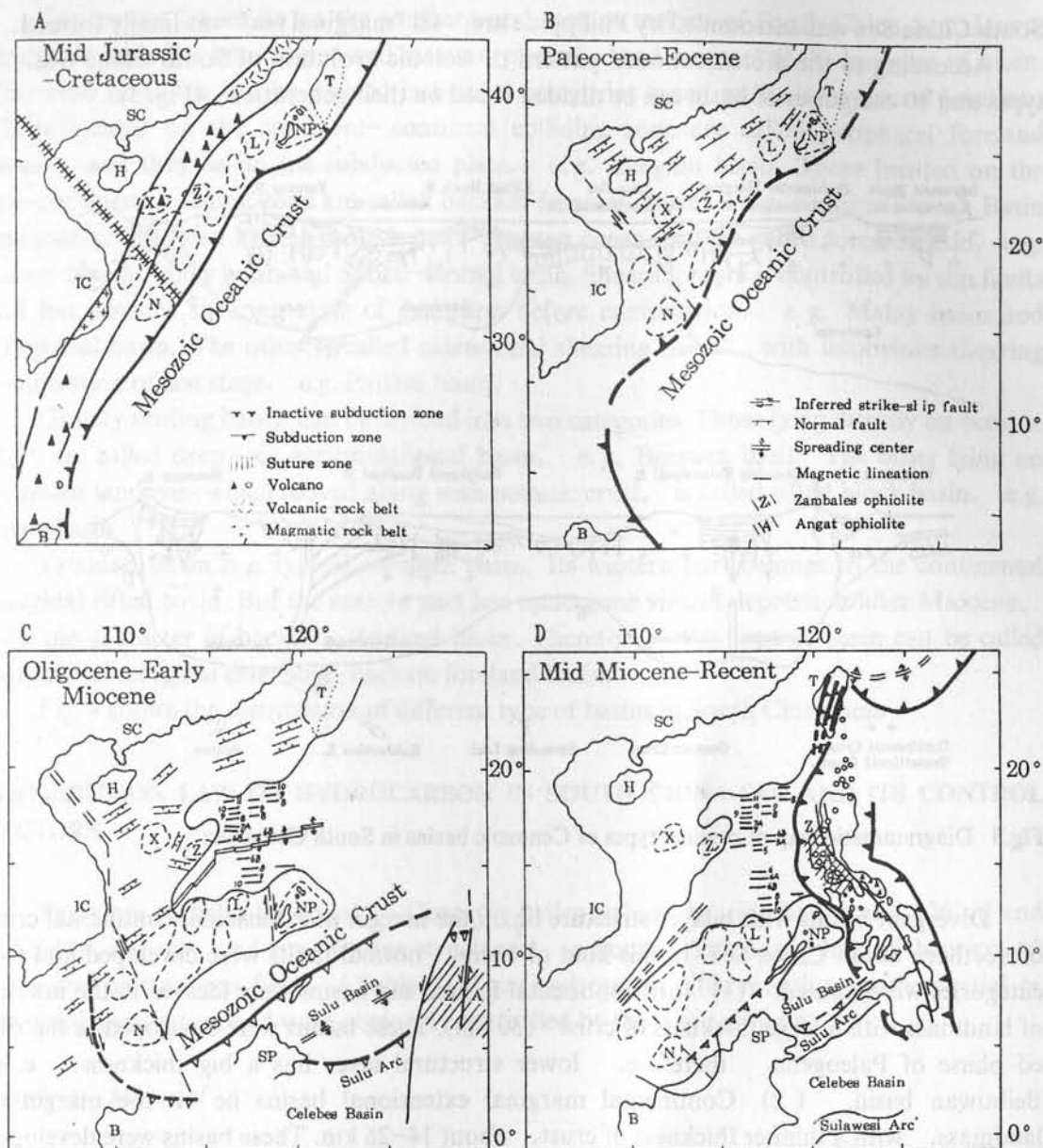


Fig.2 Sketch map of evolutionary history of south China Sea. X—Xisha, Z—Zhongsha, L—Liyue, N—Nankang, SP—South Palawan, NP—North Palawan, B—Borneo.

Formation of Marginal Sea

In late period of early Miocene — early period of middle Miocene, the spreading of sea floor was ceased, and a large scale of transgression occurred in South China Sea. Then Sabah arc upthrust northwards to the Nansha block and Philippine arc upthrust westwards to the oceanic crust of South China Sea possibly under the influence of the northwards movement of Australia plate. Meanwhile, Indo-China and South China landmass were continuously squeezed out southeastwards under the compression of India (Tapponnier *et al.*, 1982), to cause the rises and folds of middle-late Miocene in South China Sea. Because

South China Sea was surrounded by Philippine arc, its "marginal sea" was finally formed.

According to the aforementioned pattern of tectonic evolution of South China Sea, 5 types and 10 categories of basin can be divided based on their generation (Fig. 3).

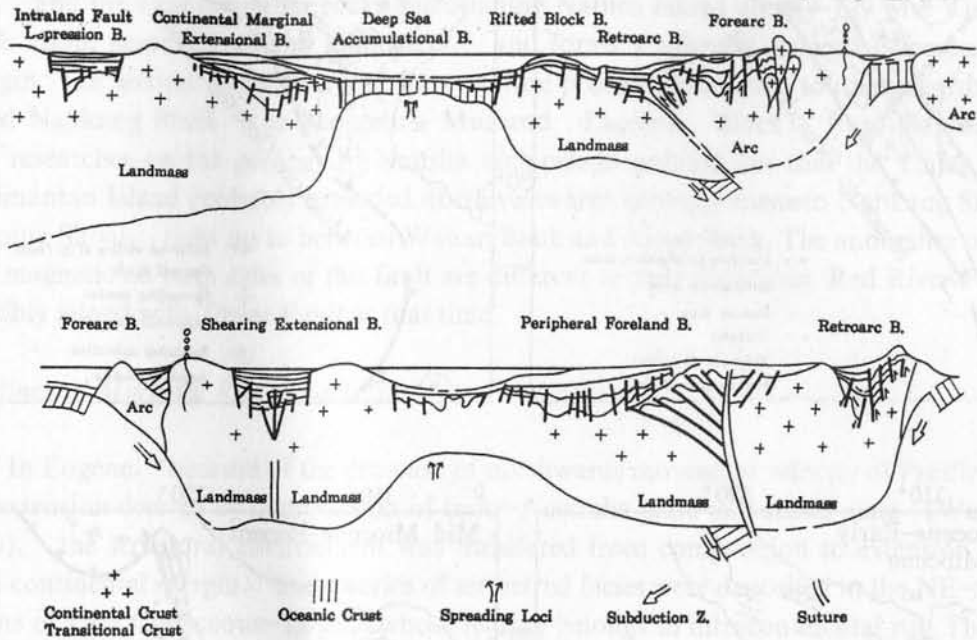


Fig.3 Diagrammatic map of original types of Cenozoic basins in South China Sea.

Divergent basins with bilayer structure lie on the margin of extensional continental crust of northern South China Sea. In this kind of basin, normal faults were developed and two categories were formed. (1) Intracontinental faulted sag basins were located in the interior of landmass with a large thickness of crust (30 km). These basins were developed in the rifted phase of Paleogene, therefore, lower structural layer has a big thickness, e.g. Beibuwan basin. (2) Continental marginal extensional basins lie on the margin of landmass, with a thinner thickness of crust, about 14–26 km. These basins were developed mainly in the faulted and subsided phase of late Cenozoic, therefore, upper structural layer has a big thickness, e.g. Zhujiang Mouth basin, Qiongdongnan basin (Table 1).

Table 1 The thickness change of Cenozoic structural layers on the northern continental margin of South China Sea

Thickness (m)	Intralund fault depression		Continental marginal extensional basin				
	Leidong	Beibu Gulf	Zhujiang Mouth			Qiong-dongnan	Taixinan
			Zhu 3	Zhu 1	Zhu 2		
Upper structural layer	1800	3000	3500	5000	6000	8000	9000
Lower structural layer	2900	6000	6000	2000	3000	3000	0–2500

Convergent basins lie on the southern and eastern margin of South China Sea. Lower structural layer has been folded and metamorphosed, and is a part of the basement of basin. This kind of basins can be divided into three categories based on their structural location. Those located on the continent-continent colliding zone are called peripheral foreland basin, and they lie on the subducted plate, e.g. Zengmu basin. Those located on the arc-continent colliding zone are called backarc foreland basin, e.g. Nansha Trough Basin and eastern Taixinan basin. Those located between ocean-arc are called forearc basin, e.g. Luzon central valley basin and Sabah-Brunei basin. Shearing basin is controlled by slip faults and has obvious shearing cycle of extension before compression, e.g. Malay basin and Yinggehai basin. The other is called extensional shearing basin, with unobvious shearing compression of last stage, e.g. Pattani basin.

Gravity settling basins can be divided into two categories. Those lying directly on oceanic crust are called deep-sea accumulative basin, e.g. Bijianan basin. The other lying on fragment landmass which moved along with oceanic crust, is called rifted block basin, e.g. Liyue basin.

Taixinan Basin is a typical complex basin. Its western part belongs to the continental marginal rifted basin. But the eastern part has undergone violent depression after Miocene, with the character of backarc-foreland basin. Therefore, this type of basin can be called continental marginal extension-backarc foreland basin.

Fig. 4 shows the distribution of different type of basins in South China Sea.

DISTRIBUTION LAW OF HYDROCARBON IN SOUTH CHINA SEA AND ITS CONTROL FACTORS

There are statistically about 16 Cenozoic hydrocarbon-bearing basins and 226 oil and gas fields (or oil- and gas-bearing structures) in South China Sea, half of them are oil fields and half are gas fields (Table 2). They had certain differentiation on the spatial or temporal distribution and were obviously controlled by the types of basin.

Supply of Material

It is mainly controlled by the supplied quantity of terrigenous materials. Those basins further away from the land have thinner sediments with less organic content due to less terrigenous clastics, therefore, there are little potential.

Rate of Deposit

The sedimentation rate depends on the tectonic setting and the type of basin. Zengmu basin, Zhujiang Mouth basin, Qiongdongnan basin, Beibu Gulf basin, Taixinan basin and Yinggehai basin in South China Sea have a higher sedimentary rate than the same type of basin in the world, so their potential is better. The rate of deposit in Liyue basin and North Palawan basin is lower, however, their hydrocarbon potential is proven to be less by the result of exploration at present. The sedimentary rate is high up to 400 m / Ma in Luzon central valley basin, but only little hydrocarbon has been found so far because of piling of much

volcanic debris, reduction of organic content and low thermal flow.

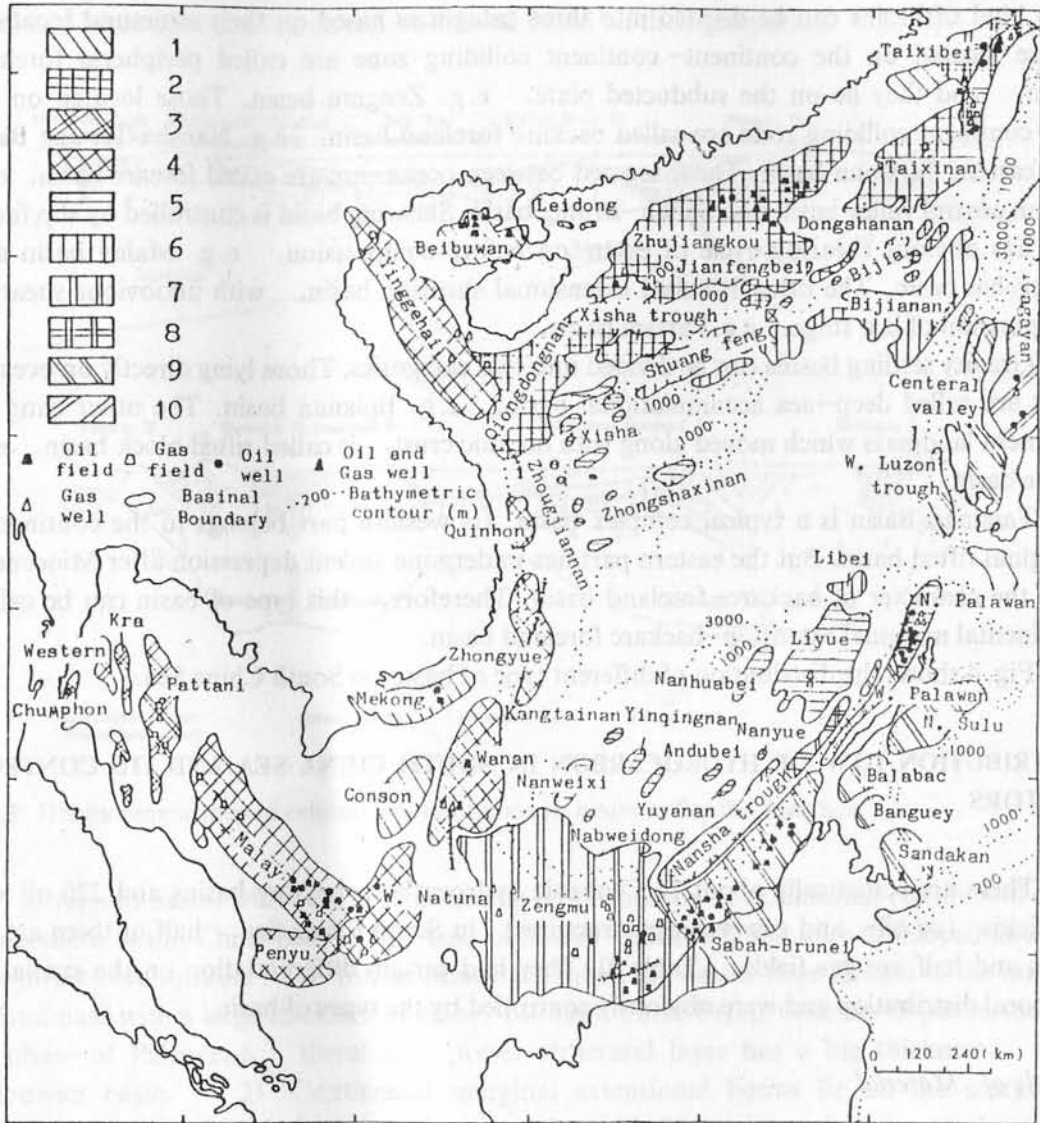


Fig.4 Distribution of Cenozoic sedimentary basins in South China Sea. 1. Intraland fault depression basin; 2. Continental marginal extensional basin; 3. Extensional shear basin; 4. Shearing extensional basin; 5. Rifted block basin; 6. Deep sea accumulative basin; 7. Peripheral foreland basin; 8. Retroarc basin; 9. Forearc basin; 10. Interarc basin.

The Type of Organic Matter and the Degree of Thermal Evolution

In the present 16 basins, the natural gas fields are relatively concentrated in four areas, Taiwan-Luzon Islands, Yinggehai-Qiongdongnan and No.3 Zhu depression, Gulf of Thailand and Nansha Islands, because those areas have a high or low degree of thermal evolution of source rock abundant in type III kerogen. But the area with a middle degree of thermal evolution is dominated by type I-II kerogen and has mainly produced oil,

only accompanied by little natural gas, e.g., Beibuwan basin, No.1 Zhu depression of Zhujiang Mouth basin.

Table 2 Statistical table of oil and gas fields (oil- and gas-bearing structures) of Cenozoic basin in South China Sea

Basins	Number of oil and gas fields / structures	Number of oil fields / structures	Number of gas fields / structures
Pattani	10		10
Chumphon	1	1	
Malay	45	19	26
W. Natuna	9	5	4
Mekong	2	2	
Wanan	4	2	2
Zengmu	53	17	36
Sabah-Brunei	38	30	8
Liyue	1		1
Central valley	1		1
N.Palawan	9	7	2
Taixinan	18		18
Zhujiang Mouth	19	18	1
Qiongdongnan	5	4	1
Beibu Gulf	8	8	
Yinggehai	3		3
Total	226	113	113

Sedimentary Cycle and Facies

Generally speaking, source rock is in the middle of sedimentary cycle, but reservoir rock is in the beginning or end of sedimentary cycle. Because paludal coal-bearing series were the important gas source rock in South China Sea, the beginning and end of the sedimentary cycle were also the developed phase of gas source rock. According to the transgressive direction in South China Sea, the age of source and reservoir beds tends to new from west to east and from north to south. The basins with multi-cycle may have many suites of source and reservoir bed for oil and gas, for example, the Mesozoic, Eocene and Neogene-Quaternary of Taixinan basin.

Turbidite fan, delta, littoral sandstones and reef carbonate rock are the most important facies of reservoir in South China Sea, and lacustrine of marine facies mudstones are the most important facies of cap bed. In case other conditions are similar, the profit reservoir and good cover has determined the formation and preservation of oil and gas fields, for example, Qiongdongnan basin and Zhujiang Mouth basin.

Time of Formation of Trap

Except east and south margin of South China Sea, the structural activity is weak in

most area, and so far it is still situated in the subsiding setting, therefore, there is good preservation but undeveloped structural condition. The hydrocarbon traps found by now are still dominated by structural traps and reef traps with certain dimensions. According to the characteristics of the type of basin in South China Sea, traps in most basins are related to the up / down of basement block faults and the factors of lithology-strata, for instance, syndepositional anticline, rolled anticline, drape anticline, faulted anticline, fault block and reef rock etc.. Their forming time is generally earlier than the time of hydrocarbon exhaustion of source rock, and is benefited to accumulate oil and gas. Minority of basins and areas that are not ideal in exploration so far, are related to the late formation of structure.

Trend of Migration

The sedimentary basins of South China Sea possessed the structure of uplift alternate with depression. Because there are well-developed strata in the low uplift or the depression edge, they have good reservoir facies and cap bed conditions, and are the good zones for migration of hydrocarbon, so oil and gas fields can be formed by accumulating the generated hydrocarbon in adjacent depression. On the contrary, there may be a vain exploration in some higher uplift zones for lack of certain conditions for field formation.

Hydrocarbon Pool-Forming Model

Thus it can be seen that different types of basin have their own characteristics of oil and gas fields. Intracontinental faulted-sag basins are predominated by self-generation and self-reservoir, new-generation and old-reservoir of Paleogene. There are strongly separating natures of basins, and a lot of changes in facies of terrestrial strata. The migration distance of oil and gas is short, and hydrocarbon distributed around the oil-producing depressions mainly become middle-small oil and gas fields.

Continental marginal rifted basins are characterized by Paleogene terrestrial hydrocarbon source rock, middle Tertiary transitional facies reservoirs and Miocene marine facies covers. The widely distributed reservoirs have good physical property and can provide a distant migration of oil and gas. they distributed mainly in the slope of depression or the margin of uplift. They may form large-middle oil and gas fields.

Shearing extensional basins unobviously separated have a high geothermal gradient, and Miocene is the hydrocarbon-producing rock and reservoir. Cover structures are irrelevant to the undulation of basement but are formed by shearing wrench. Oil and gas fields mainly distributed in the centre of depression.

There is a high geothermal gradient in foreland basins. Oligocene-Miocene marine facies is the main source rock with wide distribution and big thickness. Miocene reef buildup is the main reservoirs and traps and provides oil and gas a quite long migration. In platforms or on the margin of uplifts, large-middle oil and gas fields may be formed.

CONCLUSIONS

The evolution of South China Sea is in fact a history of the dispersion and convergence

between continental fragments, or between continental fragment and accretion zone. It had undergone four stages: (1) Andean-type continental margin, (2) shearing tensile margin, (3) little "Atlantic sea", (4) island arc marginal sea.

According to the moving character among continental and oceanic blocks, 5 types and 10 categories of Cenozoic sedimentary basins can be divided in South China Sea.

The hydrocarbon distribution on the space and the time were obviously controlled by the structural setting and the types of sedimentary basin, which appear as supply of source material, sedimentation rate, sedimentary cycle and facies, type of organic matter and degree of thermal evolution, time of formation of trap, trend of migration, and hydrocarbon pool-forming model.

REFERENCES

- Gallagher, J.J., Jr., 1986: Philippine Islands: A tectonic railroad siding. AAPG Memoir 40 (Wallace Pratt Memorial Volume), 515-527.
- Hayashi, M., 1988: The hydrocarbon potential and tectonics of Indo-China. *Journal of Petroleum Geology*, 11 (2), 219-231.
- Tapponnier, P., G. Peltzer, A.Y. Ledain, R. Armijo & P. Cobbold, 1982: Propagating extrusion tectonics in Asia: New insights from simple experiments with plasticine. *Geology*, 10 (12), 611-616.
- Taylor, B. & D.E. Hayes, 1980: The tectonic evolution of the South China Sea basin. *The Tectonic and Geologic Evolution of Southeast Asian Seas and Islands*, Geophysical Monograph, 23, American Geophysical Union, 89-104.
- Taylor, B. & D.E. Hayes, 1983: Origin and history of the South China Sea basin. *The Tectonic and Geologic Evolution of Southeast Asian Seas and Islands*, Geophysical Monograph, 27, American Geophysical Union, 23-56.
- Wan Tianfeng & Zhu Hong, 1989: The tectonic stress field of the Cretaceous-Early Eocene in China. *Acta Geologica Sinica*, 63 (1), 14-25 (in Chinese).
- Wu Jinmin, 1988: Cenozoic basins of the South China Sea. *Episodes*, 11 (2), 91-96.

PARTICLE FLUX IN THE NORTHERN SOUTH CHINA SEA

T.C. JENNERJAHN¹⁾, G. LIEBEZEIT¹⁾, S. KEMPE¹⁾, L.Q. XU²⁾, W.B. CHEN²⁾ & H.K. WONG¹⁾

1) *Institute of Biogeochemistry and Marine Chemistry, University of Hamburg, Germany*

2) *Second Institute of Oceanography, SOA, Hangzhou, China*

ABSTRACT

From September 1987 to October 1988 a sediment trap system was moored in the northern South China Sea at 18 ° 28' N, 116 ° 01' E to sample particle flux. Total flux varied between 12 and 181 mg m⁻²d⁻¹ in the shallow trap and between 19 and 122 mg m⁻²d⁻¹ in the deep trap. Flux patterns of both traps do not show significant correlations.

Biological activity in surface water enhanced by monsoon winds seems to be the dominant source of material collected in the shallow trap. Surface currents strongly affected by monsoon winds from the SW during summer and from the NE during winter probably carry suspended matter from the East China Sea and the western Pacific. Input of the major rivers discharging into the South China Sea seems to be of less importance for recent sedimentation in the investigation area. Geochemical parameters indicate that parts of the particulate matter input in the deep trap originate from lateral advection. Deep water from the western Pacific enters the South China Sea through the more than 2000 m deep Bashi Channel, the only deep connection of the northern South China Sea to the Pacific Ocean.

INTRODUCTION

Vertical flux of particulate matter is one of the most important processes in biogeochemical cycles in the ocean. At least in the open ocean it is the major contributor to marine sedimentation. Rapidly sinking particles are responsible for the chemical differentiation between the warm surface water and deep water. Water depth, settling velocity and composition of the settling particles as well as the chemistry of the water column and biological activity are responsible for the amount of sinking particulate matter that finally reaches the bottom. Average productivity of the oceans amounts to 100 g C m⁻² or 36 × 10¹⁵ g C a⁻¹ from which only 0.2% to 0.3% or 0.095 × 10¹⁵ g C will finally accumulate in the sediment (Mopper & Degens, 1977).

The results of numerous sediment trap studies suggest that vertical flux is highly variable both in total amounts and composition of the sinking particulate matter (e.g. Deuser & Ross, 1980; Honjo & Roman, 1978; Honjo *et al.*, 1982; Honjo *et al.*, 1987; Ittekkot *et al.*, 1984a, 1984b; Kempe & Jennerjahn, 1988). Furthermore, it shows large interannual fluctuation. Another important result is that fast deposition of lithogenic matter derived from the continents results from the formation of macroflocs glued together by organics of planktonic origin (McCave, 1975; Shanks & Trent, 1980; Silver & Alldredge, 1981) or is due to incorporation into fecal pellets produced by zooplankton

(Deuser *et al.*, 1983). More recent investigations indicate that only 5% of vertical particle flux is connected with fecal pellets (Pilska & Honjo, 1987), whereas macroflocs or marine snow appear to be the chief contributors.

The South China Sea is one of the largest marginal seas in the world. Studies of particulate matter input and recent sedimentation processes are of great interest in this region, as South Asian rivers and larger islands of the Pacific and the Indian Oceans are responsible for about 70% of the annual riverine input of suspended sediments into the world's oceans estimated at 13.5×10^9 tons (Milliman & Meade, 1983). Annually about 13.5×10^9 tons of suspended sediments are delivered into the oceans by world's rivers. Bedload and flood discharges may account for another $1-2 \times 10^9$ tons (Milliman & Meade, 1983). The Mekong, Hungho and Zhujiang, three of the 20 major rivers of the world as far as their sediment load is concerned (Milliman & Meade, 1983), discharge into the South China Sea.

Another important factor raising interest in studies of particulate matter transport and sedimentation in the South China Sea is the influence of monsoons. These seasonal winds strongly influence biological activity in SE Asian waters (Lafond, 1966; Nair *et al.*, 1989). Mixed layer deepening by strong monsoon winds causes nutrient injection into the euphotic zone and hence stimulates primary productivity. Enhanced primary productivity leads to an increased formation of rapidly sinking particles and thus raises flux rates.

MATERIALS AND METHODS

A sediment trap system consisting of two time-series Benthos Mark VI sediment traps (Honjo & Doherty, 1988) was moored from September 10, 1987 until March 8, 1988 (SCS-I) and from April 13 until October 7, 1988 (SCS-II) in the South China Sea at $18^{\circ} 28' N$ and $116^{\circ} 01' E$. The traps sampled vertical partial flux in preprogrammed time intervals of 15 (SCS-I), and 14.75 days (SCS-II), respectively. Total water depth amounted to 3766 m, whereas trap depths were 1000 and 3350 m, respectively. The receiving cups were filled with a saturated NaCl-solution and poisoned with $HgCl_2$ at a final concentration of 200 mg dm^{-3} .

Cup waters were analyzed for inorganic nutrients according to Grasshoff *et al.* (1983), organic phosphorus and organic carbon. Dissolved organic carbon (DOC) was determined by high temperature wet oxidation with a Carlo Erba Total Carbon Monitor model 400/P. Dissolved organic phosphorus was calculated as the difference between total dissolved phosphorus determined by alkaline peroxodisulfate oxidation and inorganic phosphate.

Samples were passed through a 1 mm sieve and the $< 1 \text{ mm}$ fraction was split in four aliquots with a rotating splitter. Two aliquots were combined and filtered through $0.45 \mu\text{m}$ Nuclepore polycarbonate filters. After washing and drying at $40^{\circ}C$ these were used for determination of total fluxes. The fractions more than 1 mm were washed and dried at $40^{\circ}C$ in Petri dishes.

The dried fractions more than 1 mm were hogogenized in an agate morta and pestle. Organic carbon was determined by temperature controlled pyrolysis (Oil Show Analyzer, Delsi Instruments, Paris; Liebezeit & Wiesner, 1989). Total phosphorus was analyzed

photometrically as phosphomolybdate complex after combustion (550°C, 1 h) and subsequent extraction with 1 mol HCl for 14 h. Biogenic opal was determined photometrically as silicomolybdate complex after alkaline hydrolysis (7 % Na₂CO₃, 85°C, 5 h). Total carbon and total nitrogen were determined by high temperature oxidation with a Carlo Erba Nitrogen Analyzer NA 1500. All other data were calculated from the measured parameters. Total flux rate results from fluxes of the residual material and the additional dissolved material after subtraction of ambient seawater concentrations.

From these data the material is subdivided into four main fractions: CaCO₃ (calculated from C_{inorg}), organic matter (calculated from C_{org} by assuming that the average composition is CH₂O, i.e. carbohydrates), biogenic opal (from silica measurement) and lithogenic matter (as difference between the above fractions and total weight).

RESULTS AND DISCUSSION

High amounts of DOC, dissolved organic phosphorus and inorganic nutrients were measured in the supernatants of the receiving cups. Ambient seawater concentrations were less than 5 % of the concentrations measured in cup waters. These high values appear to be the result of autolytic processes which is supported by extremely low nitrite values (Liebezeit & Kempe, 1989).

Due to technical problems dissolved inorganic carbon (DIC) could not be measured. Although only small amounts of DIC are to be expected regarding Liebezeit & Kempe's (1989) findings, CaCO₃ fluxes given in this paper can only be minimum values.

Averaged fluxes of the dissolved fractions of organic carbon, total phosphorus and total nitrogen were higher in the shallow trap. Percentages of dissolved organic carbon and phosphorus of total organic carbon and total phosphorus were similar in the deep trap whereas that of phosphorus was twice as high in the shallow trap (Table 1). A distinct fractionation of C/P and C/N ratios between the dissolved and the residual phase of the collected material indicates preferential release of P-containing organic molecules versus proteinaceous material (Fig. 1a). C/P ratios were lower in the dissolved than in the residual fraction, whereas an opposite behaviour was observed for the C/N ratios.

In general TOC/TP ratios of the deep trap are higher (Table 1), but do not show such a distinct fractionation (Fig. 1b). C/N ratios show a fractionation with higher ratios in the dissolved phase. These facts indicate that the organic material collected in the deep trap appears to be more refractory than that collected in the shallow trap.

Lowest TOC/TP and TOC/TN ratios in the shallow trap occurred during low flux periods. Material collected during these times consists almost exclusively of biogenic material. During NE monsoon TOC/TP ratios increase to values around 100. This could be the result of higher input of lithogenic material via (1) surface current transport from the East China Sea and the western Pacific and (2) eolian transport from the Asian landmass. The mean TOC/TP ratio of 86 is somewhat smaller than the ratio typical for marine plankton (106, Redfield *et al.*, 1963; 122, Takahashi *et al.*, 1985). However, the recent findings of Liebezeit (1991) caution against usage of TOC/TP as source indicator as about 50 to 60 % of TP appear to be of an inorganic although not necessarily abiogenic nature.

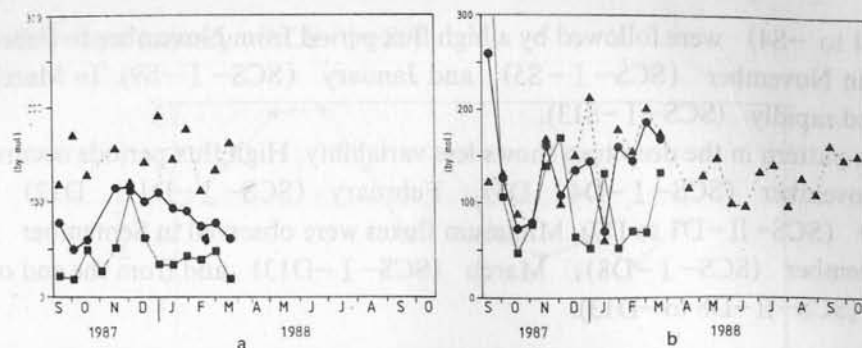


Fig.1 Molar C/P ratios of the dissolved (squares) and the residual fractions (triangles) and the total material (circles) of particle flux in the northern South China Sea (a: 1000 m water depth, b: 3350 m water depth).

Table 1 Mean fluxes of dissolved (DOC) and total organic carbon (TOC), dissolved (DOPal) and total biogenic opal (TOpal), dissolved (DP) and total phosphorus (TP), dissolved (DN) and total nitrogen (TN) and mean molar C/P and C/N ratios

	SCS-I-S	SCS-I-D	SCS-II-D
DOC ($\text{mg m}^{-2} \text{d}^{-1}$)	1.6	0.5	—
TOC ($\text{mg m}^{-2} \text{d}^{-1}$)	5.6	2.7	1.9*
DOC of TOC (%)	29.3	18.6	—
DOPal ($\text{mg m}^{-2} \text{d}^{-1}$)	0.4	0.1	0.4
TOpal ($\text{mg m}^{-2} \text{d}^{-1}$)	1.8	1.2	1.5
DOPal of TOpal (%)	22.7	11.0	25.5
DP ($\mu\text{g m}^{-2} \text{d}^{-1}$)	92.0	10.0	17.6
TP ($\mu\text{g m}^{-2} \text{d}^{-1}$)	157.2	52.6	57.6
DP of TP (%)	58.5	19.7	30.6
DN ($\mu\text{g m}^{-2} \text{d}^{-1}$)	63.7	23.7	18.8
TN ($\mu\text{g m}^{-2} \text{d}^{-1}$)	636.1	358.9	338.1
DN of TN (%)	10.0	6.6	5.6
DOC/DOP	103.5	420.1	—
C/P res. mat.	143.2	133.1	120.3
TOC/TP	86.2	132.3	—
DOC/DN tot	28.6	25.5	—
C/N res. mat.	7.4	7.6	6.8
TOC/TN	9.5	8.8	—

* Only particulate organic carbon, no analysis of dissolved fraction.

Particle flux rates vary by one order of magnitude (Fig.2) ranging from 12 (SCS-I-S4) to $181 \text{ mg m}^{-2} \text{d}^{-1}$ (SCS-I-S9) in the shallow trap and from 19 (SCS-II-DI3) to $122 \text{ mg m}^{-2} \text{d}^{-1}$ (SCS-II-D5) in the deep trap. Mean flux rates are $90 \text{ mg m}^{-2} \text{d}^{-1}$ (SCS-I-S) in the shallow trap and 78 (SCS-I-D) and $70 \text{ mg m}^{-2} \text{d}^{-1}$ (SCS-II-D) in the deep trap (Table 2). Minimum flux rates in the shallow trap in September and October 1987

(SCS-I-S1 to -S4) were followed by a high flux period from November to February with peak fluxes in November (SCS-I-S5) and January (SCS-I-S9). In March particle flux decreased rapidly (SCS-I-S13).

The flux pattern in the deep trap shows less variability. High flux periods occurred in October and November (SCS-I-D4, D5), February (SCS-I-D11, D12) and from April to July (SCS-II-D1 to D7). Minimum fluxes were observed in September (SCS-I-D1), December (SCS-I-D8), March (SCS-I-D13) and from the end of July until October (SCS-II-D8 to -D13).

Table 2 Averaged fluxes of the four main fractions CaCO_3 , organic matter (CH_2O), biogenic opal and lithogenic material in $\text{mg m}^{-2}\text{d}^{-1}$ and percentage of total flux

		SCS-I-S	SCS-I-D	SCS-II-D
CaCO_3	($\text{mg m}^{-2}\text{d}^{-1}$)	42.9*	34.7*	30.6*
	(%)	51.0*	46.3*	48.5*
CH_2O	($\text{mg m}^{-2}\text{d}^{-1}$)	12.9	6.7	4.7
	(%)	17.4	9.0	6.6
Opal	($\text{mg m}^{-2}\text{d}^{-1}$)	1.8	1.2	1.5
	(%)	2.0	1.5	2.2
Lith. mat.	($\text{mg m}^{-2}\text{d}^{-1}$)	32.4	35.3	32.9
	(%)	29.8	42.8	42.2
Total flux	($\text{mg m}^{-2}\text{d}^{-1}$)	90.0	78.3	69.9

* Only particulate CaCO_3 , no analysis of dissolved fraction.

The distinct seasonal variability of particle flux in the shallow trap is caused mainly by biological activity. This is indicated by the geochemical parameters discussed above and plankton, carbohydrate and amino acid analyses (Chen & Xu, 1990). Biological activity in south Asian waters is strongly influenced by monsoons. Monthly averaged wind speed and direction data (Fig. 2a; Royal Observatory, Hong Kong, 1989) suggest two monsoon and two short intermonsoon phases: NE monsoon lasting from October to April, SW monsoon lasting from June to August and intermonsoon phases in May and September. During winter cooler surface water enters the South China Sea through the Taiwan and Bashi Straits coming from the East China Sea and the western Pacific (Lafond, 1966). These water masses induce a counterclockwise surface current pattern (Wyrski, 1961). The incoming cool and nutrient-rich water masses enhance primary productivity.

Similarity increased wind speeds during NE monsoon in November and December (Fig. 2a) stimulate biological activity. Highest fluxes in the shallow trap are correlated with highest wind speeds (Fig. 2). In the Arabian Sea (Nair *et al.*, 1989) wind-induced deepening of the mixed layer and associated input of nutrients into the euphotic zone lead to higher primary productivity. Another important factor stimulating biological productivity might be enhanced introduction of essential trace elements associated with atmospheric dust fallout (e.g. iron: Martin & Fitzwater, 1988). During NE monsoon a high flux period was observed in the shallow trap from November 1987 to February 1988 with distinct maxima in November

(SCS-I-S5) and January (SCS-I-S9).

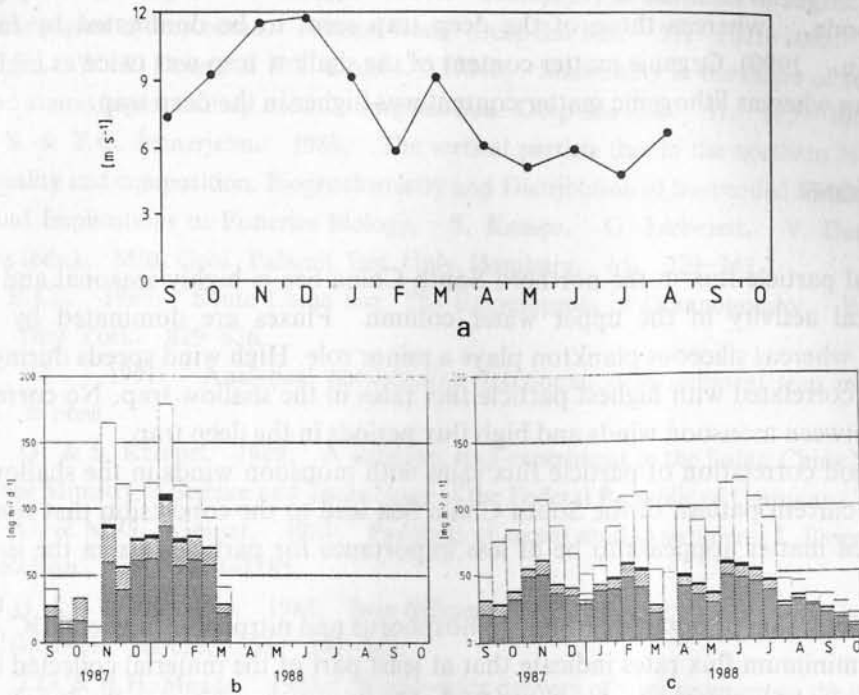


Fig.2 Wind speed data (a) and particle flux rates in the northern South China Sea subdivided into the four main fractions (from bottom to top: CaCO_3 , CH_2O , biogenic opal, lithogenic matter) in (b) 1000 and (c) 3350 m water depth, respectively, in winter 1987 / 1988.

Flux pattern of the deep trap shows less variability than that of the shallow trap and can hardly be correlated with monsoon phases. Considerable compositional changes of the material (Fig.3) show that particle flux in 3350 m water depth is affected by primary productivity in the upper water column, too. The missing correlation of flux patterns, however, delineates that processes different from biologically controlled vertical particle flux also may account for deposition of suspended matter in the deep trap.

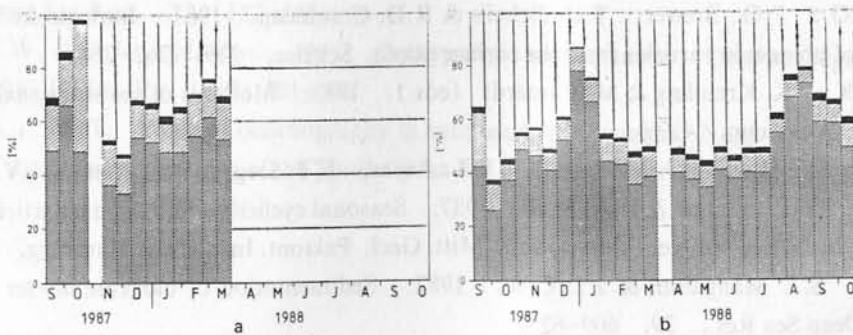


Fig.3 Relative portions of the four main fractions (from bottom to top: CaCO_3 , CH_2O , biogenic opal, lithogenic matter) of particle flux in the northern South China Sea in (a) 1000 and (b) 3350 m water depth, respectively, in winter 1987 / 1988 and summer 1988.

The relative proportions of CaCO_3 and biogenic opal of the deep trap nearly equal that of the shallow trap. CaCO_3 fluxes of the shallow trap seem to be dominated by gastropoda and pteropoda, whereas those of the deep trap seem to be dominated by foraminifera (Chen & Xu, 1990). Organic matter content of the shallow trap was twice as high as that of the deep trap whereas lithogenic matter content was higher in the deep trap.

CONCLUSIONS

Vertical particle flux in the northern South China Sea is highly seasonal and controlled by biological activity in the upper water column. Fluxes are dominated by calcareous plankton, whereas siliceous plankton plays a minor role. High wind speeds during monsoon periods are correlated with highest particle flux rates in the shallow trap. No correlation was observed between monsoon winds and high flux periods in the deep trap.

The good correlation of particle flux rates with monsoon winds in the shallow trap and the surface current pattern of the South China Sea lead to the conclusion that riverine input of suspended matter appears to be of less importance for particle flux in the investigation area.

Less dissolution of organic carbon, phosphorus and nitrogen, higher TOC / TP ratios and higher minimum flux rates indicate that at least part of the material collected in the deep trap was derived from lateral advection. Probably deep water entering the South China Sea through the Bashi Channel carries particulate matter from the western Pacific. The more than 2000 m deep Bashi Channel is the only region where deep water can enter the northern part of the South China Sea.

REFERENCES

- Chen, W.B. & L.Q. XU, 1990: A preliminary study of the sediment trap samples from the South China Sea. A report on the work done at the Institute of Biogeochemistry and Marine Chemistry. University of Hamburg, 70 p.
- Deuser, W.G. & E.H. Ross, 1980: Seasonal change in the flux of organic carbon to the deep Sargasso Sea. *Nature*, 283, 364–365.
- Deuser, W.G., P.G. Brewer, T.D. Jickells & R.D. Commeau, 1983: Biological control of the removal of abiogenic particles from the surface ocean. *Science*, 219, 262–264.
- Grasshoff, K., K. Kremling & M. Eherardt (eds.), 1983: *Methods of seawater analysis*. Verlag Chemie, Weinheim, 419 p.
- Honjo, S., B.J. Hay, S.J. Manganini, V.L. Asper, E.T. Degens, S. Kempe, V. Ittekkot, E. Izdar, Y.T. Konuk & H.A. Benli, 1987: Seasonal cyclicity of lithogenic particle fluxes at a southern Black Sea sediment trap station. *Mitt. Geol. Palaont. Inst. Univ. Hamburg*, 62, 19–39.
- Honjo, S., S.J. Manganini & J.J. Cole, 1982: Sedimentation of biogenic matter in the deep ocean. *Deep Sea Res.*, 29, 609–625.
- Honjo, S. & M. Roman, 1978: Marine copepode fecal pellets: production, preservation and sedimentation. *J. Mar. Res.*, 36, 45–57.
- Honjo, S. & K.W. Doherty, 1988: Large aperture time-series oceanic sediment traps: Design,

- objectives, construction and application. *Deep Sea Res.*, 35, 133–149.
- Ittekkot, V., E.T. Degens & S. Honjo, 1984a: Seasonality in the fluxes of sugars, amino acids and amino sugars to deep ocean, Panama Basin. *Deep Sea Res.*, 31, 1071–1083.
- Ittekkot, V., W.G. Deuser & E.T. Degens, 1984b: Seasonality in the fluxes of sugars, amino acids and amino sugars to deep ocean, Sargasso Sea. *Deep Sea Res.*, 31, 1057–1069.
- Kempe, S. & T.C. Jennerjahn, 1988: The vertical particle flux in the northern North Sea, its seasonality and composition. *Biogeochemistry and Distribution of Suspended Matter in the North Sea and Implications to Fisheries Biology*, S. Kempe, G. Liebezeit, V. Dethlefsen & U. Harms (eds.), *Mitt. Geol. Palaont. Inst. Univ. Hamburg*, 65, 229–268.
- Lafond, E.C., 1966: South China Sea. *The Encyclopedia of Oceanography*, Reinhold Publ. Corp., New York, 829–836.
- Liebezeit, G., 1991: Analytical phosphorous fractionation in sediment trap material. *Mar. Chem.*, in press.
- Liebezeit, G. & S. Kempe, 1989: A sediment trap experiment in the South China Sea. Final Report to the Ministry of Science and Technology of the Federal Republic of Germany, 22 p.
- Liebezeit, G. & M.G. Wiesner, 1989: Pyrolysis of recent marine sediments I. *Biopolymers. Adv. Org. Geochem.*, 16, 1179–1185.
- Martin, J.H. & S.E. Fitzwater, 1988: Iron deficiency limits phytoplankton growth in the northeast Pacific subarctic. *Nature*, 331, 341–343.
- Milliman, J.D. & R.H. Meade, 1983: World-wide delivery of river sediment to the oceans. *J. Geology*, 91, 1–21.
- Mopper, K. & E.T. Degens, 1977: Organic carbon in the ocean: Nature and cycling. *The Global Carbon Cycle*, B. Bolin, E.T. Degens, S. Kempe & P. Ketner (eds.), John Wiley & Sons, Chichester, New York, Brisbane, Toronto, SCOPE, 13, 293–316.
- Nair, R.R., V. Ittekkot, S.J. Manganini, V. Ramaswamy, B. Haake, E.T. Degens, B. N. Desai & S. Honjo, 1989: Monsoon related particle fluxes to the deep Arabian Sea. *Nature*, 338, 749–751.
- Pilskaln, C. & S. Honjo, 1987: The fecal pellet fraction of biogeochemical particle fluxes to the deep sea. *Global Biogeochemical Cycles*, 1, 31–48.
- Royal Observatory, Hong Kong, 1989: Marine climatological summary charts for the South China Sea 1985. Royal Observatory, Hong Kong, 137 p.
- Shanks, A. L. & J.D. Trent, 1980: Marine snow: Sinking rates and potential role in vertical flux. *Deep Sea Res.*, 27, 137–143.
- Silver, M.W. & A.L. Alldredge, 1981: Bathypelagic marine snow: Deep sea algal and detrital community. *J. Mar. Res.*, 39, 501–530.
- Wyrtki, K., 1961: Physical oceanography in southeast Asian waters. Naga report, scientific results of marine investigations of the South China Sea and the Gulf of Thailand, 1959–1961, 2.

GEOCHEMISTRY AND THEIR GENESIS OF RARE EARTH ELEMENTS OF FERROMANGANESE NODULES AND CRUSTS FROM THE SOUTH CHINA SEA

BAO GENDE & LI QUANXING

Second Institute of Oceanography, SOA, Hangzhou, China

ABSTRACT

Based on the X-ray fluorescence spectrum analysis of 15 rare earth elements in 6 ferromanganese nodules and 5 ferromanganese crusts from the South China Sea, their abundances, distribution patterns, sources and relationships with associated elements are discussed in detail in this paper. The results show that: 1) The average abundance of rare earth elements in ferromanganese nodules and crusts is 1.625 g/kg and 2.167 g/kg respectively, which is 1–2 times, 5–6 times and 15–20 times higher than that in the Pacific, in the sediments of the North Pacific and the South China Sea, respectively; 2) The distribution patterns of rare earth elements standardized by the globular aerolite in ferromanganese nodules and crusts are basically similar, that is, Ce is positively abnormal and Eu is in deficit slightly; 3) The relationships between rare earth elements and associated elements, sediments and rocks show that the source of rare earth elements in ferromanganese nodules and crusts have mainly come from slow deposition caused by weathering and leaching of medium acidic rock of the South China Sea.

INTRODUCTION

It is well known that the rare earth element of sediment, rock or ferromanganese nodule in oceanic floor can provide a lot of geological information. So such researches on source of sediment and formative mechanism of ferromanganese nodule are made by Wang *et al.* (1982, 1984), Gu *et al.* (1989), Zhao *et al.* (1990), Courtois and Claver (1980), Goldberg *et al.* (1963) and Piper (1974).

In order to study the geochemistry, formative mechanism and environment of ferromanganese nodules and crusts of the South China Sea, 15 rare earth elements out of the samples from 11 stations are identified by X-ray fluorescence spectral analysis. Meanwhile a comparison between the ferromanganese nodules, sediments of the South China Sea and the North Pacific has been made, and a formative mechanism of ferromanganese nodules and crusts has been raised. The samples were collected by Dreget Dregehammer and Piper Drege during 1987 cruise. Sampling stations and some parameters of ferromanganese nodules and crusts are provided by SIO, SOA (1989).

CHARACTERISTICS OF CONCENTRATION AND DISTRIBUTION

It can be seen from Table 1 that Σ REE (rare earth elements) in ferromanganese nodules is

higher than that in crusts in the South China Sea, and its Σ REE in ferromanganese nodules of the North Pacific, over 5 times higher than that in sediments of the North Pacific and over 10 times higher than that in sediments of the South China Sea, respectively. So rare earth elements of ferromanganese nodules and crusts from the South China Sea may be one of the potential resources of rare earth elements. As for the comparison between ferromanganese nodules and crusts, obviously, their common characteristic is that Σ Ce Light REE is higher than that Σ Heavy REE. This is in agreement with that of rare earth elements of ferromanganese nodules, sediments of the North Pacific and sediments and rock of the South China Sea. It is typical rare earth element of continental crust. However, the difference between nodules and crusts is that concentrating degree of LREE in nodules is higher than that in crusts and its Σ Ce / Σ Y is close to that of granite and far from that of sediments in the South China Sea. The result hints that there may be a relationship between rare earth elements in ferromanganese nodules (crusts) and medium acidic rock in the South China Sea.

Table 2 shows that: 1) Σ Ce is obviously richer than Σ Y in both KD17 ferromanganese crust and KD35 ferromanganese nodule of every layer; 2) In KD17 ferromanganese crust, Σ REE is higher on surface than in deep layer, while the situation in KD35 ferromanganese nodule is on the contrary, and so are Σ Ce, Σ Y, and Σ Ce / Σ Y as well. Σ Ce is approximately 4 times of Σ Y which is close to the ratio of rare earth elements in sediments of China continental shelf (Zhou *et al.*, 1990); 3) The relative difference between the highest and lowest concentration of Σ REE is over one third in both ferromanganese nodules and crusts, that is, the concentration range in nodules is from 1880.2 to 2526.3 mg / kg, and in crusts from 1583.5 to 2566.5 mg / kg. In their forming and growing processes, ferromanganese crusts and nodules may be caused either by environmental variation or by the concentration change of clastic rock contained in nodules and crusts.

DISTRIBUTION PATTERNS OF RARE EARTH ELEMENTS OF FERROMANGANESE NODULES AND CRUSTS

The distribution patterns of rare earth elements of ferromanganese nodules and crusts (Fig.1) are most similar, both of which are of negative slopes that is light REE is relatively concentrated.

Ce is in positive abnormality, and Eu in more or less deficit. The distribution pattern is obviously gentle and different from ferromanganese nodules of the North Pacific (Fig.1c) and sediments of the South China Sea and the North Pacific (Fig.1d).

As is well known, rare earth elements possess very similar chemical nature, but with the increase of atomicity, they can be separated from each other by variation of physical and chemical environments, of which the most obvious separation is that of LREE from HREE and of variable elements Ce (Ce^{3+} , Ce^{4+}) from Eu (Eu^{2+} , Eu^{3+}). Thus, the affection of sea water on ferromanganese nodules and crusts of the South China Sea is larger than that in the North Pacific and sediments of the South China Sea. On the contrary, the affection of early diagenesis of sediments on ferromanganese nodules of the North Pacific is larger than that of the South China Sea (Elderfield *et al.*, 1981). It also indicates that source of rare earth elements of ferromanganese nodules and crusts of the South China Sea may be different from the ferromanganese nodules of the North Pacific and sediments of the South China Sea.

Table 1 Concentration of rare earth elements in ferromanganese nodule (crust), sediment and rock of the South China Sea (mg/kg)

Samples	No.	La	Ce	Pr	Nd	Sm	Eu	Gd	Tb	Dy	Ho	Er	Tm	Yb	Lu	Y	ΣREE	ΣCe	ΣY	$\frac{\Sigma Ce}{\Sigma Y}$	Source
Ferromanganese crusts of the South China Sea	5	165.80	917.00	41.00	132.60	44.00	12.76	48.00	9.74	53.00	7.30	22.12	5.44	19.60	4.98	141.80	1625.14	1313.16	311.98	4.21	this paper
Ferromanganese nodules of the South China Sea	6	233.00	1315.50	52.83	170.50	52.83	13.95	55.83	7.65	59.00	5.82	22.00	4.95	19.00	4.87	149.17	2166.90	1838.61	328.29	5.60	this paper
Ferromanganese nodules of the North Pacific	5	120.54	383.66	38.39	124.45	31.75	7.72	30.21	5.24	29.33	5.35	15.26	2.40	14.81	2.24	112.77	924.46	706.51	217.95	3.24	Piper (1974)
Sediments of the North Pacific	1	87.06	134.57	23.65	99.37	31.22	6.03	25.90	4.27	25.23	5.11	14.26	2.27	13.18	2.13	158.02	632.27	381.90	250.37	1.53	Piper (1974)
Sediments of the South China Sea	53	28.63	55.80	6.31	22.65	4.71	1.09	4.27	0.68	4.00	0.82	2.43	0.34	2.18	0.43	21.81	156.15	119.19	36.96	3.22	Bao (1990)
Granite of the South China Sea	1	18.01	84.36	3.35	11.10	1.69	0.92	0.66	0.06	1.13	0.03	0.44	0	0.24	8.12	13.00	143.11	119.43	23.68	5.04	this paper
Gabbro of the South China Sea	1	27.00	101.26	7.97	38.03	10.90	9.29	10.56	2.74	13.87	6.94	7.91	1.82	6.67	2.31	47.95	295.22	194.45	100.77	1.93	this paper

Table 2 Concentration of rare earth elements in different layer of ferromanganese nodules and crusts from the South China Sea (mg / kg)

Stations and layers	Σ REE	Σ Ce	Σ Y	Σ Ce / Σ Y	Stations and layers	Σ REE	Σ Ce	Σ Y	Σ Ce / Σ Y
KD17-1	2444.30	1986.00	458.30	4.33	KD35-1	1583.50	1257.50	326.00	3.86
KD17-2	1986.90	1553.60	433.30	3.59	KD35-2	1681.90	1385.00	296.90	4.66
KD17-3	2055.10	1625.50	428.60	3.79	KD35-3	2187.80	1789.00	378.80	4.64
KD17-4	1987.30	1536.00	451.30	3.40	KD35-4	2119.10	1672.00	447.10	3.74
KD17-5	2026.20	1562.00	464.20	3.36	KD35-5	2130.90	1711.00	419.90	4.07
KD17-6	1880.20	1520.50	359.70	4.23	KD35-6	2566.50	2225.90	341.50	6.52
KD17-7	2316.20	1890.00	426.20	4.43	KD35-7	2440.60	2096.00	344.60	6.08
KD17-8	2298.70	1847.00	451.70	4.09	KD35-8	2199.70	1716.00	483.70	3.55
KD17-9	2526.30	2040.00	486.30	4.19	KD35-9	1780.00	1411.40	368.60	3.83
KD17-10	2480.10	2013.00	467.10	4.31	KD35-10	2369.70	2036.80	331.70	6.14

Note: KD17, crust; KD35, nodule.

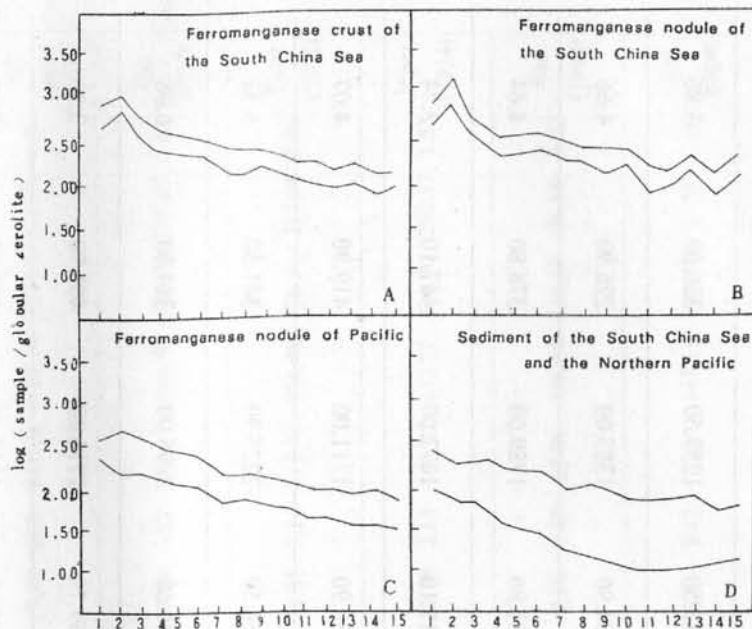


Fig.1 Distribution patterns of rare earth elements of ferromanganese nodules and crusts. 1—La; 2—Ce; 3—Pr; 4—Nd; 6—Sm; 7—Eu; 8—Gd; 9—Tb; 10—Dy; 11—Ho; 12—Er; 13—Tm; 14—Yb; 15—Lu.

The distribution patterns of rare earth elements standardized by globular aerolite in different layers of KD17 ferromanganese crust and KD35 nodule (SIO, SOA, 1989) show that the distribution patterns of rare earth elements of ferromanganese crust of different layer are basically the same. Ce is obviously in positive abnormality and Eu in more or less deficit. This shows that source of rare earth elements may be basically the same during the forming and growing processes of ferromanganese crusts, though Σ REE of every layer is different. The distribution patterns of rare earth elements from 1–5 layer of ferromanganese nodules are similar to those of crusts. Yet, they are obviously different in 6–10 layers. It is necessary further to study whether they are caused by clastic rock, nuclear or the variation of environment of the South China Sea and material source. A lot of investigation information has confirmed that the distribution pattern of rare earth elements can differ with the different material in the nuclear and on the surface of ferromanganese nodules and crusts. Yet, chemical analysis information had shown that the concentration of rare earth elements in clastic rock is less than 2000 mg/kg (Tables 1 and 2) (Goldberg *et al*, 1963, Wildman and Haskin, 1965). Perhaps, the variation of material source of rare earth elements is caused by the variation of sedimentary environment.

SOURCE OF RARE EARTH ELEMENTS OF FERROMANGANESE NODULES AND CRUSTS

Experiment of Absorption REE

KD17 ferromanganese crust and KD35 nodule were soaked by NaCl and $(\text{NH}_4)_2\text{SO}_4$, respectively. The result of chemical analysis indicates that REE in absorption state occupies

0.096% and is similar to absorption REE ore of South China granit (industrial grade is 0.1%). Because sample may change during preparing processes which may cause the decreasing of REE in ion absorption, the absorption REE in ferromanganese nodules and crusts of the South China Sea is over 0.096%. It shows that the rare earth elements in ferromanganese nodules and crusts have existed mainly in ion state instead of in crystal of clay as isomorphism, and are obviously different from the rare earth elements of sediments of the North Pacific, the South China Sea and the China Sea continental shelf (Gu *et al.*, 1989; Zhao *et al.*, 1990). The rare earth elements of ferromanganese and crusts of the South China Sea may mainly absorbed from sea water by the nucleus material.

Relationship between Rare Earth Elements and Associated Elements

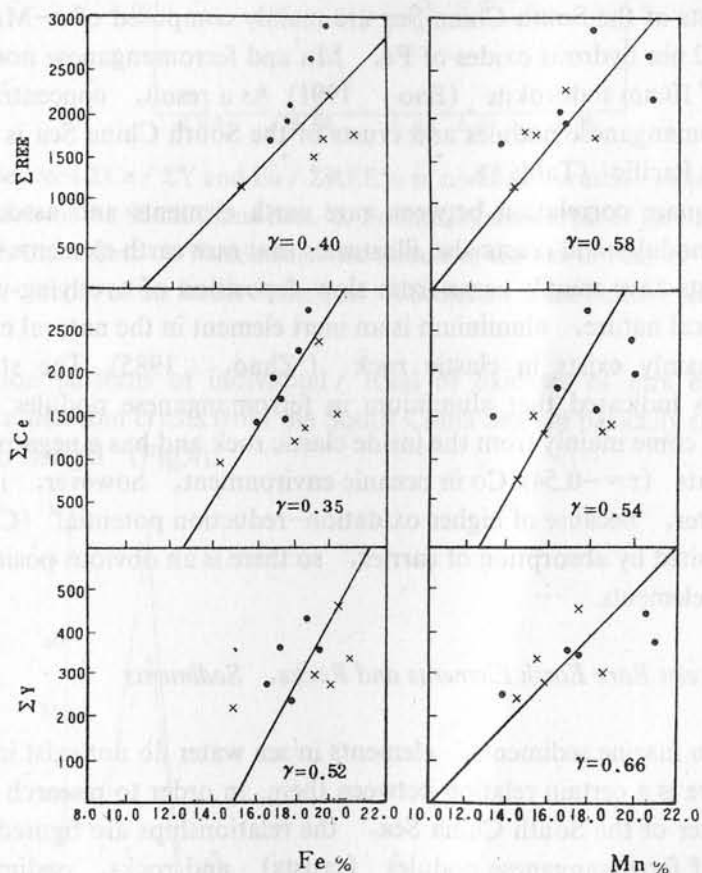


Fig.2 Relationship between REE and Fe, Mn in ferromanganese nodules (crusts).

Fig.2 shows that there is an obvious positive correlation between REE and Fe, Mn, neither ΣY nor ΣCe . This indicates that sources of rare earth elements and Fe, Mn in ferromanganese nodules and crusts are basically similar. The study of element geochemistry of ferromanganese nodules and crusts has confirmed that Fe, Mn in ferromanganese nodules and crusts are mainly from deposition of overlying water, that is, they come from deposition of hydrous oxides of soluble Fe, Mn (Courtois and Claver, 1980; Bao,

1991; Carinneo, 1981). So rare earth elements of ferromanganese nodules and crusts of the South China Sea have mainly come from slow deposition of overlying water. Geochemical experiments have confirmed that Fe, Mn metal ion formed by weathering and leaching of volcanic material can be oxidated by reaction of its solution with fresh sea water before slowly depositing as the nucleus of ferromanganese nodule. Its solution is in the state of colloid and then makes the nodules into ringlike structure. While, deposition of Fe, Mn oxides has accelerated hydrolysis of rare earth elements, that is, Ce^{3+} can be transformed into Ce^{4+} by MnO_2 (Wang *et al.*, 1984). Since Ce^{4+} is easy to deposit, Ce is in obvious positive abnormality (Fig. 1a, b). Therefore, there is an obvious positive correlation between Fe, Mn and ΣREE , ΣCe , ΣY in ferromanganese nodules and crusts caused by hydrous oxides of Fe, Mn which acts both as a catalytic agent of hydrolysis of rare earth elements and as a carrier during the deposition processes of rare earth elements. And also ferromanganese nodules and crusts of the South China Sea are mainly composed of δ - MnO_2 consisting of 2.45 nm and 1.42 nm hydrous oxides of Fe, Mn and ferromanganese nodules of the North Pacific mainly of 10 nm todorokite (Bao, 1991). As a result, concentration of rare earth elements of ferromanganese nodules and crusts of the South China Sea is much higher than that of the North Pacific (Table 1).

The least square correlation between rare earth elements and associated elements of ferromanganese nodules and crusts also illustrates that rare earth elements in ferromanganese nodules and crusts have mainly come from slow deposition of overlying water. For the elemental geochemical nature, aluminium is an inert element in the natural environment, and in general, mainly exists in clastic rock (Zhao, 1985). The study of elemental geochemistry has indicated that aluminium in ferromanganese nodules and crusts of the South China Sea come mainly from the inside clastic rock and has a negative correlation with rare earth elements ($r = -0.54$). Co in oceanic environment, however, is more stable than Mn^{2+} in sea water, because of higher oxidation-reduction potential ($Co^{3+} / Co^{2+} = 1.84$) and can be deposited by absorption of carrier, so there is an obvious positive correlation between rare earth elements.

Relationship between Rare Earth Elements and Rocks, Sediments

Like those in marine sediments, elements in sea water do not exist in an isolated state. Moreover, there is a certain relation between them. In order to research into source of elements in sea water of the South China Sea, the relationships are figured out between rare earth elements of ferromanganese nodules (crusts) and rocks, sediments of the South China Sea and nodules of the North Pacific (Figs.3 and 4).

$\Sigma Ce / \Sigma Y$ in ferromanganese nodules and crusts of the South China Sea is much than that of nodules of the North Pacific (Fig. 3), although ferromanganese nodules and crusts of the South China Sea and nodules of the North Pacific are all in the areas rich in Ce and poor in Eu ($Eu / \Sigma REE\% < 1.00$). The former is larger than 4.50, which is in the same range as granite, and the latter is less than 3.00, and close to that of sediments of the South China Sea and the North Pacific. The result further indicates that source of rare earth elements differs from that of sediments in the South China Sea, and at the same time, they may be formed by weathering and leaching of medium acidic rocks.

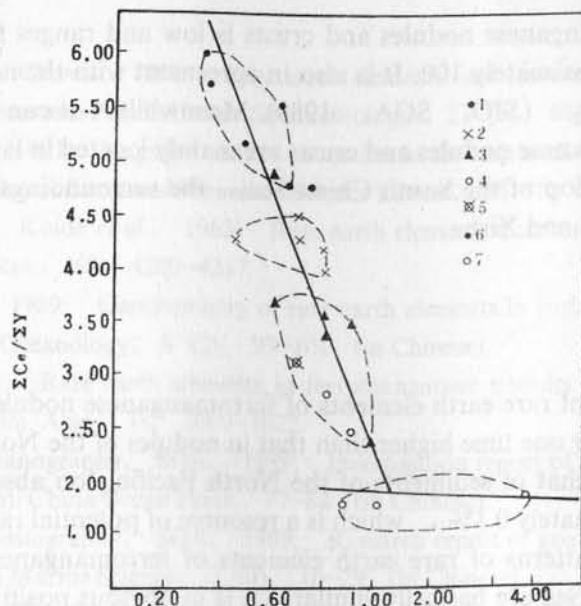


Fig.3 Correlation between $\Sigma Ce / \Sigma Y$ and $Eu / \Sigma REE\%$ in nodules, crusts, sediments and rocks. 1. Ferromanganese nodule of the South China Sea; 2. Ferromanganese crust of the South China Sea; 3. Granite of the South China Sea; 4. Ferromanganese nodule of the North Pacific; 5. Sediment of the South China Sea; 6. Gabbro of the South China Sea; 7. Sediment of the North Pacific.

The distribution patterns of individual / total of oxidates of rare earth elements in ferromanganese nodules and crusts from the South China Sea are basically similar to those of volcanicrocks from Jiangxi (Fig.4).

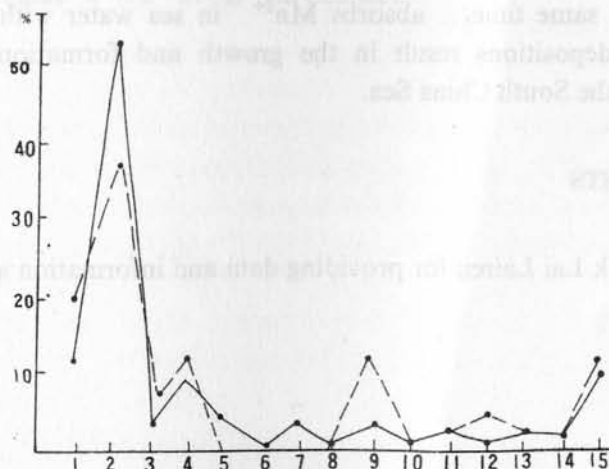


Fig.4 Distribution patterns of rare earth elements of the South China Sea and volcanic rocks of Jiangxi. 1— La_2O_3 ; 2— CeO_2 ; 3— Pr_6O_4 ; 4— Nd_2O_3 ; 5— Sm_2O_3 ; 6— Eu_2O_3 ; 7— Gd_2O_3 ; 8— Tb_4O_7 ; 10— Ho_2O_3 ; 11— Er_2O_3 ; 12— Tm_2O_3 ; 13— Yb_2O_3 ; 14— Lu_2O_3 ; 15— Y_2O_3 .

The result further indicates that rare earth elements of ferromanganese nodules and crusts in the South China Sea are mainly from weathering and leaching of volcanic material. It is in agreement with chemical analysis of the ferromanganese nodules and crusts, that is,

K / Rb of the ferromanganese nodules and crusts is low and ranges from 10 to 223, and most of them are approximately 100. It is also in agreement with the negative correlation between Ni, V and SiO₂ (SIO, SOA, 1989). Meanwhile, it can be confirmed that the areas rich in ferromanganese nodules and crusts are mainly located in large fault zones such as the lower continental slope of the South China Sea, the surroundings of Zhongsha and the area between Zhongsha and Xisha.

CONCLUSIONS

1. Concentration of rare earth elements of ferromanganese nodules and crusts from the South China Sea is over one time higher than that in nodules of the North Pacific, and over five times higher than that of sediments of the North Pacific. Ion absorption rare earth elements occupy approximately 0.1%, which is a resource of potential rare earth ore.

2. Distribution patterns of rare earth elements of ferromanganese nodules and crusts from the South China Sea are basically similar. Ce is in obvious positive abnormality with a negative slope rich in LREE, and Eu deficits in more or less degree. It is typical of rare earth elements of continental crust.

3. The source of rare earth elements of ferromanganese nodules and crusts of the South China Sea may be supposed as the following. A large amount of gas formed during the volcanic eruption reacts on sea water, forming the acidic reducible solution, which carries some Fe, Mn and rare earth elements from the lava during its flowing back through the lava. With the consumption of volcanic gases, the acidity of sea water drops and the concentration of oxygen in sea water increases. Owing to the above factors, the hydrous oxides of iron and manganese (FeOOH, MnOOH) accelerates hydrolysis of rare earth elements in sea water and at the same time, absorbs Mn²⁺ in sea water with such a cycle, the authigenic chemical depositions result in the growth and formation of ferromanganese nodules and crusts of the South China Sea.

ACKNOWLEDGEMENTS

The authors thank Lai Liren for providing data and information and Zhu Ruiming for help.

REFERENCES

- Bao Gende, 1990: Distribution and source of heavy metal in ferromanganese nodules and the relationship between nodules and sedimentary environments in North Pacific. *Ocean. Limn.*, 21 (4), 364-372 (in Chinese).
- Bao Gende, 1991: Main factors study of the controlling geochemical characteristics of ferromanganese nodules, II. Formative mechanism of different geochemical type nodules. *Science in China* (in press).
- Carinneo, B.C., 1981: Question of stability of manganese oxidates in sea water and formation of ferromanganese nodules. *Report, Academy of Sciences of the USSR*, 257 (5), 1217-1220 (in

- Russian).
- Courtois, C. and N. Claver, 1980: Rare earth elements and strontium isotopes of polymetallic nodules from southeastern Pacific Ocean. *Sedimentology*, 27 (6), 687-695.
- Elderfield, H. *et al.*, 1981: Negative cerium anomalies in the rare earth element pattern of oceanic ferromanganese nodules. *Earth and Planetary Science Letters*, 55 (1), 163-170.
- Goldberg, E.D., M. Koide *et al.*, 1963: Rare earth elements distribution in the marine environment. *J. Geophys. Res.*, 68, 4209-4217.
- Gu Senchang *et al.*, 1989: Geochemistry of rare earth elements in surface sediments of the South China Sea. *Tropic Oceanology*, 8 (2), 93-101 (in Chinese).
- Piper, D.Z., 1974: Rare earth elements in ferromanganese nodules and other marine phases. *Geochim. Cosmochim. Acta*, 38, 1007-1022.
- Second Institute of Oceanography, SOA, 1989: Investigation report of ferromanganese nodules of Pacific (1985-1986). China Ocean Press, 77-84 (in Chinese).
- Second Institute of Oceanography, SOA, 1989: Research report of geological science of the South China Sea. *Donghai Marine Science*, 7 (4), 10-29 (in Chinese).
- Wang Xianjue *et al.*, 1982: Geochemistry of rare earth elements in continental shelf sediments of East China Sea. *Geochemistry*, 1, 56-65 (in Chinese).
- Wang Xianjue *et al.*, 1984: Geochemistry of rare earth elements and trace elements in ferromanganese nodules and their genesis. *Ocean. Limn.*, 15 (6), 501-514 (in Chinese).
- Wildman, T. R. and L. Haskin., 1965: Rare earth elements in ocean sediments. *J. Geophys. Res.*, 70 (12), 2905-2910.
- Zhao Yiyang, 1985: Some geochemical patterns of shelf sediments of the China Sea. *Chin. J. Ocean. Limn.*, 3 (2), 200-211.
- Zhao Yiyang *et al.*, 1990: Rare earth elements in continental shelf sediments of the China Sea. *Acta Sedimentologica Sinica*, 8 (1), 37-43 (in Chinese).

MINERALOGY AND GEOCHEMISTRY OF HYDROTHERMAL SILICIC CHIMNEY IN THE MARIANA TROUGH

ZHANG DEYU¹⁾, CHEN SUITIAN¹⁾, TAIBI, N.G.²⁾, WANG GUANRONG¹⁾ & WU SHIY-ING¹⁾

1) *First Institute of Oceanography, SOA, Qingdao, China*

2) *Geological and Paleontological Institute, University Kiel, Germany*

ABSTRACT

Hydrothermal silicic chimneys of the Mariana Trough are chiefly composed of amorphous silica (opal) and pyrite with a small amount of marcasite, barite and quartz.

Based on the mineral association and distribution, it was speculated that the silicic chimneys might be formed by hydrothermal fluid with an initial temperature below 300°C, and that the amorphous silica which comprises the main body of the chimneys might be precipitated when the temperature of the hydrothermal fluid dropped down below 140°C due to conductive cooling or a combination of conductive cooling and seawater / hydrothermal fluid mixing.

INTRODUCTION

Since the end of 1970's when high flows ($2w/m^2$) were discovered in the spreading center of the Mariana Trough (Anderson *et al.*, 1981), the trough has become an important area for investigation of submarine hydrothermalism in the off-ridge area. In recent years, hydrothermal methane plumes with a core concentration of $74 \times 10^{-6} \text{ cm}^3/\text{kg}$ and a temperature anomaly ranging from 0.01–0.02°C were found on some of the small ridge crests in this area (Horibe *et al.*, 1986). Active hydrothermal ventings were first observed in the spreading center of the Mariana Trough by the American scientists in "Alvin" submersible in 1987. All these have confirmed the presence of hydrothermal activity in the Mariana back-arc basin.

In order to understand more about the hydrothermal activity and to collect more hydrothermal products, a joint investigation, the "Sonne" Cruise 57, was carried out in the Mariana Trough by the scientists both from Germany and China in 1988. In this cruise a number of dead hydrothermal chimneys were observed and sampled respectively by using OFOS (ocean floor observation system) and GTV (TV-monitored grab) on its small ridge crests with the water depths of 3600–3700 m (Fig. 1). These chimneys are mostly tree-trunk-shaped and generally 2 m in height and 50–80 cm in diameter. The purpose of the paper is to describe their mineral and chemical compositions, and then to speculate on their formation.

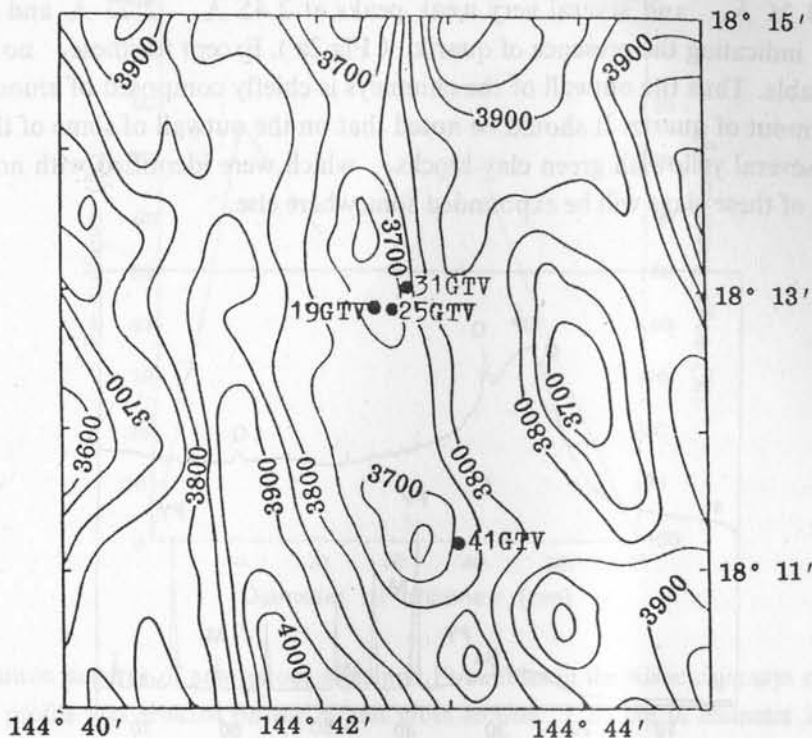


Fig.1 Locations of the hydrothermal silicic chimneys sampled in the Mariana Trough.

METHODS

Samples were taken every 10 cm on the largest cross section of the chimneys, and were washed by distilled water to remove some soluble salts. Afterwards, they were dried under 105°C overnight and then were powdered by grinding.

The samples were analysed on a Philip X-ray diffractometer with a graphite monochromator and Co radiation. The relative content of each mineral was semiquantitatively estimated by measuring the height of its major reflection peak. Some of the samples were polished, and were examined by scanning electron microscope along with other mineral grains. Chemical compositions of the chimneys were determined mainly by means of X-ray fluorescence and electron probe.

RESULTS

Mineralogy

(1) The outwall of the silicic chimneys. As shown in Fig.2a, the outwall of the chimneys gives a broad, but distinct peak centered at about 4.00 Å, which is proper to amorphous silica (opal-A; $\text{SiO}_2 \cdot n\text{H}_2\text{O}$) according to the nomenclature given by Jones and

Segnit (1971). On the broad peak of amorphous silica there are two small distinct peaks at 4.25 \AA and 3.35 \AA , and several very weak peaks at 2.45 \AA , 2.27 \AA and 1.818 \AA , respectively, indicating the presence of quartz (Fig.2a). Except for these, no other peaks were recognizable. Thus the outwall of the chimneys is chiefly composed of amorphous silica with a small amount of quartz. It should be noted that on the outwall of some of the chimneys are scattered several yellowish green clay blocks, which were identified with nontronite. A detailed study of these clays will be expounded somewhere else.

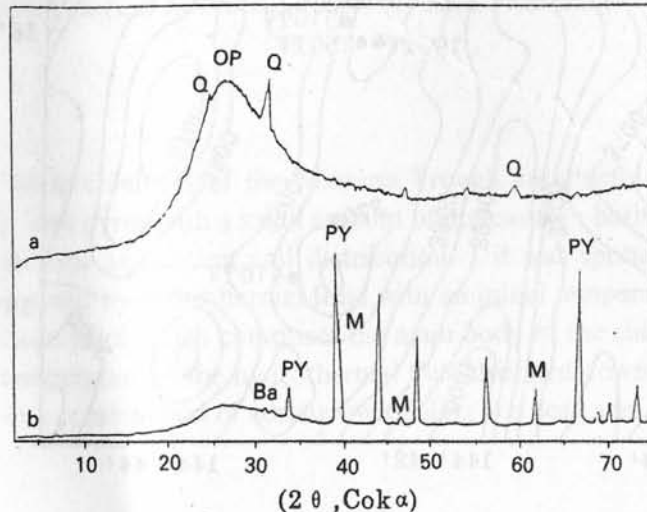


Fig.2 X-ray powder diffractograms of the silicic chimney (31GTV) in the Mariana Trough. a — The outwall of the chimney; b—The inside of the chimney; Q—Quartz; OP—Amorphous silica (Opal-A); PY—Pyrite; M—Marcasite; Ba—Barite.

(2) The inside of the silicic chimneys. X-ray powder diffractin analysis revealed that the inside of the chimney is not only composed of amorphous silica and quartz, but also of Fe sulfides and sulphate mineral (Fig. 2b). Fe sulfides consist of pyrite and small amount of marcasite. Barite is the only sulphate mineral. Semiquantitative estimation indicated that amorphous silica is no longer the most abundant phase in the inner part of the chimney; instead, pyrite becomes more abundant. Scanning electron microscope showed that the pyrite has various morphology (e.g. cubic, spheric, strawberry-like and gel-like), and that the barite is mainly tabular in shape.

(3) Mineral distribution in the silicic chimneys. As shown in Fig. 3, the amorphous silica is dominant ($> 90\%$) in the outwall of the chimney. However, towards the inside of the chimney, its content decreases apparently, being less than 35% in the center of the chimney. On the contrary, no Fe sulfides were identified in the center of the chimney, but about 60% of Fe sulfides mainly represented by pyrite were recognized in the center of the chimney. As to the distributions of quartz and barite, no distinct patterns were observed.

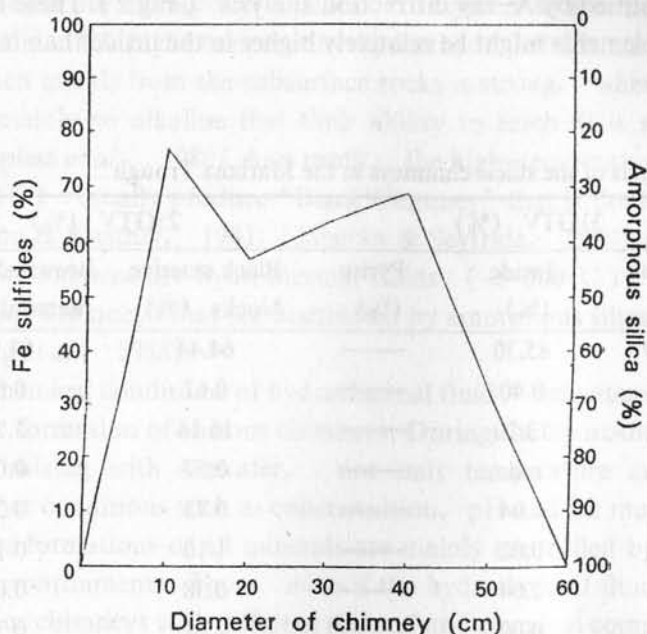


Fig.3 Distribution patterns of amorphous silica and Fe sulfides in the silicic chimneys of the Mariana Trough. This profile was selected on the largest cross section (60 cm in diameter) of chimney 31GTV.

Chemistry

(1) Major elements. Chemical analysis revealed that the contents of SiO_2 and Fe_2O_3 in the chimneys vary greatly from the outwall to the inside. As listed in Table 1, the outwall of the chimneys is almost composed of pure SiO_2 , only with little Fe_2O_3 whereas towards the inside the content of SiO_2 decreases, and the content of Fe_2O_3 increases apparently (Table 1). For other major elements, no significant changes in their contents were observed from the outwall to the inside in most of the chimneys. Such a pattern corresponds well to the mineral distributions mentioned above. However, it should be noted that the chemical compositions may not always be the same among the chimneys found in the Mariana Trough. For example, both brownish yellow materials from the outwalls of chimney 25GTV and 31GTV have similar compositions (Table 1), but black-coloured massive blocks from the inside of the chimney 25GTV have lower content of SiO_2 and higher contents of Fe_2O_3 and other major compounds than that from the inside of the chimney 31GTV (Table 1). This suggests that composition, physicochemical condition and the hydrothermal fluids by which the chimneys were formed, and the hydrothermal differentiation might be different at different places in the Mariana Trough.

As to Fe and S contents in pyrite, no significant differences were observed between chimneys 31GTV and 19GTV (Table 1).

(2) Trace elements. Unfortunately, trace elements were analyzed only for chimney 25GTV. As shown in Table 1, the contents of trace elements in the brownish yellow material are generally lower than those in the black massive blocks. On the contrary, the contents of Cu, Zn and Ni are relatively high in the black massive blocks. However, no Cu- and

Zn-sulfides were identified by X-ray diffraction analysis (Fig.2). These results suggest that the contents of trace elements might be relatively higher in the inside than in the outwall of the chimneys.

Table 1 Chemical analysis of the silicic chimneys in the Mariana Trough *

Chimneys	31GTV (%)		25GTV (%)			19GTV
	Outwall (%)	Inside (%)	Pyrite (%)	Black massive blocks (%)	Brownish yellow material (%)	Pyrite (%)
SiO ₂	94.77	85.30	—	64.44	91.06	—
Al ₂ O ₃	0.13	0.40	—	0.62	0.62	—
Fe ₂ O ₃	3.32	13.20	—	16.16	3.79	—
MnO	n.d.	n.d.	—	0.57	0.01	—
CaO	0.03	0.04	—	0.73	0.24	—
MgO	0.01	0.02	—	1.10	0.15	—
K ₂ O	0.03	0.04	—	0.38	0.08	—
Na ₂ O	0.04	0.09	—	2.66	0.34	—
TiO ₂	0.01	0.01	—	0.06	0.01	—
P ₂ O ₅	0.03	0.02	—	—	—	—
Ba	0.815	0.348	—	—	—	—
Fe	—	—	48.43	—	—	45.82
S	—	—	51.51	—	—	54.17
Total	99.09	99.95	99.99	86.72	96.30	99.99
			ppm			
Cu	—	—	—	72	2.5	—
Zn	—	—	—	77	2.0	—
Ni	—	—	—	34	<1	—
Zr	—	—	—	30	29	—
Cr	—	—	—	<10	<10	—
Y	—	—	—	7	3	—

* The results of the outwall and the inside of chimney 31GTV are averages of 6 samples.

n.d.—not determined

THE FORMATION OF THE SILICIC CHIMNEYS OF THE MARIANA TROUGH

Hydrothermal chimneys on the ocean floor are formed by submarine hydrothermal activities with changes in the physicochemical conditions when the hydrothermal fluids with high temperature under the ocean floor erupt along the ventings or cracks of basaltic rocks. Therefore, mineral and chemical compositions of the chimneys must be closely related to compositions of the hydrothermal fluids and to the physicochemical conditions of hydrothermal fluid / seawater system.

The compositions of hydrothermal fluids are directly related to temperature. The high-temperature hydrothermal fluids are commonly rich in multiple metals, whereas the

low-temperature ones are mainly rich in silica (Haymon & Kastner, 1981; Herzig *et al.*, 1988). That is, the high-temperature hydrothermal fluids are usually so acidic that their ability to leach metals from the subsurface rocks is strong, whereas the ones with low temperature are mainly so alkaline that their ability to leach Si is strong (Janecky & Seyfride 1984; Spiess *et al.*, 1980). As a result, the high-temperature hydrothermal fluids (normally $> 350^{\circ}\text{C}$) usually produce "Black Chimney" that is dominated by Cu-Zn-Fe sulfides (Haymon & Kastner, 1981; Janecky & Seyfride, 1984). On the contrary, the moderate- or low-temperature hydrothermal fluids ($< 300^{\circ}\text{C}$) tend to form "White Chimney" or "Silica Chimney" that are dominated by amorphous silica (Haymon & Kastner, 1981; Herzig *et al.*, 1988).

The physicochemical conditions of hydrothermal fluid / seawater system play a very important role in the formation of various chimneys. During the hydrothermal fluids upwelling or erupting and mixing with seawater, not only temperature and pressure must be changed, but other conditions such as concentration, pH and Eh must be changed as well. As we know, the formations of all minerals are mainly controlled by the physicochemical conditions of the environments. Thus, even if the hydrothermal fluids are cognate, they will produce various chimneys with different mineral and chemical compositions due to variations in physicochemical conditions (Haymon & Kastner, 1981; Herzig *et al.*, 1988).

As mentioned above, the chimneys of the Mariana Trough are mainly composed of amorphous silica and pyrite with a small amount of marcasite, barite and quartz. No Cu- and Zn-sulfides were recognized. Such a mineral association differs distinctly either from the "White Chimney" discovered on the East Pacific Rise (EPR), which contains a small amount of Zn sulfides such as sphalerite or wurtzite (Haymon & Kastner, 1981), or from the "Silica Chimney" found in the Galapagos spreading center, which contains no sulfides (Herzig *et al.*, 1988), and even from the "Black Chimney". This suggests that the silicic chimneys of the Mariana Trough might be formed by a kind of hydrothermal fluid with an initial temperature between those of the hydrothermal fluids by which the "White Chimney" and the "Silica Chimney" are formed.

Recent studies on the active ventings found on the EPR have revealed that the active "black smoking" has a temperature as high as 350°C and the active "white smoking" has a temperature of 300°C (Haymon & Kastner, 1981; Janecky & Seyfride, 1984; Spiess *et al.*, 1980). As to the "Silica Chimney", the initial fluid temperature was supposed to be about 175°C , according to the oxygen isotope determination and the relation between temperature and SiO_2 solubility (Herzig *et al.*, 1988). It is, therefore, reasonable that the initial fluid temperature of the silicic chimneys of the Mariana Trough might be lower than 300°C . Taking the formation temperature of pyrite (about $280\text{--}290^{\circ}\text{C}$) into account (Janecky & Seyfride, 1984), the temperature supposed above could be possible.

As to the lack of Cu, Zn sulfides in the chimneys of the Mariana Trough, there may be two possibilities: (1) the initial fluid temperature could have been too low to leach enough Cu and Zn metals from the subsurface rocks; (2) the initial fluid temperature may be very high, but it had been greatly lowered before reaching the ocean floor, thus leading to an early subsurface precipitation of Cu, Zn sulfides.

Amorphous silica is the major component of the silicic chimneys of the Mariana Trough. It is, therefore, necessary to learn its formation before explaining the formation of the chimneys. It is generally thought that the formation of amorphous silica is closely related to

SiO₂ solubility, which in turn depends on temperature and pressure (Herzig *et al.*, 1988; Janecky & Seyfride, 1984). So far as the water depth (3600–3700 m) of the small ridge crests is concerned in the spreading center of the Mariana Trough, the pressure can be regarded as a constant. Thus, SiO₂ solubility is mainly related to temperature. Generally, SiO₂ become insoluble with decrease in temperature (Janecky & Seyfride, 1984). According to previous studies on SiO₂ solubility–temperature relations (Herzig *et al.*, 1988; Walther & Helgeson, 1977; Von Damm & Bischoff, 1987), hydrothermal fluid saturated with quartz at 300°C and 500 bars will be saturated with amorphous silica at about 140°C and 260 bars. As above-mentioned, the initial fluid temperature of the silicic chimneys of the Mariana Trough was supposed to be lower than 300°C. If it were so, the formation temperature of the amorphous silica would be less than 140°C. The way of temperature decrease, however, may affect the precipitation of amorphous silica.

The simple mixing between normal seawater and hydrothermal fluid with initial temperatures between 175°C and 350°C can not cause supersaturation and precipitation of amorphous silica. But, conductive cooling or combination of conductive cooling and seawater / hydrothermal fluid mixing can lead to supersaturation and precipitation of amorphous silica at any temperatures between 40°C and 193°C. The supposed temperature for the silicic chimneys of the Mariana Trough possibly occurs under the condition of pure conductive cooling and may be the highest one in precipitation of amorphous silica. If the combination of conductive cooling and seawater / hydrothermal fluid mixing is taken into account, formation temperature of the amorphous silica will be much lower than 140°C.

The distribution pattern of the amorphous silica mentioned above may suggest that the formation of this silicate phase probably follows a model shown in Fig.4. This model can be explained as the followings.

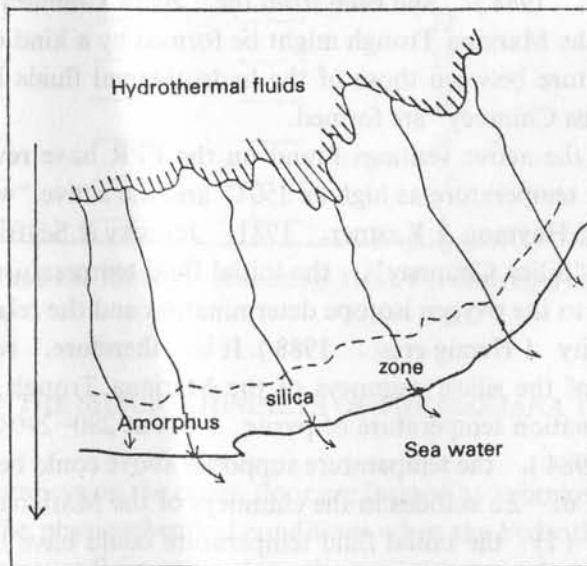
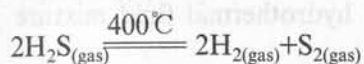


Fig.4 A possible model for the formation of amorphous silica in the silicic chimneys of the Mariana Trough.

When rising along the tubes of chimney, hydrothermal fluid with an initial temperature

of about 300°C percolates sluggishly through the porous wall of the chimney from the inside to the outside. Meanwhile, the seawater normally with 2°C percolates from the outside to the inside. Thus a mixture of seawater / hydrothermal fluid is formed. Because the fluid temperature of the inside of the chimney is always higher than that of the outside of the chimney, heat diffusion or so-called conductive cooling must occur, resulting in heat loss gradually from the inside toward the outside of the chimneys. When reaching the out-most-side of the chimney the heat is considerably lost due to hot solution. Therefore, it is most likely that supersaturation and precipitation of amorphous silica occur at the outwall of the chimney. Some of the amorphous silica may recrystallized into quartz due to the continuous reaction of hydrothermal fluid.

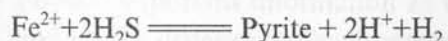
Pyrite is generally considered to be precipitated from the hydrothermal fluid with high concentration of H₂S, slightly high value of Eh and a temperature of 280–290°C (Janecky & Seyfride, 1984). If the fluid temperature is higher than 400°C, pyrite will not be formed due to the dissociation of H₂S:



When the fluid temperature decreases, however, H₂S begins to dissolve into the hot solution and to ionize:



With continuous decrease of fluid temperature, the number of S²⁻ anions will increase gradually as the concentration of H₂S increases. If a large amount of Fe is present, pyrite will be formed:



The formation of pyrite also indicates that the initial fluid temperature of the silicic chimneys of the Mariana Trough may be less than 300°C.

Barite is usually formed in an oxido-environment and under the condition of low temperature, and commonly associated with amorphous silica in hydrothermal chimneys (Haymon & Kastner, 1981). The presence of barite and its distribution feature in the silicic chimneys of the Mariana Trough suggest that it might be a post-product formed after the formation of the chimney.

CONCLUSIONS

The hydrothermal chimneys of the Mariana Trough are silicic ones distinctly different either from the "Black Chimney" and "White Chimney" discovered on the EPR, or from the "Silica Chimney" found in the Galapagos spreading center both in mineralogy and chemistry. Mineralogically, these chimneys mainly consist of amorphous silica (opal), even with a

large amount of pyrite and a small amount of marcasite, barite and quartz. Chemically, they are dominated by SiO_2 , followed by Fe_2O_3 and minor amount of other chemical elements. From the outwall to the inside of the chimneys, the amorphous silica tends to decrease (with almost pure silica in the outwall and less than 35% in the inside), whereas the Fe sulfides mainly represented by pyrite tend to increase (with no Fe sulfides in the outwall and about 60% in the inside). The distribution patterns of SiO_2 and Fe_2O_3 correspond well to those of amorphous silica and Fe sulfides.

Although the formation of the silicic chimneys of the Mariana Trough have been discussed, no precise conclusions are drawn due to the lack of some necessary evidences. But, based on their mineral associations and distribution patterns, it was speculated that initial fluid temperature of the silicic chimneys of the Mariana Trough might be less than 300°C and the formation temperature of the amorphous silica would be much lower than 140°C . Moreover, the precipitation of amorphous silica is mainly due to the heat loss caused either by conductive cooling or by a combination of conductive cooling and seawater / hydrothermal fluid mixing during the sluggish percolation of the seawater / hydrothermal fluid mixture through the porous wall of the chimneys.

REFERENCES

- Anderson, R.N., M.A. Hobert & S. Uyeda, 1981: Heat flow and hydrothermal conduction in the oceanic crust of the Mariana Trough (abs.). American Geophysical Union Chapman Conference Abstract Volume.
- Haymon, R.M. & M. Kastner, 1981: Hot spring deposits on the East Pacific Rise at 21°N : Preliminary description of mineralogy and genesis. *Earth Planet. Sci. Lett.*, 53, 363–381.
- Herzig, P.M., K.P. Beeker, P. Stoffers, H. Backer & N. Blum, 1988: Hydrothermal silica chimney fields in the Galapagos spreading center at 86°W . *Earth Planet. Sci. Lett.*, 89, 261–272.
- Horibe, Y., K. Kim & H. Craig, 1986: Hydrothermal methane plumes in the Mariana back-arc spreading center. *Nature*, 324, 131–133.
- Janecky, D.R. & Jr. W.E., Seyfride, 1984: Formation of massive sulfide deposits on oceanic ridge crests: Incremental reaction models for mixing between hydrothermal solution and seawater. *Geochim. et Cosmochim. Acta*, 48, 2723–2738.
- Jones, J.B. & F.R. Segnit, 1971, The nature of opal. 1, Nomenclature and consistent phases. *J. Geol. Soc. Aust.*, 18, 57–68.
- Spies, F.N., K.C. Macdonald *et al.*, 1980, East Pacific Rise: Hot springs and geophysical experiments. *Science*, 207, 1421–1432.
- Von Damm, K.L. & J.L. Bischoff, 1987: Chemistry of hydrothermal solutions from the Southern Juan de Fuca Ridge. *J. Geophys. Res.*, 92, 334–346.
- Walther, J.V. & H.C. Helgeson, 1977: Calculation of the thermodynamic properties of aqueous silica and the solubility of quartz and its polymorphs at high pressures and temperatures. *Amer. J. Sci.*, 277, 1315–1351.

CHEMICAL CHARACTERIZATION OF HYDROCARBONS IN SEDIMENTS FROM THE SOUTH CHINA SEA

TANG YUNQIAN¹⁾, ZHENG SHILONG¹⁾, LIU KEWEN¹⁾, SHI JIYANG²⁾, XU LIAN³⁾ & WONG, H.K.⁴⁾ & LIEBEZEIT, G.⁵⁾

- 1) *Second Institute of Oceanography, SOA, Hangzhou, China*
- 2) *Institute of Geochemistry, Chinese Academy of Science, China*
- 3) *Central Laboratory of Petroleum Geology, Ministry of Geology and Mineral Resources, China*
- 4) *Institute of Biogeochemistry and Marine Chemistry, University of Hamburg, Germany*
- 5) *National Park Administration, Wilhelmshaven, Germany*

ABSTRACT

Core 37KL contains 2-methylalkane (iso), 3-methylalkane (anteiso), as well as methy, n-dodecane cyclohexane, 4-methyl, 5-methyl and 6-methyl compounds. The content of compounds of the phenanthrene series is more than 50% of the total amount of polycyclic aromatic hydrocarbons. The isomeric end points of 5 α (H), 14 α (H), 17 α (H)-cholestane and 5 α (H), 14 β (H), 17 β (H)-isocholestane are 1.4–2.3 : 1. The ratio of 20R-cholestane to 20S-cholestane is less than 1. The epimeric value of C₃₁ hopane 22S / 22S+22R has not yet reached its equilibrium value.

INTRODUCTION

Various organic compounds such as n-alkanes, isoprenoids, steranes and terpanes provide important information as the source and diagenesis of sedimentary organic matter and on the depositional environment. For example, organic geochemistry at the molecular level offers new possibilities in the reconstruction of past depositional environments. Also the use of biological markers in the assessment of the maturity of sediments is firmly established (Mackenzie *et al.*, 1980; Mackenzie, 1984). In recent years, the distribution of aromatic compounds in crude oil and in the organic extracts of sedimentary rocks and coals are being increasingly applied to study on thermal maturation.

The aim of study is to characterize the n-alkane, sterane and terpane compounds in core samples from the South China Sea. In addition, iso-alkanes and polycyclic aromatic hydrocarbons have also been studied.

METHODS

Sample Collection and Preparation

The samples were collected during cruise 50 of the R / V Sonne in July–September, 1987, in the South China Sea by means of a Kasten corer (15 × 15 × 575–1150 cm). The

sampling stations were: 29KL—18° 26.08' N, 115° 59.22' E, core length 993 cm, water depth 3766 m; 37KL—18° 54.60' N, 115° 45.78' E, core length 833 cm, water depth 2695 m; 91KL—14° 38.3' N, 115° 7.32' E, core length 770 cm, water depth 4282 m.

The sediment samples were freeze-dried and crushed, 1:1 methylene chloride and methanol mixture are used. The extraction took place in a Soxhlet extractor. They were then treated with copper pellets to remove sulfur. The alkane fractions were separated by thin-layer and then analyzed using gas chromatography and gas chromatography-mass spectrometry.

Another extract of the mixture was separated by column chromatography using silica gel, the aromatic fraction was eluted with benzene and then analyzed using high performance liquid chromatography.

Analysis

Gas chromatography is performed by using a Varian 3700 instrument equipped with a FID detector and a quartz spring OV-1 column. It was the carrier gas.

Gas chromatography-mass spectrometry was carried out with a Finnigan-MAT instrument, the column was fitted with a quartz spring SE 54 column. Electron impact was at 70 eV. The mass spectral data were acquired and processed using an INCOS data system at 2 seconds intervals.

High performance liquid chromatography was performed in the reverse phase mode using a Varian 5060 type MCH-5 ODS. Detection was accomplished with a UV-100 ultraviolet detector. Data was collected and processed by a 3390A data system.

RESULTS AND DISCUSSIONS

N-Alkanes and Isoprenoids

The n-alkanes ranged from C₁₄ to C₃₃, main peaks occurred at C₁₇, C₂₅, C₂₇ and C₂₉. In addition, a series of iso compounds were present: i-C₁₆, i-C₁₈, i-C₁₉ and i-C₂₀. The carbon preference index (CPI) ranged from 1.34–2.49 for core 29KL and 1.70–2.28 for core 91KL respectively. The ratio of light to heavy hydrocarbons ($\sum C_{21}^- / \sum C_{22}^+$) was 0.26–1.51 (29KL) and 0.25–0.47 (91KL), for the two sections 372–400 cm and 772–800 cm of core 29KL, these ratios were particularly high, viz. 1.06 and 1.51. As a whole, the distribution preference of low molecular weight alkanes was lower than that of high molecular weight alkanes. The lower molecular weight compounds are derived primarily from marine organisms, while the high molecular weight compounds come from terrestrial vascular plants or other continental organic matter.

The South China Sea has semipelagic sediments, the terrestrial particulate matter which is in part transported by turbidity current (Li, 1987). The clay mineral assemblage has both a terrigenous component and a component dominated by volcanic activity and insular influence. The former component is rich in illite, followed by chlorite, montmorillonite and kaolinite. The latter is dominant in illite, with montmorillonite, chlorite and kaolinite as subsidiary minerals. The fact that illite is particularly abundant in all samples suggest that the

clay minerals of the South China Sea are derived largely from the Asian continent. Core 29KL is more abundant in spore pollen than 91KL. The spore pollens are made up of both arbor and non-arbor assemblage. This could be due to the fact that station 91KL was far away from land and was affected by tidal currents and turbidity currents.

From Table 1 it can be seen that the ratios of light to heavy hydrocarbons in the two cores are low, suggesting that the lower molecular weight alkanes may easily undergo biodegradation. Wehner *et al.* (1986) suggested that n-alkanes are selectively utilized by microorganisms under condition of limited oxygen and nitrogen. Two sections in the 29KL core have high ratios of light to heavy hydrocarbons. From nutrient salt studies of interstitial water, the atomic ratios of N/P (N is the total nitrogen including nitrates, nitrites and ammonium salts) ranges from 2 to 10 from surface to 307.5 cm, while at 357.5 cm depth (372 cm near station 29KL), it reaches an abnormally high value of 20. This may imply deposition by turbidity currents. In addition, at a depth of 807.5 cm (800 cm near station 29KL), the N/P ratio was 18, these characteristically high N/P ratios may be related to plankton growth, for which nitrate salts are necessary. The oxidative decomposition of plankton remains regenerated nitrogen in the order of NH_4^+ , NO_2^- and NO_3^- , with nitrate as the end product. The chemical species composition of nitrogen is determined mainly by the type of marine organisms and the oxidative decomposition of organic matter.

Table 1 Analysis of n-alkanes

Depth (cm)	Pr/Ph	Pr/nC ₁₇	Ph/nC ₁₈	Main peak		L* main peak	CPI $\sum \text{C}_{21} / \sum \text{C}_{22}^+$	
				L*	H**	H** main peak		
29KL								
22-50	1.56	0.76	0.62	17	25	0.90	1.42	0.66
175-200	1.64	0.69	0.69	17	31	0.40	2.44	0.36
372-400	1.73	0.74	0.65	17	25	1.19	1.99	1.06
572-600	1.41	0.82	0.68	17	25	0.76	2.36	0.67
772-800	1.38	0.58	0.84	17	25	1.92	1.34	1.51
972-993	1.32	0.40	0.52	17	31	0.30	2.49	0.26
91KL								
0-100	1.13	0.87	0.62	19	27	0.62	1.70	0.47
100-194	1.02	0.84	0.87	21	27	0.54	2.28	0.35
194-294	0.91	0.80	0.78	19	23	0.62	1.98	0.4
294-394	1.40	0.81	0.69	18	23	0.46	2.25	0.43
394-494	0.76	0.88	0.88	21	23	0.43	1.95	0.25
494-594	0.98	0.74	0.65	21	23	0.50	1.75	0.42
594-694	0.99	0.88	0.79	21	27	0.35	1.79	0.33
694-770	1.01	1.06	0.75	22	25	0.35	1.59	0.34

* Low molecular weight hydrocarbons

** High molecular weight hydrocarbons

Pristane (2, 6, 10, 14-tetramethylpentadecane) and phytane (2, 6, 10, 14-tetramethylhexadecane) are the products of phytanol (from chlorophyll) under different Eh condition: pristane is formed in an oxidizing environment, while phytane is

formed by hydrogenation and dehydration under reducing conditions. Thus their relative contents may be used as an indicator of the depositional environment. The Pr/Ph (pristane/phytane) ratio of 29KL is greater than 1. This reflected the fact that pristane comes directly from biological molecules prior to phytane. The total organic carbon content of 29KL lies in the range 0.29–0.94%. This suggests that the decomposition of organic matter takes place under oxidizing conditions. The Eh, pH and Fe^{+++}/Fe^{++} ratio in the central part of the South China Sea indicate that the sediment has inherited the oxidizing properties of the deep water mass of the South China Sea. In these areas the sediment has stronger oxidizing properties.

Fig. 1 and Table 2 gives the distribution of isoalkane compounds in the core 37KL, the biosynthetic isocompounds (2-methyl) and anteiso compounds (3-methyl) lie in the ranges 32–40% and 33–37% respectively. The distribution of carbon number is from C_{16} to C_{21} . Anteiso compounds are abundant especially in the two layers 0–22 cm and 22–50 cm, but 7-methyl heptadecane and 8-methyl heptadecane which are present in fresh water plankton are absent. 2-methyl and 3-methyl carboxylic acids are widespread in lipids of bacteria. Isoalkanes may come from hydroxylation of branched chain unsaturated the hydrocarbons, or the decarboxylation and dehydroxylation of carboxylic acid or fatty alcohol which contain side chains (Kaneda, 1977). Although the study of iso-alkanes is inferior to that of n-alkanes, it provides valuable information on the palaeoenvironment and an interpretable record of the biochemistry of the primitive life forms (Summons, 1987).

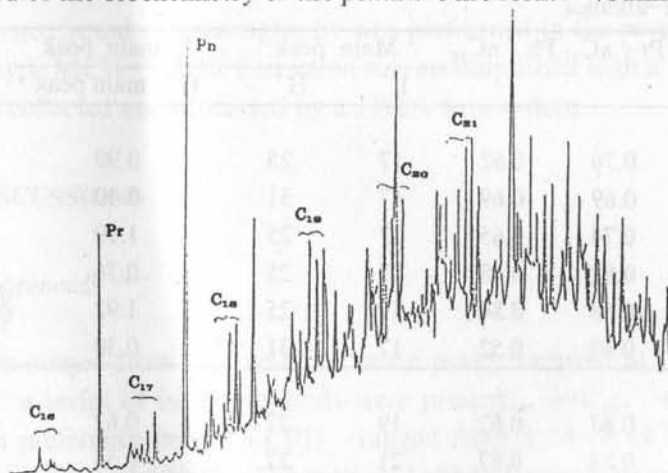


Fig. 1 Gas chromatogram of iso-alkanes (37KL).

Table 2 2-methyl and 3-methyl compounds in the 37KL sediment

Depth of sample (cm)	C_{16}		C_{17}		C_{18}		C_{19}		C_{20}		C_{21}	
	I	A	I	A	I	A	I	A	I	A	I	A
0–22	1.1	0.5	1.0	1.7	6.4	5.9	11.6	10.21	0.9	15.6	8.1	8.6
22–50	0.6	0.5	1.2	1.9	4.5	4.2	7.5	6.8	8.9	13.4	8.4	9.7
172–200	1.6	1.0	3.9	5.3	7.6	6.9	7.4	5.8	6.6	9.6	5.7	6.8
372–400	0.9	0.4	3.3	3.9	6.7	5.4	7.8	6.5	7.6	9.5	7.0	7.0
572–600	1.3	0.9	2.9	3.5	8.0	5.7	9.1	6.4	9.7	11.7	8.6	8.2
772–800	1.1	0.4	4.5	7.0	9.0	6.8	9.0	7.7	4.5	10.1	4.3	5.1

I: 2-methyl (iso) alkane; A: 3-methyl (anteiso) alkane

Polycyclic Aromatic Hydrocarbons

Polycyclic aromatic hydrocarbons are widespread in nature. They are produced from incomplete combustion of fossil fuels such as coal and petroleum, and from spill of petroleum and its products. They also occur in nature as aromatic derivatives of natural precursors originating from bacterial lipids (hopane series), or from terrestrial higher plant terpenoids (amyrin series) (Garrigues *et al.*, 1986). The main route whereby polycyclic aromatic hydrocarbons are transported into the ocean is through the atmosphere followed by rain scavenging and settling. They can also be delivered to the ocean by runoff.

Chrysene and benzo(a)pyrene of polycyclic aromatic hydrocarbons are carcinogenic (Pruell & Quinn, 1985). The Ames assay indicates a significant mutagenic activity in the fraction which contains polycyclic aromatic hydrocarbons with 4–6 aromatic rings. The majority of this activity is found in the fraction composed of 5–ring compounds (West *et al.*, 1986). Perlyene is present in terrestrial matter and characterizes the original reducing depositional environment of rapid transportation. In addition, it can be derived from pigments of marine biomass (perihydroxy perylenequinone). Perlyene is a palaeoenvironmental indicator of an early depositional anoxic environment (Didyk *et al.*, 1978; Tan & Heit, 1981). The components of polycyclic aromatic hydrocarbons in the 37 KL samples are listed in Table 3, 4, and gas chromatograms are shown in Fig. 2.

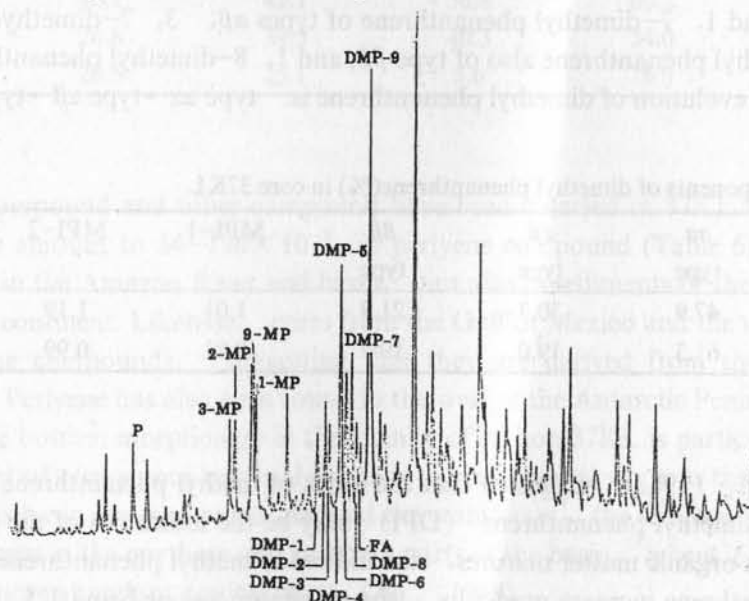


Fig. 2 Gas chromatogram of polycyclic aromatic hydrocarbons (37KL).

Table 3 The distribution of the methyl phenanthrene components in core 37KL

Depth (cm)	3-methyl phen-anthrene	2-methyl phen-anthrene	9-methyl phen-anthrene	1-methyl phen-anthrene
22–50	19.1	27.5	31.4	22.0
372–400	19.4	30.3	30.5	19.7

The phenanthrene series is made up of phenanthrene, methyl phenanthrene, dimethyl phenanthrene trimethyl phenanthrene, tetramethyl phenanthrene, ethyl phenanthrene, diethyl phenanthrene, methyl acenaphthene phenanthrene, dimethyl acenaphthene phenanthrene, methyl benzene phenanthrene and benzene phenanthrene. Due to the different positions of the alkyl substituting group of the phenanthrene ring, their stabilities are distinct. The methyl group of 3-methylphenanthrene and 2-methyl phenanthrene of the isomeric compounds of methyl phenanthrene is situated at the β position, which are stable. On the other hand, 1-methyl phenanthrene and 4-methyl phenanthrene are reactive, and 9-methyl phenanthrene (α position) is even more reactive. During thermal evolution, there is a transformation from the medium or α position to the β position.

The total amount of 2-methyl phenanthrene and 3-methyl phenanthrene in core 37KL are about 47 and 50% respectively, while that of 1-methyl phenanthrene at the α position are 20 and 22%, 4-methyl phenanthrene is absent. Because of the efficient hindrance effect of the methyl group with carbon at the fourth position and hydrogen at the fifth position, it is difficult to methylate at these positions. Thus, the content of 4-methyl phenanthrene is very low to vanishing (Garrigues, 1983).

The isomerized compounds of dimethyl phenanthrene, viz. 3, 6-dimethyl phenanthrene and 2, 7-dimethyl phenanthrene are of the stable $\beta\beta$ type; 1, 6-dimethyl phenanthrene and 1, 7-dimethyl phenanthrene of types $\alpha\beta$; 3, 7-dimethyl phenanthrene and 2, 6-dimethyl phenanthrene also of type $\beta\beta$; and 1, 8-dimethyl phenanthrene is of type $\alpha\alpha$. The order of evolution of dimethyl phenanthrene is: type $\alpha\alpha$ \rightarrow type $\alpha\beta$ \rightarrow type $\beta\beta$.

Table 4 The components of dimethyl phenanthrene(%) in core 37KL

Depth (cm)	$\alpha\alpha$ type	$\alpha\beta$ type	$\beta\beta$ type	MPI-1	MPI-2	DPI
22-50	47.9	30.3	21.9	1.01	1.19	1.35
372-400	61.3	19.0	19.7	0.81	0.99	1.12

Radke *et al.*, (1982) suggested that the index of methyl phenanthrene (MPI-1 and MPI-2) and dimethyl phenanthrene (DPI) may be the indicators of the maturity of organic matter. As organic matter matures, the indices of methyl phenanthrene-1 and -2 and dimethyl phenanthrene increase gradually, the maximum values being 1.5, 1.75 and 1.85 (Radke *et al.*, 1982). Thus, our results suggest that the degree of maturity of the matter of 37 KL is low.

The three fluorene series of polycyclic aromatic hydrocarbons come possibly from the same precursors (Table 5); their basic structure is a five ring. In a slightly oxidizing or slightly reducing environment, furan dominates. Under normal reducing conditions, the α -carbon atom is saturated by hydrogen and fluorene is abundant; in a strongly reducing environment, it will be reduced to thiophene, so that thiophene compounds are enriched (Lin *et al.*, 1987).

Table 5 The main components of polycyclic aromatic hydrocarbons% from core 37KL, as well as from East China Sea

Depth (cm)	Phen- anth- rene	Chry- sene	Py- rene	Fluo- rene	Fu- ran	Thio- phene	Fluo- anth- rene	Constituents of the fluo series		
								Fluo-	Fu-	Thio-
22-50	69.31	1.85	5.86	1.40	0.91	4.75	1.75	19.8	12.9	67.3
372-400	53.23	1.55	2.85	2.00	1.00	5.54	0.87	23.4	11.7	64.9
E-1	29.98	15.74	3.22	4.53	0.00	3.55	17.68	56.1	0.0	43.9
E-2	11.31	27.00	16.08	4.65	0.00	4.22	13.01	52.4	0.0	47.6

Fluo: Fluorene; Fu: Furan; Thio: Thiophene; E-1: East China Sea-1; E-2: East China Sea-2.

Table 6 The compounds of polycyclic aromatic hydrocarbons ($\times 10^{-9}$)

Depth (cm)	Phen- anthrene	Benzo(e)- pyrene	Benzo(a)- pyrene	Perlyene	1,2,3,4-diben- zopyrene
0-22	14.1	26.4	27.7	37.5	12.2
22-50	27.7	40.1	28.7	40.0	12.0
175-200	41.7	49.0	49.8	136.2	26.6
372-400	40.1	42.1	56.8	60.2	14.2
572-600	26.8	39.5	40.3	54.0	9.8
772-800	26.5	25.1	5.6	76.9	14.1

Perlyene compound and other compound have been detected in 37KL using HPLC instrument. They amount to $54-136 \times 10^{-9}$ in perlyene compound (Table 6). Perlyenes are found not only in the Amazon River and basin, but also in sediments of the open ocean far away from any continent. Likewise, cores from the Gulf of Mexico and the western Atlantic contain perlyene compounds, suggesting that they are derived from the continent via turbidity flows. Perlyene has also been found in the west of the Antarctic Peninsula (Tang *et al.*, 1989). The bottom morphology in the vicinity of station 37KL is particularly favorable for the transport of terrigenous material through the continental slope to the deep basin. At the center of this basin are seamounts. Around the seamounts, the sediment thickness is less than 1000 m except in the northern and southern parts of the basin, where it reaches 2-3 km because of the more abundant detrital input (Jin, 1989).

Steranes and Terpanes

Core samples contain cholestane ($C_{27} H_{48}$), ergostane ($C_{28} H_{50}$) and sitostane ($C_{29} H_{52}$); with sitostane as the dominant nomolog in the series. They are abundant in the non-biological configuration ($C_{29} \alpha\alpha\alpha 20S/20R$), which has values of >0.8 . At the depth range 394-494 cm of core 91KL, it even reached the abnormally high value of 3.04. In addition, the ratio of C_{29} isositostane to sitostane ($C_{29} \alpha\beta\beta/\alpha\alpha\alpha$) is also over 0.6. This shows

that the $\alpha\alpha\alpha$ -R configuration has been converted to $\alpha\alpha\alpha$ -S, $\alpha\beta\beta$ -R and the $\alpha\beta\beta$ -S configurations, namely a biological to geological conversion. On the whole, the values of $\alpha\alpha\alpha$ -20S (C_{27} or C_{28} or C_{29}) are less than the content of 20R+20S for the corresponding carbon number. For example, the 20S / 20S+20R of C_{29} $\alpha\alpha\alpha$ sterane ratio has not reached the end value of 50–55% (Mackenzie, 1984).

The amount of C_{27} cholestane is 23–28%, and that of C_{28} ergostane and C_{29} sitostane 26–31% and 43–49% respectively. The abundance of C_{28} sterane at the depth interval 394–494 cm of core 91KL is up to 41%. Other parameters such as C_{29} $\alpha\alpha\alpha$ S / R, $\alpha\alpha\alpha C_{28}$ regular sterane / C_{29} regular sterane and $\alpha\alpha\alpha C_{27}$ regular sterane / C_{29} regular sterane also exhibit high values. In general, the precursors of the three steranes mentioned above are believed to reflect autochthonous or allochthonous input. A high proportion of C_{29} steranes indicate a significant input of terrigenous organic matter, since the precursor C_{29} sterols such as 24-ethylcholest-5-en-3 β -ol is abundant in vascular plants. Although Volkman (1986) suggests that marine organisms can be a major source of 24-ethylcholest-5-en-3 β -ol and other sterols presently used as biomarkers for terrigenous organic matter, there is consensus that C_{29} sterane is attributable to terrestrial higher plants.

The spore and pollen assemblage results show that core 29KL is richer in spore and pollen than core 91KL. In particular, very meagre assemblages are found in the interval 280–450 cm of core 91KL. There is only a slight increase in scattered growth of pine and herbs at 450–600 cm. Because station 91KL is far away from land and the tidal current and turbidity current are effective, few spore and pollen are expected.

In general, the isomerized end point of 5 α (H), 14 α (H), 17 α (H)-cholestane and 5 α (H), 14 β (H), 17 β (H)-isocholestane is 1 : 3. The 20S : 20R of cholestane is 1 : 1. The isomerized end point of the cores 29KL and 91KL lies within the range 1.4–2.3 : 1, and the ratio of 20S : 20R in cholestane is less than 1 (except for the section 394–494 cm of 91KL, which has the value of 1.8. Thus, sediments at these stations have not yet reached the isomerized end point. $(5\alpha, 14\beta, 17\beta-20S+5\alpha, 14\beta, 17\beta-20R) / (5\alpha, 14\alpha, 17\alpha-20S+5\alpha, 14\alpha, 17\alpha-20R) + (5\alpha, 14\beta, 17\beta-20S+5\alpha, 14\beta, 17\beta-20R)$ is an indicator of the maturity of organic matter, the isomerized end point of C_{27} $\beta\beta / \alpha\alpha+\beta\beta$ being 75%. But for the cores 29KL and 91KL, the values are 31–38% and 32–41%. The isomerized end point of C_{29} 20S / 20S+20R is 50–55% (Mackenzie, 1984), but for core 29KL, it is 42–50% and for core 91KL, it is 43–48%. Thus, sediments from the two cores studied have by and large not yet attained maturity.

Pentacyclic triterpanes exist in nature as three series of compounds: sedimentary hopanes which are derived from the defunctionalization and configurational isomerization of a bacterial 17 β (H), 21 β (H)-hopanetetrol (Ourisson *et al.*, 1979); 17 β (H), 21 α (H)-hopanoids and 17 α (H), 21 β (H)-hopanoids which have been found in recent sediments (Dastillung *et al.*, 1980). Biologically synthesized hopanes generally have the 17 β (H), 21 β (H) configuration which is thermodynamically less stable than the 17 α (H), 21 β (H) configuration. The relative amounts of hopanes vary with maturity. As the degree of maturity increase, the 17 β (H), 21 β (H)-hopanes and moretane decrease, 17 α (H), 21 β (H)-hopane becomes predominant (Seifert & Moldowan, 1980; Mackenzie, 1984). The pentacyclic triterpanes of the two cores 29 and 91KL contain all of the three series of compounds mentioned above. In particular, the presence of 17 β (H), 21 β (H) suggest that

the sediments are relatively immature. In addition, the ratio of homohopane (C_{31} 22S / 22R+22S) is less than the equilibrium value for complete maturity (approximately 0.6) (Mackenzie, 1984). The C_{27} 17 β (H), 21 α (H) compounds near the 17 α (H)-22, 29, 30-trisnorhopane except 17 α (H), 21 β (H) compound are found in all the sediment samples. Furthermore, C_{29} , C_{30} and C_{31} 17 β (H), 21 α (H) compounds were also present. The 22S concentration of C_{31} 17 α (H), 21 β (H)-30-22S and 17 α (H), 21 β (H)-30-22R at the depth interval 770-800 cm of core 29KL sample is slightly higher than that for the 22R configuration. For other depth intervals, 22R is enriched relative to 22S.

17 α (H)-22, 29, 30-trisnorhopane (Tm) and 18 α (H)-22, 29, 30-trisnorneohopane (Ts) are used as sensitive indicators of oil in sediments. The Tm / Ts ratio in the two cores ranges from 1.05 to 1.61, the actual value being a function of the depositional environment and the distribution of organic matter. From the relative amounts of C_{27} , C_{28} and C_{29} steranes (Table 7), it is clear that they are derived mostly from terrigenous higher plants, which, however, are both qualitatively and quantitatively different for the two core location. Core 29KL has both arbor and non-arbor spore assemblages, the arbor pollen being dominated by of needle pine (56%), and the non-arbor pollen by the grass family (68%). The pteridophyte spores are represented chiefly by golden locks and spinulose tree fern. The arbor pollen of core 91KL contains mainly pine with quercus, castanopsis and needle pine occurring secondarily. The Tm / Ts ratio of the two cores is over 1, indicating low maturities. The epimerized value of C_{31} hopane 22S / 22S+22R is 39-46% (as high as 55% for core 29KL 772-800 cm). These values are not near the stable state value of 60%. The C_{20} side chain epimerized amount (C_{29} S / S + R) of C_{29} sterane 5 α (H), 14 α (H), 17 α (H) is 43-56% (except that core 91KL 394-494 cm, it is 74%). This is near equilibrium end point of 55%. The nuclei isomerization 20R / 20S 14 α (H), 17 α (H) \rightleftharpoons 20R / 20S 14 β (H), 17 β (H), the sterane ratio $\beta\beta / \alpha\alpha$ is only 31-41%, the equilibrium end point is, however, 75% (Seifert & Moldowan, 1981), implying that isomerization has not reached its end point.

CONCLUSIONS

1. The distribution of carbon number in the organic matter of sediments from the South China Sea ranges from C_{16} to C_{33} . The ratio of pristane to phytane suggested that the depositional environment at station 29KL was slightly more reducing than that at station 91KL.

2. The iso-alkane compounds contained some substituting alkyl groups in addition to the 2-methyl (iso-) and 3-methyl (anteiso-) compounds.

3. The presence of perlyene, the low ratio of light to heavy hydrocarbons and the pre-dominance of C_{29} sterane demonstrated that terrestrial higher plants were the major source of organic matter, although there are also marine inputs.

4. The low maturity of the sedimentary organic matter from the South China Sea is demonstrated by the fact that: (1) the amount of C_{27} or C_{28} or $C_{29}\alpha\alpha$ -S is lower than the total amount of $\alpha\alpha$ -R+S; (2) the isomerized end point of 5 α (H), 14 α (H), 17 α (H)

Table 7 Geochemical parameters of the sterane compounds in the core 29 and 91KL

Depth (cm)	$\frac{\alpha\alpha\alpha + \alpha\beta\beta^*}{C_{27}C_{28}C_{29}}$			$\frac{C_{29\alpha\alpha\alpha}}{20S}$	$\frac{C_{29}}{\alpha\alpha\alpha}$ S/R	$\frac{C_{29}}{\alpha\beta\beta}$	$\frac{C_{28}}{13\beta17\alpha}$ reg.st.	$\frac{C_{27}}{13\beta17\alpha}$ reg.st.	$\frac{\alpha\alpha\alpha}{C_{28}st.}$	$\frac{\alpha\alpha\alpha}{C_{27}st.}$	chole- stane(%)	Isocho- lestane (%)	Rear. st.(%)	$\frac{4 - me.st.}{C_{29}reg.st.}$	$\frac{C_{29-31}}{\sum\beta\alpha}$
				$\frac{20S}{20S + 20R}$		$\frac{\alpha\beta\beta}{\alpha\alpha\alpha}$			$\frac{C_{28}st.}{C_{29}st.}$	$\frac{C_{27}st.}{C_{29}st.}$					$\frac{\sum\alpha\beta}{\sum\beta\alpha}$
29K1															
22-50	27.1	28.7	44.2	0.45	0.82	0.86	0.10	0.11	0.65	1.05	51.2	38.0	10.8	0.08	0.26
175-200	27.5	27.5	45.0	0.45	0.82	0.75	0.11	0.12	0.62	1.03	53.1	34.7	12.2	0.04	0.35
372-400	25.6	27.0	47.4	0.48	0.93	0.67	0.11	0.09	0.50	0.84	53.0	35.6	11.4	0.04	0.34
572-600	23.2	29.4	47.4	0.52	1.10	0.60	0.13	0.10	0.61	0.70	53.4	34.7	11.9	0.03	0.35
772-800	28.1	28.5	43.4	0.56	1.30	0.68	0.09	0.10	0.62	1.06	55.1	34.5	10.4	0.03	0.45
972-993	22.5	28.2	49.3	0.45	0.81	0.70	0.10	0.09	0.58	0.69	55.6	33.9	10.5	0.03	
91KL															
0-100	25.1	30.0	45.9	0.45	0.81	0.72	0.06	0.06	0.67	0.89	55.5	37.6	6.9	0.02	0.38
100-194	25.5	27.6	46.9	0.45	0.83	0.67	0.11	0.09	0.54	0.86	52.8	36.6	10.6	0.04	0.44
194-294	25.3	29.0	45.7	0.47	0.88	0.74	0.12	0.11	0.67	0.86	51.6	36.5	11.9	0.05	0.52
294-394	23.0	28.2	48.8	0.43	0.77	0.80	0.11	0.11	0.59	0.73	49.9	29.3	20.8	0.04	0.35
394-494	23.9	40.9	35.2	0.74	3.04	1.04	0.30	0.17	1.25	1.28	43.6	35.9	20.5	0.05	0.40
494-594	27.5	26.2	46.3	0.49	0.80	0.71	0.15	0.09	0.64	0.87	50.1	38.0	11.9	0.05	0.41
594-694	23.1	28.6	48.3	0.44	0.75	0.73	0.10	0.09	0.57	0.78	52.9	36.8	10.3	0.06	0.47
694-770	25.7	31.2	43.1	0.49	0.84	0.80	0.14	0.14	0.75	0.94	48.1	38.3	13.6	0.05	0.38

* Distribution of carbon number (%). st.: sterane; reg. st.: regular sterane; me. st.: methyl sterane; rear: rearrangement.

cholestane and $5\alpha(\text{H})$, $14\beta(\text{H})$, $17\beta(\text{H})$ isocholestane have not yet reached their equilibrium values; (3) the occurrence of $17\beta(\text{H})$, $21\beta(\text{H})$ and the relative proportions of $17\alpha(\text{H})$, $21\beta(\text{H})$, and $17\beta(\text{H})$, $21\alpha(\text{H})$, and the ratio of $17\alpha(\text{H})$ -22, 29, 30-trisnorhopane (Tm) to $18\alpha(\text{H})$ -22, 29, 30-trisnorneohopane (Ts). All point to immaturity; and (4) the indices of methyl phenanthrene and dimethyl phenanthrene are low.

ACKNOWLEDGEMENTS

This research was financed by the National Laboratory of Organic Geochemistry, Institute of Geochemistry, Chinese Academy of Sciences.

REFERENCES

- Brassell, S.C., A.M.K. Wardroper, I.D. Thomson, J.R. Maxwell and G. Eglinton, 1981: Specific acyclic isoprenoids as biological markers of methanogenic bacteria in marine sediments. *Nature*, 290, 693-696.
- Dastillung, M., P. Albrecht and G. Ourisson, 1980: Aliphatic and polycyclic alcohols in sediments: Hydroxylated derivatives of hopane and of 3-methyl hopane. *J. Chem. Research*, 168-169.
- Didyk, B.M., B.R.T. Simoneit, S.C. Brassell and G. Eglinton, 1978: Organic geochemical. *Nature*, 272, 216-222.
- Garrigues P., A. Saptorahardjo and C. Gonzalez, 1986: Biogeochemical aromatic markers in the sediments from Mahakam Delta (Indonesia). *Org. Geochem.*, 10, 959-964.
- Garrigues, P. and M. Ewald, 1983: Identification of monomethylated polycyclic aromatic hydrocarbons in crude oils by liquid chromatography and high resolution Shpol'skii effect fluorescence spectrometry. *Anal. Chem.*, 55, 2155-2159.
- Jin Qingming (ed.), 1989: South China Sea geology and oil gas resources. Geological Publishing House, Beijing, China, 266-307 (in Chinese).
- Kaneda, T., 1977: Fatty acids of the genus *Bacillus*: an example of branched-chain preference. *Bacterial Rev.*, 41, 391-418.
- Li Cuizhong, 1987: Sediments type and sedimentation of the central South China Sea Basin. *Donghai Haiyang*, 5, 18-35 (in Chinese).
- Lin Renzhi, Wang Peirong, Dai Yunjian, Zhang Zebo, Huang Guanghui and Bao Jianong, 1987: Polyaromatic hydrocarbons in fuels and their significance in petroleum geochemistry. Proceedings of the Third National Symposium on Organic Geochemistry of China (in Chinese).
- Mackenzie A.S., 1984: Applications of biological markers in petroleum geochemistry. *Advances in Petroleum Geochemistry*, Brooks J. and D. Welte (eds.), Academic Press, London, 115-214.
- Mackenzie, A.S., R.L. Patience, J.R. Maxwell, M. Vandenbroucke and Durand, 1980: Molecular parameters of maturation in the Toarcian shales, Paris Basin—I. Changes in the configurations of acyclic isoprenoid alkanes, steranes and triterpanes. *Geochim. Cosmochim. Acta*, 44, 1709-1721.

- Ourisson, G., P. Albrecht and M. Rohmer, 1984: The microbial origin of fossil fuels. *Sci. Am.*, 251, 44-51.
- Ourisson, G., P. Albrecht and M. Rohmer, 1979: The hopanoids, palaeochemistry and biochemistry of a group of natural products. *Pure Appl. Chem.*, 51, 709-729.
- Pruell, R.J. and J.G. Quinn, 1985: Polycyclic aromatic hydrocarbons in surface sediments held in experimental Mesocosm. *Toxicol. and Environ. Chem.*, 10, 183-200.
- Radke, M., D.H. Welte and H. Willsch, 1982: Geochemical study on a well in the western Canada Basin: Relation of the aromatic distribution pattern to maturity of organic matter. *Geochim. Cosmochim. Acta*, 46, 1-10.
- Seifert, W.K. and J.M. Moldowan, 1980: The effect of thermal stress on source-rock quality as measured by hopane stereochemistry. Douglas A.G. and Maxwell J.R. (eds.), Pergamon Press, Oxford, 1979, 229-237.
- Seifert, W.K. and J.M. Moldowan, 1981: Palaeoreconstruction by biological markers. *Geochim. Cosmochim. Acta*, 54, 783-794.
- Summons, R.E., 1987: Branched alkanes from ancient and modern sediments, isomer discrimination by GC/MS with multiple reaction monitoring. *Org. Geochem.*, 11, 281-289.
- Tan, Y.L. and M. Heit, 1981: Biogenic and abiogenic polycyclic aromatic hydrocarbons in sediments from two remote Adirondack lakes. *Geochim. Cosmochim. Acta*, 45, 2267-2279.
- Tang Yunqian, Yang Zhanxiang, Xu Luqiang and Zhou Jian, 1989: Alkane and aromatic hydrocarbons in sediments in the sea area near the Antarctic Peninsula. *Proceedings of China First Symposium on South Ocean Expedition*, 82-87 (in Chinese).
- Tissot, B.P., 1984: Geochemistry of resins and asphaltenes. *Rev. Inst. Fr. Petrole.*, 39, 561-572.
- Volkman, J.K., 1986: A review of sterol markers for marine and terrigenous organic matter. *Org. Geochem.*, 9, 83-89.
- Wehner, H., M. Teschner and K. Bosecker, 1986: Chemical reactions and stability of biomarkers and stable isotope ratios during in vitro biodegradation of petroleum. *Org. Geochem.*, 10, 463-471.
- West, W.R., P.A. Smith, G.M. Booth, S.A. Wise and M.L. Lee, 1986: Determination of genotoxic polycyclic hydrocarbons in a sediment from the Black River (Ohio). *Arch. Environ. Contam. Toxicol.*, 15, 241-149.